UNIVERSITY OF SOUTHAMPTON

DIRECT AND INDIRECT CHANNELS TO MOLECULAR DISSOCIATION AT METAL SURFACES

A thesis submitted to the University of Southampton in support of candidature for the degree of Doctor of Philosophy

by Claire Mormiche

Department of Chemistry
August 2002

UNIVERSITY OF SOUTHAMPTON

ABSTRACT

FACULTY OF SCIENCE

DEPARTMENT OF CHEMISTRY

Doctor of Philosophy

DIRECT AND INDIRECT CHANNELS TO MOLECULAR DISSOCIATION AT METAL SURFACES

by Claire Mormiche

The influence of well-defined (100) steps on the dynamics of the dissociative chemisorption of methane, hydrogen and ammonia on Pt(533) has been investigated using molecular beam techniques and TPD spectroscopy.

For CH_4 on Pt(533), the enhancement in dissociation is associated with the additional direct sticking mediated by the step sites which exhibit an effective activation barrier 300meV lower than the (111) terraces. The lowest activation barrier appears for incident trajectories with an angle of ~5-10° compared to the surface normal. An enhanced surface temperature dependence is also observed on the Pt(533) surface over Pt(111), resulting either from the lower barrier to dissociation or the lower effective Debye temperature of the Pt atoms, at the step.

H_2 adsorption on Pt(533) exhibits 3 channels to dissociation, a direct channel which is the main one above 30 meV, and two indirect channels. One accommodated channel which influence the sticking below 25 meV and one unaccommodated channel which has a decreasing influence up to 150 meV where $S_0(H_2)$ stays constant at ~ 0.05. The unaccommodated indirect channel is not available on CO and O steps-decorated surface. The production of water from hydrogen adsorption on the O/Pt(533) is limited by the formation of hydroxyl.

Ammonia adsorption is molecular at $T_s < 400$ K and does not seem to depend strongly on the platinum surface plane, however desorption from the (100) steps of Pt(533) appears as extra shoulders on the TPD spectra. Ammonia decomposes on Pt(533) at $T_s > 360$ K but does not on Pt(111). The dissociation of NH_3 occurs in two steps: NH_2 is formed and H_2 produced at 400 K, then N_2 and H_2 both desorb at 530 K. An indirect channel to NH_3 initial dissociation at 400 K is evidenced. The dissociation of NH_3 on oxygen steps-decorated Pt(533) is enhanced, producing H_2, H_2O, N_2 and NO on the whole surface, while on CO/Pt(533) the steric effect of CO slowly blocks the adsorption and decomposition of NH_3.

The interaction of H_2 and O_2 with uranium has also been studied by TPD and molecular beam techniques. A direct channel for O_2 dissociative adsorption and an indirect channel for H_2 dissociation are evidenced. The desorption of hydrogen from surfaces with varying oxygen coverages is also presented.

ACKNOWLEDGEMENTS

First of all I would like to thank my supervisor Prof. Brian Hayden for giving me the chance to work in his research group, for believing in my abilities and for calming me down when everything seemed to go wrong. Thanks also to Dr Tim Nunney who had to deal with my constant mood swings, my many questions and not least for being forced to read this work hundreds of times.

Thanks to Bernd Riedmuller who initiated me with the beam machine and colaborated with us on the methane chapter.

A big thanks too to Mike Rendall for solving many computer problems and cheering me up with the installment of the cake day rota.

Thanks to Dr John Davies for being there, listening to my problems and making me enjoy my evenings especially at the Donjon.

Thanks again to all the members of my group, Naruo, Scott, Oliver and Ben for taking the piss out of me each time I was moaning (*i.e.* every day).

Thanks to Chris for smiling all the time and teaching me what's "beer".

Thanks to Sam and Sheila who have assumed, from time to time, to be my English godparents.

I cannot forget Dave, Rob, Alan and John for repairing everything without delay and always with a smile.

Thanks to all my friends at Southampton University for making me forget that work is not everything.

Finally I would like to thank the one I am more used to call "My Baby", *i.e.* the beam machine, who has been a very good girl during these three years and has not broken down too often.

GLOSSARY

AES	Auger Electron Spectroscopy
B3LYP	Becke's Three Parameter Hybrid Functional Using the LYP Correlation Functional
CAE	Constant Analyser Energy
CAT	Constant Analyser Transmission
CID	Collision Induced Desorption
CRR	Constant Retard Ratio
DFT	Density Functional Theory
DRS	Direct Recoil Spectroscopy
EELS	Electron Energy Loss Spectroscopy
EMT	Effective Medium Theory
ESCA	Electron Spectroscopy for Chemical Analysis
ESDIAD	Electron Stimulated Desorption Ion Angular Distribution
EXAFS	Extended X-Ray Absorption Fine Structure
FAT	Fixed Analyser Transmission
FEM	Force Electron Microscopy
FRR	Fixed Retard Ratio
GGA	Generalized Gradient Approximations
HREELS	High Resolution Electron Energy Loss Spectroscopy
IRAS	Infrared Reflection Absorption Spectroscopy
LEED	Low Energy Electron Diffraction
LDA	Local Density Approximation
MBRS	Molecular Beam Relaxation Spectroscopy
ML	Monolayer (1ML = 1 adatom per surface lattice atom)
PES	Potential Energy
QMS	Quadrupole Mass Spectrometer
RLS	Rate Limiting Step
SIMS	Secondary Ion Mass Spectroscopy
STM	Scanning Tunnelling Microscopy
TOF	Time Of Flight
TPD	Temperature Programmed Desorption Spectroscopy
UHV	Ultra High Vacuum
UPS	Ultraviolet Photoelectron Spectroscopy
XPS	X-ray photoelectron Spectroscopy

TABLE OF CONTENTS

CHAPTER I: THEORY OF ADSORPTION 1
I.1 INTRODUCTION 1
I.2 POTENTIAL ENERGY SURFACES 2
I.3 PHYSISORPTION 4
I.4 CHEMISORPTION 6
I.4.1 Direct Dissociation 6
I.4.2 Indirect Dissociation 8
I.5 AIMS 10
I.6 REFERENCES 11

CHAPTER II: INSTRUMENTATION 12
II.1 INTRODUCTION 12
II.2 FIRST CHAMBER: THE NOZZLE SKIMMER CHAMBER 12
II.3 SECOND CHAMBER: THE CHOPPER CHAMBER 14
II.4 THE MAINCHAMBER 14
II.4.1 The Variable Aperture 15
II.4. 2 Sample Mounting and Cleaning 15
II.4.2.1 Platinum 15
II.4.2.2 Uranium 19
II.5 SUPERSONIC MOLECULAR BEAMS 20
II.5.1 The Beam Line 28
II.5.2 Kinetic Energy of the Particles in the Beam Line 29
II.6 REFERENCES 32

CHAPTER III: EXPERIMENTAL METHODS 33
III.1 TEMPERATURE PROGRAMMED DESORPTION 33
III.2 KING & WELLS METHOD 35
III.2.1 Sticking Probability 37
III.2.2 Titration Method 39
III.3 X-RAY PHOTOELECTRON SPECTROSCOPY 41
III.4 REFERENCES 48

CHAPTER IV: DYNAMICS AND KINETICS OF DISSOCIATIVE ADSORPTION OF METHANE ON Pt(533) 50
IV.1 INTRODUCTION 50
IV.1.1 Methane Adsorption on Transition Metals 50
IV.1.2 Platinum 50
IV.1.3 Adsorbate-Substrate Bonds between CH_4 and Pt 51
IV.1.4 Molecular Orbitals of CH_4 and Energy Diagram Correlation with Pt 52
IV.1.5 Structural Effects 55
IV.1.6 CH_4 Adsorption on Platinum Surfaces 56
IV.2 EXPERIMENTAL 58
IV.3 RESULTS AND DISCUSSION 59

IV.3.1 Methane Temperature Programmed Desorption..... 59
IV.3.2 King & Wells Method..... 59
IV.3.3 Titration of CO and CO_2..... 60
IV.3.4 Dependence of $S_0(CH_4)$ on Incident Energy..... 62
IV.3.5 Influence of the (100) Steps on $S_0(CH_4)$..... 65
IV.3.6 Angular Dependence of $S_0(CH_4)$..... 68
IV.3.7 Dependence of $S_0(CH_4)$ on Surface Temperature..... 72
IV.4 CONCLUSION..... 76
IV.5 REFERENCES..... 76

CHAPTER V: DYNAMICS AND KINETICS OF DISSOCIATIVE ADSORPTION OF HYDROGEN ON Pt(533)..... 80
V.1 INTRODUCTION..... 80
V.1.1 Adsorbate-Substrate Bonds..... 81
V.1.2 Dissociative Adsorption of H_2..... 82
V.1.3 Structural Effects..... 83
V.2 EXPERIMENTAL..... 85
V.3 RESULTS AND DISCUSSION..... 85
V.3.1 Hydrogen Temperature Programmed Desorption..... 85
V.3.2 King & Wells Method..... 92
V.3.3 Dependence of $S_0(H_2)$ on Incident Energy..... 93
V.3.4 Consequences of Pre-adsorbed Oxygen on $S_0(H_2)$..... 96
V.3.5 Maxwell-Boltzmann Distribution..... 104
V.3.6 Dependence of $S_0(H_2)$ on Surface Temperature..... 107
V.3.7 Dependence of $S_0(H_2)$ on Hydrogen Coverage..... 110
V.3.8 Water Formation on Platinum..... 115
V.3.9 Consequences of Pre-adsorbed Carbon Monoxide on $S_0(H_2)$..... 124
V.3.10 Dependence of $S_0(H_2)$ on Surface Temperature..... 129
V.3.11 Dependence of $S_0(H_2)$ on Hydrogen Coverage..... 130
V.4 CONCLUSION..... 134
V.5 REFERENCES..... 136

CHAPTER VI: DYNAMICS AND KINETICS OF ADSORPTION OF AMMONIA ON Pt(533)..... 142
VI.1 INTRODUCTION..... 142
VI.1.1 Ammonia Production..... 142
VI.1.2 Ammonia Adsorption on Transition Metals..... 142
VI.1.3 Molecular Orbitals of NH_3 and Energy Diagram Correlation with Pt..... 144
VI.1.4 NH_3 Adsorption on Platinum Surfaces..... 147
VI.1.5 Decomposition of NH_3..... 152
VI.2 EXPERIMENTAL..... 154
VI.3 RESULTS AND DISCUSSION..... 154
VI.3.1 Ammonia Temperature Programmed Desorption..... 154
VI.3.2 Temperature Programmed Desorption of N_2 and H_2..... 157

VI.3.3 Summary..... 162
VI.3.4 King & Wells Method..... 166
VI.3.5 Dependence of $S_0(NH_3)$ on Incident Energy..... 166
VI.3.6 Dependence of $S_0(NH_3)$ on Ammonia Coverage..... 169
VI.3.7 Dependence of $S_0(NH_3)$ on Surface Temperature..... 172
VI.3.8 Consequences of Pre-adsorbed CO on NH_3 Adsorption/Desorption..... 179
VI.3.9 Summary..... 187
VI.3.10 King & Wells Method..... 191
VI.3.11 Dependence of $S_0(NH_3)$ on Incident Energy..... 191
VI.3.12 Consequences of Pre-adsorbed Oxygen on NH_3 Adsorption/Desorption..... 194
VI.3.13 Summary..... 207
VI.3.14 King & Wells Method..... 210
VI.3.15 Dependence of $S_0(NH_3)$ on Incident Energy..... 210
VI.4 CONCLUSION..... 211
VI.5 REFERENCES..... 213

CHAPTER VII: DYNAMICS AND KINETICS OF ADSORPTION OF DISSOCIATIVE ADSORPTION OF HYDROGEN ON A POLYCRYSTALLINE URANIUM SURFACE..... 218
VII.1 INTRODUCTION..... 218
VII.1.1 Oxygen/Uranium and Hydrogen/Uranium Interactions..... 220
VII.2 EXPERIMENTAL..... 222
VII.3 RESULTS AND DISCUSSION..... 223
VII.3.1 Hydrogen Temperature Programmed Desorption..... 223
VII.3.2 XPS Measurements..... 229
VII.3.3 King & Wells Method..... 233
VII.3.4 Consequences of Pre-adsorbed Oxygen on Hydrogen TPD..... 236
VII.3.5 Dependence of S_0 of Oxygen on Incident Energy..... 240
VII.4 CONCLUSION..... 242
VII.5 REFERENCES..... 242

CONCLUSION..... 245

FUTURE WORK..... 249

APPENDIX A..... 251

APPENDIX B..... 258

CHAPTER I: THEORY OF ADSORPTION

I.1 INTRODUCTION

In the early 1950's, as many new techniques were developed, the study of gas-phase molecular processes became of great interest. Surface chemistry only became wide-spread in the 1960's due to industrial applications such as catalysis, electrochemistry, oxidation, biological sciences, etc. To study particle-surface interactions well characterised conditions are required since these interactions are sensitive to surface contamination and surface structure, thus the availability of economical ultrahigh vacuum (UHV) systems which can provide such conditions is also necessary. New surface instrumentation and techniques have been developed that permit the study of surface properties on the atomic scale (such as EXAFS, ESCA, HREELS, FEM, IRAS, LEED, STM and TPD). As a result of this sudden availability of surface characterisation techniques, macroscopic surface phenomena, such as adsorption, catalysis and diffusion, are being reexamined on the molecular scale.

An example of surface reactions between a molecule in gas phase and a surface is adsorption. On approaching the surface, each atom or molecule encounters an attractive potential that ultimately will bind it to the surface under proper circumstances. It is always an exothermic process [1].

Surfaces are of such interest because they are a special kind of defect in the solid state, *i.e.* they are not periodic in one direction giving rise to localised electronic and vibrational properties. To simplify the study of the surface, a single crystal with low Miller index is generally used, which gives a known ordered arrangement of atoms. The one studied in these experiments is more complex because of the presence of surface irregularities (steps) that can influence a variety of surface phenomena, ranging from crystal growth to heterogeneous catalysis. Steps are also important participants in atoms transport along the surface. For the stepped Pt(533) crystal surface studied here their equilibrium concentration is around 20 to 25 % of the total surface area.

I.2 POTENTIAL ENERGY SURFACES

The adsorption of a molecule at a surface, which leads to change the potential energy, ***PE***, of this molecule, can be represented by the one-dimensional potential energy model of Lennard-Jones [2] (**figure I.1**), where **z** is the molecule-surface separation. ε is the well depth and σ is the bond length at zero ***PE***.

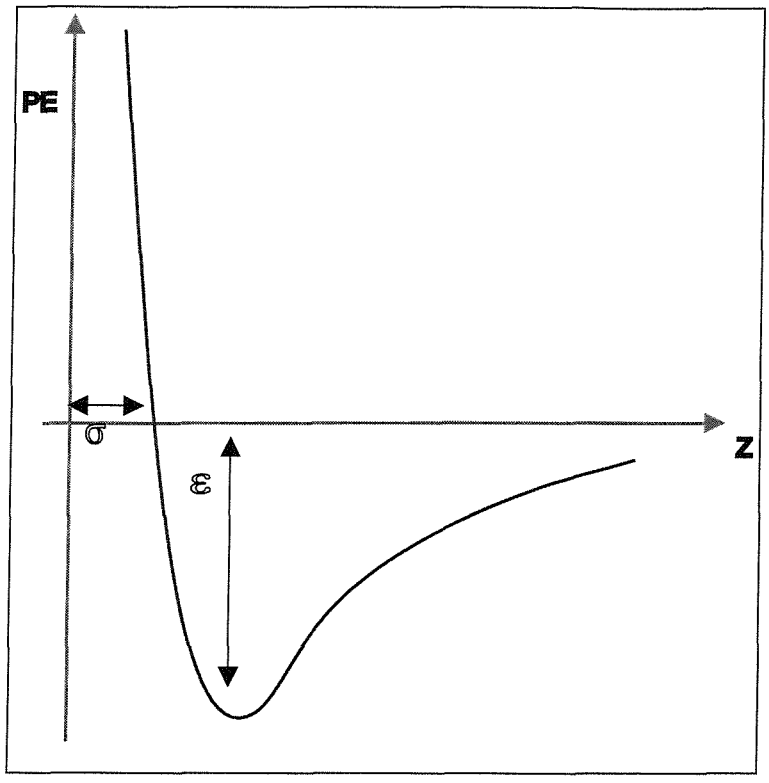

Figure I.1: Lennard-Jones Potential Model.

But this theoretical model is not adequate for interactions where further degrees of freedom need to be considered, such as the vibrational and rotational energies of the molecule, the site of impact on the surface and the orientation of the molecule to the surface of impact. Thus a two-dimensional potential energy surface (***PES***) model is useful (**figure I.2**), where the two degrees of freedom most commonly represented are the molecule-surface separation, z, and the molecular bond length, r.

This ***PES*** consists of an elbow connecting the two following channels: the entrance channel representing the incoming molecule (*i.e.* high distance to the surface z and small bond length r) and the exit channel which represents the adsorbed atoms (*i.e.* small z and large r).

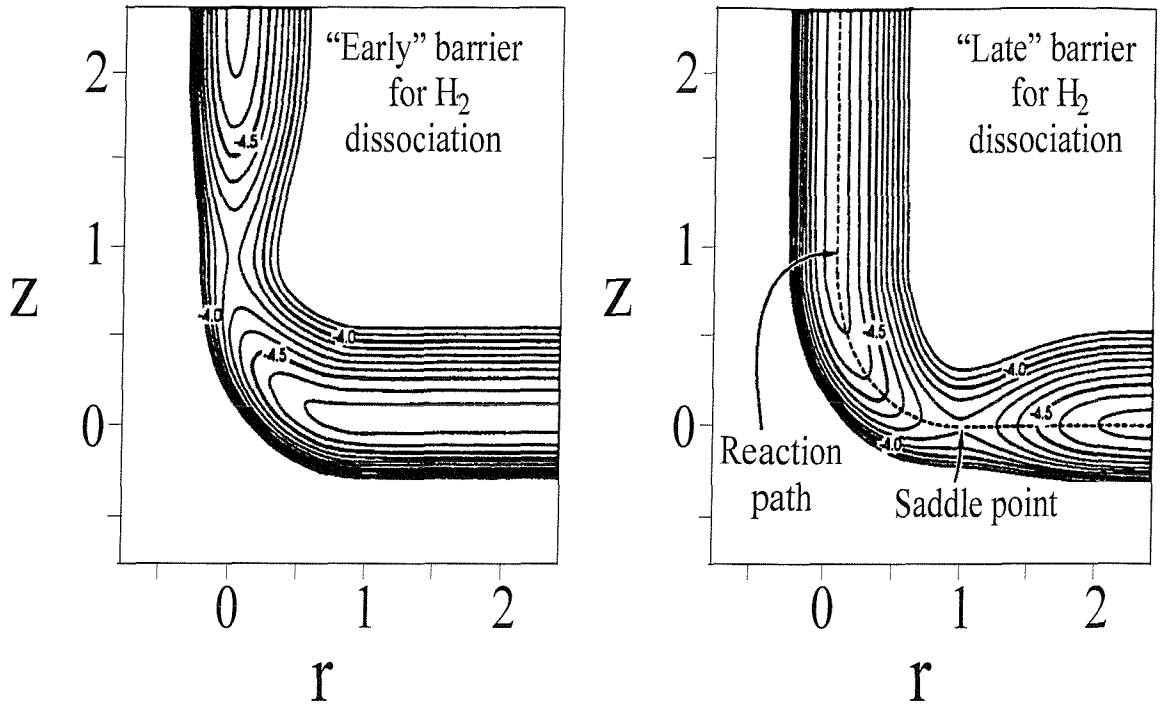

Figure I.2: Two-dimensional ***PES*** model for an early and a late barriers to H_2 dissociation [3].

The transition from the molecular state to the atomically adsorbed state occurs at the saddle point. The precise location of this point is important because it explains the dependence of the dissociation probability on both vibrational and translational energy. In moving across the surface unit cell, the position of the saddle may change in the z direction (geometric corrugation) and in addition the magnitude of the barrier may also vary (energetic corrugation). If geometric corrugation occurs, then the most efficient trajectory may not be normal to the surface but at some angle θ_I, changing with the impact site. Hence it allows both normal and parallel momentum to couple to the barrier to dissociation, and therefore a total rather than normal energy dependence may be observed. In contrast the effect of parallel momentum on an energetically corrugated surface is to decrease the probability of dissociation. Here motion across the surface reduces the time available to access the minimum barrier [4]. Moreover, the saddle point or barrier to dissociation can be defined as early, when the translational energy of the incident molecule couples well with

the barrier and aids dissociation, or late where the inter-molecule bond is being stretched a lot compared with its equilibrium position at the saddle point, hence the vibrational energy of the incident molecule will couple well with the barrier and aid dissociation. The results of quantum mechanical simulations of H_2 dissociation on various surfaces, led the authors Darling and Holloway to conclude that hydrogen dissociative adsorption on Cu and Fe can only be reconciled with a late barrier, while on Ni and Pd it appears to be an early barrier [5]. Experimentally Hayden and Lamont also concluded in the existence of a late barrier for H_2 dissociation on Cu(110) [6]. The influence of the vibrational energy also leads to isotopic effects due to the difference in the vibrational energy level spacing in H_2 and D_2. The influence of the rotational energy has also been observed for H_2 on Cu(111), by permeation-desorption experiments [7].

Hence even the two-dimensional ***PES*** model can be inadequate to describe molecule-surface interactions because they depend on many parameters.

There are two types of adsorption in heterogeneous catalysis: physisorption and chemisorption which differ especially by the strength of the adsorbate-surface bond much more intense for a chemisorbed species. As a direct result the desorption temperatures of a chemisorbed species are much higher than those of physisorbed species. Incidentally, physisorption has very little catalytic importance while chemisorption is generally required for catalytic activity at a surface.

I.3 PHYSISORPTION

Physisorption is characterised by Van der Waals forces: the London dispersion (or dispersion forces) and dipole-dipole interactions [8].

If two molecules have a permanent dipole moment respectively μ_1 and μ_2, then the energy of the dipole-dipole interaction between them in the gas phase is:

$$E_{dd} = -\frac{2}{3kT(4\pi\varepsilon_0)^2} \times \frac{(\mu_1\mu_2)^2}{r^6} \qquad (1)$$

Where r is the bond length, and T the temperature of the gas.

The molecule ***1*** of dipole μ_1, approaching a second molecule ***2*** is responsible for the presence of an electric field which polarises the charges on molecule ***2***. This may induce a dipole moment of magnitude $\alpha_2\mu_1$, where α_2 is called the polarisability of molecule ***2***. Hence the dipole-induced dipole attractive energy is given by:

$$E_{ind} = -\frac{\mu_1^2\alpha_2 + \mu_2^2\alpha_1}{(4\pi\varepsilon_0)^2 r^6} \qquad (2)$$

The third term is the London forces arise from the interaction between the instantaneous fluctuations in the electron distribution in molecule ***1*** with that of molecule ***2*** (even though these molecules do not have any permanent dipoles).

$$E_L = -\frac{3}{2}\left(\frac{E_1E_2}{E_1 + E_2}\right)\frac{\alpha_1\alpha_2}{(4\pi\varepsilon_0)^2 r^6} \qquad (1)$$

Where E_1 and E_2 are approximately equal to the energies of the first electronic transitions of these molecules.

As the molecules approach more closely, the Pauli repulsion rises and the resulting equation for the intermolecular potential energy, E_{LJ} (often referred to as the Lennard-Jones potential) is expressed by:

$$E_{LJ} = 4\varepsilon\left[\left(\frac{\sigma}{r}\right)^{12} - \left(\frac{\sigma}{r}\right)^{6}\right] \qquad (3)$$

Where ε is the well-depth at the equilibrium separation and σ is the bond length at zero ***PE*** (see **figure I.1**).

When a molecule approaches a surface, the interaction results in a (9-3) potential energy, which is similar in shape to the (12-6) potential.

Physisorption is not surface specific, there is no real bond between the molecule and any particular surface atom, the molecule occupies an area of the surface depending on its size.

To be trapped, a molecule must lose sufficient of its normal kinetic energy by either transfer to the surface or to another degree of freedom. The energy of adsorption is between 0.052 and 0.52 eV.

Note that physisorption is never activated.

I.4 CHEMISORPTION

Chemisorption leads to a strong bonding where molecular orbitals between the surface atom and the adsorbate are formed, and charge transfers take place; thus there is formation of ionic or covalent bonds. Chemisorption is surface specific, varying from metal to metal and from plane to plane. The energy of adsorption varies between 0.52 and 5.2 eV.

Dissociative chemisorption "underpins" most surface reactions and is one of the simplest examples of surface chemistry, involving the breaking of molecular bonds in favour of new bonds to a surface. Since dissociated species can react to form new compounds, it is not surprising that this process is a key step in many complex reaction mechanisms, including most examples of heterogeneous catalysis [9]. Thus, there is a constant interest in understanding dissociative chemisorption, such as the dissociative chemisorption of methane on platinum. There are two general mechanisms of this process, giving rise to direct and indirect channels. The direct dissociation channel where the molecule dissociates on first impact with the surface, is the most accessible dynamically. The indirect channel where the potential energy surface presents a too high barrier for direct dissociation to take place, leads to trapping of the incident molecule in a molecular precursor state. Dissociation takes place subsequently after a single or many vibrational periods [10] through partition between desorption and dissociation [11]. Note that these two channels can coexist as we will see for H_2 dissociation on Pt(533) (**chapter V**).

I.4.1 Direct Dissociation

Direct dissociation requires (a) clean surface site(s) to be successful, and this results in a coverage dependence of the sticking probability. In 1918, Langmuir [12] proposed a model for this coverage dependence that assumes each dissociating molecule AB requires

two vacant sites to adsorb both A and B parts. Since the chance of one site being vacant on the surface for A to adsorb is $(1-\theta)$ where θ is the proportion of saturation coverage, the chance of two spaces for A and B to be vacant is $(1-\theta)^2$, then the probability of finding two sites, S, results in the coverage dependence:

$$S = a(1-\theta)^2 \qquad (4)$$

Desorption into the AB form will only occur when adsorbed A and B parts are in adjacent sites.

Many systems deviate from this predicted behaviour due to the possibility of lateral interactions between adsorbates or adsorbate induced surface reconstructions which the Langmurian model ignores. In the case of hydrogen dissociation on W(100), S follows a $(1-\theta)$ dependence, which was interpreted as the dissociative step occurring on only one vacant site followed by the subsequent migration of one of the hydrogen atoms to another site [13].

There are two mechanisms of direct dissociation: activated and non-activated. The activated mechanism is characterised by the energy barrier in the reaction coordinate being above the zero-point energy level. The non-activated one is characterised by the barrier being below the zero-point energy level (**figure I.3**). If the incident kinetic energy of the molecule is lower than the barrier, the molecule just reflects from the surface, but if it is higher then dissociation happens immediately. Non-activated process typically demonstrate high dissociation probability extending to zero incident energy.

An increase in the dissociation probability with the incident beam energy E_i, for both mechanisms, is often seen as this allows access to non-optimised trajectories, there being a range of saddle points (some activated) for different orientations and impact sites.

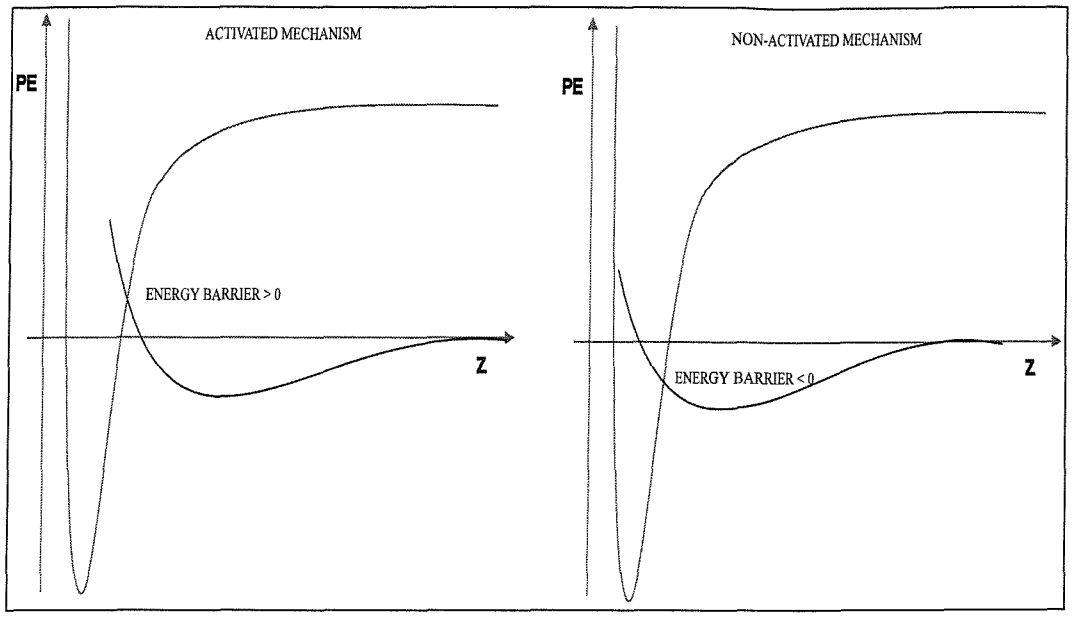

Figure I.3: Comparison between the two types of direct dissociation.

To overcome the barrier to dissociation in the activated mechanism, the energy can be supplied by the translational energy or energy partitioned in the internal degrees of freedom of the molecule (vibration, rotation) by change of seeding and of the gas molecules temperature. As seen earlier, the most effective parameter to dissociation depending on the barrier (*i.e.* late or early) will be varied. Hence, the increase of the sticking probability with the incident kinetic energy of the molecule is a characteristic of direct dissociation. Moreover there is no dependence on the surface temperature, because the time of residence on the surface before dissociation is much too short to allow thermal equilibrium, unless dissociation occurs via tunnelling through an entrance channel activation barrier. For example in the dissociation of CH_4 on Pt(111) and Pt(533) (**chapter IV**), the initial dissociative sticking probability rises almost exponentially with T_s at low incident energies, changing to a linear variation at high energies [14]. In this latter case a marked isotope effect must occur.

I.4.2 Indirect Dissociation

The molecule cannot dissociate straight away, thus it is trapped on the surface into a precursor state as physisorbed (and highly mobile) or chemisorbed (less mobile) molecular species (**figure I.4**), until finding a favourable site of dissociation, where the energy barrier

in the reaction coordinate is sufficiently low. An example of precursor chemisorbed species is N_2 on Fe(111) [15].

Unlike direct dissociation, this type of dissociation is characterised by a strong decrease of the sticking probability with increasing surface temperature and translational energy. The rate of trapping into a shallow precursor well depends in the ability to dissipate energy during collision with the surface, which can be done by the excitation of surface phonons or by the non-adiabatic excitation of electron-hole pairs. If the energy of the incident molecule cannot be transferred to the surface the molecule cannot trap, hence the molecule will simply scatter back into the gas phase from the repulsive wall of the potential. The existence of the precursor has been experimentally confirmed by the observation of sticking probability profiles for a number of systems in which ***S*** is initially independent of the coverage [16], as we will see for H_2 on Pt(533) at low incident energies (**chapter V**).

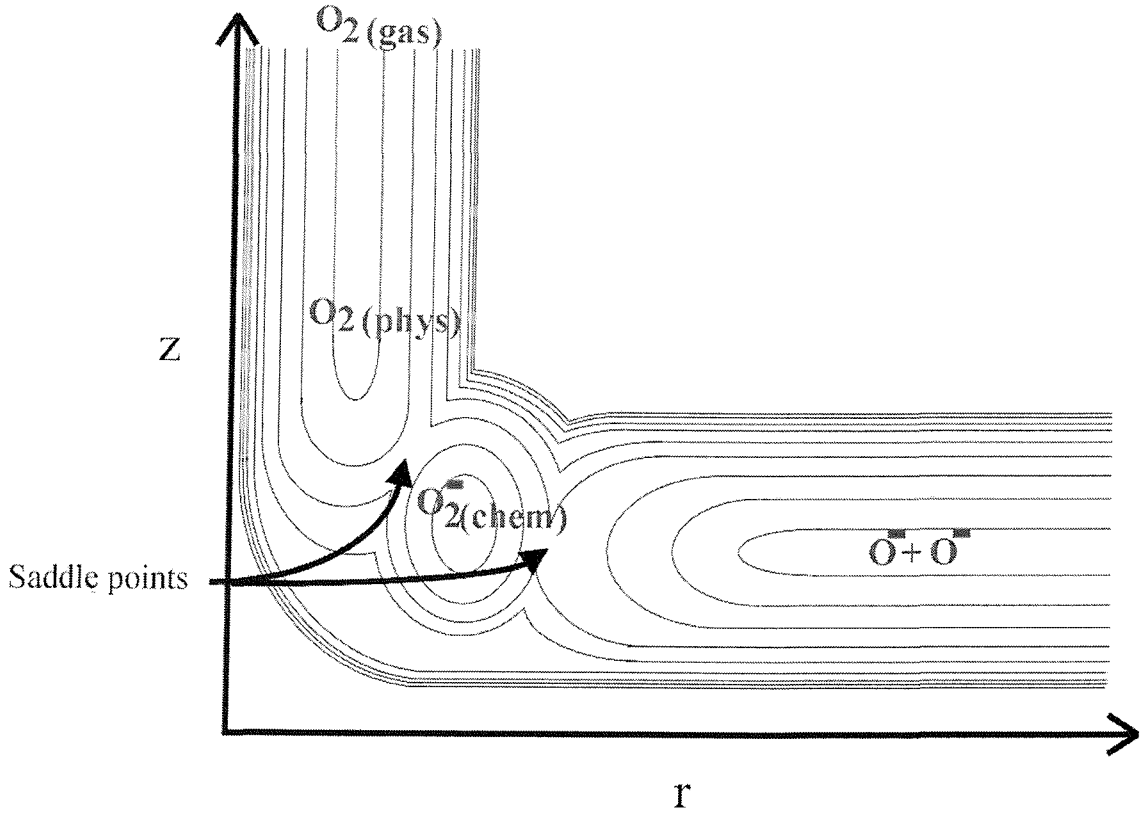

Figure I.4: Two dimensional potential for adsorption on a surface through a precursor state.

Notice that there are two types of precursor state, the intrinsic state where the incident molecule collides with the surface over an empty site and an extrinsic precursor

state where the molecule collides over a filled site. In this last case, the molecule is trapped on the surface until finding a "hole" to dissociate. This hole could be a low energy pathway to dissociation may be due to geometrical or oriental effects. The intrinsic state is characterised by the initial sticking probability S_0 decreasing with increasing the surface temperature, T_s, while the extrinsic one shows no T_s dependence and a coverage independence.

I.5 AIMS

Since steps and defects can have such a distinct effect on processes at the surface, one of our aims is to study the dynamical interaction of several types of molecules, such as CH_4, NH_3 and H_2 with a Pt(533) crystal surface. An attempt to quantify the influence of the step edge on dissociative mechanism will be performed by comparing the present results with the results on Pt(111) from the literature.

The dynamical interactions of CH_4 molecules with a stepped platinum (533) surface has been investigated in order to show the influence of the surface temperature, angle of incidence and incident kinetic energy on the dissociation of CH_4.

In both H_2 and NH_3 studies, oxygen and carbon monoxide have been chosen to decorate the (100) steps prior to hydrogen or ammonia adsorption in order to block adsorption on the steps. However the data obtained in **chapters V** and **VI** show that the effect of both preadsorbates is more complex than expected. Temperature programmed desorption measurements as well as sticking probability data are presented, which highlight the processes of adsorption and decomposition as well as their dynamics and kinetics.

In **chapter VII** an attempt to clarify the mechanism taking place in the hydrogen-uranium reaction, as well as the influence of an oxide layer on the hydrogen adsorption is undertaken. Measurements of the initial dissociative sticking coefficient, S_0, of hydrogen on polycrystalline uranium are also performed.

I.6 REFERENCES

[1] Somorjai G. A., *"Introduction to surface chemistry and catalysis"*. Wiley-Interscience Publication (New York), chap.1, p. 13, **1994.**

[2] Lennard-Jones J. E., *Trans. Faraday Soc.*, 28: 333, **1932.**

[3] Halstead D. and Holloway S., *J. Chem. Phys.*, 93: 2859, **1990.**

[4] Darling G. R. and Holloway S., *Surf. Sci.*, 304: L461, **1994.**

[5] Darling G. R. and Holloway S., *J. Chem. Phys.*, 97: 5182, **1992.**

[6] Hayden B. E. and Lamont C. L. A., *Faraday Disc.*, 91: 415, **1991.**

[7] Michelsen H. A., Rettner C. T. and Auerbach D. J., *Phys. Rev. Lett.*, 69: 2678, **1992.**

[8] Alberty R.A. and Silbey R.J., *"Physical Chemistry"*, John Wiley & Sons, Inc. (New York), chap. 12, p.415, **1992.**

[9] Xi G., Wang J., Li S. and Shao S., *J.Vac.Sci.Tech.A*, 9: 1688, **1991.**

[10] Gasser R. P. H., *"An Introduction to Chemisorption and Catalysis by Metals"*, Oxford University Press, chap. 3, p.40, **1985.**

[11] Butler D.A. and Hayden B. E., *Surf. Sci.*, 337: 67, **1995.**

[12] Langmuir I., *J. Am. Chem. Soc.*, 40: 1361, **1918.**

[13] Alnot P., Cassuto A. and King D. A., *Surf. Sci.*, 215: 29, **1989.**

[14] Luntz A. C. and Bethune D. S., *J. Chem. Phys.*, 90: 1274, **1989.**

[15] Ertl G., Lee S. B. and Weiss M., *Surf. Sci.*, 114: 515, **1982.**

[16] King D. A. and Wells M. G., *Surf. Sci.*, 29: 454, **1972.**

CHAPTER II: INSTRUMENTATION

II.1 INTRODUCTION

All experiments were performed under Ultra-High Vacuum (UHV) conditions. The UHV reaction chamber (**figure II.1**) has a typical base pressure below 1×10^{-10} mbar and is equipped with facilities for ion bombardment, X-Ray Photoelectron Spectroscopy (XPS from VG), Low Energy Electron Diffraction (LEED screen from Omicron) and a rotatable Quadrupole Mass Spectrometer (QMS from VSW). The rig includes three connected vacuum chambers, each of which has its own discrete pumping system, and is pumped by two turbo pumps and three diffusion pumps, backed by three rotary pumps. The sample is mounted on a xyzθ rotatable manipulator (which can be cooled using liquid nitrogen) situated at the top of the chamber. The main chamber is interfaced to a two-stage molecular beam line.

The beam gas mixtures are controlled by a mica beam flag inside the main chamber. This flag and an additional fixed QMS for background gas analysis (from Vacuum Generators QXK300) allow for the measurement of sticking coefficients by the King & Wells technique (see **chapter III**).

The main difference from previous experiments performed on this system [1] is that the gas inlet to the first stage is attached to a gas mixing board equipped with mass flow/pressure meters and controllers.

II.2 FIRST CHAMBER: THE NOZZLE SKIMMER CHAMBER

Gas mixtures are expanded through a 30 μm quartz nozzle (**figure II.1**), into the main chamber. The supersonic beam used in our experiments was generated in the nozzle/skimmer chamber by a pressure behind the nozzle P_n (between 0.1 and 2.5 bar), measured by a barometer.

This nozzle is resistively heated by a tungsten filament coiled around it, separated by a thin layer of carbon film used to protect the quartz tube. The temperature is monitored by a K-type thermocouple (Ni/Cr-Ni/Al) which is located just at the exit of the nozzle, allowing

for accurate temperature measurement of the gas mixtures. A dust filter is positioned just before the nozzle to prevent blockages (tube with a grid inside).

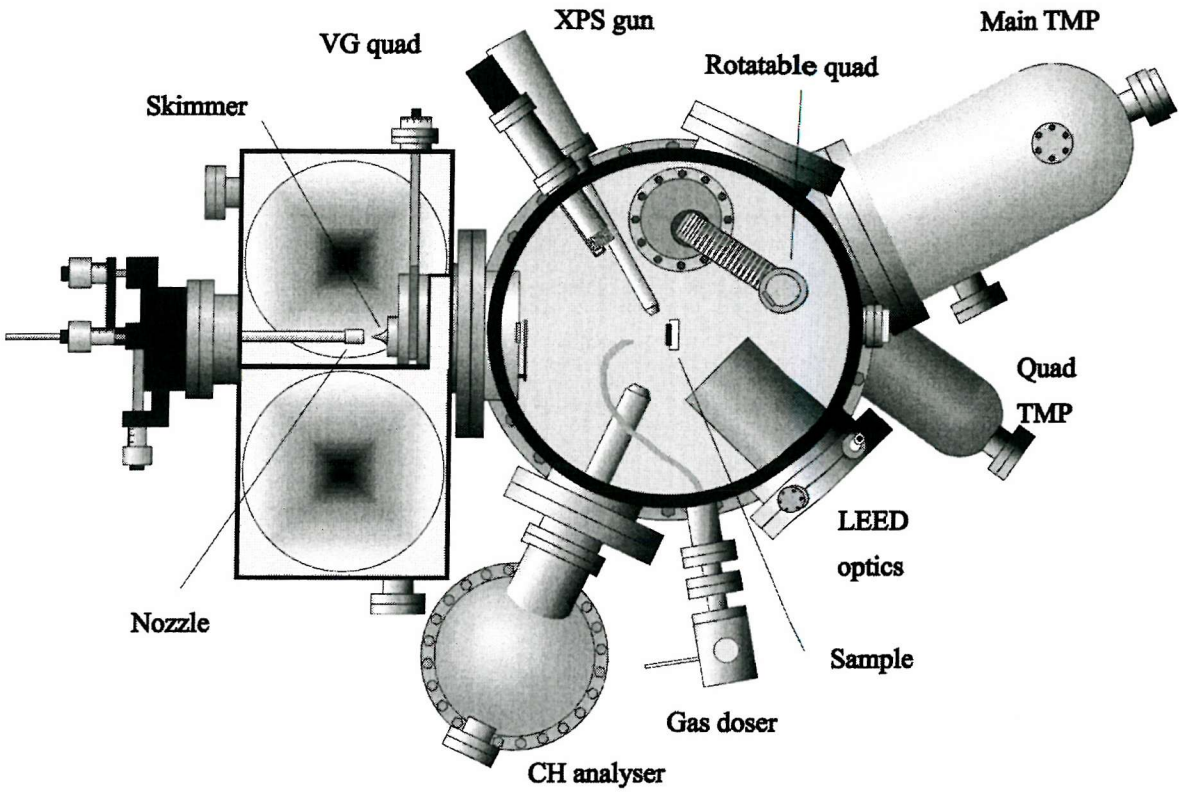

Figure II.1: Top view of the UHV Supersonic Molecular Beam System.

The orientation and position of the nozzle can be adjusted by x and y tilt (± 4 mm corresponding to ± 2.5°) motions and x, y (± 12.5 mm), z (25 mm) displacements to allow alignment of the beam with the skimmer and the aperture [2]. The skimmer is a thin stainless steel cone with a 300 μm orifice, designed to extract the centre line beam while deflecting the majority of gas away from the beam axis. The position of the skimmer can be adjusted in the x and y directions. This chamber is pumped by a 6" oil diffusion pump Edwards EO6 (pumping speed 1000 l s^{-1}) with a water cooling system, which is backed by an Edwards E2M18 two-stage rotary pump (pumping speed 5 l s^{-1}). The backing system was modified after one year to allow a more efficient pumping, thus the E2M18 rotary pump was replaced by a E2M40. The base pressure of this chamber, measured by a penning gauge, is below 1×10^{-7} mbar with an increase in pressure to 1×10^{-4} mbar upon opening to the beam.

II.3 SECOND CHAMBER: THE CHOPPER CHAMBER

This chamber (**figure II.1**) is also pumped by an Edwards EO6 diffusion pump with a water cooling system and backed by an Edwards E2M12 two-stage rotary pump (pumping speed 3.3 l s^{-1}). The base pressure of this chamber is 1×10^{-8} mbar with an increase in pressure to 5×10^{-7} mbar on opening to the beam. The methane and hydrogen sticking measurements never required the chopper, thus the nozzle-aperture-flag system (see **chapter III**) was found to be appropriate for the measurements by the King & Wells method. However, the rotating disk chopper is necessary to modulate the beam, thus it is essential for time-of-flight measurements (not performed here).

The chopper chamber is mounted adjacent to the nozzle chamber with only a small overlap in the direction of the beam to minimise the distance from the skimmer to the sample surface. Thus, the distance from the skimmer to the exit of this second stage is *ca.* 15.2 cm and to the sample *ca.* 31.4 cm [2].

II.4 THE MAIN CHAMBER

The main chamber contains facilities for several UHV techniques, in particular a differentially pumped pulse counting mass spectrometer which can be rotated in both vertical and horizontal planes for measurement of scattered flux. However, only the ion gun (sputtering) and the fixed quadrupole mass spectrometer (background gas analysis) were utilised in these experiments. The main chamber is pumped by a turbo-molecular pump Leybold with water cooling system (pumping speed 1000 l s^{-1}) backed by an Edwards EO4 diffusion pump with a water cooling system and backed by an Edwards E2M18 two-stage rotary pump (pumping speed 5 l s^{-1}). Another turbo-molecular pump Leybold with water cooling system (pumping speed 151 l s^{-1}) differentially pumps the rotational QMS also backed by the diffusion and the rotary pumps. The turbo-pumps are required to achieve base pressures of typically under 1×10^{-10} mbar rapidly. With a full molecular beam the pressure can rise from 5×10^{-10} to 1×10^{-7} mbar, depending on the size of the aperture and the flow selected.

II.4.1 The Variable Aperture

The variable aperture is a stainless steel plate containing several holes which can be moved across the beam prior to its entrance into the main chamber. The size of the apertures varies from 0, 0.5, 1.3, 3 to 4 mm. Thus, the beam diameter at the crystal surface can vary between 0 and 10 mm.

For our sticking probability experiments, an intermediate aperture of 1.3 mm was used, in order to have a sufficient quantity of gas for detection, but low enough so as not to increase the background pressure intensity too greatly. For TPD experiments both 1.3 and 3 mm apertures were used which did not seem to influence the results.

II.4.2 Sample Mounting and Cleaning

II.4.2.1 Platinum

The platinum single crystal used in this study is aligned and polished to within 0.5° of the (533) plane and is 10 mm in diameter (**figure II.2**). The crystal was cut and polished, by Metal Crystals & Oxides Ltd (Cambridge), then the step direction of the crystal was determined by Laue X-ray back-scattering. It is mounted by two 0.30 mm tungsten wires on two nickel bars, that are in turn connected to a copper support. These bars are electrically insulated from the oxygen-free copper support using mica wafers. A chromel-alumel thermocouple is spotwelded to the edge of the crystal for temperature measurements.

The copper support can be cooled using liquid nitrogen to a minimum sample temperature of 115 K. Thus the mica wafers must be sufficiently thin to retain thermal conductivity.

Note that firstly the W wires were spotwelded onto the sides of the crystal, but their lifetime was relatively short due to the weakness introduced on the weld point. Thus it was decided to spark-erode some grooves on the crystal sides so that the crystal could be "sandwiched" between two tensioned 0.25 mm W wires.

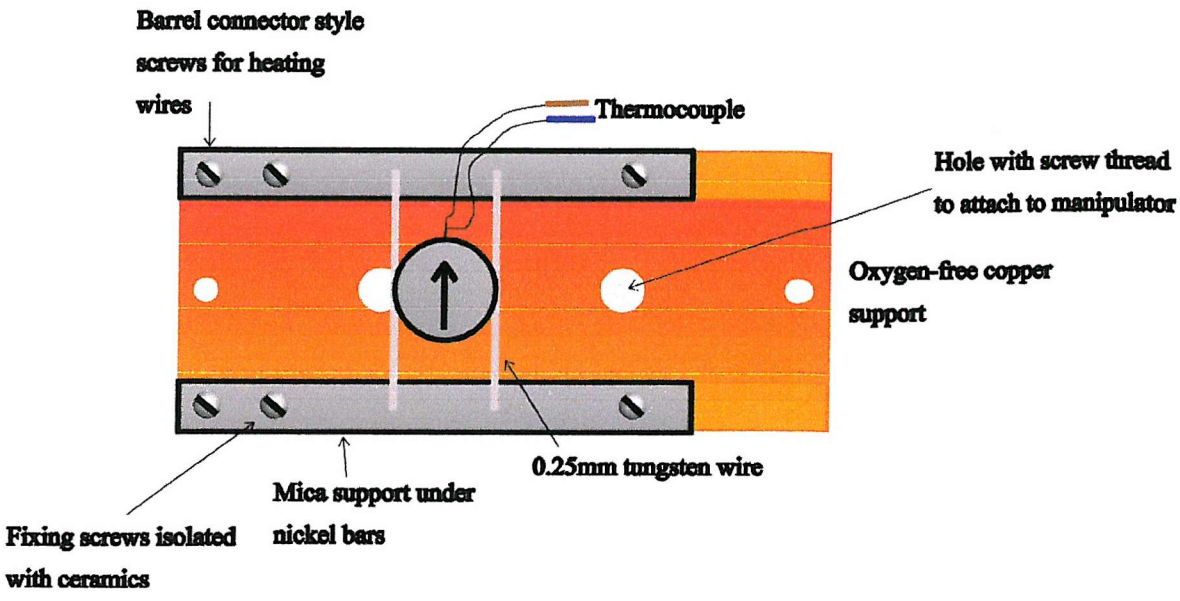

Figure II.2: Sample mount for the Pt(533) crystal.

After pumping down the system and performing baking, the ion gun is used to clean the sample, by sputtering the surface with argon ions. The noble gas is fed directly into the ionisation chamber, where a discharge is initiated by electrostatic fields. Positive ions are extracted via the accelerating voltage through a small aperture, and focussed crudely on their way to the sample.

The interaction of relatively heavy particles, possessing a kinetic energy of 0.5 to 3 keV and a solid surface, results in a complex sequence of events. After sputtering, the argon ion is stopped at a certain depth on the surface, as a result of losing energy via elastic scattering off atomic cores and inelastic scattering of electronic shells. Thus, the lattice atoms can move and some will be ejected from the surface.

The consequence of this phenomenon is the expulsion of metal and contaminant atoms. There are two types of contaminants for platinum: the bulk impurities which are the more difficult to control, such as calcium, sulphur, phosphorus and silicon. The second source of contaminants is due to the gas molecules present in the sample surrounding, such as oxygen, hydrogen, carbon and hydrocarbons, and is therefore highly dependent on the quality of the vacuum.

The sputtering of the Pt sample is performed for several hours at $T_s = 300$ K with 3 keV Ar ions, and then at $T_s = 973$ K with 1 keV Ar ions to allow a better diffusion of the

bulk contaminants to the surface. After each treatment the sample is annealed at 1200 K to facilitate the repair of the surface structure.

Subsequent cleaning is achieved by dosing some oxygen onto the surface, with $T_s = 620$ K and a pressure between 1×10^{-9} mbar and 1×10^{-8} mbar (depending on the surface cleanliness), followed by annealing at 1200 K for 10 minutes to remove surface carbon and obtain the dissolution of any silicon into the bulk.

The Kinetic Theory of Gases [3] leads us to conclude that the contamination of the surface by atoms and molecules from the gas phase is less than 3-4 % of a monoatomic layer if the sample is left, without any treatment, in a 10^{-10} mbar vacuum for 1 hour. Thus, after several hours, the contamination of the surface cannot be neglected so it is essential to clean the crystal before a series of experiments. Once more, oxygen is dosed at a pressure between 5×10^{-9} mbar and 1×10^{-8} Torr for 15 minutes at $T_s = 620$ K. The sample is then annealed at 1200 K for 20 minutes. This prevents the effects of silicon contamination and removes carbon by the formation of carbon monoxide and carbon dioxide which are then desorbed, leaving a clean platinum surface. It is also necessary to clean the sample between experiments. Here the sample is annealed between runs to 1200 K for 5 to 20 minutes.

Because the temperature programmed desorption (TPD) spectra are sensitive to the amount of disorder and the presence of contaminants on the surface, the cleanliness of the surface is first checked by comparing the TPD obtained for the adsorption of oxygen with that found in the literature (**figure II.3**) [4] as well as the one performed with the same Pt(533) sample in the same UHV system by Gee and Hayden [5].

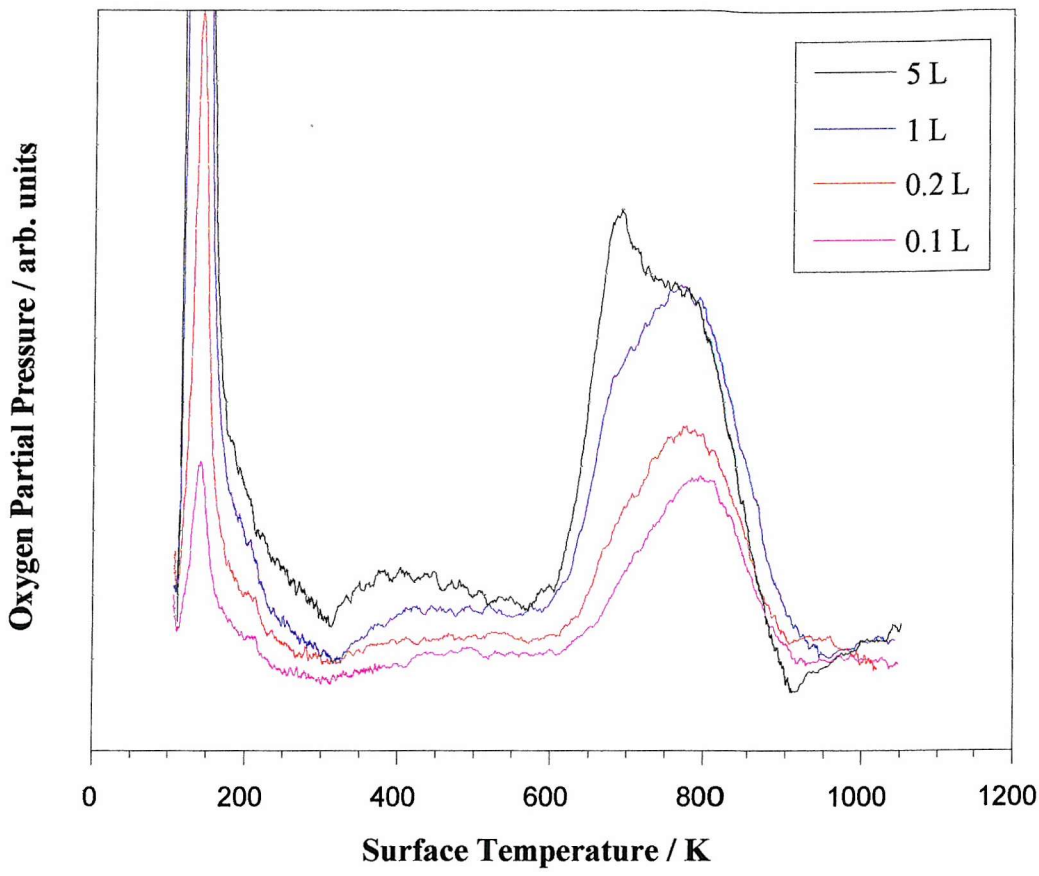

Figure II.3: Typical TPD of O_2 following exposure of Pt(533) to O_2. O_2 was dosed using a capillary source at T_s = 110 K, and the heating rate was 1-1.5 K s^{-1}.

Note that in the present case, a capillary source was used to dose the oxygen, thus the energy of the molecules is defined by a Maxwell-Boltzmann distribution, with the most probable speed (corresponding to the maximum in the distribution) V equal to:

$$V = \sqrt{\left(\frac{2RT}{M}\right)} = 399.5\ m\ s^{-1} \qquad (1)$$

The sticking probability, S, is also found to be very sensitive to the presence of contaminants, thus the cleanliness of the surface is also checked comparing the initial sticking probability of oxygen $S_0(O_2)$ at a surface temperature of 300 K and with a kinetic energy E_i = 0.52 eV, thus $S_0(O_2)$ = 0.39 (**figure II.4**) with that obtained earlier by Gee in similar conditions [5]. The technique of King and Wells [6] used for these measurements is described in detail in **chapter III**.

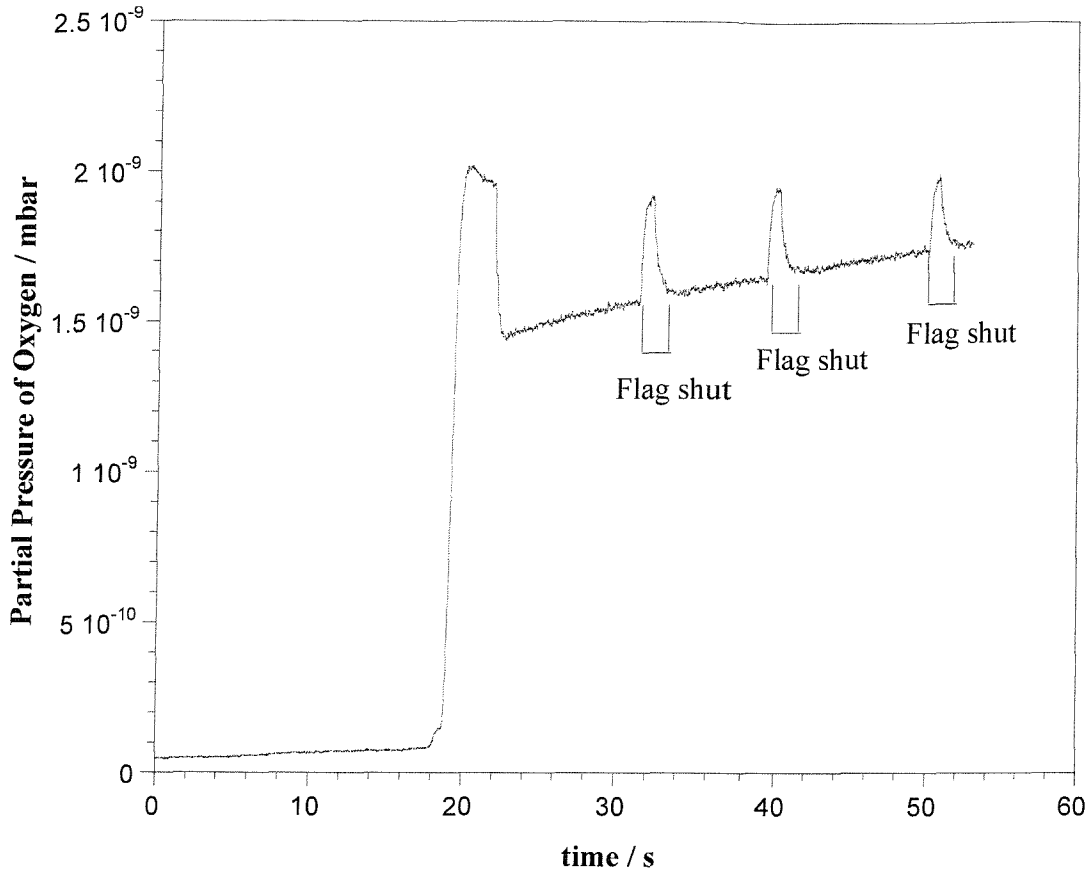

Figure II.4: Typical sticking probability measurement of oxygen on a Pt(533) surface. $E_i = 0.52$ eV, $T_s = 308$ K.

II.4.2.2 Uranium

The uranium polycrystalline sample used in this study has a 10×13 mm^2 surface area and it was spotwelded by two 0.25 mm tungsten wires and mounted on the same support than the platinum sample.

This sample was largely oxidised, thus an extreme cleaning was necessitated to obtain an oxygen free metal surface. For this purpose, the surface was cleaned by numerous 60 min argon-bombardment with 1 to 3 keV ions (angle $\Theta_I = 20°$ from normal incidence) at $T_s = 300$ K and at 675 K. Each sputter was followed by 30 min to 1 h annealing at 825 K. A 10 min annealing was also performed after each experiment, however after 5 to 7 experiments the surface was too contaminated to go further and sputtering was necessary.

Note that several obstacles had to be overcome prior to obtaining some data. Firstly mounting the sample (by spot-welding two tungsten-wires of 0.25 - 0.30 mm diameter) and the thermocouple (~0.25 mm diameter) proved to be difficult, due to the oxidation of the

sample. The second problem was due to the thickness and size of the samples (from 2 to 4 mm width) and to the rather low thermal conductivity of U (27 $W\,m^{-1}\,K^{-1}$ at 300 K) leading to effective resistive heating, therefore requiring a rather large current to be applied in order to heat the surface. Using quite extreme welding conditions eventually proved to be successful.

The cleanliness of the surface was checked by comparing some temperature programmed desorption of H_2 on U with the results obtained previously by Balooch and Hamza [7]. The sample cleanliness was also monitored by XPS.

Moreover the sticking probability being very sensitive to the presence of contaminants, the initial sticking probability of H_2 on U obtained on the present surface was compared to $S_0(H_2) = 0.04$ obtained by TPD measurements [7].

II.5 SUPERSONIC MOLECULAR BEAMS

In 1919, Gerlach and Stern [8] developed the first effusive molecular beam source, but this source had a large energy distribution, therefore a poor signal to noise ratio. Thus in 1951, Kantrowitz and Grey [9] suggested to replace it with a supersonic jet characterised by a much narrower energy distribution. This idea was put into practice by Kistiakowsky and Slichter [10], whom found the need to use a new type of pump, the diffusion pump, to keep a low background pressure so that molecular collisions have no consequences on the high beam collimation.

Figure II.5 shows the schematic diagram for the supersonic molecular beam source used in the present work. The beam is formed from the expansion of a high pressure of gas, P_n, behind the nozzle (which is considered constant) through a 30 μm hole into the first stage chamber (maintained at high vacuum by continuous pumping) of pressure P_b. P_b is much lower than P_n, therefore the gas can be approximated as an isentropic flow, with neglectible viscous and heat conduction effect. The gas starts from a neglectible small velocity, called the stagnation state. As the area of the nozzle decreases, the pressure difference (P_n-P_b) accelerates the gas towards the sample. The gas density decreasing along

the beam axis, until at some distance the flow changes from a continuum to a free molecular flow with virtually no molecular collisions.

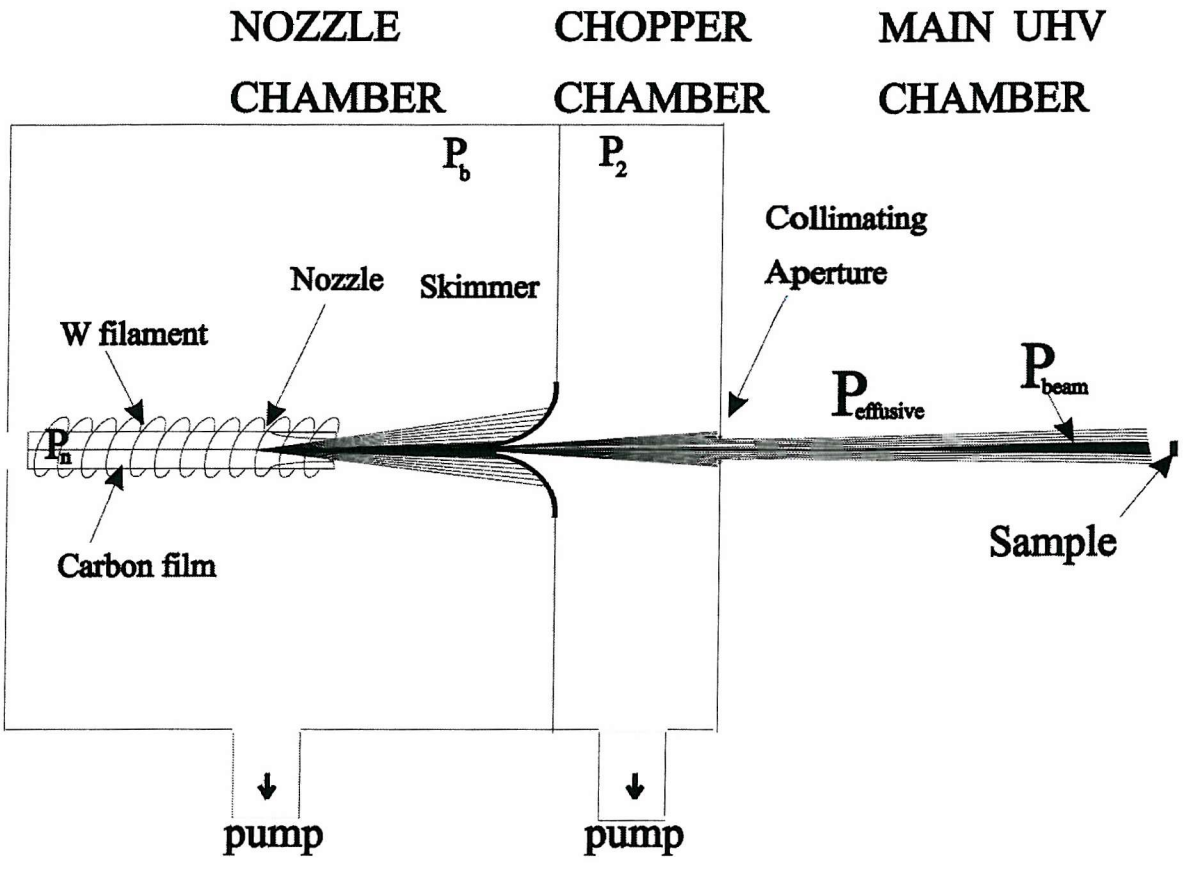

Figure II.5: Schematic diagram of a supersonic molecular beam source.

As we will see later, the most probable speed of the gas molecules can be calculated and the distribution of speeds, $P(V_i)$, is found to be approximately Maxwellian.

$$P(V_i) = 4\pi V_i^2 \left(\frac{m}{2k_B \pi T_n}\right)^{\frac{3}{2}} \exp\left(-\frac{mV_i^2}{2k_B T_n}\right) \qquad (2)$$

With Vi and m respectively the speed and the mass of molecule i, and k_B the Boltzmann's constant.

However as the expansion occurs, the temperature of the gas, T_n, drops drastically, therefore the distribution becomes very narrow.

The ratio of the molecules speed to the speed of the sound is defined by the Mach number.

$$M = \frac{ObjectSpeed}{SoundSpeed} \qquad (3)$$

Hence **figure II.6** shows the effect of T_n on $P(V_i)$ and M.

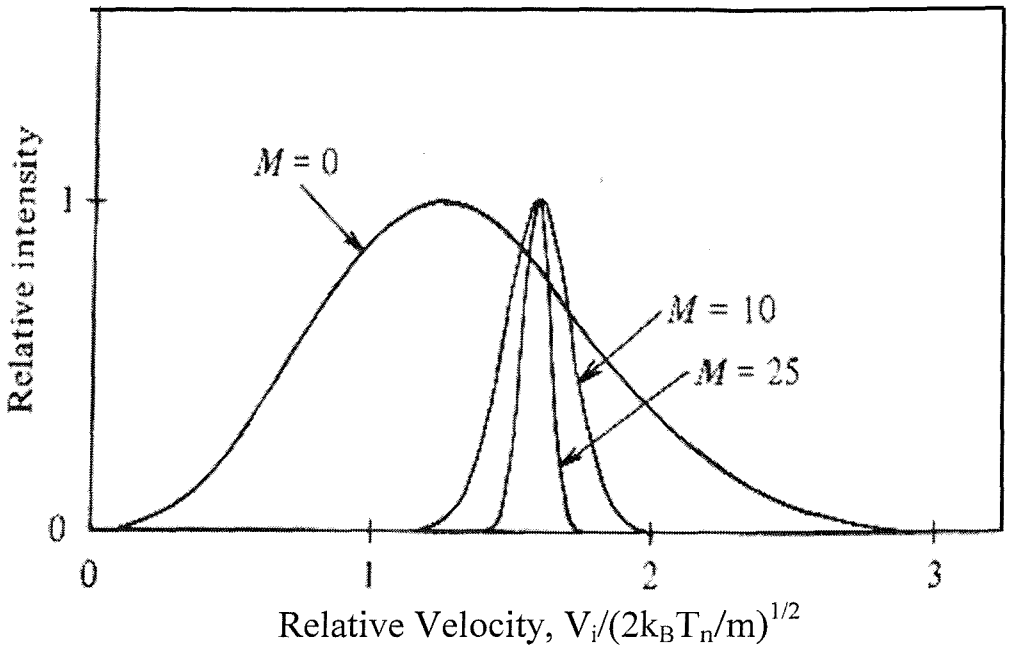

Figure II.6: Normalised supersonic nozzle (M=10 and M=25) and effusive beam (M=0) velocity distributions.

As seen in the supersonic beam expansion (**figure II.7**), in the zone of silence, the molecules of the incident beam are characterised by supersonic speeds (M>>1). The core of the expansion is isentropic, thus the molecular flow is independent of the boundary conditions. However as M continues to increase, overexpansion occurs at the boundary with the background pressure and the beam becomes compressed by a series of shock waves. Shock waves are very thin nonisentropic regions of large density, pressure, temperature and velocity gradients; they provide a mechanism to change the direction of a supersonic flow and to reduce the Mach number to subsonic values if a change in direction is not sufficient to meet a boundary condition. Hence rapidly the molecules slow down and reach the speed of sound on the mach disk (M=1), then they become even slower (M<1). The position of the mach disk (relative to the nozzle exit), x_m, is determined by a function containing the ratio

of the pressures, P_n (nozzle pressure) and P_b (the background pressure), and the nozzle diameter d.

$$x_m = 0.67\left(\frac{P_n}{P_b}\right)^{\frac{1}{2}} d \qquad (4)$$

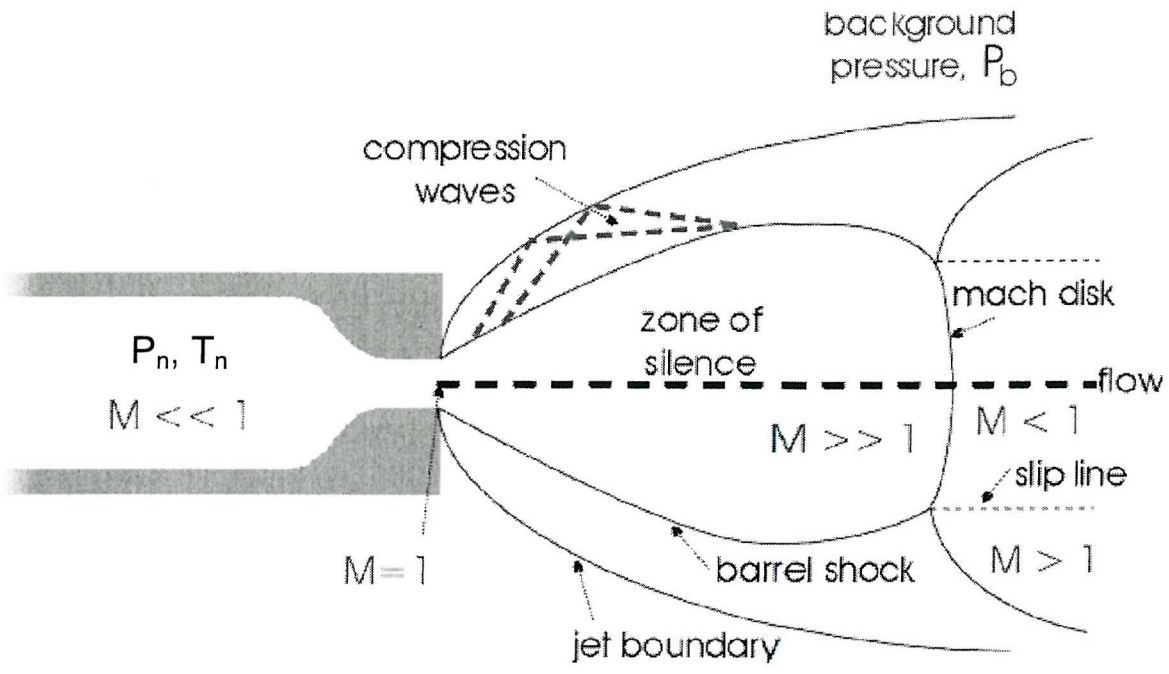

Figure II.7: Supersonic beam expansion [11].

Therefore in order to maintain the supersonic beam over large distances (so that it can hit the sample surface located in the main chamber without passin through the Mach disc shock), a skimmer is placed in the zone of silence (at ~ 100d from the nozzle). Hence it extracts the centre line beam while deflecting the majority of gas away from the beam axis causing P_b to increase very fast (up to a maximum of 1×10^{-5} mbar for this system). The skimmer is also designed to avoid the creation of shock waves in front of or inside itself.

The shape of the nozzle must also be considered. In fact depending on the size of the nozzle walls the divergence of the free jet expansion varies. This phenomenon is also minimised by keeping P_n high.

The selected beam flow enters the second stage chamber but only the centre line beam passes through the aperture into the main chamber, there is a large number of incident molecules which are deflected back into the second chamber. If the pressure in this second chamber, P_2, is too high there will be some molecular collisions close to the aperture, which

will perturb the beam. In the present experiments P_2 increased to a maximum of 5×10^{-7} mbar. The beam entering the main chamber is formed of two components, $P_{effusive}$ which takes in account the diffusion of the molecules and P_{beam} which takes in account the number of molecules which will directly collide with the sample surface (see **figure II.5**).

As the expansion occurs and the temperature of the gas drops, vibrational and rotational relaxation can occur. The extent of relaxation depends on the number of collisions experienced by each molecule and the energy difference between the vibrational and rotational states. Typically a molecule can experience 100-1000 collisions during the expansion which is believed to be sufficient to cool its vibrational and rotational states. The vibrational relaxation of a small diatomic like hydrogen requires 10^4 collisions due to the larger energy level spacing and so the amount of vibrational cooling will be small. Large polyatomics generally have much shorter relaxation periods of only 10-100 collisions and so for these molecules vibrational cooling will be almost complete. Rotational relaxation is usually much faster due to the smaller energy level spacing. This can be approximated to by the linear relaxation model which states that the rate of cooling from T_r to temperature T can be predicted by the equation:

$$\frac{dT_r}{dt} = \frac{(T - T_r)}{\tau} \qquad (5)$$

Where τ is the relaxation time defined as $\tau = \frac{Z}{\nu}$ the ratio of the required number of collisions Z to the collision frequency ν. $\nu = \sigma \times \mathbf{n} \times \mathbf{v}$ with σ the "effective" molecular cross section, $\mathbf{n}$ the number of molecules and $\mathbf{v}$ the uniform velocity of the molecules. For molecules where the required number of collisions is large, such as 300 for hydrogen, the specific heat ratio is $\gamma \sim 5/3$, while for small numbers of required collisions, such as 3 in the case of nitrogen, $\gamma \sim 7/5$.

The terminal velocity of the gas molecules colliding with the sample surface in the main chamber can be obtained by the following reasoning:

As well as conservation of mass and of momentum, the first law of thermodynamics predicts the conservation of energy. The energy can be transformed, *e.g.* from potential to kinetic energy, but there is no loss or gain.

$$dE_0 = dE_1 \qquad (6)$$

$\boldsymbol{dE_0}$ and $\boldsymbol{dE_1}$ being the energies of the system respectively at state 0 and state 1.

Moreover it relates the change in internal energy $\boldsymbol{dU}$ to the heat absorbed by a system $\boldsymbol{\delta Q}$ and the work done on the system $\boldsymbol{\delta W}$:

$$dU = \delta Q + \delta W \qquad (7)$$

While $\boldsymbol{\delta Q}$ and $\boldsymbol{\delta W}$ depend on the initial and final states and the process which produces the final state, $\boldsymbol{dU}$ only depends on the initial and final states but not the process.

For the control volume, ***cv***, the rate of change of energy $\frac{dU_{cv}}{dt}$ is equal to the rate of heat added to ***cv***, $\frac{\delta Q}{dt}$, the rate of work done, $\frac{\delta W}{dt}$, and the rate of energy flow into $m_0 E_0$ and out ***cv***, $-m_1 E_1$.

$$\frac{dU_{cv}}{dt} = \frac{\delta Q}{dt} + \frac{\delta W}{dt} + m_0 E_0 - m_1 E_1 \qquad (8)$$

With

$$Q = \lim_{dt \to 0} \frac{\delta Q}{dt} \qquad (9)$$

and

$$W = \lim_{dt \to 0} \frac{\delta W}{dt} \qquad (10)$$

For a steady state there is conservation of energy and mass, hence $\frac{dU_{cv}}{dt} = 0$ and $m_0 = m_1 = m$ is the mass of the gas molecules.

Hence: $$Q + W = m(E_1 - E_0) \qquad (11)$$

The energy E is the sum of kinetic, potential, internal and chemical energies, however potential and chemical energies are neglected.

Hence: $$Q+W = m(E_{kin1} + U_1 - E_{kin0} - U_0) \quad (12)$$

With $E_{kin1} = \frac{1}{2}mV_1^2$ and $E_{kin0} = \frac{1}{2}mV_0^2$ and the initial molecules speed $V_0 = 0$ at the nozzle exit while V_1 represents the speed of the gas molecules as the gas expands.

Moreover considering an adiabatic system, $Q = 0$ and $W = -(P_1V_1 - P_0V_0)$, hence:

$$-P_1V_1 + P_0V_0 = \frac{1}{2}mV_1^2 + U_1 - U_0 \quad (13)$$

It is convenient to introduce a new function, the enthalpy of a gas, $\boldsymbol{H}$, which is defined by:

$$H = U + PV \quad (14)$$

Since the enthalpy is defined in terms of other thermodynamic quantities, the only gain is in term of convenience.

Therefore:

$$H_1 - H_0 = -\frac{1}{2}mV_1^2 \quad (15)$$

Moreover:

$$dH = dU + d(PV) \quad (16)$$

$$dH = dQ + dW + PdV + VdP \quad (17)$$

$$dH = dQ - PdV + PdV + VdP \quad (18)$$

$$dH = dQ + VdP \quad (19)$$

Considering an isobaric system: $dP = 0$

Hence: $$dH = dQ \quad (20)$$

As the gas expands the number of collisions and the temperature of the gas quickly decrease. The change in enthalpy from $\boldsymbol{H_0}$ to $\boldsymbol{H_1}$ is related to the molar heat capacity $\hat{\boldsymbol{C}}_p$

$$\hat{C}_p = \frac{dQ}{dT}\Big)_P = \frac{\partial H}{\partial T}\Big)_P \quad (21)$$

Hence $$dH = H_1 - H_0 = \hat{C}_p\, dT \qquad (22)$$

With $dT = T_1\text{-}T_0$ the temperature difference after and before expansion.

We conclude in: $$-\frac{1}{2} m V_1^2 = \hat{C}_p\, dT \qquad (23)$$

Considering that substantial cooling occurs (which is the case for molecules coming out of the nozzle), then $T_0 >> T_1$, moreover considering $\hat{C}_p$ independent of the temperature, thus:

$$V_1 = \sqrt{\frac{2}{m} \hat{C}_p T_0} \qquad (24)$$

For an ideal gas:

$$\hat{C}_p = \left(\frac{\gamma}{\gamma - 1} \right) R \qquad (25)$$

With γ the ratio of heat capacities C_p/C_v.

Hence the terminal velocity of the expanding gas can be expressed as:

$$V_\infty = \sqrt{\left(2 \left(\frac{RT_0}{m} \right) \left(\frac{\gamma}{\gamma - 1} \right) \right)} \qquad (26)$$

Using a mixture of i ideal gases with mole fractions x_i, the terminal velocity of the beam becomes:

$$V_\infty = \sqrt{\left(2(RT_0) \frac{\sum \left(x_i \frac{\gamma_i}{\gamma_i - 1} \right)}{\sum x_i m_i} \right)} \qquad (27)$$

Experimentally the speed of the gas molecules was calculated differently (see in **part II.5.1**) for low seeding percentage of reactant gas in the seeded gas. However be aware that inaccuracies will arise due to the approximations performed when using the previous equations, notably on C_p, C_v, x_i and T_0 however there is good agreement between the two methods.

II.5.1 The Beam Line

Because of the use of several gases for each experiment (reactant gases and seed gases) a new beam line has been used for our experiments (**figure II.8**). This line is arranged so that up to 5 different gases can be available at any time. Each gas is leaked into the beam line through a flow-controller (**MFC**) which allows the gas to be regulated. Since the gas mixing board is equipped with only 3 flow-controllers, the mixture can only be a 3 gas-mixture. Typical gas loads of 25-70 ml min^{-1} were used for the expansion. The beam line is evacuated using a rotary pump (E2M5, pumping speed 1.39 l s^{-1}), thus it is possible to change the mixture wanted relatively quickly without having any risk of contamination by the precedent mixture. The MFC installed are originally calibrated with one specific gas and allow a maximal flow to pass through. Hence each MFC had to be re-calibrated depending on the gas used taking into account the specific heat and density at specific temperature and pressure.

As will be seen in **chapter III**, the reacting gas only goes up to 16 % of the seeding gas. Thus, the seeding gases like helium, hydrogen and argon necessitated a flow-controller at 200 ml min^{-1}. But the reacting gases such as methane, oxygen or hydrogen necessitated only a flow-controller with a maximum of 20 ml min^{-1}.

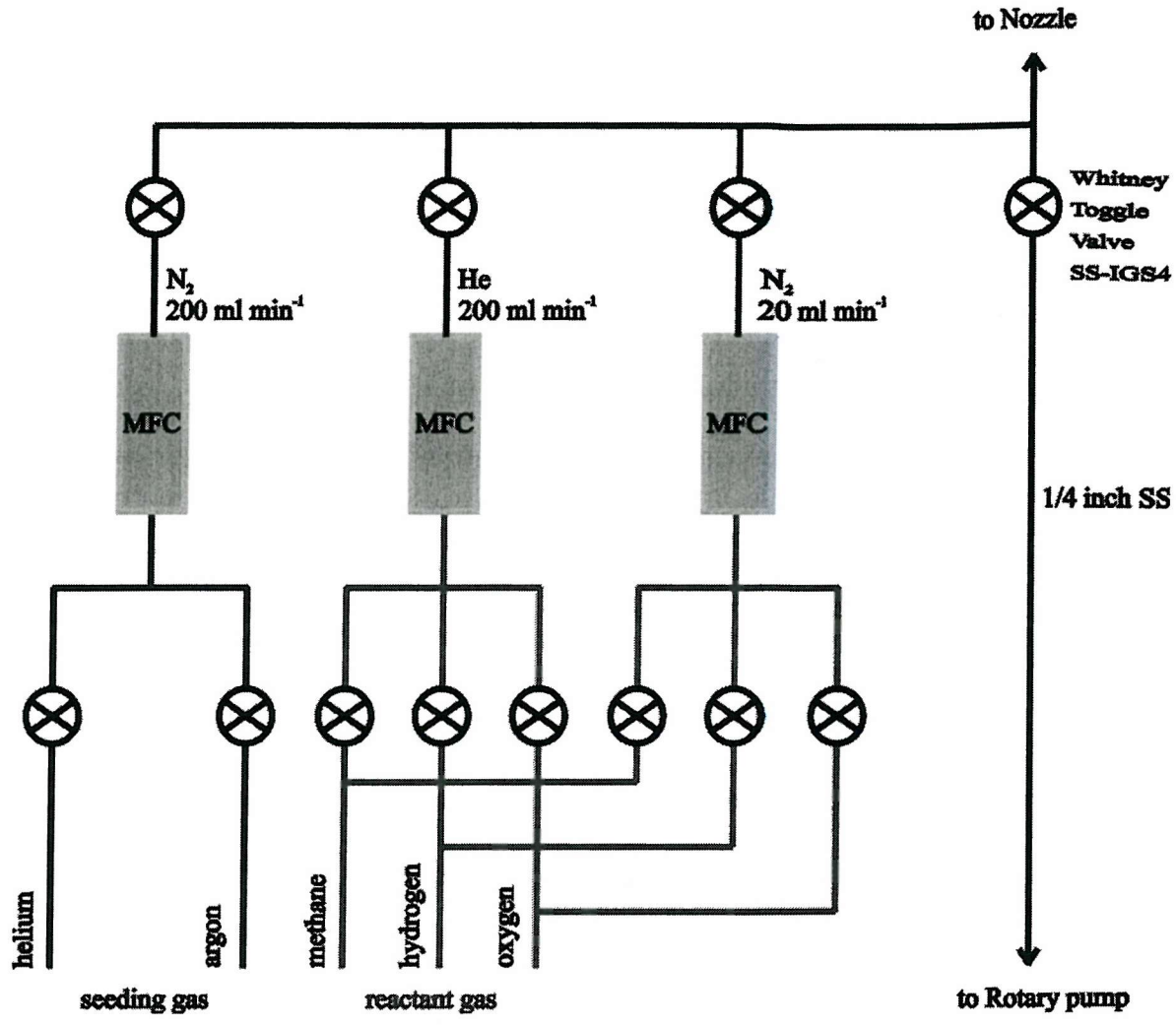

Figure II.8: Schematic of the beam line.

II.5.2 Kinetic Energy of the Particles in the Beam Line

Unfortunately, there were no facilities available at the time to employ a direct beam time-of-flight (TOF) method to determine the seeded beam kinetic energy E_i and velocity spread experimentally. However, the following E_i calculations led to some values in good agreement with previous results obtained by Gee *et al.* [5,12] on the same system when TOF measurements were performed.

It is not possible to consider the total energy of a particle constant because it is in a whole system of particles, where many collisions occur. But the kinetic (incident) energy of this particle can still be calculated. This is going to depend of the seed gas, the amount of the reactant gas in the seed gas and also the gas temperature, T_n. The continuum flow of gas mixture in nozzles permits the use of the "seeding" technique, in which a light gas

accelerates heavier gas molecules to high velocities, or vice versa. Thus, the kinetic energy of the seed gas particles in the beam-line is:

$$E_{i(seed)} = \left(\frac{1}{2}\right) \times m_{(seed)} V_{(seed)}^2 \qquad (28)$$

Where $\boldsymbol{m_{(seed)}}$ is the mass of a seed gas particle and $\boldsymbol{V_{(seed)}}$ its velocity.

Kinetic theory shows that the molar translational energy of a monoatomic ideal gas, such as He and Ar used as seed gas in the present experiments, is $\frac{1}{2}k_B T_n$ in one specific direction. Due to the 3 degrees of freedom in x, y, z directions the total $E_{trans} = \frac{3}{2}k_B T_n$, so that it is independent of the pressure or the molar mass of the gas molecules. A monoatomic gas has no vibrational or rotational degree of freedom, therefore the internal energy of this particle is:

$$U = E_{trans} + E_{vib} + E_{rot} = \frac{3}{2}k_B T_n \qquad (29)$$

The molar enthalpy of a monoatomic ideal gas, $\boldsymbol{H}$, is larger than the internal energy by PV, hence with the ideal gas law P6=k_BT,

$$H = \frac{3}{2}k_B T_n + kT_n \qquad (30)$$

$\boldsymbol{H}$ represents a reserve of energy for the gas molecule which is in the present case totally transferred to the kinetic energy of the gas, $\boldsymbol{E_{i(seed)}}$, therefore:

$$H = E_{i(seed)} \qquad (31)$$

And:

$$\frac{5}{2}k_B T_n = \frac{1}{2}mV_{(seed)}^2 \qquad (32)$$

Thus:

$$V_{(seed)}^2 = \frac{5k_B T_n}{m_{(seed)}} \qquad (33)$$

H_2 was also used for the seeding, but its kinetic energy is different. Below 80 K the rotational degrees of freedom are "frozen out" and the specific heat is like that of an ideal gas, hence only the 3 translational degrees are taken in account, hence $E_i = \frac{3}{2}k_B T_n + k_B T_n$. At $300 < T_n(K) < 500$, the rotational degrees of freedom are manifest, giving two more degrees of freedom, hence $E_i = \frac{5}{2}k_B T_n + k_B T_n$. Near the dissociation temperature of 3200 K there is evidence of two more degrees of freedom, implying that vibration is now affecting the specific heat, hence $E_i = \frac{7}{2}k_B T + k_B T$. Between 500 and 1000 K (as used here), the incident energy is approximated to:

$$Ei_{(seed)} = (3.6) \times k_B T_n \qquad (34)$$

The kinetic energy of the reactant gas particles in the beam-line is also:

$$E_{i(react)} = \frac{1}{2} \times m_{(react)} V^2_{(react)} \qquad (35)$$

Where $m_{(react)}$ is the mass of a reactant gas particle and $V_{(react)}$ its velocity.

If the percentage of reactant particles is less or equal to 1 %, the kinetic energy of these particles is assumed to be equal to the kinetic energy of the seeding gas, thus the mass ratio of the different gases is not taken into account.

If the percentage of reactant particles is greater than 1 % but less than 5 %, we can approximate the velocity of the reactant gas particles to the velocity of the seeded gas particles. Thus:

$$E_{i(react)} = \frac{1}{2} \times m_{(react)} V^2_{(seed)} \qquad (36)$$

Hence, in He, Ne and Ar with equation (33):

$$E_{i(react)} = \frac{5}{2} \times \frac{m_{(react)}}{m_{(seed)}} \times k_B T_{nozz} \qquad (37)$$

This formula gives a reasonable approximation of the incident energy for helium [1].

And in H_2 with equation (34):

$$E_{i(react)} = 3.6 \times \frac{m_{(react)}}{m_{(seed)}} \times k_B T_{nozz} \qquad (38)$$

II.6 REFERENCES

[1] Gee A., PhD. thesis, University of Southampton, **2000**.

[2] Jones J. D., PhD. thesis, University of Southampton, **1994**.

[3] Woodruff D. P. and Delchar T. A., "*Modern Techniques of Surface Science*", Cambridge University Press, chap. 1, **1994**.

[4] Rar A. and Matsushima T., *Surf. Sci.*, 318: 89, **1994**.

[5] Gee A. T. and Hayden B. E., *J. Chem. Phys.*, 113: 10333, **2000**.

[6] King D.A. and Wells M.G., *Surf. Sci.*, 29: 454, **1972**.

[7] Balooch M. and Hamza A. V., *J. Nuclear Mat.*, 230 : 259, **1996**.

[8] Gerlach W. and Stern O., *Z. Phys.*, 8: 110, **1921**.

[9] Kantrowitz A. and Grey J., *Rev. Sci. Instr.*, 22: 328, **1951**.

[10] Kistiakowsky G. B. and Slitcher W. P., *Rev. Sci. Instr.*, 22: 333, **1951**.

[11] Miller D. R., *Atom. Mol. Beam Meth.*, 1: 14, **1988**.

[12] Gee A. T., Hayden B. E., Mormiche C., Nunney T. S., *J. Chem. Phys.*, 93: 5240, **1990**.

CHAPTER III: EXPERIMENTAL METHODS

III.1 TEMPERATURE PROGRAMMED DESORPTION

TPD relies on using changes in the surface temperature to probe the strength of the adsorbate-surface bonds. It permits the determination of the nature, surface coverages and binding energies of adsorbed species. Because these energies may change from site to site on the surface, TPD may also be indicative of the surface structure. The surface residence time, τ, of the adsorbate species depends exponentially on the temperature T_s [1]:

$$\tau = \tau_0 \times \exp\left(\frac{-E_{des}}{RT_s}\right) \qquad (1)$$

With R the gas constant, E_{des} the activation energy of desorption and τ_0 which corresponds to the period of vibration of the bond between the adsorbed molecule and the substrate and is frequently taken to be about 10^{-13} s.

Thus, the adsorbate-covered surface is simply heated to rupture the adsorbate-surface bonds resulting in desorption. If the adsorbate is not resupplied from the gas phase, its surface concentration diminishes rapidly with increasing temperature until the surface becomes clean.

All the TPD experiments done in this study were characterised by continuous pumping to keep a large pumping speed compared to the desorption rate (~ 500 l s^{-1}). Thus, the chamber pressure is simply proportional to the desorption rate with the maximum pressure corresponding to the maximum rate of desorption (see **figure III.1(b)**). If the chamber is not continuously pumped, the pressure will rise up to a maximum illustrated in **figure III.1(a)**. In the case where the pumping speed is too small compared to the desorption rate the pressure profile will look like **figure III.1(c)**.

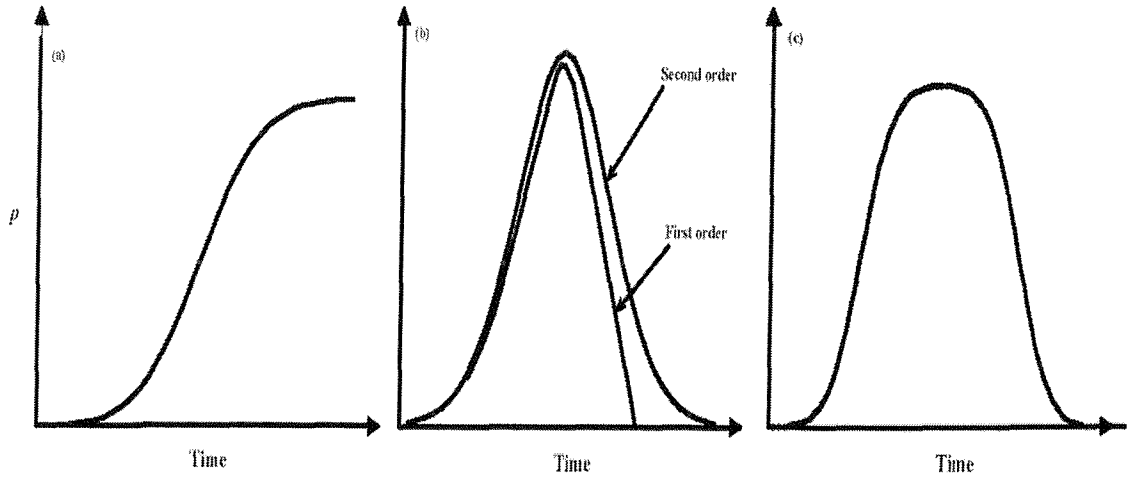

Figure III.1: Pressure versus time traces during a TPD measurement for (a) no pumping, (b) a fast pumping, and (c) a slow pumping.

In the present case, the TPD data are usually obtained by applying a linear temperature ramp up to 17 K s^{-1}, depending on the requirements of each specific experiment, thus:

$$T_s = T_{s0} + \left(\frac{dT_s}{dt}\right) \times t \qquad (2)$$

where T_{s0} is the initial surface temperature and $\frac{dT_s}{dt}$ is the heating rate. A non-linearity of the heating rate can lead to ambiguous interpretation of the data.

Expressing the desorption rate using an Arrhenius equation [2] gives:

$$\frac{d\theta}{dt} = \nu \times \theta^n \times \exp\left(-\frac{E_{des}}{RT_{sp}}\right) \qquad (3)$$

For a specific species of which the maximum desorption occurs at a given surface temperature, T_{sp}, and if one assumes a certain order for the desorption process, n, then the energy of desorption, E_{des}, and the pre-exponential factor, $\nu \times \theta^n$, can be determined, knowing the surface coverage θ (in molecules cm^{-2}). The frequency factor, ν, is of the order of the vibrational frequency of the bond broken in the reaction coordinate, and is approximated to 10^{13} Hz (1 Hz = 1 s^{-1}) in all the present calculations.

With $\frac{d^2\theta}{dt^2} = 0$ for the maximum rate of desorption, and assuming that the frequency factor and E_{des} are independent of θ and t, then E_{des} can be obtained from equation (4) if it is a first order desorption process and from equation (5) if it is a second order desorption process:

$$\frac{E_{des}}{RT_{sp}^2} = \nu \times \frac{dt}{dT_s} \times \exp\left(-\frac{E_{des}}{RT_{sp}}\right) \qquad (4)$$

Notice that first order desorption are independent of the coverage θ. This behaviour is evidenced by a constant peak temperature T_{sp} when increasing θ.

$$\frac{E_{des}}{RT_{sp}^2} = \nu \times 2 \times \theta \times \frac{dt}{dT_s} \times \exp\left(-\frac{E_{des}}{RT_{sp}}\right) \qquad (5)$$

Many factors can complicate the analysis of desorption spectra, such as the variation of E_{des} (or ν) with θ, especially if there are different sites of adsorption [3], for example on a Pt(533) surface due to the presence of terraces and steps.

If there is redistribution of the adsorbates, the population of the various desorbing phases cannot be equated to the population of the various adsorbed phases, hence TPD cannot explain what has adsorbed but only what has desorbed. Another difficulty of studying with TPD method is ensuring that the sample heats uniformly.

The TPD is most useful for molecules which adsorb reversibly and do not chemically alter during the temperature rise, such as CO and O_2 molecules. Methane adsorption was too complicated to be studied by TPD because it does not desorb as CH_4 molecule but fragments at the surface; this will be detailed in **chapter IV**. The desorbed atoms and molecules are detected with a fixed quadrupole mass spectrometer, as described in the instrumentation section.

III.2 KING & WELLS METHOD

King and Wells [4] perfected a method to obtain absolute values of the sticking probability, S (defined as the ratio of adsorption rate to collision rate), and of the surface

coverage, θ. This method is relatively simple in operation and gives results with high degree of accuracy, however it is limited to sticking probability larger than 5 %. It has been used, for example, to study CH_4 dissociative adsorption on platinum [5, 6], H_2 dissociation on platinum [7, 8, 9], O_2 dissociation on platinum [10].

This method has been shown to be a useful tool here for determining the $S(\theta)$ function on polycrystalline (*i.e.* U) and single crystal (*i.e.* Pt(533)) sample surfaces, and possesses major advantages [4]:

(1) only a centre section of the target is sampled, thus avoiding crystal edge effects;

(2) this technique is more accurate for fast adsorption processes than the uptake flash filament technique;

(3) the randomised gas density component of the adsorbing gas in the crystal chamber during adsorption does not rise above 1×10^{-9} Torr and is run for a maximum 60 s, thereby considerably reducing the amount of contaminants produced at the chamber walls by the impinging gas;

(4) this technique can be used for angular distributions of reflected gas molecules during adsorption and of adsorbates. It is also used to study the adsorption and desorption kinetics.

Moreover, this method is useful to study the adsorption/desorption behaviour of molecules, such as CH_4, which experience dissociation on the surface and do not desorb in their initial form. These molecules cannot be evidenced by the TPD technique, therefore the method of King & Wells is preferable to quantify their adsorption rate. Notice that this last method has its own limitation. Hence for very low sticking coefficients another method will be used here, the titration method, notably for CH_4 adsorbing on Pt (533).

Figure III.2 shows a typical sticking probability measurement for hydrogen on Pt(533). The pressures P_0, P_a, P_1 and P_2 at times t_0, t_a, t_1 and t_2 respectively, will be detailed later.

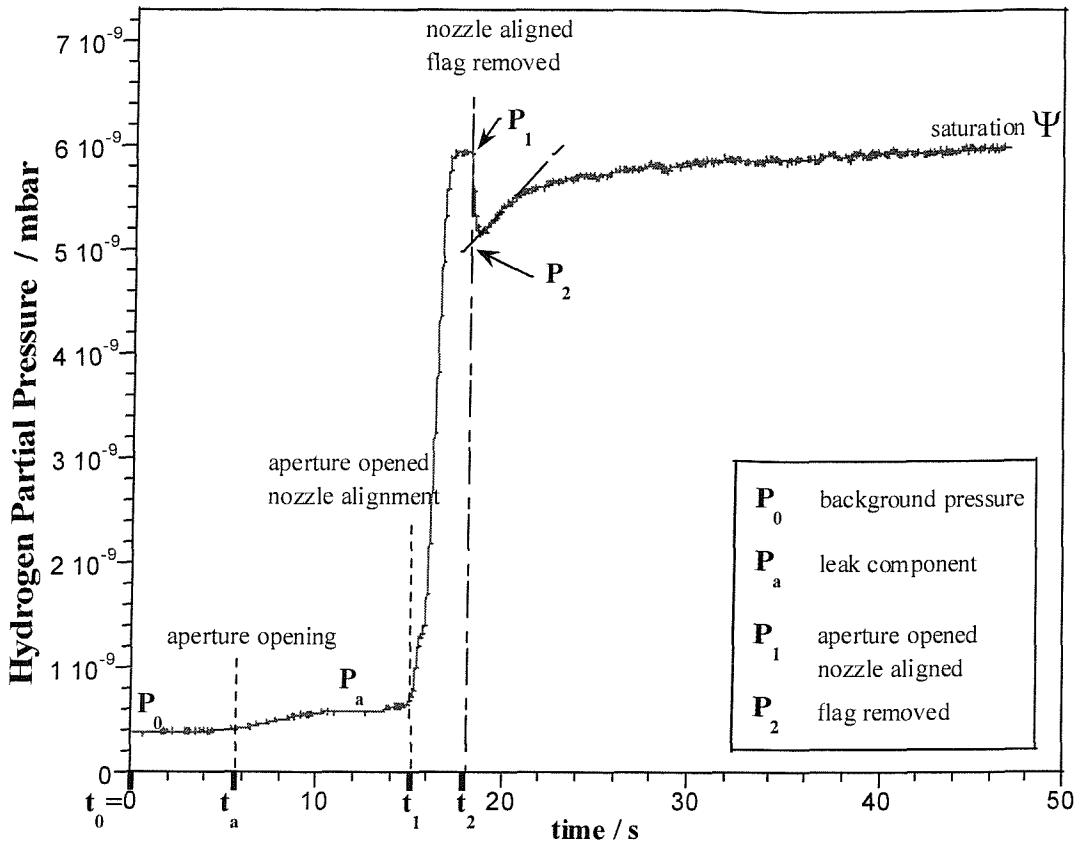

Figure III.2: Typical mass spectrometer response during sticking probability measurements of H_2 on Pt(533) by the King and Wells method.

III.2.1 Sticking Probability

As seen in the preceding chapter, a supersonic molecular beam is created and the nozzle, skimmer and aperture are used to open the path of the beam to various points. In practice, the aperture is first opened, then the nozzle is placed in face of the skimmer, and at last the flag, which is the most important step, is removed from the front of the sample. Hence the changes of pressure obtained in the reaction chamber are monitored by a fixed quadrupole mass spectrometer and contribute to obtain some sticking probability measurements.

At time t_0 corresponding to the beginning of the experiment, the beam gas must not influence the pressure of the main chamber. Hence the background pressure measured in the reaction chamber P_0.

At time t_a the aperture is opened. In theory the pressure in the reaction chamber should not rise because the nozzle which brings the molecular flow is not aligned to the beam path. However in several cases we observe a slight increase of the pressure, P_a, as seen in **figure III.2**.

At time t_1 the nozzle is aligned to allow the beam into the reaction chamber and the pressure rises to P_1 due to the flux of the beam.

At time t_2 the flag inside the reaction chamber is removed from the front of the sample, allowing the beam to hit the sample surface. Hence at time t_2 the fraction of molecules adsorbing on the surface to the total number of molecules beamed on it is defined as the initial sticking probability, S_0, and leads to a sudden decrease of the reaction chamber pressure to P_2. Note that P_2 does not correspond to the minimum of the sticking but is taken after extrapolation (see **figure III.2**). This takes in account the time lag of the QMS to "read" the pressure and also the fact that the QMS is positioned at a relatively large distance from the sample.

Hence S_0 can be expressed with a simple ratio of pressures:

$$\frac{(P_1 - P_2)}{(P_1 - P_0)} = S_0 \qquad (6)$$

The formula of the initial sticking probability was also corrected by the effusive component of the beam F_d (fraction of the molecules that are scattered by the variable aperture on entering the chamber and that contribute to the diffuse background intensity).

In theory, at time t_0 the beam must not influence the pressure in the reaction or in the second stage chambers. However, by monitoring the pressure in the second stage, a clear increase of the pressure is observed. Then at time t_a when the aperture is opened a slight increase P_a (effusive component in **figure III.2**) is observed in the reaction chamber. Following the alignment of the nozzle to the beam path there is a noticeable effusive component P_{eff} of the beam in the second stage chamber which is narrowed by the skimmer

(see **chapter II**) and consecutively by the aperture at the entrance of the main chamber. Hence the total effusive component of the beam is given by:

$$F_d = \frac{P_a + P_{eff}}{\psi} \qquad (7)$$

F_d was estimated to be *ca.* 21 % for this system by Butler [2]. This latter value was obtained by comparing the results of sticking probability measurements of nitrogen on W(100) at 300 K obtained with this system and those of Rettner *et al.* [11].

Hence:

$$S_0 = \frac{(P_1 - P_2)}{(P_1 - P_0) \times (1 - F_d)} \qquad (8)$$

Whereas the sticking probability is easily obtained experimentally, it still depends on several parameters: the surface coverage (which varies with the surface temperature and the dosing time), the beam energies (kinetic and vibrational) that were controlled by the nozzle temperature and the seeding, and the angle of incidence.

In fact the sticking probability varies from S_0 to zero as the surface coverage increases up to saturation. Hence at time t the sticking probability becomes:

$$S = \frac{(P_1 - P_t)}{(P_1 - P_0) \times (1 - F_d)} \qquad (9)$$

At time t, the area under the uptake curve is proportional to the number of molecules adsorbed on the crystal surface, *i.e.* the coverage θ coverage, hence:

$$\frac{\theta}{\theta_{sat}} = \frac{\int_{t1}^{t} (P_1 - P_t)dt}{\int_{t1}^{\infty} (P_1 - P_t)dt} \qquad (10)$$

III.2.2 Titration Method

When the sticking probabilities are too small to be obtained accurately by the King & Wells method (less than 5%), the sticking coefficients have to be determined by the titration method [12]. This method has also the advantage of measuring the sticking

probability of incident molecules which adsorb dissociatively on the surface, such as CH_4. It consists of titrating the atom or molecule left on the surface after adsorption of the incident molecule. For this purpose a specific gas, of which the molecules interact with the atoms or molecules left on the surface, is dosed on the surface in known conditions. Hence the new species formed on the surface after reaction are quantified with the fixed quadrupole mass spectrometer.

In the case of CH_4, the deposited carbon which is left on the surface after dissociative adsorption is titrated with oxygen. The O_2 is dosed at ~ 550 K thus it instantly reacts with the surface carbon producing CO and CO_2. The desorption rates of CO and CO_2 are related to the dissociative adsorption of methane, thus they are also related to the sticking probability of methane on the surface.

These measurements lead to relative sticking probabilities values obtained by:

$$S_{rel} = \frac{A_{total}}{t_1 \times \Psi} \qquad (11)$$

with:

$$A_{total} = \sum c_i A_{spei} \qquad (12)$$

where A_{total} is the total amount of carbon on the surface, c_i is the calibration coefficients related to the detection sensitivity of species i, and A_{spei} is the amount of carbon in the titrating species i, Ψ is the maximum pressure of the titrated species obtained by extrapolation of the incident reacting gas pressure on the K&W spectrum (**figure III.2**) but for time t_1 (in practice when the flag is removed from the front of the sample). The coefficients are obtained experimentally by calibrating the pressure given by the ion gauge against the detector output of the QMS for each species i.

Because all the parameters necessitated here are in relative units, it is necessary to scale the relative sticking probabilities obtained with the results of the K&W method in order to realise absolute sticking probabilities. This was performed by measuring an initial sticking probability with the K&W method (sufficiently high to be trustworthy), and then comparing it to the relative sticking obtained by the titration method.

This method was only used in the case of CH_4 on Pt(533), which will be detailed in **chapter IV**.

III.3 X-RAY PHOTOELECTRON SPECTROSCOPY

X-ray photoelectron spectroscopy (XPS) also known as electron spectroscopy for chemical analysis (ESCA) is a surface and subsurface sensitive technique that provides straightforward data interpretation and chemical bonding information. Minimal sample preparation is required, non-destructive depth information can be obtained, and no charging problems are encountered for metal samples while they exist for oxides samples (hence need to use an electron gun to replace the electrons photoemitted in this last case). XPS is sensitive to surface contaminants at the level of about 1 % of a monolayer, similar to Auger electron spectroscopy.

XPS was first developed by Siegbahn and coworkers in the 1960s [13]. Photoelectron spectroscopy is a particularly simple process and consists of the excitation of electrons in an atom or molecule from the sample surface by means of monoenergetic X-rays, where $h\nu > 100$ eV. The photoemitted electron can originate from deep levels in the atom: the core levels. The X-rays may penetrate far into the bulk (10^3 to 10^4 Å), however XPS takes the advantage of the short mean free path of the electrons in the solid, *i.e.* the electrons cannot escape without inelastic collisions except from within a few nanometers of the surface (0.3 to 3 nm depending on the kinetic energy of the electrons). Moreover to be more surface selective one can enhance the sensitivity of XPS to the surface valence band by the use of grazing angle incidence radiation and grazing angle emission electron collection. The average distance that an electron can travel without being scattered inelastically is defined as the inelastic mean free pathlength, λ. Hence the relation between λ and the intensity of the photoelectron signal in the solid by inelastic scattering events has been established:

$$I = I_0 \exp\left(\frac{-d}{\lambda \cos\theta_e}\right) \qquad (13)$$

With I the intensity at the surface, I_0 the intensity of the photoelectrons from distance d below the surface, and θ_e the angle of the emission relative to the surface normal. As θ_e increases, the distance d decreases, hence the photoelectrons are more likely to be generated at the surface or subsurface.

The electrons photoemitted from inner core levels of atoms are detected by an electron energy analyser. The Einstein photoelectric equation, outlined in 1905 [14], using the condition of the conservation of energy, connects the kinetic energy E_{kin} of these electrons to their binding energy E_B, relative to the vacuum level:

$$E_{kin} = h\nu - E_B \qquad (14)$$

Where $h\nu$ is the energy of the incident X-rays. E_B is of the order of several hundred eV. Note that the energy of the photoelectron is discrete and thus characteristic of the atom.

In a solid, the binding energy of the ejected electrons is relative to the Fermi level (highest occupied electronic state), thus a small additional amount of energy (a few eV) is required to remove the electron from the solid surface into the vacuum, and is known as the workfunction of the solid, ϕ, hence the Einstein relation is modified:

$$E_{kin} = h\nu - E_B - \phi \qquad (15)$$

This equation assumes that the photoelectron suffers no change in energy between emission from the surface and detection in the spectrometer, *i.e.* the process is elastic. Note that in entering the analyser the E_{kin} of the photoelectrons is changed, hence the workfunction, ϕ', of the spectrometer has to be taken in account too.

The equations given above obey Koopman's theorem, which specifies that all the electrons in the system, apart from the electrons photoemitted, are insensitive to the photoemission event. This insensitivity neglects the phenomenon of relaxation. In fact, some electrons in the photoemitting atoms relax to lower energy states to screen the core hole created during photoemission, leading to a surplus of energy for the photoelectrons, E_a. Because the photoemission is a rapid process, the system does not always reach a stable equilibrium. In fact, E_a can be lower than expected due to some processes of excitation

called shake-up and shake-off giving rise to energy satellites. All the above phenomena are defined as final state effects. The chemical environment of the photoemitting atoms must also not be neglected, and small but detectable shifts of core-level energies, closely related to charge transfer in the outer electronic level, can be detected. In fact, the weakly bound valence electrons screen the core hole, leading to an additional energy term, E_r. These phenomena are defined as initial state effects. E_a and E_r are of the order of a few eV or less.

$$E_{kin} = h\nu - E_B - \phi + E_a + E_r \qquad (16)$$

From the evaluation of the binding energy of the ejected electrons, one may identify the elements present in the sample. Any photon whose energy exceeds the work function of the solid ($h\nu > \phi$) can be used for photoelectron spectroscopy, which simply excludes the near ultraviolet, visible and higher wavelength (whose energy ranges are much lower than the X-ray one). Since the electrons occupy discrete energy levels, the resulting spectrum shows distinct and separate peaks corresponding to these levels. The width of the observed features depends on three factors: the inherent width of the exciting radiation, the lifetime of the core hole being probed, and the resolution of the analyser [15].

Figures III.3 and **III.4** show the excitation and relaxation of an atom by an X-ray. The vacancy (core hole) obtained after photoemission of an electron in the level K can relax either by emission of an Auger electron or by emission of a photon.

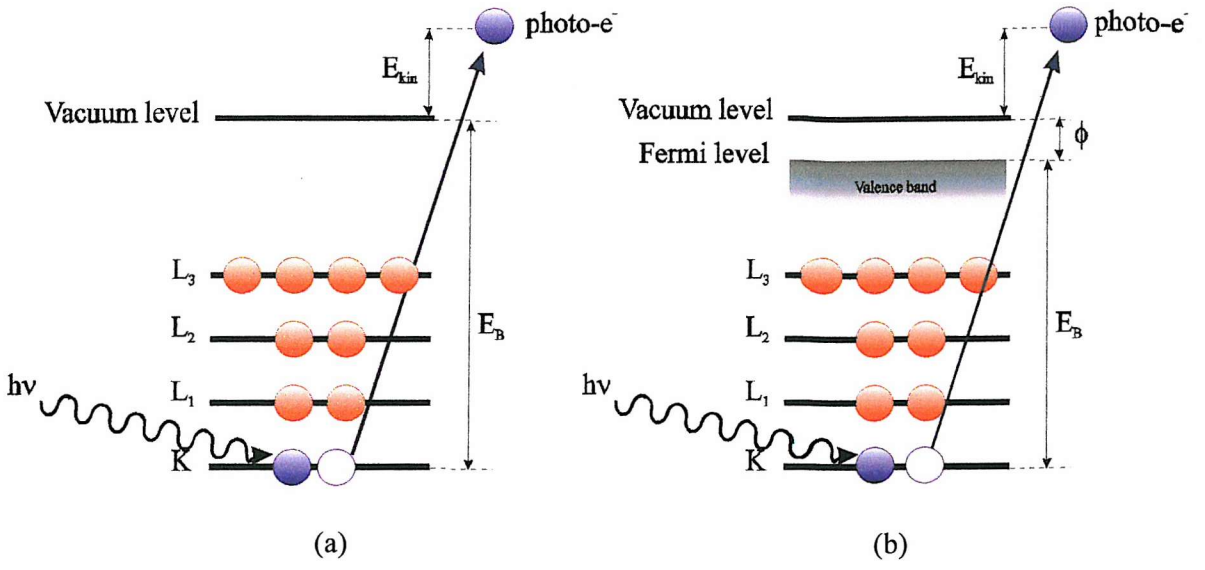

Figure III.3: Interaction of incident X-rays, of energy $h\nu$, with electrons from inner core level K of an atom from (a) the gas phase and (b) from a solid, resulting in photoemission.

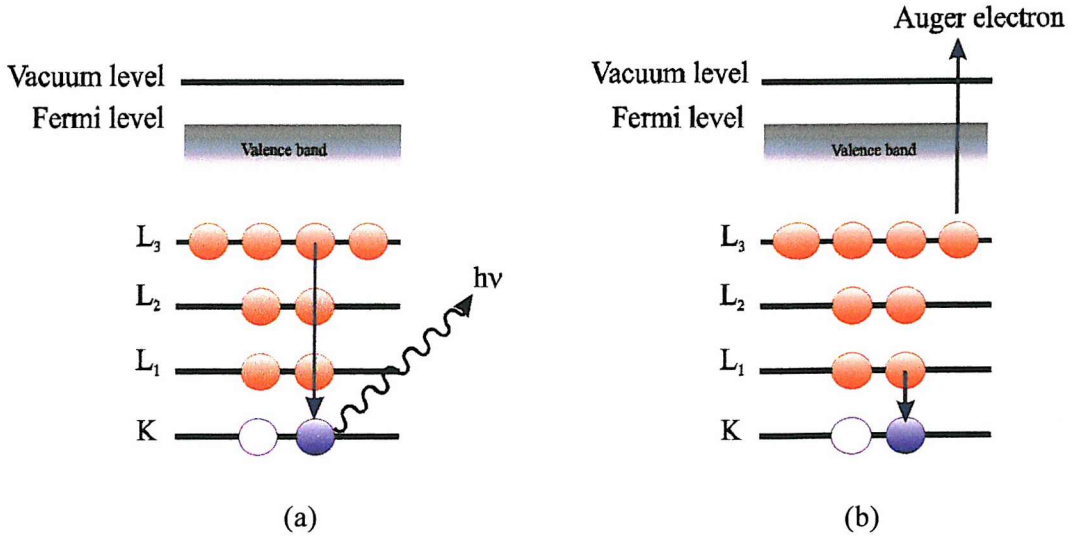

Figure III.4: Relaxation of the surface atom, (a) by X-ray fluorescence and (b) through the Auger process.

Fluorescence is important for core levels with energy E ≥ 10 keV and elements with high atomic number. The fluorescence yield, or the radiate probability, E_f, is defined as the ratio of the emitted X-rays (thus depending on $h\nu$) to the number of primary vacancies created. E_f increases with the atomic number, and is larger for the K line emissions than L and M. For atomic number ≥ 50, the fluorescence yield tends to unity. Notice also that the fluorescence occurring at depths below the surface is at the origin of secondary electrons,

resulting from inelastic photoemission [15] which contribute to a large background in the XPS spectrum.

The kinetic energy of the Auger electron is simply the difference between the initial and final states, and is therefore independent of the energy of the incident photon $h\nu$. Hence it is easy to separate the satellite peaks due to the Auger relaxation from the XPS peaks by varying the energy of the incident photons.

As a first approximation, the core ionisation energies are supposed to be insensitive to the bonds between atoms because they are too tightly bound to be greatly affected by the changes that accompany bond formation. This insensitivity turns out to be largely true, and the core ionisation energies are characteristic of the individual atom rather than the overall molecule. Consequently, XPS gives lines characteristic of the elements present in a compound or alloy. However, it is not entirely true as seen previously. Hence, the charge redistribution of valence electrons induces changes in the binding energy of the core electrons, so that information on the valence state of the element is readily obtainable. The binding energy of an electron is a function of both the attractive potential of the electron with the nucleus and the repulsive Coulomb potential with the surrounding electrons in the atom. For example, the C(1s) electron is more tightly bound in CO_2 than in CO. This gives rise to a chemical shift in the spectrum which can be explained basically in terms of several eV. Thus, the gain of negative charges on atoms lowers the core ionisation energies, while the loss of negative charge (*e.g.* oxidation) which correspond to a decrease in the valence electron density, is accompanied by an increase in the binding energy E_B of the core electrons.

In the present case, the X-ray source available consists of a dual anode, coated with Al on one face and Mg on the other face, which can be bombarded with high energy electrons (see **figure III.5**). These electrons are emitted by the thoria-coated filament, through which is flowing around 5 A current and is at near earth potential, and are rapidly accelerated toward the high voltage potential of the anode at 15 kV. The emission current is set up to 20 mA, thus the X-ray source runs at 300 W. In most cases the electron energy is chosen to be appreciably higher than the K-shell binding energy of the target and lines associated with the filling of K-shell holes dominate the spectrum.

The emission from this target consists of characteristic narrow line emissions associated with the filling of core holes created by the incident electron beam superimposed on a low continuum background up to the energy of the incident electron due to the bremsstrahlung.- The bremsstrahlung is a radiation emitted by a charged particle under acceleration. The energy emitted by an accelerated particle is proportional to $1/m^2$, with m the rest mass of the particle. Hence the bremsstrahlung plays a particularly important role for light particles; up to energies of 100 GeV. - The energies of the two lines $K_{\alpha 1,2}$, corresponding to an unresolved doublet associated with decays from $2p_{1/2} \rightarrow 1s$ and $2p_{3/2} \rightarrow 1s$, are 1253.6 eV for Mg with a full width at half-maximum of 0.7 eV, and 1486.6 eV for Al, with a full width at half-maximum of 0.85 eV. Note that the signal-to-background ratio is poor because of inelastic processes. The small satellite peaks due to the $K_{\alpha 3,4}$ emission could be present in the kinetic energy spectrum. $K_{\alpha 3,4}$ is also due to the decay $2p \rightarrow 1s$, but it involves a doubly ionised target ion. The use of a very thin Al window, acting as a partial filter for unwanted x-ray lines, prevents this latter feature. Thus the photon source is nearly monochromatic hence the bremsstrahlung is reduced. There is also a very low possible transition from 3p to 1s energy levels, called K_β. The Al window also isolates the anode field and prevents stray electrons from affecting the experiments.

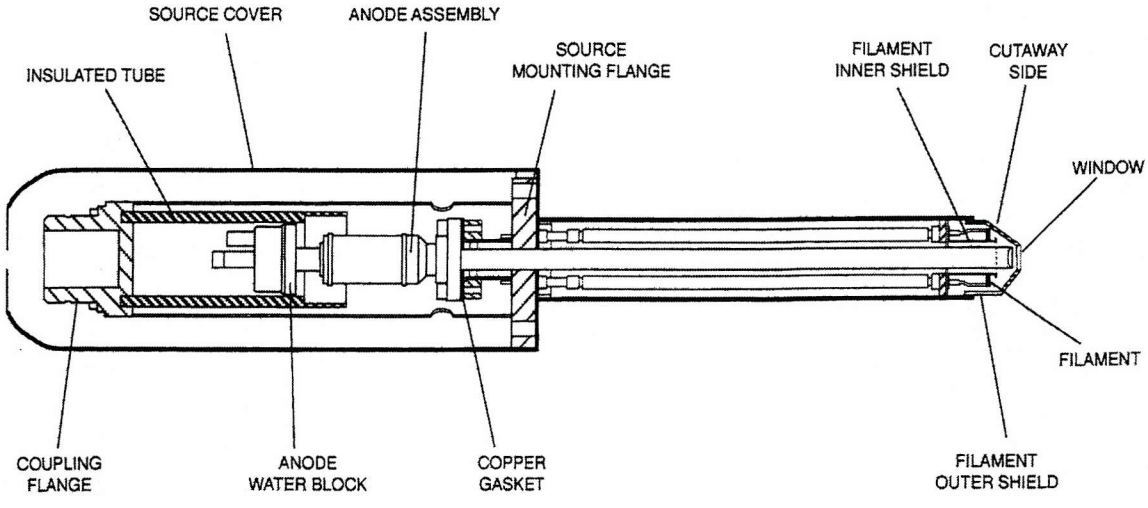

Figure III.5: Reproduction of the dual anode X-ray Source (VG Microtech). The anode is water cooled. The gun is differentially pumped with respect to the rest of the UHV system.

Valence band electrons have a very low photoelectric cross section compared to the core electrons, meaning that their binding energy to the nucleus is weaker, hence as seen in

equation (23) the kinetic energy of the electrons ejected from the valence band is larger than the core electrons one. Hence by varying the kinetic energy we can emit valence or core electrons whom can give different informations of the surface.

The water-cool system is essential for several reasons, first of all considerable power is fed into the metallic target which could consequently outgas giving unacceptable rise of pressure if the cooling did not prevent it. Secondly, the cooling limits the rise in temperature of the XPS source, otherwise all the elements like the anode and the copper gasket could evaporate until complete disappearance of their material!

The electrons are focussed onto the entrance of the analyser by a series of electrostatic lenses. The kinetic energy of the photoelectrons is measured using an electrostatic deflector which produces different deflections in the paths of these electrons as they pass between charged plates. As the field strength is increased, electrons of different speeds, and therefore different kinetic energies, reach the detector. Thus the electron flux can be recorded and plotted against kinetic energy to obtain the photoelectron spectrum. Present techniques give energy resolution of ~ 1 eV.

There are many types of collector and analyser, *i.e.* hemispherical or cylindrical. The present one is a 100 mm mean radius hemispherical one with an integral dual element transfer lens (see **figure III.6**).

There are two modes of operation: the FAT/CAE (CAT) mode, where the pass energy $\boldsymbol{HV}$ is held constant ($\boldsymbol{H}$ is a constant determined by the geometry of the system, and $\boldsymbol{V}$ is the potential difference between the two hemispheres) and the electrons are retarded at the entrance slit by a negative potential $\boldsymbol{R}$, before entering the hemispheres, and the FRR/CRR mode, where the retarded potential is constant, and the pass energy is a fixed ratio of the kinetic energy. With the pass energy constant, the resolution across the entire $\boldsymbol{E_{kin}}$ range is constant, making it preferable for XPS. The CRR mode is generally used for applications where good resolution is required at low $\boldsymbol{E_{kin}}$, such as AES or ISS. The CAE mode, used here gives:

$$E_{kin} = HV + R \qquad (17)$$

With $\boldsymbol{HV}$ set at 50 eV, and $0 < E_{kin}(eV) < 1486.6$ (for Al).

Allowing for the analyser work function and the work function of the solid ϕ_{tot} ~ 5 eV, E_{kin} is in fact:

$$E_{kin} = HV + R + \phi_{tot} \qquad (18)$$

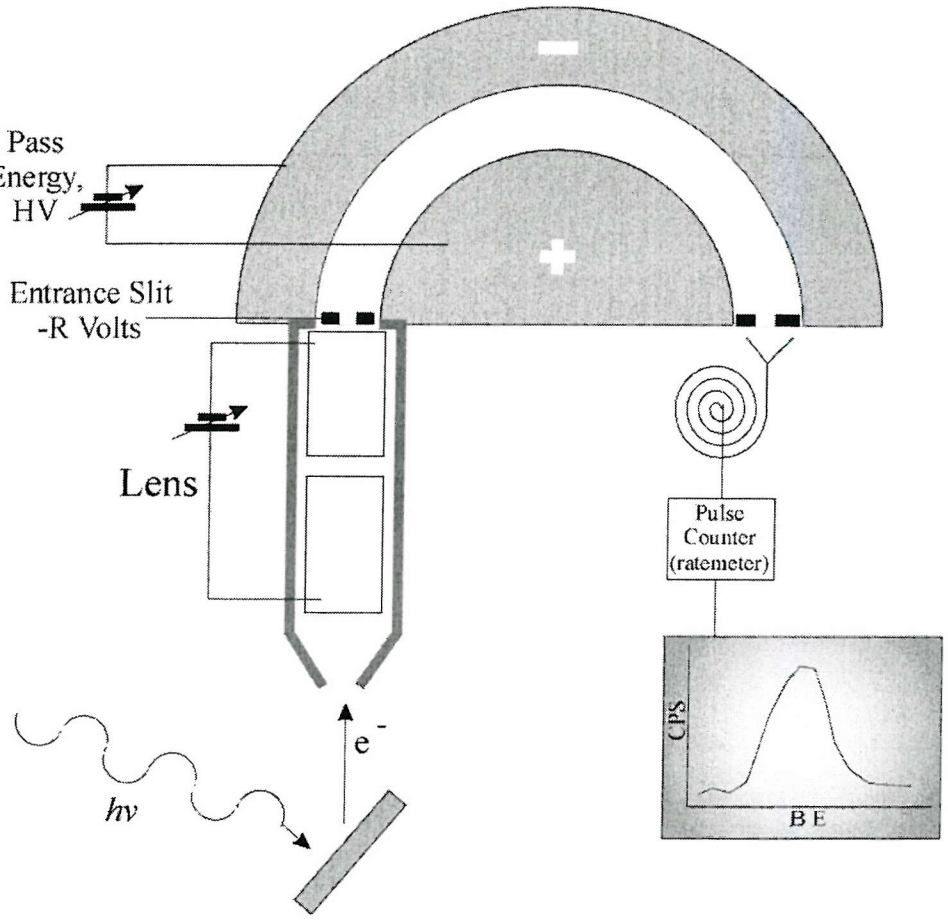

Figure III.6: Reproduction of the diagram of the analyser (VG Microtech).

III.4 REFERENCES

[1] Somorjai G. A., "*Introduction to surface chemistry and catalysis*". Wiley-Interscience, chap. 4, **1994**.

[2] Butler D. A., Ph. D. thesis, University of Southampton, **1994**.

[3] Jones J. D., Ph. D. thesis, University of Southampton, **1994**.

[4] King D. A. and Wells M. G., *Surf. Sci.*, 29: 454, **1972**.

[5] Schoofs G. R., Arumainayagam C. R., McMaster M. C. and Madix R. J., *Surf. Sci.*, 215: 1, **1989**.

[6] Luntz A. C. and Bethune D. S., *J. Chem. Phys.*, 90: 1274, **1989**.

[7] Luntz A. C., Brown J. K. and Williams M. D., *J. Chem. Phys.*, 93: 5240, **1990**.

[8] Samson P., Nesbitt A., Koel B. E. and Hodgson A., *J. Chem. Phys.*, 109: 3255, **1998**.

[9] Gee A. T., Hayden B. E., Mormiche C., Nunney T. S., *J. Chem. Phys.*, 112: 7660, **2000**.

[10] Gee A. T., Hayden B. E., *J. Chem. Phys.*, 113: 10333, **2000**.

[11] Rettner C. T., DeLouise L. A., and Auerbach D. J., *J. Chem. Phys.*, 85: 1131, **1986**.

[12] Rettner C. T., Pfnür H. E., and Auerbach D. J., *Phys. Rev. Lett.*, 54: 2716, **1985**.

[13] Siegbahn K., Nording C. N., Fahlman A., Nordberg R., Hamrin K., Hedman J., Johansson G., Bermark T., Karlsson S. E., Lindgren I., Lindberg B., "*ESCA: Atomic, Molecular and Solid state Structure Studied by Means of Electron Spectroscopy*", Aimqvist and Wiksells, Uppsala, **1967**.

[14] Einstein A., *Ann. Physik*, 17: 132, **1905**.

[15] Ebert H. D., Ph.D. thesis, University of Southampton, **1990**.

CHAPTER IV: DYNAMICS AND KINETICS OF DISSOCIATIVE ADSORPTION OF METHANE ON Pt(533)

IV.1 INTRODUCTION

IV.1.1 Methane Adsorption on Transition Metals

The interest in CH_4 chemisorption systems is partly motivated by the increasing importance of using natural gas as a raw material in the chemical industry, but from a fundamental point of view, it is also interesting to study the strongly activated chemisorption of certain molecules on metal surfaces. Alkanes, particularly methane, form an abundant natural resource, and the catalytic activation of alkanes offers promise for conversion to useful petrochemicals.

CH_4 is one of the major industrial sources of H_2 because of the reaction which occurs at metal surfaces:

$$CH_4 + H_2O \rightarrow CO + 3H_2 \qquad (1)$$

This process called steam reforming is performed by reaction with steam over a catalyst (typically nickel). An excess of steam avoid carbon deposition on the catalyst.

Because H_2 is an essential component in many important industrial processes [1], it has been relevant to study the interaction of CH_4 with several metal surfaces such as tungsten W(110) [2, 3], copper Cu(100) [4] and platinum Pt(111) [5, 6, 7].

IV.1.2 Platinum

Platinum is one of the most versatile, heterogeneous metal catalysts. It is used in many different reactions: for the conversion of aliphatic straight-chain hydrocarbons to aromatic molecules to branched molecules (isomerisation), for hydrogenation on a large

scale in the chemical and petroleum-refining industries, etc. It is also used as an oxidation catalyst for ammonia oxidation, an important step in the production of fertilisers. Platinum is the catalyst for the oxidation of CO and hydrocarbons in the control of car emissions, and is perhaps the most widely used and most active electrode for catalysed reactions in electrochemical cells. Its chemical stability in both oxidising and reducing conditions makes this metal an ideal catalyst in many applications. For this reason it is of considerable importance to scrutinise the catalytic activity of Pt on the atomic scale, to learn what makes this metal so versatile as a catalyst and so selective for important catalytic transformations [8].

Mined mostly in South Africa and in the USSR, platinum, along with rhodium (which occurs as an impurity in platinum ores), is very rare and therefore expensive. Its regeneration and recovery must be an important part of any technology that uses this metal. It is a soft, silver-white and very heavy metal.

Transition elements of group VIIIA such as platinum, are known in only one crystalline form, but as with most metals, undergo structural changes when the temperature and/or the pressure is changed. Platinum forms a face centred cubic (fcc) lattice, with each platinum atom having 12 equivalent nearest neighbours at 2.7741 Å. The radius of a platinum atom is 1.3870 Å in a unit cell of 3.9231 Å along each side at 298 K.

IV.1.3 Adsorbate-Substrate Bonds between CH_4 and Pt

The Effective-Medium Theory (EMT) defines the formation of a surface chemical bond to be adsorption accompanied by charge transfer and charge redistribution between the adsorbate and the substrate, producing strong bonds of covalent or ionic character [9, 10, 11]. Changes in the electronic and atomic structure of the bonding partners are determined and compared with their electronic and atomic (or molecular) structures before they formed the surface bond. A transition metal-surface such as platinum, has d-electrons that lie in a band around the Fermi level. These d-states can interact with adsorbate states giving rise to bonding and antibonding shifts. The d-electron contribution to the bonding depends on the degree of filling of the antibonding states (since the bonding states are already filled). Thus, early transition metals with fewer d-electrons form stronger chemical bonds [12]. Because platinum has a filled $5d^{10}$ orbital, the chemical bonds available with an adsorbate will be

weaker than for tungsten which has a configuration of $5d^4$, because Pt has more electrons available to go in the antibonding states.

However, other theories also point out that d-electron metals, such as Ni, Pd, or Pt, in which the d-bond is mixed with the s and p electronic states provide a large concentration of low-energy electronic states and electron vacancy states [13]. Therefore Pt is ideal for catalysis because of the multiplicity of degenerate electronic states that can readily donate or accept electrons to and from adsorbed species [14].

The surface bonds must not be too strong otherwise the reaction intermediates will block the adsorption of new reactant molecules due to long surface residence times and the reaction will be impaired. If the adsorbate-substrate bonds are too weak, the necessary bond-scission processes will be absent. Hence the catalytic reaction will not occur [14].

Platinum is a good catalyst as it forms bonds strong enough to induce bond dissociation in the reactant molecules (CH_4), but sufficiently weak that only short residence times for the surface intermediates ensue and rapid desorption of the product molecules occurs.

The experiments done on metal catalysts and the theoretical models are in good agreement. Indeed, one of the predictions of these models is that the heat of chemisorption of atoms should increase from right to left in the periodic table and it has been well observed [10, 12].

IV.1.4 Molecular Orbitals of CH_4 and Energy Diagram Correlation with Pt

CH_4 is a tetrahedral molecule with H-C-H angles all equal to ~ 109.5°, and C-H bonds length close to 1.10 Å. The bonding energy of CH_4 in the gas phase is 4 times the bonding energy of one C-H bond ~ 414 kJ mol^{-1}. This is in good agreement with the theoretical calculations obtained by Anderson and Maloney [15] of 1.21 Å for the C-H bond length and the C-H strength of 531 kJ mol^{-1}.

The $1s^1$ atomic orbitals of the four H atoms and the $1s^2\ 2s^2\ 2p^2$ atomic orbitals of the C interact together. They give four bonding orbitals $1a_1^2$, $1t_{2x}^2$, $1t_{2y}^2$ and $1t_{2z}^2$, corresponding to the C-H bonds, and the anti-bonding orbitals $2a_1$, $2t_{2x}$, $2t_{2y}$ and $2t_{2z}$. These orbitals of the free molecule in the gas phase are represented in **figure IV.2**.

The energy levels of platinum are characterised by unoccupied s-p and occupied s-d bands. The filled areas indicate single occupied levels.

Anderson and Maloney [15] performed a molecular study of the activation of methane on iron, nickel and platinum surfaces. The platinum surface was modelled by using a 10 atom-cluster. The atoms with which CH_4 interact directly in the transition state are shaded (see **figure IV.1a**). Kua and Goddard [16] used nonlocal density functional methods (B3LYP) to examine the structures and energetics of a number of organic fragments on Pt surfaces. They calculated the optimum geometry of CH_3 in the on-top, bridge and three-fold hollow sites of a Pt(111) surface using an 8 atoms-Pt cluster. Hence they conclude that the most stable structure for CH_3 is in the on-top site with a binding energy of 225 kJ mol^{-1} and a C-Pt distance of 2.07 Å. Therefore the approach by Anderson and Maloney to insert a Pt(111) surface atom into a methane C-H bond is of great interest.

The calculated activation energy for inserting a Pt(111) surface atom into a methane C-H bond is 43 kJ mol^{-1}, and occurs when the bond is stretched 0.36 Å. The stretching causes one of the 3-fold degenerate t molecular orbitals, $1t_{2x}$, to become destabilised. Its bending of 30° away from the tetrahedral direction (see **figure IV.1b**) contributes further to the destabilisation and also leads to a small stabilisation in the $1t_{2z}$ orbital. The low-lying $1a_1$ orbital is destabilised by the distortion. Interactions with the surface consist of a small stabilisation of the $1a_1$ orbital and mixing of both of the rehybridised orbitals $1t_{2x}$ and $1t_{2z}$ with the Pt surface orbitals to form clearly defined C-H-Pt and C-Pt σ bonding orbitals. The main occupied anti-bonding counterpart orbital energy levels lies in the doubly occupied d band region of Pt, participation of the CH $2t_{2x}$ orbital in it removes almost all H contribution so that this orbital has a C-Pt σ bonding character.

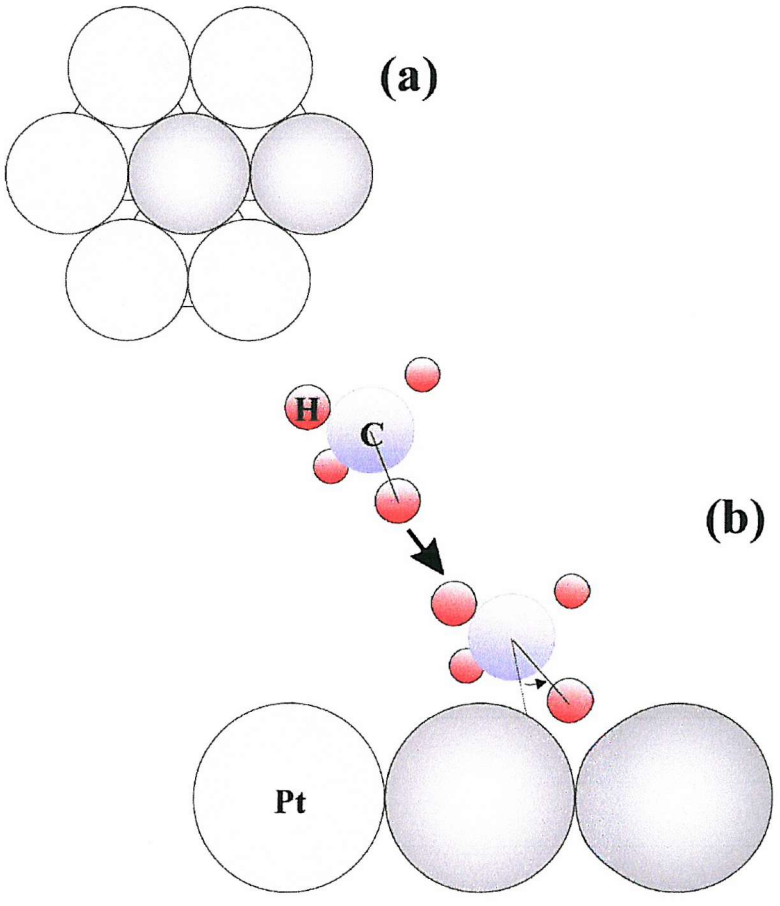

Figure IV.1: **(a)** cluster model used for the calculations [15], **(b)** Calculated transition-state structure for CH_4 above a Pt(111) surface atom.

This approach is relevant to the present study of CH_4 on the Pt(533) surface, because it helps understanding how the CH_4 molecules stick on the (111) terraces of this surface, and how they might decompose. No molecular orbital study of the interaction between CH_4 and a stepped Pt surface seems to exist. However we can obtain an idea on the CH_4-Pt bond likely to occur at the (100) steps. The number of coordination on a Pt atom on a (111) terrace is 9, while on top of a step atom it is 7. As the number of coordination is lower at the step, the electron density will be lower, therefore the Fermi level of the d band goes lower, hence it will lead to a stronger bond due to the lowering of the σ bond with the adsorbate than on the terrace. At the lower edge of the step the coordination number is 10 therefore the binding energy with the molecule will be much weaker.

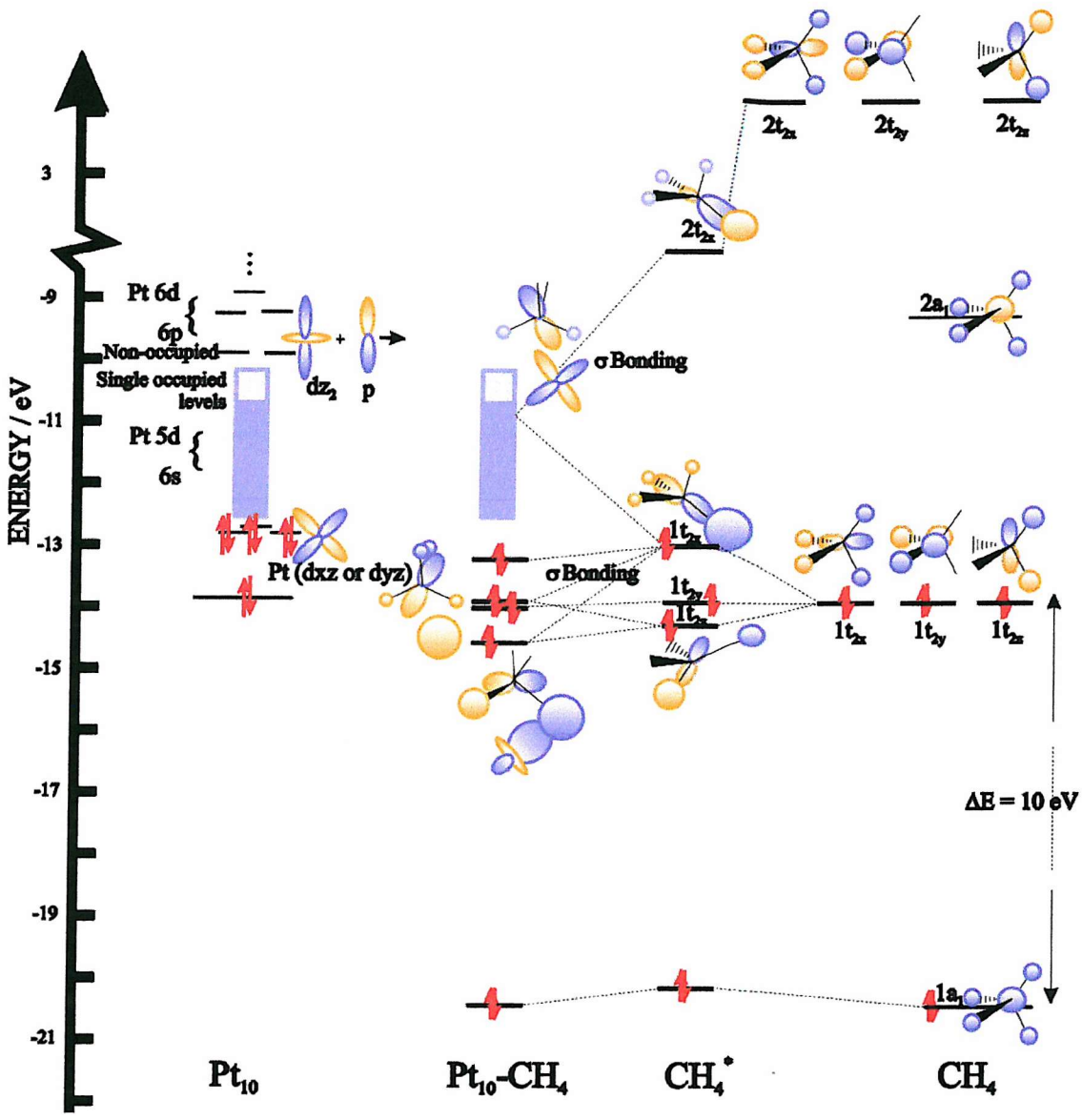

Figure IV.2: Molecular orbital diagram for CH_4 interacting with a 10 atoms Pt cluster reproduced from Jean and Volatron data [17] and Anderson and Maloney data [15].

IV.1.5 Structural Effects

Because different reactions are sensitive to different structural features of the catalyst surface, one has to prepare a catalyst with the appropriate structure to obtain maximum activity and selectivity. It has been observed that the terrace structure, the step or kink concentrations, or a combination of these structural features is needed to achieve optimum reaction rates for a given reaction [14].

Rendulic and Winkler [18], who studied the adsorption of H_2 on nickel, have shown that the sticking coefficient varies with surface geometry. In fact the difference in chemical

behaviour of terrace, step and edge atoms arises not only from their different structural environment but also from their different electronic charge densities that result from variation of the local atomic structure. Previous studies on H-H and O-O bond-breaking processes have already shown that steps can substantially lower the activation energy barrier for dissociation. These surface irregularities can be of great importance in a variety of surface phenomena, ranging from crystal growth to heterogeneous catalysis [19]. Brønsted, Evans and Polanyi established a linear relation between the activation energy barrier $\Delta \mathbf{E}_{act}$ and the adsorption energy of the products $\Delta \mathbf{H}_{ads}$ for an elementary reaction such as the activation energy for the H-H bond cleavage on a metallic surface [20-21]. They concluded that as $\Delta \mathbf{H}_{ads}$ increases, $\Delta \mathbf{E}_{act}$ decreases. This relation is applied in many areas of chemistry including heterogeneous catalysis, where it is often used to rationalise observed variations in catalytic activity from one catalyst to the next or to estimate activation barriers [22]. In the case of NO dissociation on Pd(211) [23], for example, the associated activation barrier was calculated to be lower at the step edge, and could be attributed to the stronger binding of N_{ads} and O_{ads} at the step site. Similar observation have been made for NO dissociation on a stepped Ru(0001) surface [24]. However, NO adsorption and dissociation on a stepped Rh(533) surface was found to proceed mainly on terrace sites at low coverages ($\theta < 0.25$) [25]. In the case of N_2 dissociation on Ru(0001), the activation energy for N-N bond cleavage at steps is in the order of 0.4 eV, a value which is substantially lower than sites at the close packed surface of 1.3 eV. The adsorption energy of the product N_{ads} in this case does not reflect this strong reduction in barrier height. Rather the lowering of the barrier was attributed to differences in transition state geometry and electronic effects [26].

IV.1.6 CH_4 Adsorption on Platinum Surfaces

Several studies of CH_4 adsorption on Pt(111) have already been published which indicate that the rate-limiting step is believed to be the breaking of one of the C-H bonds of CH_4 by the metal [1, 5, 6]. The initial dissociative chemisorption of CH_4 molecules on metal surfaces, or "C-H bond activation", is characterised by a high activation barrier. There are two different ways to break a CH_4 molecule leaving a CH_3 radical and a H atom on the surface. The first, which is found to be common to all the metal surfaces studied so far, is by the direct chemisorption channel where the incident translational and vibrational energies of

the molecule help to overcome the activation barrier for dissociation, hence high incident energies are necessitated. The surface temperature has also been shown to influence the CH_4 dissociation [27-30]. Using a molecular beam technique, it is possible to control the mean vibrational and translational energy of the beam through control of the nozzle temperature and seeding. The second way to CH_4 dissociation, which has been observed on Ir(110) [31] and Pt(110) [32] at low incident translational energies, is the trapping mediated channel: the CH_4 molecule traps first in a precursor state, thus the lifetime on the surface is important, and subsequently overcomes the activation barrier if the surface temperature is sufficiently high, and partitions between dissociation and desorption are favourable. There are three suggested trapping processes, the non-adiabatic creation of electron-hole pairs, the selective trapping mechanisms -where the normal momentum is transferred to another molecular degree of freedom- and surface phonon excitation [33]. It has been suggested that the precursor on the surface is structure sensitive and that it results in an increase of the dissociation probability. This was observed for the hydrogen adsorption on highly defected Pt(111) surfaces [34]. Whereas for the direct channels, maximum chemisorption probabilities in the order of 0.2 to 0.3 were found at high energies, the low energy channels exhibit maximum probabilities in the order of defect concentrations typical for single crystal surfaces prepared under UHV-conditions ($\approx 10^{-3}$).

It has been demonstrated that surface steps tend to increase the sticking coefficient for some gases, such as H_2 on Ni(997) compared to H_2 on Ni(111) [19], and also to enhance the turnover for some chemical reactions on surfaces, such as the ammonia synthesis over iron surface being dependent on the surface orientation (111), (211), (210) *etc.* [35]. In fact, some studies indicate that the H-H and C-H bond-breaking processes are more facile on stepped surfaces than on the flat crystal faces. The effect of step edges on the dissociation mechanism of CH_4 on Pt has not been previously studied hence the dynamical interactions of CH_4 molecules with a stepped platinum (533) surface will be investigated.

The (533) plane in the fcc system is separated by $14.4 \pm 0.5°$ from the (111) plane. The structure of this crystal face is a stepped (111) surface (**figure IV.3**). Hence also the alternate notation Pt(S)-[4(111)×(100)] which indicates that the (111) terraces are 4-atom rows wide and separated by monoatomic steps made up of (100) planes.

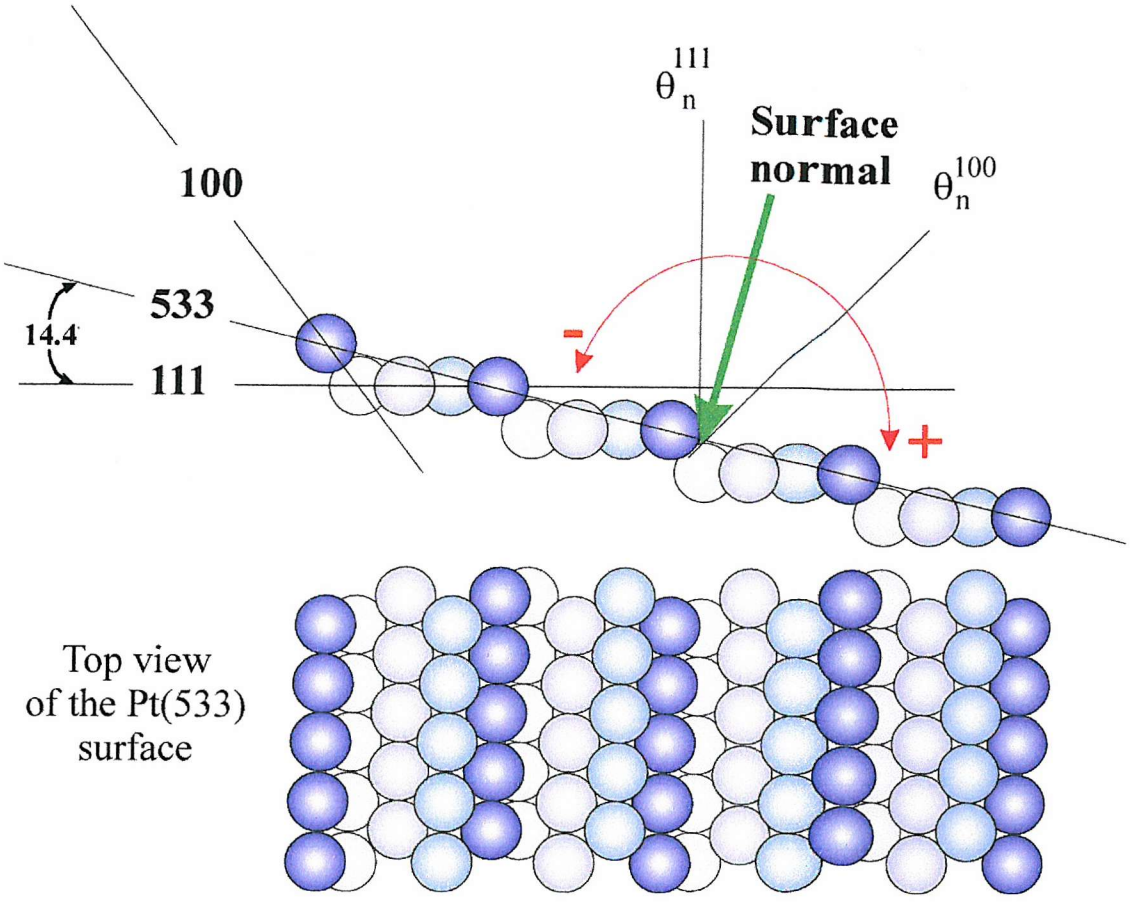

Figure IV.3: Idealised atomic surface structure for the stepped Pt(533) crystal.

IV.2 EXPERIMENTAL

Experimentally the interaction of CH_4 with the Pt surface has been studied with molecular beam techniques. The experiments were carried out in the UHV chamber detailed in **chapter II**. The (533) platinum single crystal was initially cleaned by cycles of annealing and sputtering, then only oxygen treatments at 723 K were necessitated to remove the surface carbon and to lead to the dissolution of any silicon into the bulk as described in **chapter II**. Then an anneal up to 1200 K for 10 minutes was performed between experimental runs.

The mixture required to obtain the initial sticking coefficient of CH_4 on the platinum surface depended on the required energy. Thus argon, helium, hydrogen and neon, each with a purity of 99.9995 %, were used as seeding gases (**chapter II**). Methane had a purity of 99.995 % (All BOC Gases).

The nozzle temperature did not exceed 900 K to prevent cracking of methane [36]. The surface temperature was varied $115 < T_s(K) < 800$ during the methane dosing, but it was held at 523 ± 30 K during titration by oxygen.

For all experiments presented here, the incident angle, Θ_I, is defined as zero when impinging normal to the (533) plane. Positive angles are defined as scattering into the steps. The crystal was aligned with respect to the optical surface normal. θ_n^{111} and θ_n^{100} denote the surface normals of the (111)-terraces and the (100)-steps.

IV.3 RESULTS AND DISCUSSION

IV.3.1 Methane Temperature Programmed Desorption

TPD experiments were not the best way to quantify the methane adsorption because CH_4 only desorbs as a CH_4 molecule if the surface temperature is very low, indeed Arumanayagam *et al.* [37] observed molecular methane desorbing from Pt(111) at 140 K. Otherwise CH_4 dissociates on the surface and thus desorbs as several different species, depending on the surface temperature. The CH_4 molecule can dissociate, losing hydrogen atoms sequentially, leaving a carbon atom on the surface. The hydrogen atoms recombine to form H_2 gas if the temperature is sufficient, *i.e.* above the H_2 step-desorption temperature which peaks around 380 K [38].

Thus, there are two methods that permit the quantification of CH_4 adsorption, the King & Wells method [39] and the titration method [40]. The carbon coverage on the surface could have also been monitored by XPS, but the unavailability of the XPS equipment at the time of these measurements excluded it.

IV.3.2 King & Wells Method

As seen in **chapter III**, this method permits a direct measurement of the initial dissociative sticking probability S_0. In practice King and Wells [39] have found that the experiment has an estimated error of ± 0.02. This error and the limit of the signal-to-noise at

low values of the sticking probability results in the minimum calculable value of S_0 being around 5 %.

$$S_0 = \frac{(P_1 - P_2)}{(P_1 - P_0) \times (1 - F_d)} \qquad (2)$$

Figure IV.4 shows a pressure-time profile for CH_4 using the King & Wells method. The mixture used was 1.41 ml min^{-1} CH_4 / 70 ml min^{-1} He, at a nozzle temperature of 881 K and a surface temperature of 566 K.

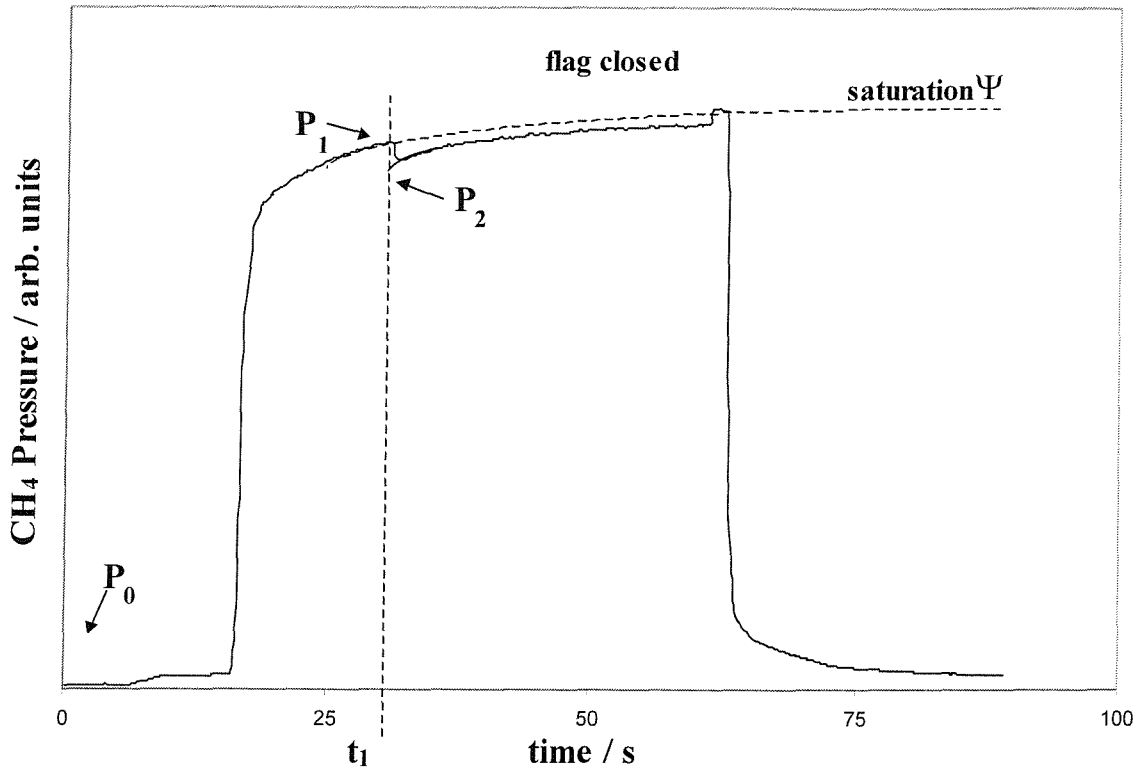

Figure IV.4: Typical mass spectrometer response during sticking probability measurements of CH_4 by the King & Wells method, T_s = 566 K, T_n = 881 K, E_i = 759 meV.

IV.3.3 Titration of CO and CO_2

For sticking probabilities smaller than 5 %, the sticking coefficients were determined by measuring the total amount of adsorbed carbon as a function of CH_4 exposure. We assume that the amount of dissociatively adsorbed methane is proportional to the amount of adsorbed carbon C_{ads} produced by thermal decomposition of the initially formed CH_x fragment. Therefore the deposited carbon was titrated with oxygen, which leads to the

formation of CO and CO_2 (**figure IV.5**). The methane was dosed at a surface temperature of approximately 550 K such as to decompose the CH_x fragments and desorb H_2 and CO adsorbed from the background during the experiment. Note that associative desorption of CH_4 or the formation of other C_yH_x product was never observed at this T_s. Then a pure oxygen beam was dosed at the same surface temperature, and the formation of CO and CO_2 was followed with a QMS (**figure IV.5**). The desorption rates of CO and CO_2 are related to the dissociative adsorption of methane, thus they are also related to the sticking probability of methane on the surface. However, the signals are corrected for the differences in detection sensitivities, accomplished by calibrating the corrected reading of the ion gauge against the detector output of the QMS for CO and CO_2. Consequently, the sum of the corrected time integrals of the CO and CO_2 desorption signals was proportional to the amount of surface carbon deposited.

The relative sticking probability of methane on platinum is obtained by:

$$S_{rel} = \frac{A_{total}}{t_1} \times \psi \qquad (3)$$

With:

$$A_{total} = x \times A_{CO} + A_{CO2} \qquad (4)$$

where $\mathbf{A_{total}}$ is the total amount of carbon on the surface, $\mathbf{A_{CO}}$ and $\mathbf{A_{CO2}}$ are the amounts of carbon entering the formation of CO and CO_2 respectively. x is a calibration coefficient estimated to be 0.185 for this system (i.e. the ratio of the ionisation cross sections of CO to CO_2), ψ is the maximum pressure obtained by extrapolation of the methane pressure on the K&W spectrum (**figure IV.4**) but for time $\mathbf{t_1}$.

This titration method is known to be very sensitive for measuring accurately and reliably small amounts of surface C and has been successfully applied in slightly different ways in the past [29, 32, 40].

Clearly, as neither the flux nor the amount of carbon was determined on an absolute scale, the initial slope of the carbon uptake curves yields a relative value for the initial sticking probability. Hence it is necessary to scale the relative probability obtained with the results of the K&W method in order to obtain absolute sticking probabilities.

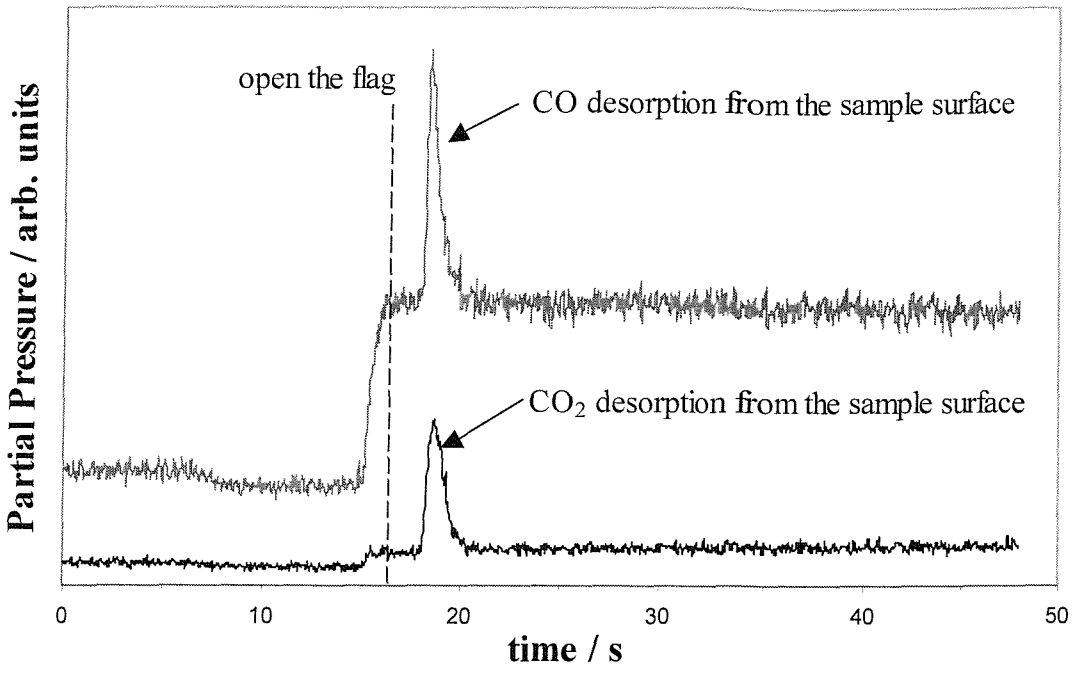

Figure IV.5: CO and CO_2 formation during the reaction of adsorbed carbon deposited by dissociative adsorption of CH_4 with oxygen, T_s = 427 K. The oxygen was dosed for 48 s.

Note that depending on the amount of C on the surface, the ratio of CO to CO_2 formed varies. Considering an approximately constant amount of oxygen being dosed onto the surface, if there is a small amount of C then can easily form CO_2 and a little bit of CO. However, if there is a lot of C on the surface then it is easier to form CO than CO_2.

IV.3.4 Dependence of $S_0(CH_4)$ on Incident Energy

Figure IV.6, shows the variation of the initial dissociative sticking probability of CH_4 on Pt(533), $S_0(CH_4)$, as a function of incident energy, at T_s = 600 K. Beam energies were varied between 26 and 1455 meV by varying the nozzle temperature as described previously. The CH_4 was seeded in helium, neon, argon or hydrogen. The impact conditions are chosen such that the beam impinges 5 degrees off the (533) normal meaning with an angle of ~ 10 degrees to the (111) terrace normal (see **figure IV.3**). Note that by using a mixture of CH_4 and H_2 at T_s = 600 K there should not be any risk of hydrogen influencing the sticking probability of methane on the surface because hydrogen does not adsorb on the surface at such high surface temperature (see **chapter V figure V.1**).

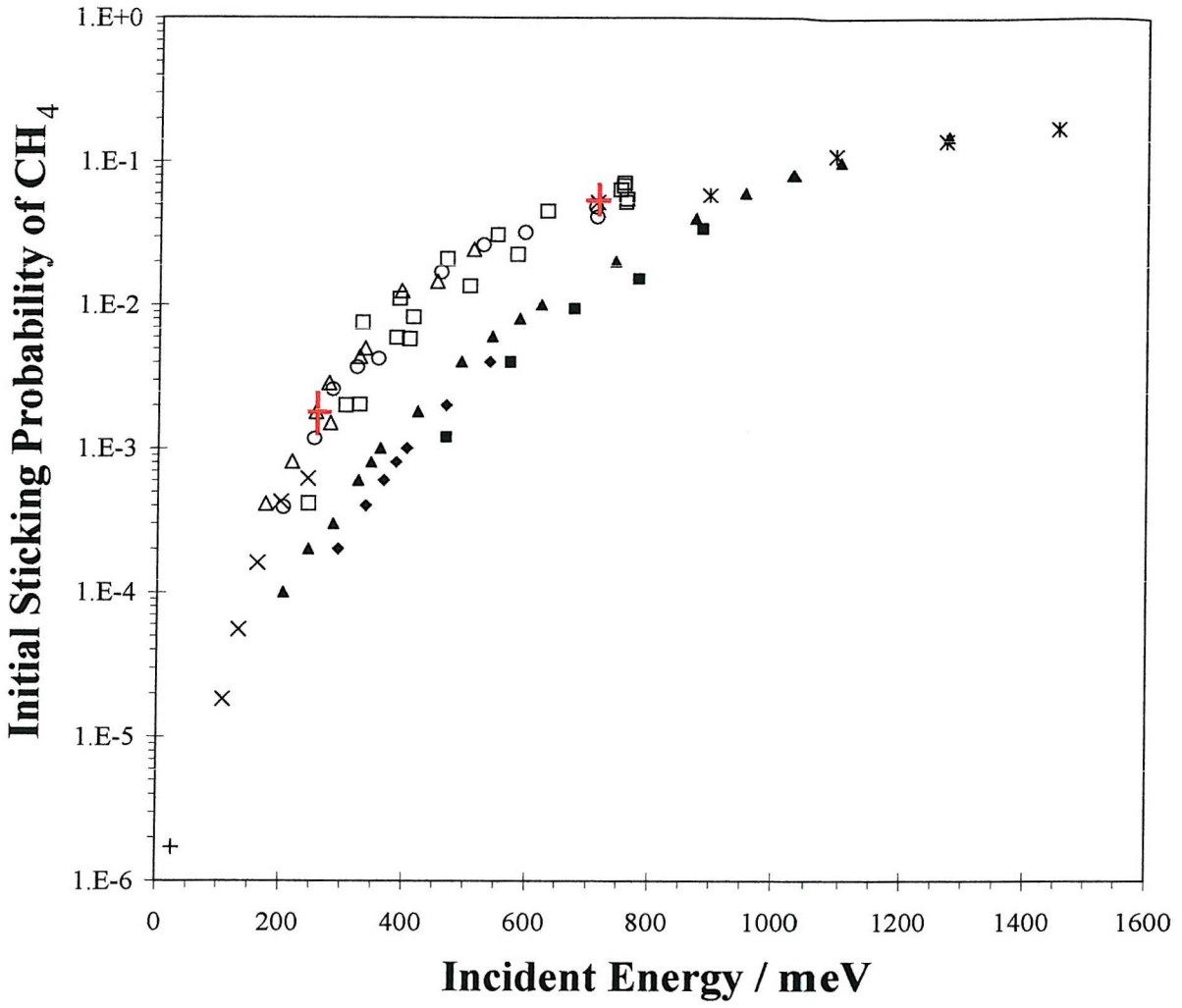

Figure IV.6: $S_0(CH_4)$ on Pt(533) at T_s = 600 K versus the incident energy of the beam, with CH_4 seeded 3 % in Ar (+), 3 % in Ne (×), 16 % in He (△), 9 % in He (○) 2 % in He (□), in H_2 (✳). The data for $S_0(CH_4)$ on Pt(111) versus E_i at T_s = 800 K and two nozzle temperature (T_n = 300 (♦) and 680 K (▲)) from Luntz [28] and at T_s = 550 K (■) from Oakes [6] are also plotted.

As it has also been reported for the dissociative chemisorption of CH_4 on Pt(111) [6, 28], W(110) [2], Ni(111) [38], Ni(100) [27], Ru(0001) [29], and Pd(110) [41], the initial sticking probability of CH_4 is dramatically enhanced by translational energy, and shows a nearly exponential dependence on E_i. This is characteristic of a molecule whose total energy is less than the height of the entrance channel barrier, thus its dissociation is only possible via an entrance channel tunnelling mechanism. This channel has been evidenced for CH_4 dissociative adsorption on W(110) by Rettner *et al.* [2], while for CH_4 on Ni(111) Lee *et al.* [38] interpreted the strong energy dependence of $S_0(CH_4)$ in term of CH_4 angular deformation mode upon surface impact which is essentially a conversion of translational energy into vibrational motion associated with the ν_2 (H-C-H bending mode) and ν_4

(umbrella) vibrational modes in CH_4, and that tunnelling also plays a role in the final C-H bond breaking.

$S_0(CH_4)$ increases on the stepped Pt surface more than two orders of magnitude upon increasing the translational energy of the beam from 26 to 300 meV and are significantly higher than the values obtained by Luntz *et al.* [5, 28] and Oakes *et al.* [6] on Pt(111) also shown in **figure IV.6**. The curvature of S_0 versus E_i flattens around 700 meV, which indicates that the translational energy appears to couple less efficiently into the reaction coordinate. Above 850 meV, $S_0(CH_4)$ on Pt(533) (obtained by varying T_n) tends to the same value as $S_0(CH_4)$ on Pt(111) (corresponding to $T_n = 680$ K and a variable seeding mixture) [27].

The present results have utilised a method where the nozzle temperature is varied hence it does not avoid the variation of the internal energy which can be large, due to the variation of the vibrational energy. Luntz *et al.* [5, 28] studied the effect of the vibrational energy by performing experiments at $T_s = 800$ K with the nozzle temperature constant at 300 K in one set of data and at 680 K in the other data set as seen in **figure IV.6**, only the seeding gas ratio was varied. A higher nozzle temperature results in noticeably higher value of S_0 at constant E_i. This is a consequence of enhanced dissociative sticking of vibrationally excited molecules which is characteristic of activation barriers with saddle points close to the exit channels [3, 28, 38]. Note that increasing $\mathbf{T_n}$ should also cause some rotational excitations, however since CH_4 is spherical these latter excitations are expected to play little role in the dissociation. In the present case the scatter in data points for S_0 on Pt(533) is larger than that associated with the different vibrational contribution to sticking. For example, at $E_i = 700$ meV $S_0(CH_4)$ is relatively insensitive to a nozzle temperature change of *ca.* 500 K for the H_2 and He seeded beams. The vibrational contributions are small compared to the difference in S_0 observed between Pt(111) and Pt(533) over a wide range of E_i and as a result we will disregard the small changes induced by vibrationally excited molecules, while Rettner *et al.* for CH_4 on W(110) [2] and Lee *et al.* for CH_4 on Ni(111) [38] reported a stronger increase in S_0 with incident vibrational energy for smaller T_n variation than 500 K.

IV.3.5 Influence of the (100) Steps on $S_0(CH_4)$

It has been found on Pt(111) that $S_0(CH_4)$ also depends on the surface temperature. At low energy (E_i = 420 meV), $S_0(T_s)$ follows an Arrhenius expression, whereas at higher energy (E_i = 1270 meV) $S_0(T_s)$ scales linearly [5, 28]. **Figure IV.7** shows the variation of the $S_0(CH_4)$ on Pt(533) with the surface temperature for $100 < T_s(K) < 1000$, at 5° from normal incidence. The incident kinetic energy was kept constant at E_i = 700 meV by seeding 1 % of CH_4 in 99 % of He at T_n = 810 K and also at E_i = 400 meV by seeding 2 % of CH_4 in 99 % of He at T_n = 465 K.

Thus, there is a clear surface temperature dependence of the initial dissociative sticking probability S_0. This dependence has also been observed in the case of CH_4 dissociation on Pt(111) by Luntz and co-workers [1, 5, 28] and by Oakes *et al.* [6] as well as in the case of CH_4 dissociation on Pt(110) by Walker [32].

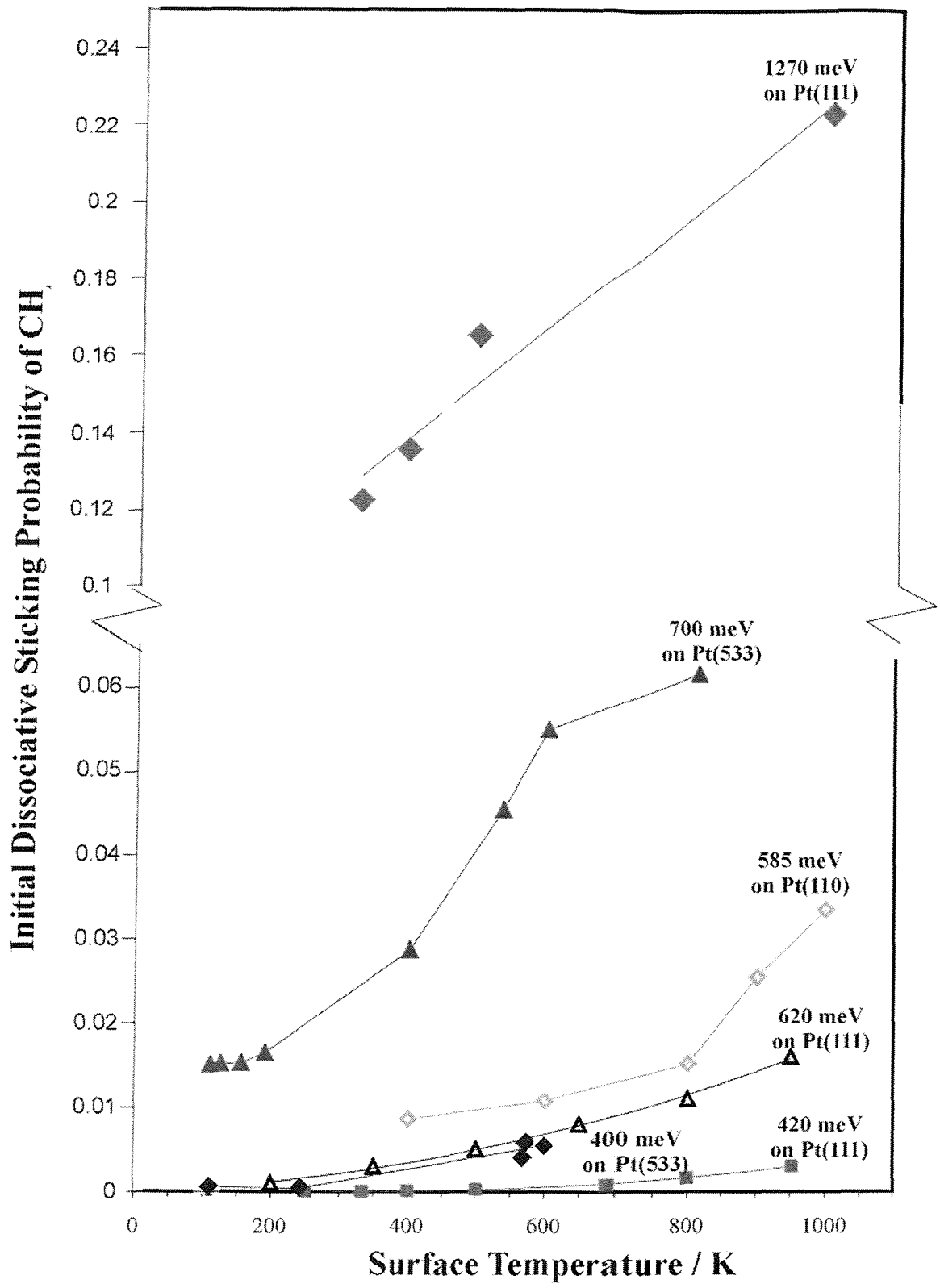

Figure IV.7: $S_0(CH_4)$ as a function of T_s for E_i at 400 (◆)and 700 meV (▲). The data were measured at 5° from the surface normal. Results obtained on Pt(111) by Luntz *et al.* [1] and on Pt(110) by Walker *et al.* [32] are also shown.

The T_s dependence of the sticking is not linear over the whole energy range and depends on E_i, hence in order to make a more quantitative comparison of measurements made on Pt(111) at $T_s = 800$ K [28] with the Pt(533) measurements at $T_s = 600$ K (**figure IV.6**) we estimated $S_0(CH_4)$ on Pt(111) at $T_s = 600$ K using a coefficient $f(E_i)$. This should avoid any distortion of the curve. For comparison we have plotted S_0 scaled linearly versus E_i in **figure IV.8**. The Pt(111) results have been multiplied by this coefficient to account for the difference in T_s. Moreover in order to take account geometrically of the lower proportion of (111) sites on the Pt(533) surface, the Pt(111) data have also been multiplied by 0.65. The resulting estimate of the contribution of the (111) terraces (fine line) has been subtracted from the Pt(533) data (solid circles) in order to establish the contribution of the (100) steps (open circles).The result is a lower energy onset for dissociative sticking of methane at the step sites, with an apparent saturation of the sticking above *ca.* 1000 meV. Following the procedure of Michelsen *et al.* [42], we have assumed that a Gaussian distribution of barrier heights is responsible for the activation at the step sites, and fitted the step contribution to sticking, $S_0^{100}[E_i]$, with the function:

$$S_0^{100}[E_i] = \frac{A}{2}\left(1 + erf\left(\frac{E_i - E_t}{w}\right)\right) \qquad (5)$$

The constants **A**, $\mathbf{E_t}$ and w have been varied to obtain the best fit curve (**figure IV.8**) with $\mathbf{E_t} = 570$ meV, the "sticking threshold" which is the energy at which the sticking probability reaches half of its limiting high energy value $\mathbf{A} = 0.054$, and $w = 250$ meV which determines the width of the sticking function. As a result of the procedures used to estimate the (111) terrace contribution, there is some associated error in the effective mean and spread of barrier heights represented in the associated constants, and the corrected sticking data on Pt(111) may have been overestimated. Consequently there may be a small increase in $S_0^{100}[E_i]$ for $E_i >> \mathbf{E_t}$. On the other hand, the observation that at high incident energies the dissociation probability reaches a saturation value smaller that unity is not very surprising and has been observed for other systems such as H_2 on Cu [41]. Moreover, theoretical work has shown that with increasing degrees of freedom considered in the computation, the saturation value of the dissociation probability decreases [43, 44]. Nevertheless, the results of the fit suggest that steps offer a low energetic bypass to dissociative chemisorption with a reduction of the barrier height of roughly 250-280 meV (**figure IV.8**). This channel most

likely saturates and at incident energies above 700 meV the observed increase in activity can be attributed to dissociation on the (111) terraces.

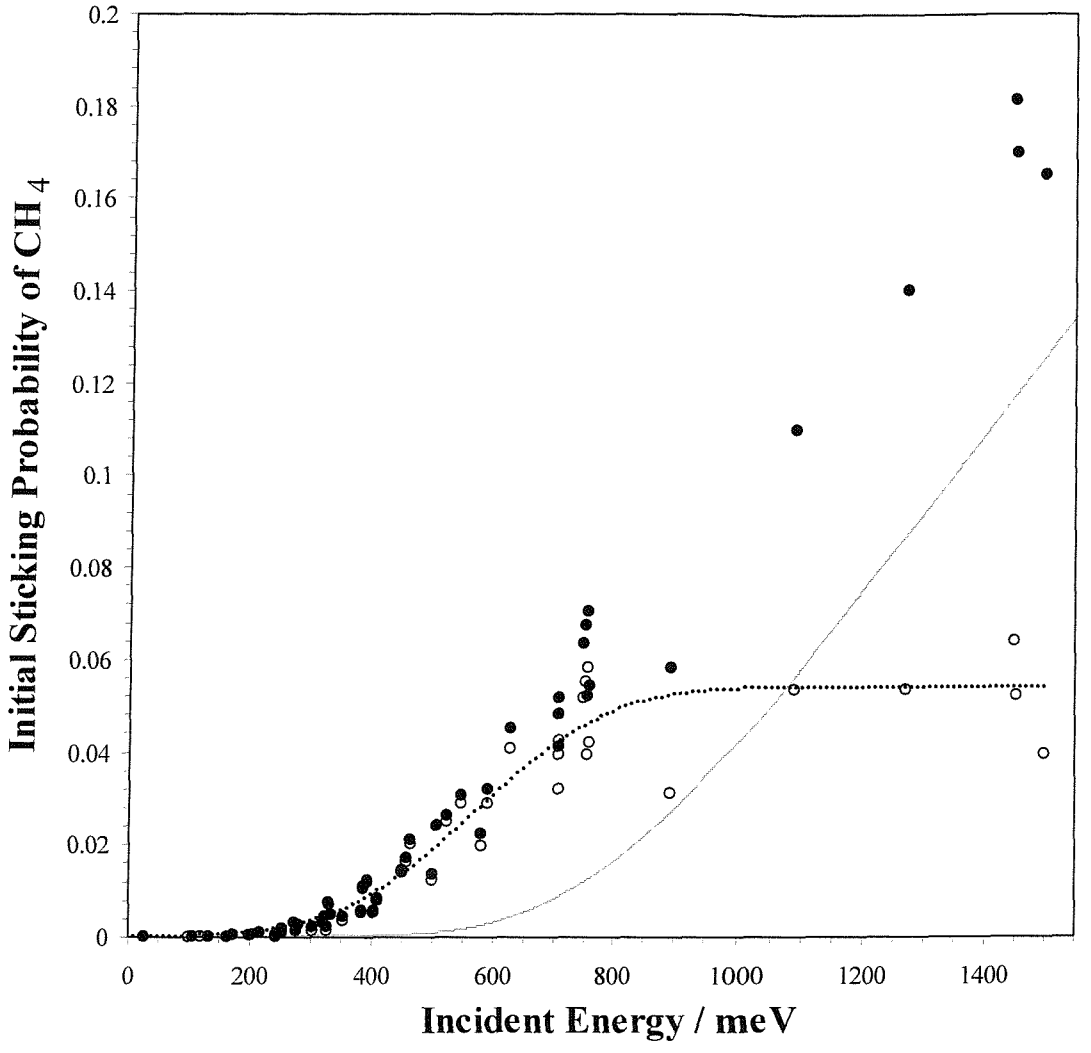

Figure IV.8: $S_0(CH_4)$ on Pt(533) at $T_s = 600$ K versus the translational energy plotted on a linear scale (●). The results from Luntz [28] are T_s and geometrically corrected (fine line). The dotted line indicates the fitted (100) step contribution $S_0^{100}[E_i]$ from the Δ(Pt(533) data – Pt(111) fit) values (○).

IV.3.6 Angular Dependence of $S_0(CH_4)$

The initial sticking probability of methane was measured directly by the reflection-detection technique as a function of incident angle at $E_i = 1450$ meV and $T_s = 600$ K (**figure IV.9**). This energy was chosen because from **figure IV.8** it is observed that the influence of the steps on the overall dissociative adsorption activity of CH_4 is constant at

approximately 0.055 above ~ 700 meV. The incident angle is defined as zero when impinging normal to the (533) plane and positive when impinging into the (100) step edges.

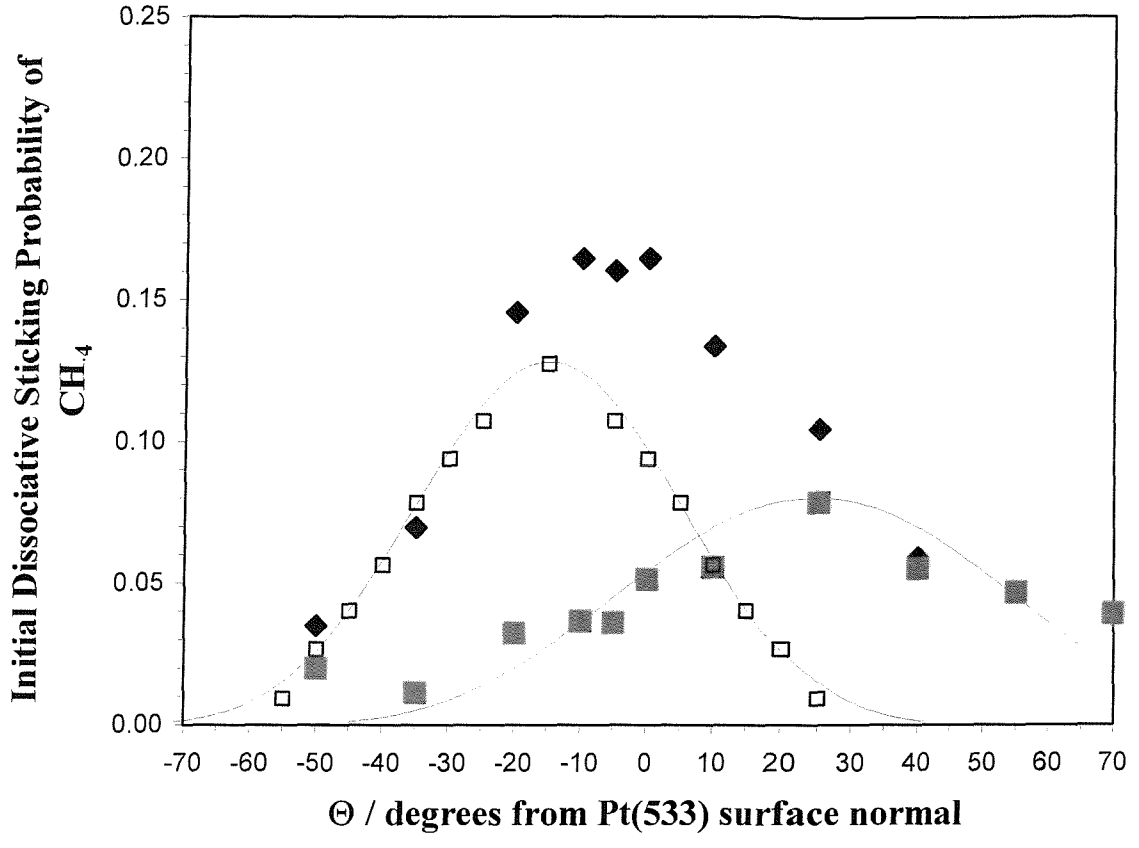

Figure IV.9: Angular dependency of $S_0(CH_4)$ at E_i = 1450 meV and T_s = 600 K (◆). The contribution from the terraces obtained from Schoofs data (□) at 985 meV (×0.72) is indicated by a plane line [45]. The contribution of the steps (■) is also indicated by a plain line.

At high energies the angular dependency of S_0 should show a sharp $\cos^{n-1}\Theta_I$ distribution which peaks around the surface normal. Such a behaviour is expected by applying detailed balancing where the sticking process can be related to the recombinative desorption of $CH_3 + H \rightarrow CH_4$ [46]. The adsorption-desorption equilibrium yields a similar angular dependency for the desorbing flux $\boldsymbol{F}$ where F is proportional to $\cos^n\Theta_I$.

In fact, a relatively sharp distribution is observed which peaks at -5° from the surface normal which accounts for recombination occurring over an activation barrier [47]. This distribution can be fitted with a $\cos^{n-1}\Theta_I$ at negative angles, while at positive angles the non-$\cos^{n-1}\Theta_I$ tendency indicates the contribution of the steps. If one assumes that terraces and

steps act as two independent active surfaces one should be able to deconvolute the data into the sum of two $\cos^{n-1}\Theta_I$ distributions as described by the following:

$$S_0^{533}[\Theta_I] = A_{111}S_{0,0}^{111}\cos^{n_{111}-1}\left(\Theta_I - \theta_n^{111}\right) + A_{100}S_{0,0}^{100}\cos^{n_{100}-1}\left(\Theta_I - \theta_n^{100*}\right) \quad (6)$$

Where $\mathbf{A_{111}}$ and $\mathbf{A_{100}}$ are geometric correction factors for the catalytic active area seen by the molecular beam dependent on Θ_I, $S_{0,0}^{111}$ and $S_{0,0}^{100}$ are maximum sticking coefficients of terraces and steps with respect to the local surface normals θ_n^{111} and θ_n^{100*}. θ_n^{100*} is used as a fit parameter because due to the short length of the step edge a strict geometrically determined surface normal might not exist. To reduce the amount of fit parameters the angular dependencies of the (111) terraces has been obtained directly from the Pt(111) data from Schoofs *et al.* [45]. Note that Schoofs *et al.* performed their experiments at a surface temperature of 500 K and an energy of 985 meV, hence their results should also be multiplied by a factor $f(T_s, E_i, \text{geometry})$ Hence we obtain $\theta_n^{111} = -15$, $\mathbf{A_{111}} \times S_{0,0}^{111} \sim 0.13$ and $n_{111} \sim 8$. Inserting these known parameters into the previous equation, the parameters for the (100) steps can be obtained from a fit to the data in **figure IV.10**. Therefore the maximum of the step contribution corresponds to a sticking of $\mathbf{A_{100}} \times S_{0,0}^{100} \sim 0.08$ at an angle $\theta_n^{100*} = 25°$ compared to the Pt(533) plane normal. If fitted with a cosine function, the step contribution data would reveal a value of $n_{100} \sim 4$ smaller than for the terraces contribution which is in good agreement with the lower barrier height observed at the steps.

Note that the maximum sticking occurs at -5° which indicates that dissociation is most efficient for molecules which impinge nearly perpendicularly to the (533) surface normal. This behaviour suggests that step dissociation proceeds via a concerted interaction with two surface planes. For such an interaction one would expect a smaller barrier height because the surface provides an angular, instead of a flat, dissociation site which might be advantageous to attack the tetrahedral symmetry of the molecule. This picture is in agreement with the "splat"-model introduced by Lee *et al.* [38] which assumes that the dissociation of methane requires the deformation of the C-H bonds to allow the carbon atom to reach close contact to the surface. Note that this deformation was also introduced earlier on in the energy correlation diagram in **section IV.1.4**.

This geometric reasoning is in agreement with recent quantum calculations of nitrogen dissociation on Ru(0001) [26]. Rather different symmetries for the transition states at steps and terraces are found and the barrier height reduces by 900 meV! The authors attributed the decrease in barrier height at the step partly to the fact that the configuration of the transition state at the step comprises of an additional Ru-atom. This lowers repulsive adsorbate-adsorbate interactions caused by the two nitrogen atoms which compete for the surface atoms.

The concept of enhanced catalytic activity at defects has also been discussed in terms of the Brønsted-Polanyi relation [24]. Within this concept, the lowering of the barrier height is associated with a stronger bonding of reactants and products to the surface. Generally, due to the lower coordination numbers of step atoms, reactants and products are more strongly adsorbed.

The frequently observed rate enhancement associated with defects or steps has also been observed for methane on different Pd-surfaces [48]. The rate of dissociation increases in the order Pd(111)<Pd(311)<Pd(679) [49, 50]. However, no attempt was made to link the reaction to a specific site. In contrast to these observations, increasing the defect character of a Pt(111) surface by Ar-ion bombardment seems not to affect the dissociation probability at all [45]. The interpretation of this observation is difficult because defects induced by sputtering are very ill-defined and as experiments are performed at elevated temperatures reactive structures might disappear before they interact with methane molecules. Unfortunately, no molecular beam study of CH_4 dissociation on Pt(100) is available to our knowledge which rules out a direct comparison between the activity of a (100)-surface and of a (100)-step. Measurements on a Ni(111) [38] and Ni(100) [27] surfaces revealed that the more open (100)-structure substantially enhances the initial dissociative sticking probability. The sticking versus energy curve measured at similar conditions shifts $\approx$ 250 meV to lower energy for the more open surface. A smaller shift $\approx$ 150 meV) is observed between the direct dissociation channels on Ir(110) [31] and Ir(111) [30]. The energy differences, especially the ones for Ni, are in the order of the energy difference observed in our study. For these reasons, it is difficult to judge whether the Pt(533) steps offer a new low energetic route to

dissociation because the total reactivity could also consist of the Pt(111)- and Pt(100)-activities weighted by the ratio of the catalytically available surface areas.

IV.3.7 Dependence of $S_0(CH_4)$ on Surface Temperature

The data in **figure IV.10** account for the variations of the initial dissociative sticking of methane on Pt(533) surface. The impact conditions are identical to those of **figure IV.8** and the incident energy of the beam is controlled has seen before. It is evident from the plot that the dissociative adsorption is enhanced at elevated surface temperatures. The threshold energy is clearly shifted to lower energy.

A modest effect of T_s has also been observed on Pt(111) surface as shown in the present figure. Because of the limited overlap between the energy scales of our measurements and those on the Pt(111) surface, no attempt was made to quantitatively determine the step contribution to S_0. However, a comparison of the two curves by eye indicates a significant effect associated with the (100) steps, in fact the effect of thermal activation on the stepped surface is distinctly higher than on the flat surface.

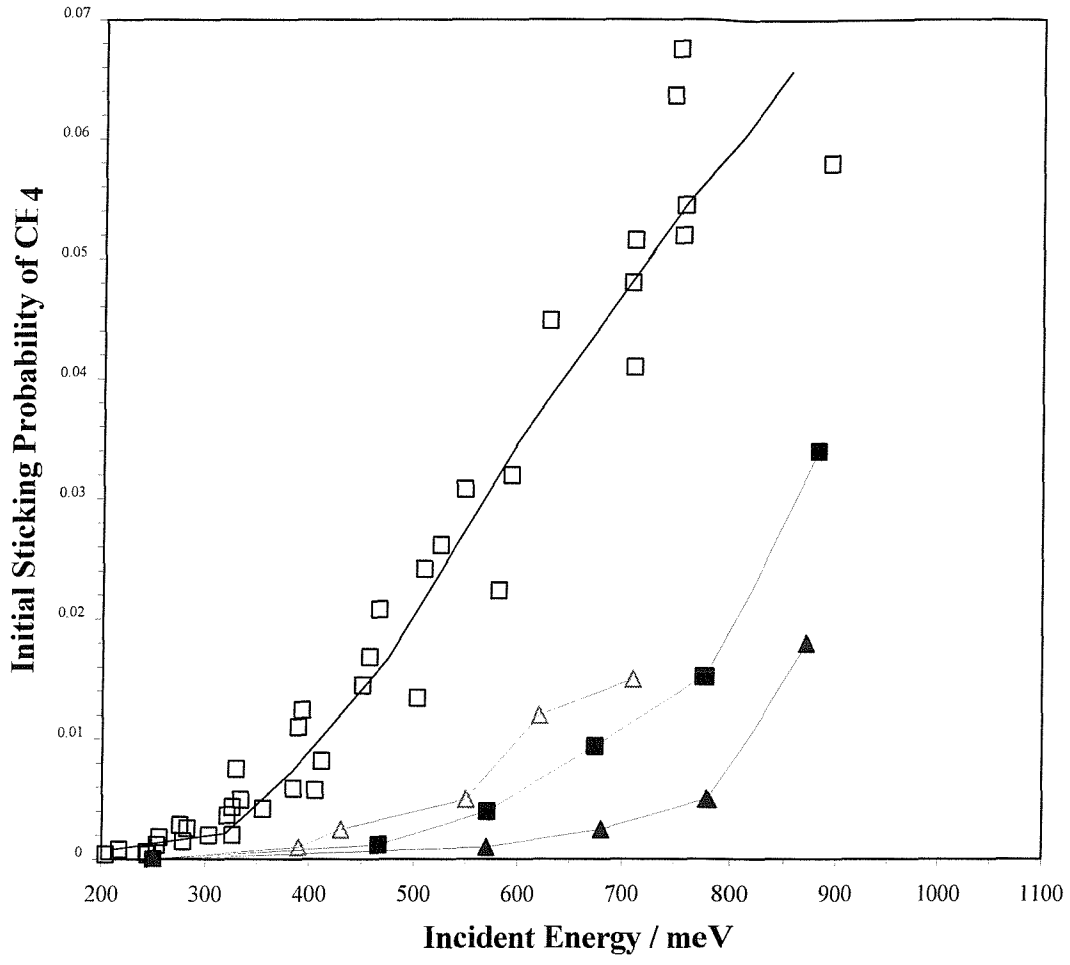

Figure IV.10: $S_0(CH_4)$ on Pt(533) versus E_i for T_s = 110 K (△) and 600 K (□). The results from Oakes *et al.* [6] for $S_0(CH_4)$ on Pt(111) for T_s = 150 (▲) and 550 K (■) are also shown.

Figure IV.11 shows the influence of T_s at a fixed incident energy of 700 meV. For a comparison the results of $S_0(CH_4)$ on a Pt(111) surface are depicted [1]. On Pt(533), whereas at temperatures below 150 K the sticking appears to be independent of T_s, between 200 and 600 K it increases substantially. In contrast the thermal activation on the Pt(111) surface is much lower.

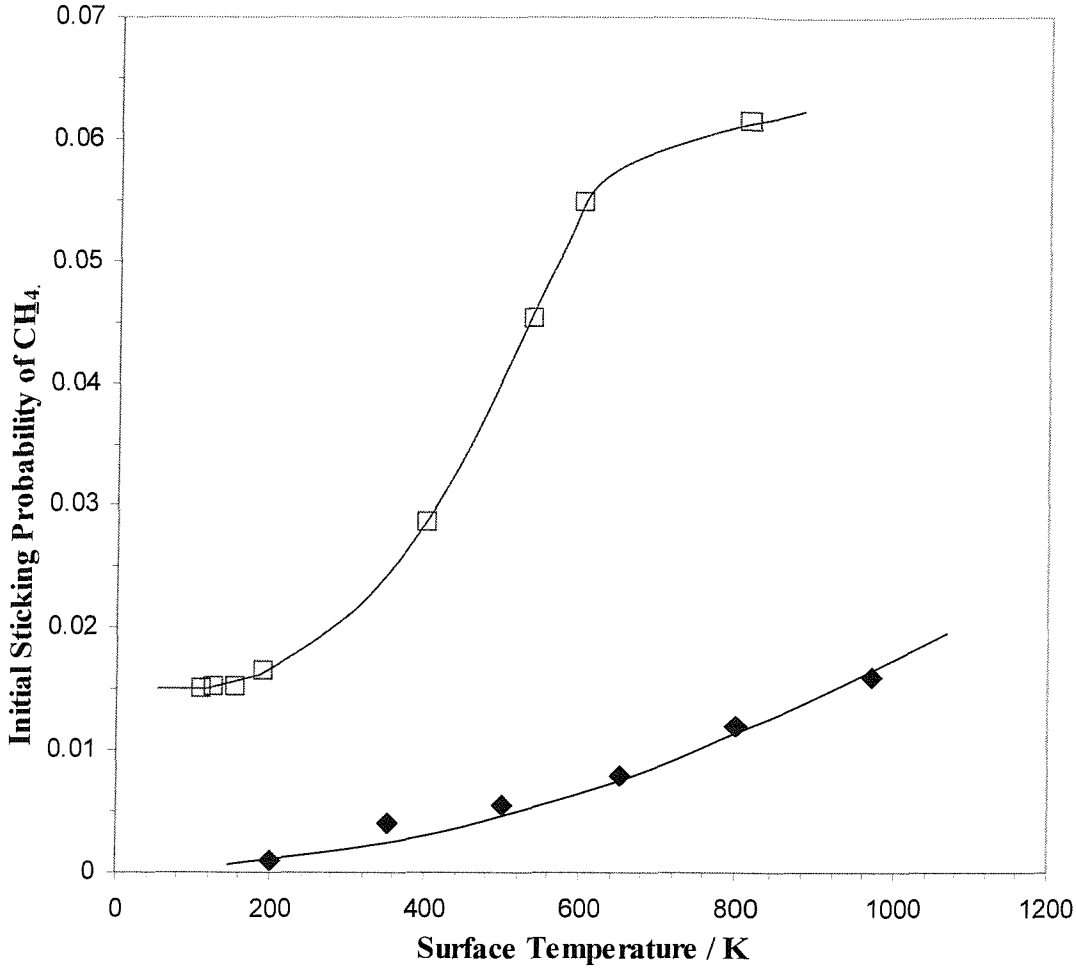

Figure IV.11: $S_0(CH_4)$ on Pt(533) versus T_s for $E_i = 700$ meV (□). The results from Luntz *et al.* [1] for $S_0(CH_4)$ on Pt(111) for $E_i = 620$ meV are also shown (◆).

Figure IV.12 shows the variation of the logarithm of $S_0(CH_4)$ with $1/T_s$ at $E_i = 700$ meV. For comparison the results from Luntz and Harris of $S_0(CH_4)$ on a Pt(111) surface, for $E_i = 420$, 620 and 1270 meV are also depicted [1, 5]. These data illustrate the non-Arrhenius behaviour of the sticking at energies below ~ 800 meV while at high energy, an Arrhenius dependence seems to exist, however notice the limited number of data points.

The influence of T_s becomes weaker as the incident energy E_i increases (if changes in $\ln(S_0)$ are considered). Hence in comparison to the Pt(533) data, the influence of T_s on S_0 at 620 meV on Pt(111) is overestimated and should even be lower at 700 meV.

Note that the slow disappearance of the T_s effect with increasing energy can be attributed to a surface "recoil" effect [48] which means that collision energy is adsorbed by the lattice. Consequently less energy is available to surmount the barrier.

Note that Schoofs *et al.* [45] did not demonstrate dependence of $S_0(CH_4)$ on T_s on Pt(111). Their data was taken at relatively high incident energy E_i = 705 meV where there is likely to be only a weak dependence on surface temperature which could not be observed due to the limited number of data points taken in that study.

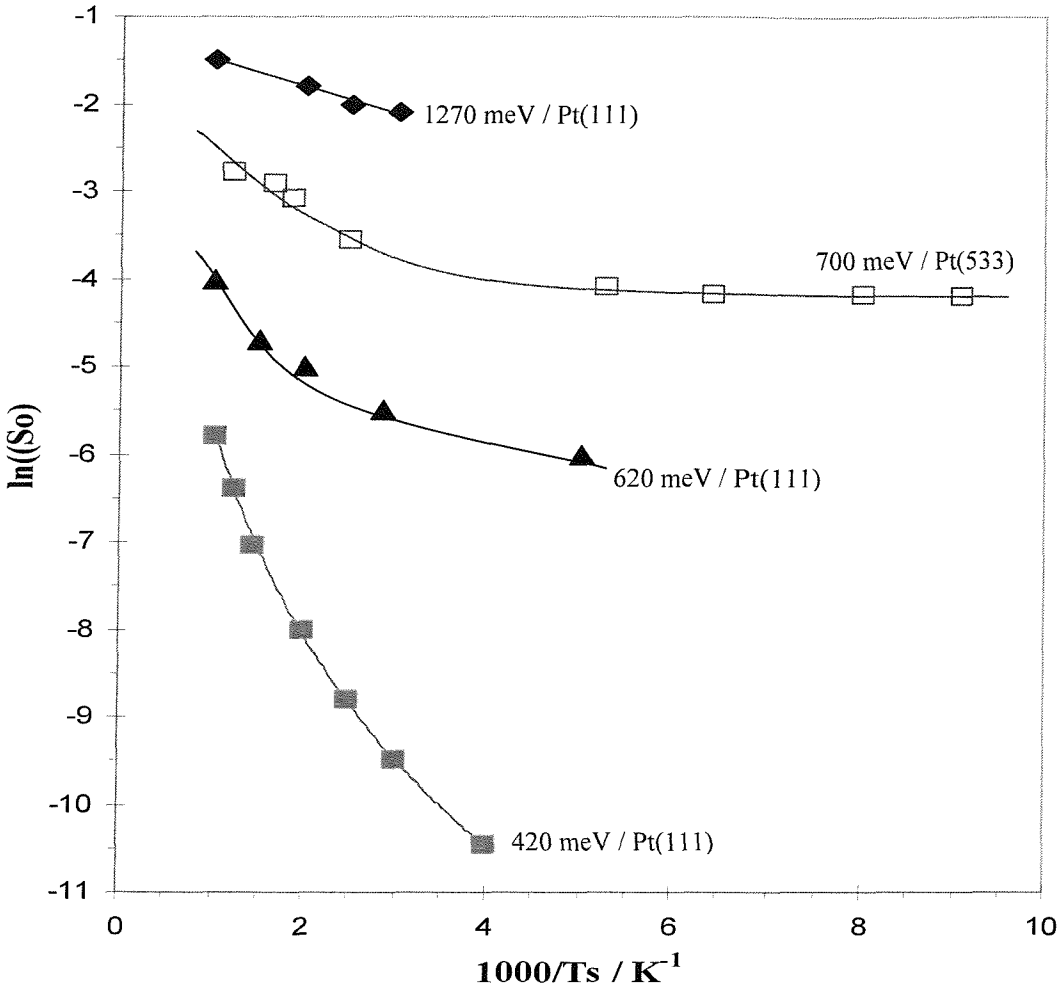

Figure IV.12: Ln(S_0) versus 1000 / T_s at E_i = 700 meV on Pt(533) (□). The results from Luntz *et al.* [1, 5] for $S_0(CH_4)$ on Pt(111) for E_i = 420 (■), 620 (▲) and 1270 meV (◆) are also shown.

The influence of T_s on dissociative chemisorption of methane has been treated theoretically by various models [5, 49-51]. One of the most recent models is the quantum dynamic model [1, 51-53] which was preceded by the thermally assisted tunnelling model developed by Harris and Luntz [5]. In this model the surface temperature is introduced by treating the surface as a single oscillator. The increase in activity with T_s can be explained in terms of a 'kick' from the surface cube which assists the molecule in surmounting the barrier. This theoretical attempt models T_s effects, occurring in dissociative chemisorption

of methane on various metal surfaces, reasonably well [52, 53]. Such a model is basically consistent with the tendency of **figure IV.11**. One striking observation of the surface temperature effect is that T_s has a considerably larger influence on the dissociative chemisorption probability at the (100)-steps than on the (111)-terraces. One possible explanation could be that because of the lower activation barrier at the (100)-step surface energy couples more efficiently into the reaction coordinate. Clearly the onset of thermal activation occurs at a temperature which is typically in the order of a Pt surface Debye-temperature, *e.g.* $T_D = 118$ K for Pt(100) [54] and $T_D = 230$ K for Pt(111) [55]. Therefore, the initial dissociation probability measured at 110 K reflects the efficiency of the (100)-step to introduce gas-phase energy into the reaction coordinate.

Another explanation could be the quality of the surface structure. So far we have assumed that the Pt(533)-surface is perfectly ordered at any temperature. Clearly, at higher temperature surface roughening will substantially influence the steps and terraces of the surface. A less ordered structure might increase the effective catalytic surface area attributed to the steps which would lead to a higher dissociation probability. Unfortunately, on the basis of these experiments we cannot estimate the magnitude of this effect.

In summary, the dynamics of dissociative adsorption of methane at Pt (100)-steps strongly resembles the behaviour on the (111)-terraces. The major differences are a substantially lower barrier height and a more pronounced surface temperature effect. In the energy and temperature range studied, no indication was found for a reaction mechanism other than the direct dissociation channel. The results suggest that the higher surface corrugation in combination with the step geometry is responsible for the lowering of the activation barrier.

IV.4 CONCLUSION

The dynamics of dissociative chemisorption of methane on Pt(533) have been studied using molecular beam techniques. A strong enhancement of dissociation with translational energy is seen. A comparison to the reactivity of Pt(111) reveals that dissociation of methane occurs already at lower translational energies.

The strong dependency of the initial sticking coefficient of CH_4 on surface temperature, also evidenced on Pt(111) [1, 21] and on Pt(110) [20] first appeared in direct conflict with the E_i dependence. The E_i dependence is consistent with a tunnelling mechanism in a direct channel to dissociation, whereas the T_s dependence implies that the dissociation takes place through an equilibrated precursor in an indirect channel. However, a theoretical model [30] has shown that these two dependencies are entirely compatible. This involves a **thermally assisted tunnelling** channel, caused by a coupling of the tunnel barrier to the lattice which dominates over most of the accessible temperature and energy range. This phenomena dominates the dissociation of a CH_4 molecule into a CH_3 radical and an H atom on stepped surfaces as on flat surfaces [5].

By correcting the data for the different catalytic areas 'seen' by the methane molecules, the energy dependence of the step associated dissociation probability has been determined. The dynamics of step enhanced dissociation indicates saturation above ~ 1000 meV. Dissociation is further activated by translational energy on the terraces. The influence of surface temperature is larger at the steps than on the terraces.

IV.5 REFERENCES

[1] Luntz A. C. and Harris J., *Surf. Sci.*, 258: 397, **1991**.

[2] Rettner C. T., Pfnur H. E., and Auerbach D. J., *Phys. Rev. Lett.*, 54: 2716, **1985**.

[3] Rettner C. T., Pfnur H. E., and Auerbach D. J., *J. Chem. Phys.*, 84: 4163, **1986**.

[4] Alstrup I., Chorkendorff I. and Ullmann S., *Surf. Sci.*, 264: 95, **1992**.

[5] Harris J., Simon J., Luntz A. C., Mullins C. B. and Rettner C. T., *Phys. Rev. Lett.*, 67: 652, **1991**.

[6] Oakes D. J., McCoustra M. R. S. and Chesters A., *Faraday Discuss.*, 96: 325, **1993**.

[7] Arumainayagam C. R., McMaster M. C., Schoofs G. R. and Madix R. J., *Surf. Sci.*, 222: 213, **1989**.

[8] Somorjai G. A., "*Introduction to surface chemistry and catalysis*". Wiley-Interscience, chap.7, p. 500, **1994**.

[9] Nørskov J. K., *Phys. Rev. B.* 26: 2875, **1982**.

[10] Nørskov J. K., *Rep. Prog. Phys.*, 53: 1253, **1990**.

[11] Nørskov J. K., *Prog. Surf. Sci.*, 38: 103, **1991**.

[12] Somorjai G. A., "*Introduction to surface chemistry and catalysis*". Wiley-Interscience, chap.6, p. 401, **1994**.

[13] Christmann K., Ertl G. and Pignet T., *Surf. Sci.*, 54: 365, **1976**.

[14] Somorjai G. A., "*Introduction to surface chemistry and catalysis*". Wiley-Interscience, chap.6, p. 450-452, **1994**.

[15] Anderson A. B., and Maloney J. J., *J. Phys. Chem.*, 92: 809, **1988**.

[16] Kua J. and Goddard III W. A., *J. Phys. Chem. B*, 102: 9492, **1998**.

[17] Jean Y., and Volatron F., "*Structure electronique des molecules*", Ediscience, International, Tom II, p. 40, **1994**.

[18] Rendulic K. D. and Winkler A., *Int. J. Modern Phys. B.*, 7: 941, **1989**.

[19] Steinruck H. P., Luger M., Winkler A. and Rendulic K. D., *Phys. Rev. B.*, 32: 5032, **1985**.

[20] Brønsted N., *Chem. Rev.*, 5: 231, **1928**.

[21] Evans M. G., and Polanyi N. P., *Trans. Faraday Soc.*, 34: 11, **1938**.

[22] Boudart M., Ertl G., Knözinger H. and Weitkamp J., "*Handbook of heterogeneous catalysis*", Wiley-VCH, Weiheim, p.1, **1997**.

[23] Hammer B., *Faraday Discuss.*, 110: 323, **1998**.

[24] Hammer B., *Surf. Sci.*, 459: 323, **2000**.

[25] Esch F., Baraldi A., Comelli C., Lizzit S., Kiskinova M., Cobden P. D., and Nieuwenhuys B. E., *J. Chem. Phys.*, 110: 4013, **1999**.

[26] Dahl S., Logadottir A., Egeberg R. C., Larsen J. H., Chorkendorff I., Törnqvist E. and Nørskov J. K., *Phys. Rev. Lett.*, 83: 1814, **1999**.

[27] Holmblad P. M., Wambach J., and Chorkendorff I., *J. Chem. Phys.*, 102: 8255, **1995**.

[28] Luntz A. C. and Bethune D. S., *J. Chem. Phys.*, 90: 1274, **1989**.

[29] Larsen J. H., Holmblad P. M., and Chorkendorff I., *J. Chem. Phys.*, 110: 2637, **1999**.

[30] Seets D. C., Reeves C. T., Ferguson B. A., Wheeler M. C., and Mullins C. B., *J. Chem. Phys.*, 107: 10229, **1997**.

[31] Seets D. C., Wheeler M. C., and Mullins C. B., *J. Chem. Phys.*, 107: 3986, **1997**.

[32] Walker A. V., and King D. A., *J. Chem. Phys.*, 112: 4739, **2000**.

[33] Butler D. A., PhD thesis, University of Southampton, **1994**.

[34] Poelsema B. Verheij L. K. and Comsa G., *Surf. Sci.*, 152/153: 496, **1985**.

[35] Strongin D. R., Carrazza J., Bare S. R. and Somorjai G. A., *J. Catal.*, 103: 213, **1987**.

[36] Walker A. V. and King D. A., *Phys. Rev. Lett.*, 82: 5156, **1999**.

[37] Arumainayagam C. R., McMaster M. C., Schoofs G. R. and Madix R. J., *Surf. Sci.*, 222: 213, **1989**.

[38] Lee M. B., Yang Q. Y. and Ceyer S. T., *J. Chem. Phys.*, 87: 2724, **1987**.

[39] King D. A. and Wells M. G., *Surf. Sci.*, 29: 454, **1972**.

[40] Valden M., Xiang N., Pere J. and Pessa M., *Appl. Surf. Sci.*, 99: 83, **1996**.

[41] Valden M., Xiang N., Pere J., and Pessa M., *Chem. Phys. Lett.*, 257: 289, **1996**.

[42] Michelsen H. A., and Auerbach D. J., *J. Chem. Phys.*, 94: 7502, **1991**.

[43] Kroes G. J., Baerends E. J., and Mowrey R. C., *J. Chem. Phys.*, 107: 3309, **1997**.

[44] Kroes G. J., Baerends E. J., and Mowrey R. C., *Phys. Rev. Lett.*, 78: 3583, **1997**.

[45] Schoofs G. R., Arumainayagam C. R., McMaster M. C. and Madix R. J., *Surf. Sci.*, 215: 1, **1989**.

[46] Rendulic K. D. and Winkler A., *Surf. Sci.*, 299/300: 261, **1994**.

[47] Van Willigen W., *Phys. Lett.*, 28: 80, **1968**.

[48] Hand M. and Harris J., *J. Chem. Phys.*, 92: 7610, **1990**.

[49] Ukraintsev V. A. and Harrison I., *J. Chem. Phys.*, 101: 1564, **1994**.

[50] Pasteur A. T., Dixon-Warren St J., Ge Q. and King D. A., *J. Chem. Phys.*, 106: 8896, **1997**.

[51] Luntz A. C. and Harris J., *J. Vac. Sci. Techn.*, 10: 2292, **1992**.

[52] Luntz A. C., *J. Chem. Phys.*, 102: 8264, **1995**.

[53] Carré M.-N. and Jackson B., *J. Chem. Phys.*, 108: 3722, **1998**.

[54] Lyon H. B. and Somorjai G. A., *J. Chem. Phys.*, 67: 3707, **1966**.

[55] Feder R., Pleyer H., Bauer P. and Muller N., *Surf. Sci.*, 109: 419, **1981**.

CHAPTER V: DYNAMICS AND KINETICS OF DISSOCIATIVE ADSORPTION OF HYDROGEN ON Pt(533)

V.1 INTRODUCTION

A number of catalyst systems have been used for hydrogenation reactions. A few are rather specific in application but the majority of these catalysts are generally useful for a variety of different reactions. The most common hydrogenation catalysts are nickel, platinum, palladium, rhodium and ruthenium.

An ever-increasing number of industries are finding important uses for large quantities of hydrogen of varying degrees of purity. H_2 is used to harden oils and fats in the food industry, to improve the octane number of gasoline, to produce synthetic gasoline and lubricating oils, to desulfurize hydrocarbon materials in the petroleum industry, and to provide reducing atmospheres in the heat treatment of metals. Hydrogen is, in particular, an essential component in catalytic synthesis, *e.g.* that of ammonia on iron-based catalysts:

$$3\ H_2 + N_2 \rightarrow 2\ NH_3 \qquad (1)$$

the methanol production on copper-based catalysts:

$$CO + 2\ H_2 \rightarrow CH_3OH \qquad (2)$$

$$CO_2 + 3\ H_2 \rightarrow CH_3OH + H_2O \qquad (3)$$

and the production of higher-molecular-weight hydrocarbons over iron or ruthenium surfaces:

$$2\ CO + 4\ H_2 \xleftarrow[\text{At } 550 < T_s(K) < 650]{\text{Fe catalyser, P = 6 atm, } C_3H_6} C_2H_4(C_3H_6) + 2\ H_2O \qquad (4)$$

$$x\ CO + y\ H_2 \xleftarrow[\text{At } 550 < T_s(K) < 650]{\text{Fe catalyser, } C_2H_4\ (C_3H_6)} C_{5\text{-}9}H_{12\text{-}20} + 2\ H_2O \qquad (5)$$

Smaller uses for H_2 are found in the electric lamp industry, for lead burning in chemical plants with oxygen, with acetylene in the cutting and welding of metals, and as a fuel in rockets and guided missiles [1]. Thus, it has been relevant to observe the dynamical interaction of H_2 with several metal surfaces such as copper Cu(110) [2], iron Fe(110) [3], tungsten W(100) [4], nickel Ni(111), Ni(997), Ni(110) [5] and platinum Pt(111) [6]. The relative simplicity of the hydrogen molecule made possible the study and the interpretation of the dynamical parameters of its adsorption and desorption on all these sample surfaces.

V.1.1 Adsorbate-Substrate Bonds

Christmann *et al.* [7] showed that transition metals, such as Ni or Pt, are unique in the fact that their d-band is mixed with the s and p electronic states therefore providing a large concentration of low energy electronic states and electron vacancy states. This is ideal for catalysis because of the multiplicity of degenerate electronic states that can readily donate or accept electrons to and from adsorbed species, which lead to the formation of a proper surface chemical bond. In the case of H_2 chemisorption, Harris *et al.* [8] showed that these metal states serve as sinks for the s electrons of H_2.

Hammer and Norskov [9] performed a theoretical approach, based on density functional theory (DFT) total energy method, to study the dissociation of H_2 on Pt(111), Cu(111), Al(111) and $Cu_3Pt(111)$. This method first allows the hydrogen molecular orbitals to mix with the metal sp orbitals which has the effect of both broadening and lowering the H_2 orbital energy. These orbitals then react with the 5d-band of the metal producing some bonding σ_u^*-d and anti-bonding σ_g-d interactions. The σ_u^*-d is relatively low in energy and therefore stabilises the attraction between H_2 and Pt. Moreover, the σ_g-d is pushed in energy above the Fermi level and consequently is emptied, therefore resulting in an attractive interaction. In comparison, the 3d band of Cu which does not extend as much as the 5d of Pt, leads to a weaker coupling with the H_2 orbitals, therefore the bonding interaction σ_u^*-d is higher in energy, resulting in a weaker attraction between H_2 and Cu. Moreover, the σ_g-d interaction is lower than the Fermi level, therefore it is filled with electrons which results in a repulsive interaction.

Thus, because of the strength of the bonds between the platinum atoms and the H_2 molecules, Pt is employed for hydrogenation on a large scale in the chemical and petroleum-refining industries. It is the most important material for heterogeneous catalysis of hydrogenation reactions.

V.1.2 Dissociative Adsorption of H_2

Chemical reactions at surfaces represent the interaction of a system with a limited number of degrees of freedom (the molecule) with the half-infinite solid which possesses in principle an infinite number of degrees of freedom. During the dissociative adsorption of H_2 on a metal surface, there is little energy transfer to the substrate phonons due to the large mass mismatch. Thus the crucial process in the understanding of the dissociation is the conversion of the kinetic and internal energy of the molecule into the translational energy of the atoms relative to each other, the subsequent energy dissipation to the solid is not relevant for the dissociation. Hence the loss of translational energy through the non-adiabatic coupling to electronic excitation (more particularly the electron-hole pair) has been suggested to be an important trapping mechanism particularly for light molecules [10, 11].

Depending on the height of the potential energy surface barrier, the dissociative adsorption of H_2 at the surface can occur via a direct or an indirect channel. The direct channel involves the dissociation of the molecule during the period of the initial surface collision, and is the most accessible dynamically, it is evidenced by the initial sticking probability increasing linearly with the translational energy. The adsorption can be activated, such as for H_2 adsorbing on Cu which features a large barrier in the order of 1 eV [12, 13]. The adsorption can also be non-activated such as for H_2 on Ni [5,14] and Pt [6]. When the potential energy surface presents too high a barrier for direct dissociation to take place, the molecule can take the route of the indirect channel. In this case, it is trapped into a precursor state during the initial collision, which is fully accommodated at the surface and therefore dependent on the surface temperature. Dissociation takes place subsequently, depending upon partition between desorption and dissociation [15]. In this last case, increasing the translational energy increases the probability of inelastic or elastic scattering,

lowering the sticking probability. This is the case for H_2 on Pd(100) [16], Pd(110) and Pd(111) [17], W(111) [18] and W(100) [4,18,19]. Steering of molecules in a direct channel has also been suggested as an explanation for the sticking behaviour of H_2 on W(100) [20-23] and on Pd(100) [24-27]. It has been pointed out, however that it does not account for all the experimental observations for H_2 dissociative adsorption on W [4, 28] and on Pt [29].

V.1.3 Structural Effects

The surface structure of a transition metal catalyst can also play a key role in the interaction with H_2. In fact, the enhanced reactivity of polycrystalline thin film surfaces for H_2 dissociation over that of the single crystal surfaces was soon noticed by Bernasek *et al.* [30], who attributed it to the presence of step and defect sites.

The identification of the **active sites** on the surface of a catalyst has become one of the important goals of research in surface chemistry. The concept of special "active sites" associated with low-coordinated surface atoms was introduced as early as 1925 by Taylor [31]. Several authors established that rough surfaces with vacancies, adatoms, steps and kinks are much more chemically active than flat surfaces at a given gas temperature. Steps and defects supply high binding energy sites for adsorbates, and the same local electronic structure can result in concomitant reductions in the activation energies to molecular dissociation, as will be seen in **part V.3**. If the reduction in activation energy is sufficient, an indirect channel to dissociation may be introduced by the presence of such sites, while terraces exhibit higher energy barriers only overcome at high E_i through a direct dissociation channel. The vicinal planes of flat surfaces are therefore proposed as useful model surfaces for high area supported metal catalysts which will expose a high density of such defect sites. The understanding of reactions, rather than adsorption, on such surfaces can be difficult, even in the case of perhaps the simplest reaction involving hydrogen dissociation on vicinal surfaces [5, 16, 29, 32-42].

In fact, it was observed by Rendulic *et al.* when comparing H_2 adsorption on Ni(997) and on Ni(111) [43], that structural imperfections such as steps and kinks seem to correspond to the "active sites" in surface reactions. Two channels to H_2 dissociation were found on Ni(997); a direct channel due to the H_2 dissociation on the (111) terraces dominating at high gas temperatures, and an indirect channel due to the H_2 dissociation on

the steps dominating at low gas temperatures. This first channel was also observed on flat Ni(111) while the second channel was observed by Steinruck *et al.* [5] on Ni(110). Christmann *et al.* [33] when comparing H_2 adsorption on Pt(997) and on flat Pt(111) also found a strong influence of the steps and the same channels as previously mentioned for nickel surfaces.

On Pt(533), which has four atom wide (111) terraces separated by a one atom (100) step, S_0 shows a decrease with incident translational energy up to 150 meV [29]. There is evidence that this behaviour is due to two processes, one of which shows a dependence on the surface temperature, T_s, and operates in the range 0-30 meV, the other being available up to 150 meV and being independent of T_s. The first of these channels is due to trapping into a conventional accommodated physisorbed precursor, which is possible within this very low energy regime even for such a badly mass-matched system. The second, surface temperature independent channel on Pt(533) is associated with the (100) steps. By comparison with H_2 dissociation on W(100) [4] and on W(100)-c(2×2)Cu [15, 28], where step sites are responsible for the majority of the process at low energy, this channel is suggested to be due to an unaccommodated precursor, and that steps are the active sites. The alternative proposal is that steering (translational and rotational) in a direct dissociation channel is responsible. Extending the model as applied to H_2 dissociation on W(100) [20, 22, 23] and Pd(100) [24-27] does not produce a satisfactory outcome, since the steering would have to be strong enough in the translational co-ordinate to allow molecules to impinge primarily on the step sites, *i.e.* over the width of the (111) terrace.

A series of H_2 sticking measurements have been carried out using supersonic molecular beams on an oxygen precovered Pt(533) surface [44]. The results are compared to those previously obtained on the clean Pt(533) [29] and on Pt(111) surfaces [6, 45], in order to establish the role of the steps sites on the overall dissociation dynamics, and to investigate the existence of other effects. Oxygen has been chosen since it decorates the (100) steps at low coverages, and is shown to block hydrogen dissociation at those sites. Previous studies have shown that at 300 K, oxygen saturates the available step sites before adsorbing at the terrace [46, 47]. However notice that there is reaction between hydrogen and the adsorbed oxygen to produce water at this temperature which will be detailed later on.

V.2 EXPERIMENTAL

The experiments were carried out in the UHV chamber described in **chapter II**. The platinum single crystal used in this study is a stepped Pt(533) crystal. The crystal was cleaned by annealing between experiments to 1200 K for 5 to 20 minutes depending on its degree of cleanliness, but necessitated other sort of treatments before a series of measurements as described previously in **chapter II**.

In order to obtain the initial dissociative sticking coefficient of H_2 on the platinum surface, $S_0(H_2)$, the gas-mixture was varied depending on the energy required. Thus argon, helium and neon, each with a purity of 99.9995 %, were used as seeding gases (**chapter II**), and H_2 was used as the seeded gas with a purity of 99.9995 % too (all BOC Gases).

The nozzle temperature was varied between 307 and 880 K. The sample was cooled by liquid nitrogen at all times and the temperature of the surface was held at a constant 128 K during the H_2 dosing by this cooling. The sample was held at 307 K during the measurement of $S_0(H_2)$ with incident energy by the King & Wells method [48].

The oxygen required to cover the steps was dosed from a capillary source placed a few centimetres from the face of the sample, and the oxygen had a purity of 99.998 %.

V.3 RESULTS AND DISCUSSION

V.3.1. Hydrogen Temperature Programmed Desorption

Using a molecular beam technique, a pure flow of hydrogen was dosed on to a platinum (533) crystal surface. The series of thermal desorption spectra taken up to saturation coverage at an exposure estimated as 72 L is reproduced in **figure V.1**.
The dosing was carried out with the nozzle at room temperature, on a surface at 128 K, using a 1.3 mm aperture resulting in a beam diameter at the sample of 3.25 mm. Therefore only ~ 11 % of the surface was hit by the beam. Subsequent thermal desorption was monitored by a quadrupole mass spectrometer measuring the resulting background pressure

rise in the reaction chamber. Use of a largest aperture (3 mm) gave similar results, showing that diffusion is negligible.

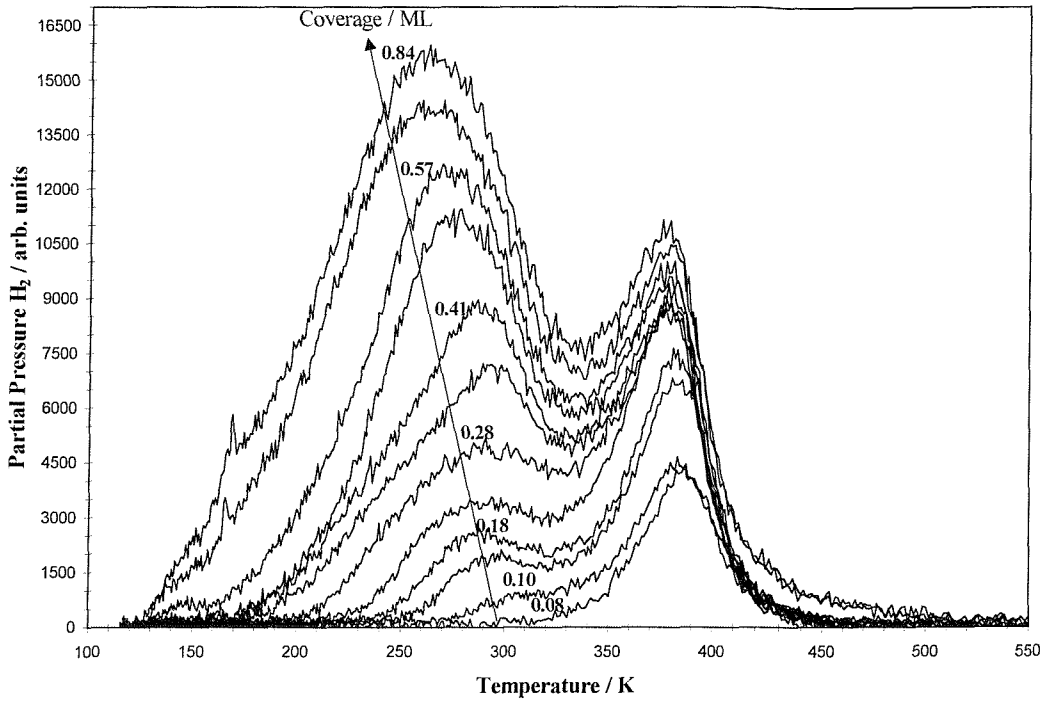

Figure V.1: TPD of Hydrogen from the Pt(533) surface at coverage $0.08 < \theta_H$ (ML) <0.84, obtained at T_s = 128 K and T_{nozz} = 307 K. The heating rate varied from 1 to 2 K s^{-1}.

With a small hydrogen coverage θ_H = 0.08 ML, only one peak is observed, at 380 K (note that the small variation of the heating rate does not show any obvious displacement of the maximum temperature). No such peak was observed in TPD at a heating rate of 10 K s^{-1} for hydrogen on Pt(111) [7], or on the platinum surface Pt(997) [33] which has a lower step density of Pt(111) step sites. However, Christmann *et al.* [7] showed that the hydrogen TPD from a Pt(111) surface bombarded with argon and not annealed, reveals a high temperature shoulder at 400 K, which was associated with hydrogen adsorbed at steps or defects induced by the bombardment. Therefore the 380 K peak present in **figure V.1** is attributed to the recombinative desorption of atomic hydrogen preferentially adsorbed on the (100) steps of Pt(533). The symmetry of this peak and the temperature at its maximum, which shifts slightly to lower temperature with increasing coverage, are suggestive of second order desorption kinetics [49]. Hence equation (6) can be solved to obtain the activation energy of

desorption (or binding energy), $\mathbf{E_{des}}$, for this latter peak. Considering a linear change of sample temperature with time ($T_s = T_0 + \frac{dT_s}{dt} \times t$):

$$\frac{E_{des}}{RT_{sp}^2} = \frac{2\theta\nu}{\frac{dT_s}{dt}} \times \exp\left(-\frac{E_{des}}{RT_{sp}}\right) \qquad (6)$$

With θ the coverage, **R** the gas constant in J mol^{-1}, $\mathbf{T_{sp}}$ the peak temperature and ν the rate constant (*i.e.* the number of translational degrees of freedom $\times \frac{1}{2}kT_{gas}$).

Hence:

$$\ln\left(\theta T_{sp}^2\right) = \ln\left(\frac{E_{des}}{2R\nu}\right) + \ln\left(\frac{dT_s}{dt}\right) + \frac{E_{des}}{RT_{sp}} \qquad (7)$$

$\ln\left(\theta T_{sp}^2\right)$ plotted against $\frac{1}{T_{sp}}$ gives a straight line (see **figure V.2**) which is characteristic of a second-order reaction with fixed activation energy, the latter is obtained from the slope $\frac{E_{des}}{R}$.

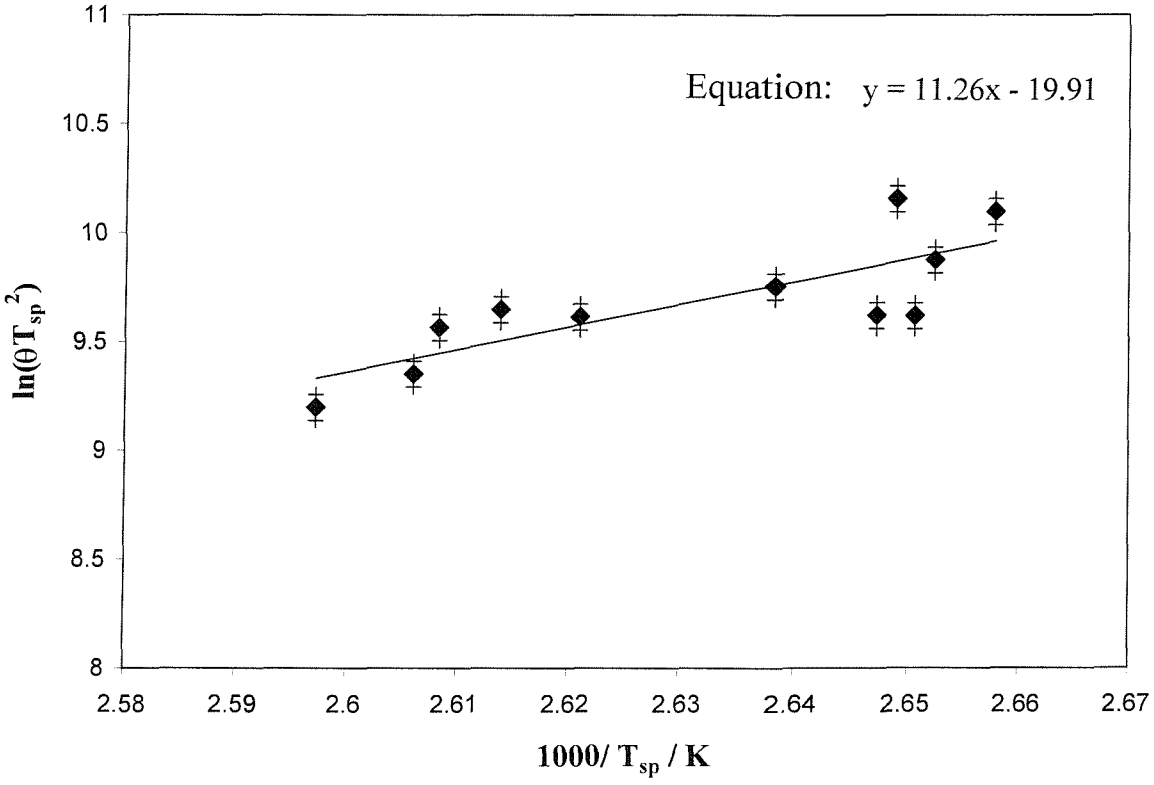

Figure V.2: $\ln\left(\theta T_{sp}^2\right)$ as a function of $\frac{1}{T_{sp}}$ for a second-order reaction.

Therefore $\mathbf{E_{des}}$ = 94 kJ mol^{-1}, which is in good agreement with the results of Hatzikos [50] for H_2 on Pt(100)-(1×1) of 93.85 kJ mol^{-1}and the results of Thomas [50] for H_2 on Pt(100)-(1×1) of 95.31 kJ mol^{-1}.

Hence ν the rate constant can be obtained by substitution of $\mathbf{E_{des}}$ in equation (6), thus $\nu = 5.4 \pm 1.5 \times 10^{12}$ s^{-1}.

When the coverage increases, a second peak, below 310 K, is observed which corresponds to the recombinative desorption of atomic hydrogen adsorbed on the terraces (111), as seen by Christmann [7] on Pt(111). This corresponds also to second order desorption kinetics as shown by Lu and Rye [52]. The energy of desorption of hydrogen atoms $\mathbf{E_{des}}$ on the (111) terraces of Pt(533) can also be estimated by a similar plot to **figure V.2** (see **figure V.3**).

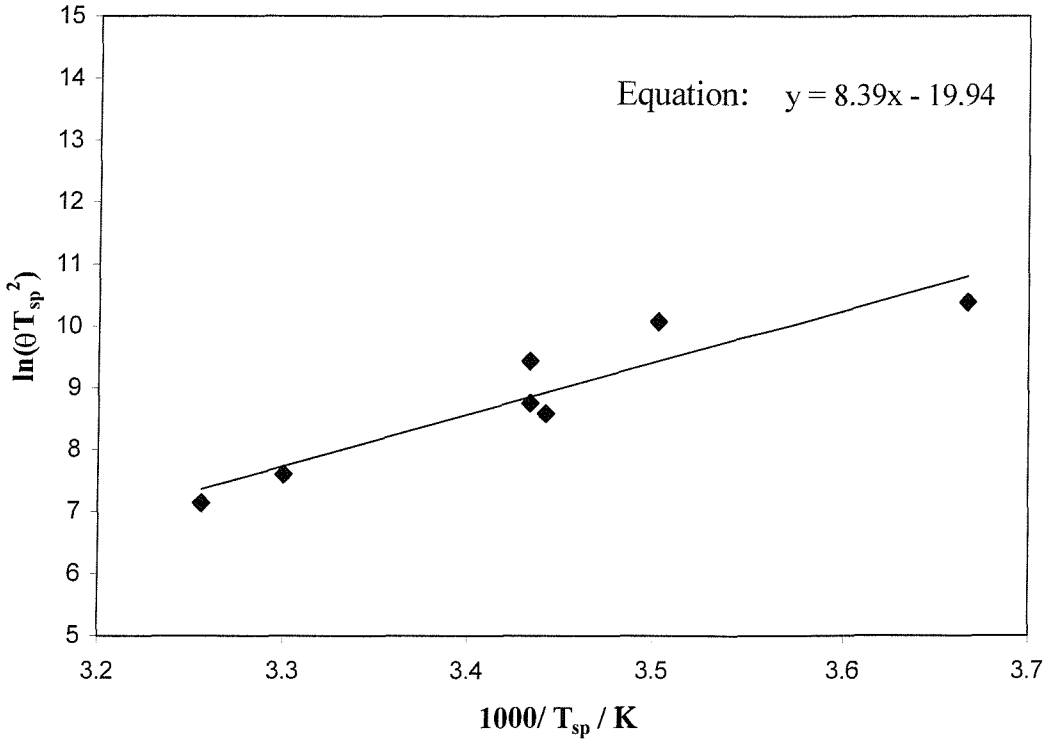

Figure V.3: $\ln\left(\theta T_{sp}^2\right)$ as a function of $\frac{1}{T_{sp}}$ for a second-order reaction.

Therefore $\mathbf{E_{des}}$ = 70 kJ mol^{-1}, which is in relatively good agreement with the data from Lu and Rye of 73.22 kJ mol^{-1} on Pt(111) [52]. And ν the rate constant is found around $\nu = 9 \pm 7 \times 10^{12}$ s^{-1}.

Brønsted, Evans and Polanyi [53, 54] established a linear dependence of the activation energy, ΔE_{act}, for an elementary reaction (such as the activation energy for the H-H bond cleavage on a metallic surface), and the adsorption energy of the products, ΔH_{ads}. They concluded that a larger ΔH_{ads} results in a smaller ΔE_{act}.

There appears to be a large group of reactions that fit this relation, notably the activation of NO [55] and N_2 [56]. In this last case Dahl *et al.* [56] performed some DFT calculations for N_2 adsorption on several metals surfaces, such as Fe, Mo, Pd, Cu, Ru, and Co, on flat and stepped surfaces.

Hence in the present case, the binding energy of hydrogen at (100) steps, directly related to ΔH_{ads}, being larger than the binding energy of hydrogen on the (111) terraces, results in a lower activation energy ΔE_{act} at these step sites. Therefore the steps are found to be the best reactive sites for H_2 activated adsorption.

The previous series of TPD spectra are useful to observe the evolution of the H_2 coverage with the H_2 exposure (**figure V.4**) and to calculate the saturation coverage of atomic hydrogen on Pt(533). Christmann and Ertl [33] showed that the amount of desorbing hydrogen atoms per cm^2, n_H, from a surface of area **A**, and gas temperature T_{gas}, could be evaluated for each specific hydrogen exposure from the area below the corresponding thermal desorption trace $\int pdt$. Using the effective hydrogen pumping speed of the vacuum system, S_{eff}, corresponding to the ratio V/τ where **V** is the volume of the vacuum chamber and τ the time constant for the evacuation of the gas. The amount of atomic hydrogen n_H can be calculated by equation (8):

$$n_H = 2 \times \left(\frac{S_{eff}}{A k_B T} \right) \times \int p dt \qquad (8)$$

With P_s the lowest limit of pressure attainable with the present system, C the volume to be exhausted, and S_{eff} the pumping speed of the system independent of the pressure **P** (which means that S_{eff} is large compared to the rate of desorption), then the plot of $\log(P-P_s)$ versus **t** (the time of pumping back down to the base pressure) is linear, hence the slope is given by equation (9):

$$\frac{\Delta \log(P - P_S)}{\Delta t} = \frac{S_{eff}}{2.303 \times C} \qquad (9)$$

The volume of the chamber ***C*** has been estimated to be 0.107 m^3. Hence $\mathbf{S_{eff}}$ was estimated to be 0.234 $m^3 s^{-1}$.

The area **A** was calculated to be 0.785×10^{-4} m^2 and T = 300 K.

The number of platinum atoms per cm^2 on the Pt(533) surface, $\mathbf{n_{Pt}}$, calculated geometrically is:

$$n_{Pt} = 1.462 \times 10^{15} \; at \; cm^{-2}$$

Defining the coverage θ as the number of hydrogen atoms per platinum atoms in the surface:

$$\theta = \frac{n_H}{n_{Pt}} \qquad (10)$$

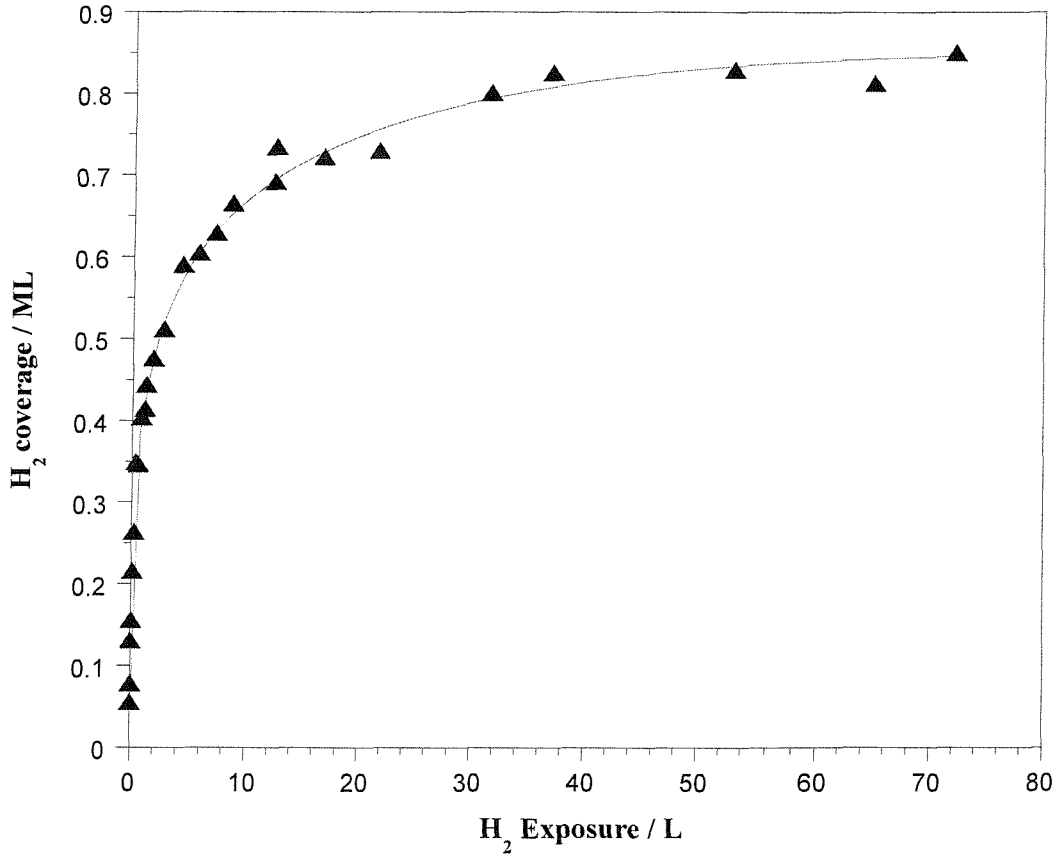

Figure V.4: H_2 coverage up to saturation as a function of exposure at normal incidence, using a pure beam of hydrogen, E_i = 95 meV and T_s = 115 K. A guide line is also shown.

The saturation coverage was then estimated to be 0.84 ± 0.05 ML at $T_s = 128$ K, which is similar to that calculated by Christmann *et al.* [33, 7] previously estimated it to be 0.8 ± 0.05 ML on Pt(111) and Pt(997) at $T_s = 150$ K.

Previous results showed that hydrogen adsorbs on the steps or defects until their total saturation, then it starts to adsorb on the terraces. Therefore it should be expected that above 0.10 ML the area of the TPD peak corresponding to H_2 adsorbed on the (100) steps at 380 K should stay constant while the (111) terraces peak should grow. However, from **figure V.1** it seems that the 380 K peak grows slightly too above 0.10 ML.

One goal of this study is to estimate the influence of the steps on the total hydrogen coverage. Thus, after a deconvolution of the TPD peaks from **figure V.1**, it was found that at saturation, which necessitated an exposure of 72 L, the steps account for 21.6 ± 0.4 % of the total H_2 coverage (**figure V.5**). The (100) step peak saturates at a coverage of 0.18 ± 0.02 ML which corresponds to a filling of half of the four-fold sites at the (100) step edges with atomic hydrogen. It is likely that the hydrogen atoms occupy high coordination sites at the inside edge of the step on the basis of HREELS measurements which show a preference for three-fold hollow sites on the Pt(111) terrace [57]. This result is in good agreement with the equilibrium concentration of steps on the Pt(533) surface which was found to be 20 % of a monolayer according to the geometry of this surface -an alternate notation being Pt(S)-[4(111)×(100)] which indicates that the (111) terraces are 4-atom rows wide and separated by steps made up of (100) planes one-atom row high (see **figure IV.3 chapter IV**).

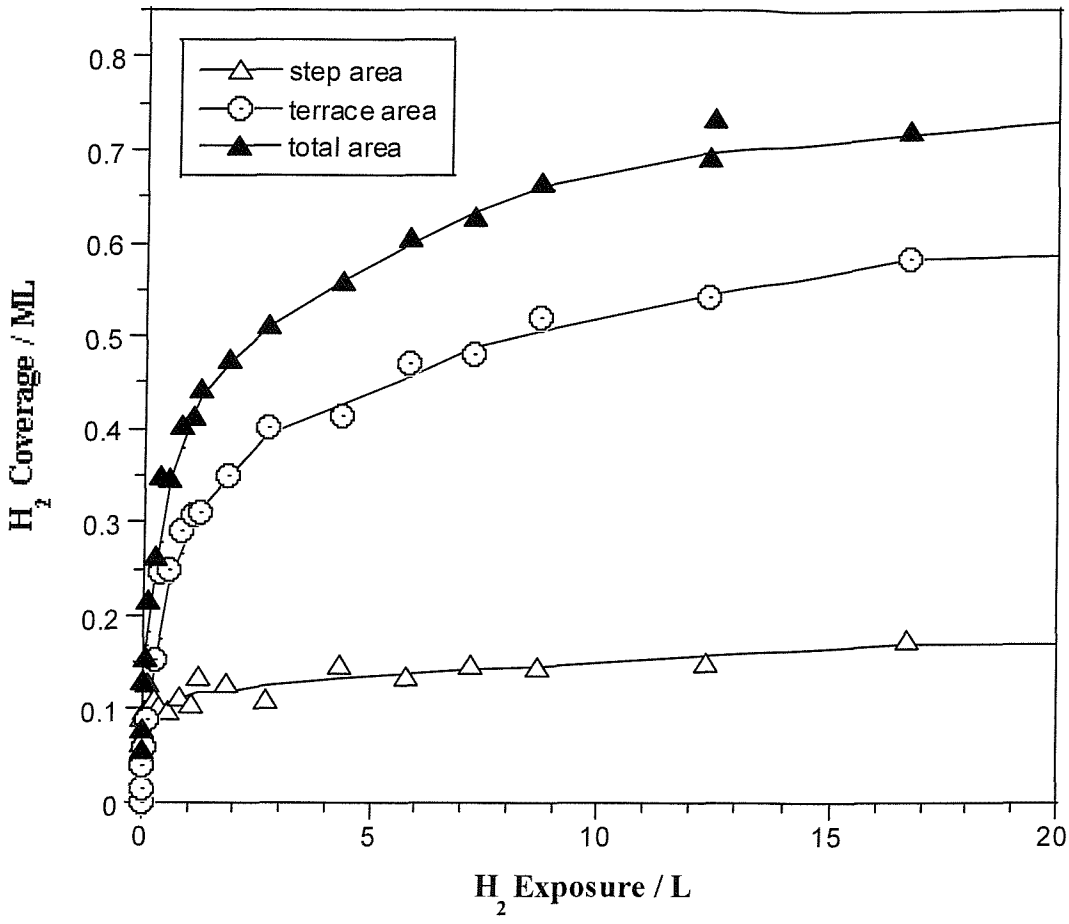

Figure V.5: H_2 coverage on the steps, the terraces and in total, as a function of exposure at normal incidence, using a pure beam of hydrogen, $E_i = 95$ meV and $T_s = 115$ K, the aperture used is 1.3 mm diameter. Guide lines for each set of data are shown.

V.3.2 King & Wells Method

As seen in **chapter III**, this method [48] permits a direct measurement of the initial dissociative sticking probability S_0 with a minimum calculable value of S_0 (see equation (11)) being around 5 %.

$$S_0 = (P_1-P_2)/((P_1-P_0)\times(1-F_d)) \qquad (11)$$

Figure V.6 shows a pressure-time profile for H_2 using the King & Wells method. The mixture used was 0.5 ml min^{-1} H_2 / 49.5 ml min^{-1} He, at a nozzle temperature of 304 K, giving an incident kinetic energy of 65.5 meV, calculated as explained in **chapter II**. The surface temperature was 306 K.

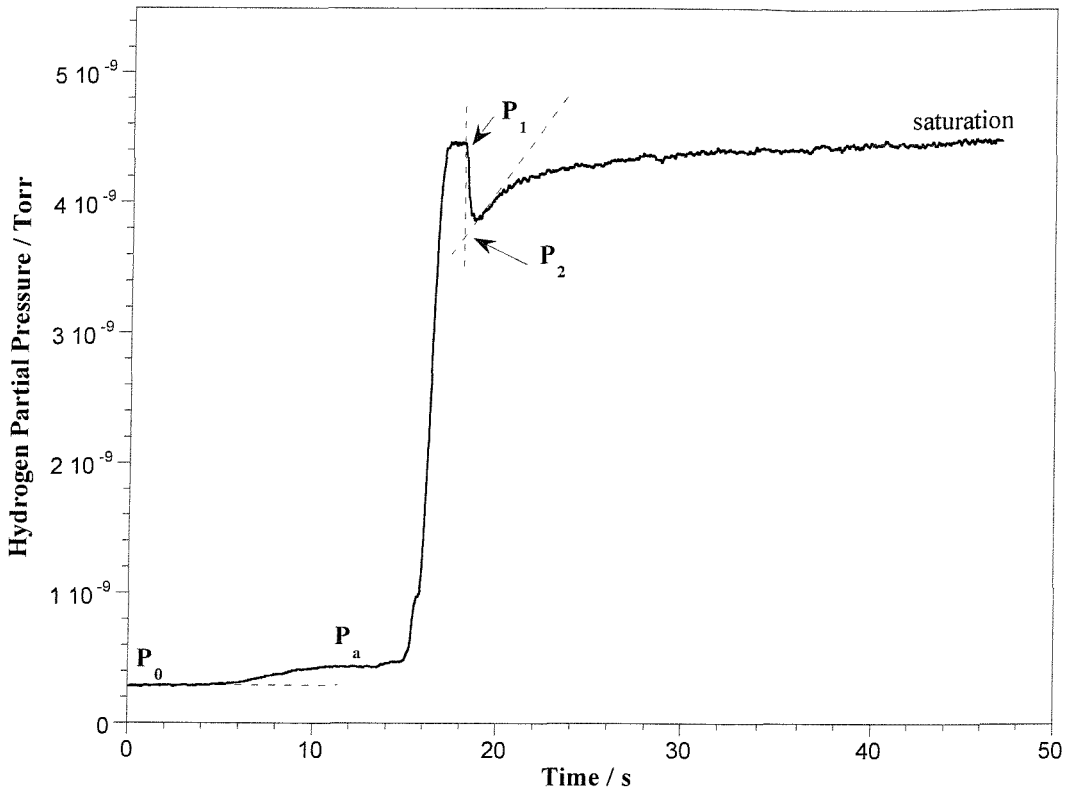

Figure V.6: Typical mass spectrometer response during sticking probability measurements of H_2 by the King & Wells method, T_s = 306 K and E_i = 65.5 meV.

V.3.3 Dependence of $S_0(H_2)$ on Incident Energy

Luntz *et al.* [6] and Samson *et al.* [45] found that with the direction of incidence normal to the surface, the S_0 of D_2 and H_2 on Pt(111) at T_s = 300 K is relatively small at low energy and increases steadily with E_i (**figure V.7**). They concluded that $S_0(H_2)$ and $S_0(D_2)$ can in no way be dominated by steps or defects, and must reflect a direct dissociation of D_2 and H_2 on the terraces of the Pt(111) surface. Thus the hypothesis proposed by Poelsema *et al.* [34] that H_2 dissociates only at steps and other surface defects on Pt(111), which led these authors to conclude that a highly mobile molecular bound state carries the molecule from the adsorption site to the dissociation site, has been dismissed. In fact the dissociation of H_2 molecules happens via a non-activated (where the energy barrier in the reaction coordinate is under the zero-point energy level, the consequence is a non-dependence of the S_0 with the surface temperature) direct dissociation (where the molecules dissociate at first impact with the surface) channel. For Pt(111), a steady increase in sticking probability with E_i is observed reflecting dissociation over a distribution of barriers corresponding to different collision geometries, molecular orientations, and sites perhaps in the dimensions of

the surface unit cell [45]. Notice that neither Luntz nor Samson measured the $S_0(H_2)$ on Pt(111) at E_i under 40 meV, therefore the behaviour of the initial sticking probability at low energy is not none.

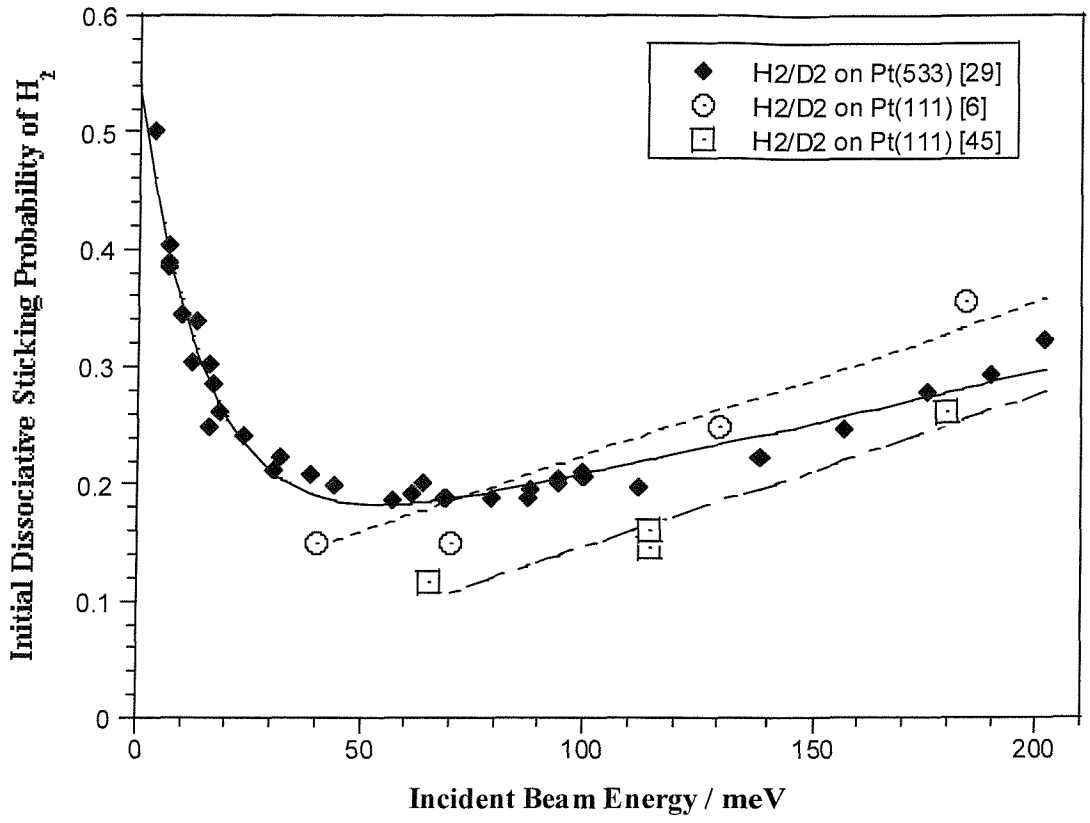

Figure V.7: Initial sticking probability of D_2 and H_2 on clean Pt(111) by Luntz *et al.* [6] (opened circles) and by Samson *et al.* [45] (opened squares) and on clean Pt(533) by Gee *et al.* [29] (filled diamonds), as a function of incident beam energy, T_s = 300 K, $\Theta_i = 0°$. Lines of best fit of each set of data are shown.

The results obtained by Gee *et al.* [29] on the $S_0(H_2)$ and $S_0(D_2)$ on a stepped Pt(533) surface are also presented on **figure V.7**. They were measured by the reflection/adsorption technique, in the energy range 6.4 – 200 meV. Beam energies were controlled by a combination of nozzle temperature and seeding and the temperature of the surface was held at 300 K during all the measurements.

Notice that some sticking measurements were performed at the same beam energy E_i but at different nozzle temperatures, therefore using different seeded gas mixtures. No noticeable difference was observed indicating no significant internal state dependence on the sticking probability under these conditions. Moreover, results for both D_2 and H_2 were obtained in the region $0 < E_i$ (meV) < 100 and indicated that there is no (or little) apparent

isotope effect on dissociative sticking at these energies. Any mechanism requiring energy dissipation and accommodated molecular trapping should lead to some isotope effect in the trapping probability. It appears therefore that it is translational energy that is dominating the dissociative sticking probability at these energies.

Above 100 meV the trend presented by Gee is similar to that of the Samson and Luntz data, thus it is believed to correspond to the dissociation of H_2/D_2 on the 4 atom wide (111) terraces of Pt(533) through the same channel as evidenced on Pt(111). Below 100 meV a completely different behaviour is encountered which was associated with the presence of the (100) steps on the Pt(533) surface. The falling of $S_0(H_2)$ on Pt(533) with increasing E_i is a sign of hydrogen molecular trapping into a precursor state during the initial collision (where the potential energy surface presents a too high barrier for direct dissociation to take place). The molecules interaction is very weak, thus the increase of the incident energy of the molecules will lead to less molecules accommodating on the surface and finding a proper site to dissociate, and more will directly scatter back into the gas phase. This is an indirect channel and it requires a precursor with sufficient lifetime and mobility to locate such sites, although full accommodation of this species would not be a pre-requisite. Another explanation for the observed tendency of $S_0(H_2)$ to decrease with increasing E_i under 100 meV is the steering. This phenomenon has been suggested by White *et al.* on the basis of an ab-initio potential for the $H_2/W(100)$ system [22]. There are some points of impact on the surface and some molecular orientations for which the molecule sees an energy barrier, while for other points of impact and orientations there is no barrier. These are just the conditions for which steering should play an important role. At the lowest incident energies the modest (mainly attraction) forces experienced by the free hydrogen molecule are strong enough to permit its slow reorientation and translation across the tungsten surface in order to find a favourable site for dissociation. As the E_i increases, the forces tending to move the molecule will act for a too short time to significantly alter its position or orientation, hence the steering becomes less effective, thus the $S_0(H_2)$ decreases. The steering is largely a direct process thus there is no molecular precursor state involved. Whereas this second explanation may seem suitable for the $H_2/W(100)$ system although this has been disputed [4], it is unlikely to be for the $H_2/Pt(533)$ system because it would require the hydrogen to translate all along the 4-atoms wide (111) terraces before reaching the steps - where the dissociation was proved to occur - which is unlikely. Gee *et al.* [29] also

concluded on the existence of another component (surface temperature dependent) of the indirect channel at low energies, which will be discussed later.

Thus, at low E_i the adsorption is mostly dominated by the indirect channel, whereas at high E_i it is mostly dominated by the non-activated direct channel. Thus:

$$S_0 = S_0^{a}(E_i) * n^{a} + S_0^{a1}(E_i) * n_n^{a1} + S_0^{a2}(E_i, T_s) * n_n^{a2} \qquad (12)$$

where $\mathbf{S_0^{a}}$ is the initial sticking probability of hydrogen on activated sites, $\mathbf{S_0^{a1}}$ is the initial sticking probability of hydrogen on non-activated sites non-surface temperature dependent, $\mathbf{S_0^{a2}}$ is the initial sticking probability of hydrogen on non-activated sites surface temperature dependent, and $\mathbf{n^{a}}$, $\mathbf{n_n^{a1}}$ and $\mathbf{n_n^{a2}}$ are the respective relative concentrations of these sites (with $n^{a} + n_n^{a1} + n_n^{a2} = 1$).

V.3.4 Consequences of Pre-adsorbed Oxygen on the $S_0(H_2)$

The major interest in our study is to demonstrate whether or not the difference between the initial dissociative sticking probability of H_2 on a flat Pt(111) surface and on a stepped Pt(533) surface, is due to the effect of the steps as Christmann and Ertl [33], Rendulic and Winkler [43] and Gee [29] suggested. Because Pt(533) is a stepped (111) surface, it was decided to block the (100) steps to deactivate them whilst leaving the (111) terraces virtually unaffected. Thus, this precovered platinum surface could be considered a "virtual" Pt(111) surface. In order to understand the choice of oxygen to block the steps, one has to consider the effect of contamination by a dopant and some of the results obtained in the past.

It is well accepted that traces quantities of electropositive or electronegative adsorbates can dramatically influence the catalytic properties of metals through long-range electronic effects. Many studies, both experimental and theoretical, have shown that electronegative species such as Cl, S, O and P tend to poison surface reactions, while electropositive species such as Na, K and Cs often promote these reactions. Thus, extended electronic effects can conclude to a modification of catalytic reactions. Notice that these pre-adsorbates can also just induce a steric blocking of the dissociation sites. Identifying the

conditions under which local or non-local effects will dominate is critical to understand the influence of adsorbates on surface reactions [58].

Winkler and Rendulic [59] found that in the case of the densily packed Ni(111) surface, the initial dissociative sticking probability of hydrogen, $S_0(H_2)$, is very small. With a small pre-coverage of oxygen they observed a small decrease of this sticking which was attributed to the filling of the defect sites by the adsorbed oxygen atoms. Increasing slightly the oxygen pre-coverage gave rise in an increase of $S_0(H_2)$, which demonstrates that the chemisorbed oxygen atoms represent active sites for H_2 dissociation. Increasing the oxygen coverage further leads to the formation of (2×2)-oxygen islands, which makes the surface inert for hydrogen adsorption, therefore reducing $S_0(H_2)$ down to zero when the (2×2)-oxygen overlayer is completed.

On a stepped nickel surface, even a very small number of oxygen atoms already cause a large decrease in $S_0(H_2)$, which again proves that the oxygen initially dissociatively adsorbs on the step sites. Again, when the steps are totally filled with the pre-adsorbed oxygen, a slight oxygen contamination on the terraces will enhance the H_2 dissociation probability.

Thus, the steps have been proved to be very important quantitatively and qualitatively for $S_0(H_2)$.

In the case of D_2 dissociative adsorption on Pt(111), $S_0(D_2)$ [58], O_2 is one of the rare co-adsorbates that causes the work function of platinum to increase. Thus, if long-range electronic effects dominate, one naively expects that increasing the oxygen coverage will increase the $S_0(D_2)$ as seen in the case of $S_0(H_2)$ over a nickel(111) surface. However, the contrary is observed which indicates that O_2 steric poisoning of the chemisorption of D_2 on Pt(111) dominates over any electronic effects.

Therefore, the dominance of the steric effects over the long-range interactions shows oxygen to be an ideal pre-adsorbate to block the Pt(533) steps for hydrogen dissociative adsorption whithout affecting the hydrogen sticking probability on the (111) terraces. Notice that there is no evidence of a repulsive O-H interaction unlike that found for CO-H which could affect the initial dissociative sticking probability of hydrogen expected from the terraces [60].

The sites and the geometry of dissociative adsorption of oxygen molecules on Pt(111) and on Pt(100) are already well known. The saturation O coverage produced by

dosing Pt(111) with O_2 at 300 K with a gas doser is 0.26 ± 0.03 ML [61], which is very similar to the value of 0.25 ML obtained by dosing O_2 at 150 K on Pt(533) with a molecular beam source [62]. Note that we found a value of 0.35 ML at saturation by dosing O_2 with a capillary source at T_s = 110 K. On Pt(111) the O occupies three-fold hollow sites [63-66]. Wang *et al.* [47] studied the adsorption of oxygen on Pt(533) with HREELS and TPD, they concluded that the binding site for oxygen at steps (both atomic and molecular) is on the exposed step edge, consistent with recent theoretical predictions and scanning tunnelling micrographs [67]. McClellan *et al.* [68] studied the oxygen adsorption on a stepped Pt(321) surface at 100 K and 285 K by HREELS and TPD, and by comparison with oxygen adsorption on Pt(111) at 100 K [69, 70] they concluded that oxygen adsorbs atomically on the steps and on the terraces when O_2 is dosed at 285 K. Moreover, as seen in **figure V.9**, the oxygen adsorbs initially on the (100) step sites in four-fold hollow sites until their complete saturation, then on the (111) terraces in three-fold hollow sites.

The dissociative adsorption site behaviour of H_2 and O_2 molecules on the stepped platinum (533) surface are modelled in **figure V.8**. The hydrogen or oxygen atoms have the same behaviour of adsorption on Pt(533). In fact, the hydrogen also first adsorbs on the (100) step edges in a four-fold hollow site [29, 71]. Then hydrogen adsorbs on the (111) terrace in a three-fold hollow site [57,62].

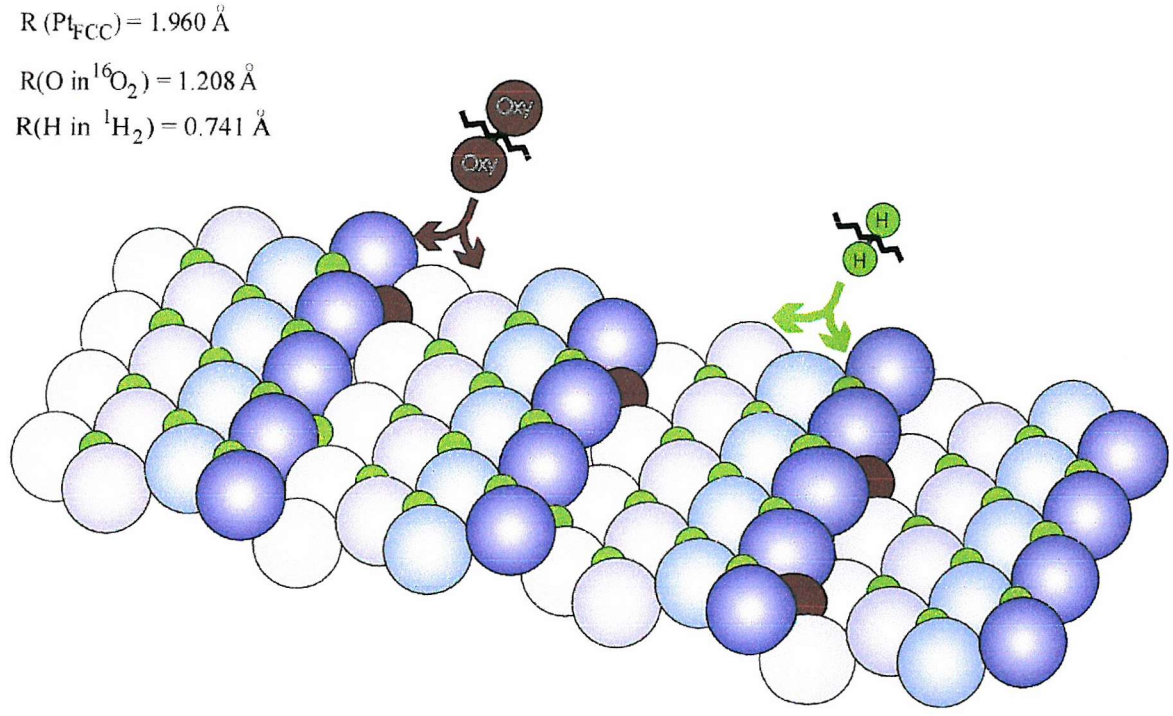

Figure V.8: Idealised atomic surface for the stepped Pt(533) crystal with oxygen and hydrogen adsorbed atoms.

Thus, in order to block the steps, the surface was exposed at T_s = 300 K to 0.12 ML of oxygen which is achieved under the present conditions with an exposure of 0.12 ± 0.02 L. This exposure, which is expected to correspond to the filling of the steps, without any significant oxygen deposition on the terraces, was determined from the oxygen TPD on the Pt(533) surface, identifying the recombinative desorption of atomically adsorbed O of the terraces and the steps (**figure V.9**).

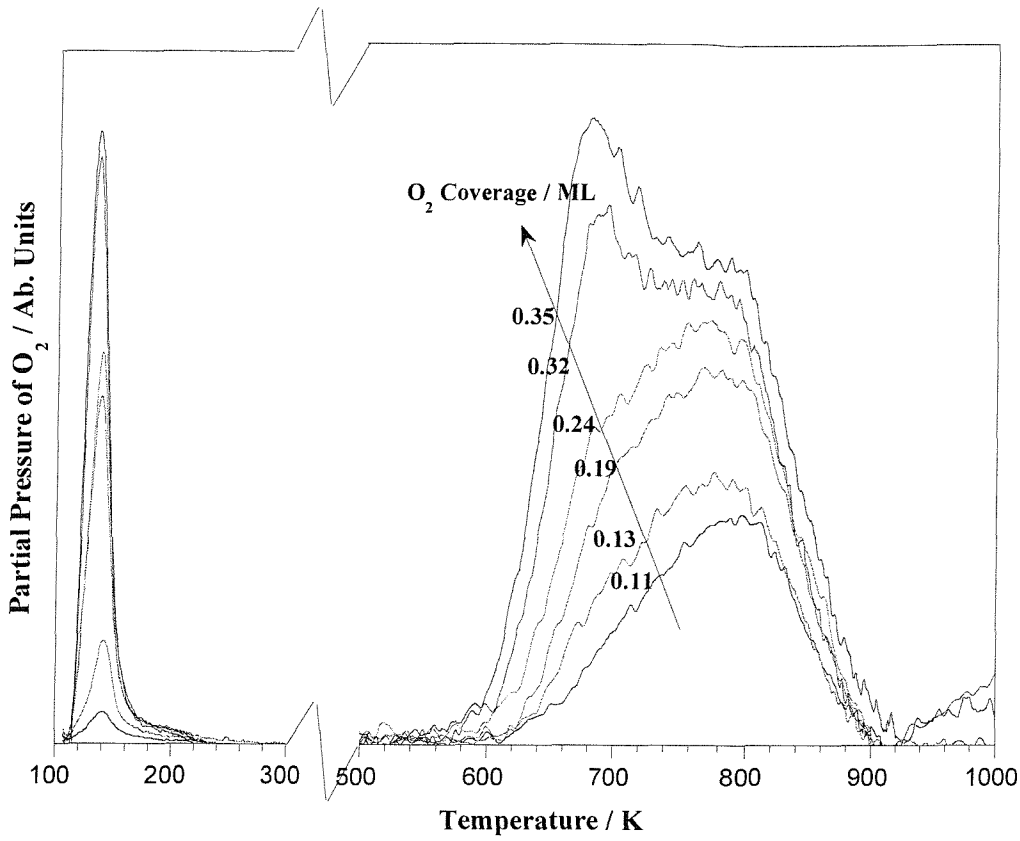

Figure V.9: TPD of O_2 following exposure of Pt(533) to O_2. O_2 was dosed using a capillary source at T_s = 110 K. The coverage was 0.11-0.35 ML and the heating rate was 1-1.3 K s^{-1}.

A series of dissociative sticking measurements for hydrogen were made on the Pt(533) surface following the exposure of the surface at 300 K to 0.12 ML of O_2. The following results were performed with a similar method to Gee *et al.* [29], selecting the incident energy of the H_2 molecules by varying the nozzle temperature, T_n, and the seeding. Previous experiments on Pt(533) [29] concluded that it is the translational energy that is dominating the dissociative sticking probability in the range of energy studied, therefore, the variation of the internal energy due to T_n and the seeding were not taken into account.

Figure V.10 presents the variation of the initial sticking probability of hydrogen $S_0(H_2)$ (within an error of $\pm$ 0.02) with E_i on an oxygen step-decorated Pt(533) crystal surface [44]. $S_0(H_2)$ was measured at a surface temperature of 307 K. Beam energies were varied between 3 and 180 meV. The H_2 was seeded in argon, neon or helium. These results are presented together with the results obtained for H_2 and D_2 on clean Pt(533) by Gee *et al.* [29] and the results obtained on Pt(111) by Samson *et al.* [45].

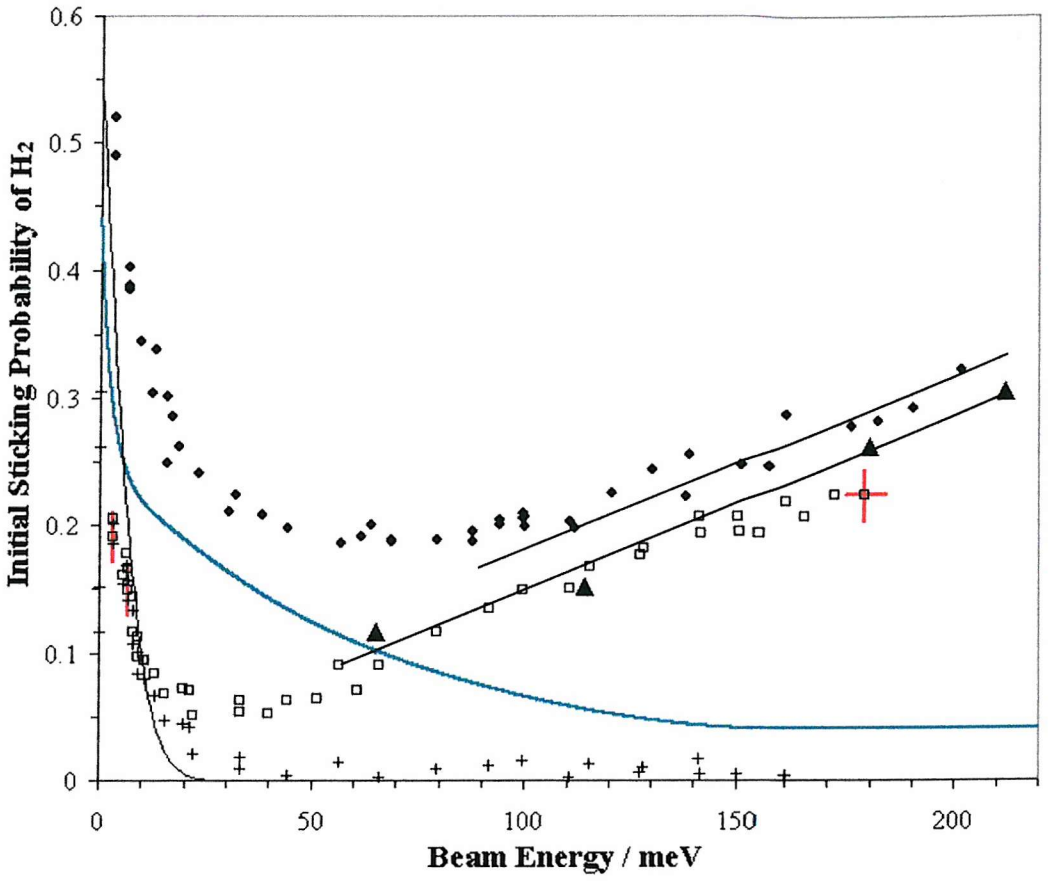

Figure V.10: Initial sticking probability of hydrogen and deuterium on clean Pt(111) $T_s = 300$ K (▲) [45], on clean Pt(533), $T_S = 300$ K, $\Theta_I = 0°$ (♦) [29] and of hydrogen on O-precovered Pt(533), $T_S = 307$ K, $\Theta_I = 0°$ (□) [44 this work].The heavy curve is the difference in the Pt(533) and Pt(533)-O sticking probabilities. The linear curves are fits of the direct contribution on both Pt(533) and Pt(533)-O. The crosses (+) represent the indirect component of the sticking obtained by substracting from S_0 on Pt(533)-O. The light curve is a hard cube calculation of S of physisorbed hydrogen on platinum.

The results reveal that there are two clearly resolved energetic regions to the dissociative adsorption of hydrogen on the step-decorated surface. The O-precovered Pt(533) data show the same trend of $S_0(H_2)$ at energies above 30 meV as previous results. In fact the steady increase of $S_0(H_2)$ with increasing E_i, is qualitatively similar to that found on the clean Pt(533) surface (**figure V.10**), and is characteristic of dissociative adsorption on the (111) terraces through a direct channel. At energies below 30 meV, $S_0(H_2)$ on O/Pt(533) is strongly inhibited by the energy of the molecule, this was also observed on clean Pt(533). However, it is evident that there is a strong effect of the step decoration on the initial sticking of H_2, especially at low energies where the sticking is associated with the indirect channel. At higher energies, $S_0(H_2)$ is only slightly lower on the step decorated surface compared to the clean Pt(533) surface. In addition, the gradient of the linear increase in

$S_0(H_2)$ with E_i on Pt(533), step decorated Pt(533), and Pt(111) is the same. This is the energy regime in which dissociative adsorption of hydrogen takes place by direct dissociation on the (111) terraces.

The first component of the indirect channel, observed by Gee [29] for H_2 adsorption on Pt(533) at low energies, related to the presence of the steps, is no longer available during the adsorption of H_2 on O-precovered Pt(533) due to the deactivation of the steps by O. The subtraction of these results, from those on the clean surface give the contribution of the indirect unaccommodated dissociation component of the low-energy channel, *i.e.* the steps (heavy curve). This proportion of $S_0(H_2)$ decreases with increasing energy over the range $0 < E_i(meV) < 150$ to a constant value. This constant difference at high energy is associated with *ca.* 18 % of the direct (111) terrace mediated channel blocked by the adsorbed oxygen. In all other respects the heavy curve is similar to that in which the step contribution to the indirect channel measured on clean Pt(533) was extracted (figure 3 in [29]) by subtraction of the direct channel measured on the Pt(111) surface. Therefore, these present results suggest that all dissociation via the unaccommodated indirect channel takes place at the step sites.
At $E_i < 30$ meV, on the O-decorated Pt(533) surface a non-negligible initial sticking strongly inhibited by E_i is also observed. We suggest this sticking to account for hydrogen dissociative adsorption via an accommodated physisorbed precursor. There is no data of $S_0(H_2/D_2)$ available on Pt(111) at these low energies, therefore we do not know if there is a similar indirect channel on that surface, hence we cannot be sure that the small channel evidenced on the stepped platinum surface at very low energies is due to the hydrogen molecules being directly accommodated on the step sites or on the whole surface. **Figure V.10** shows an estimate of this channel component (light curve) obtained using a hard cube calculation (see **appendix A**) of a physisorbed species with a 30 meV well depth.

In order to check the influence of pre-adsorbed oxygen on the (111) terrace, and compare it with the observation of Michelsen [58] for Pt(111), $S_0(H_2)$ was measured across the energy range $3 < E_i(meV) < 180$ for an oxygen pre-coverage varying from 0 to 0.35 ML (**figure V.11**), *i.e.* condition in which the terraces will also be saturated by oxygen.

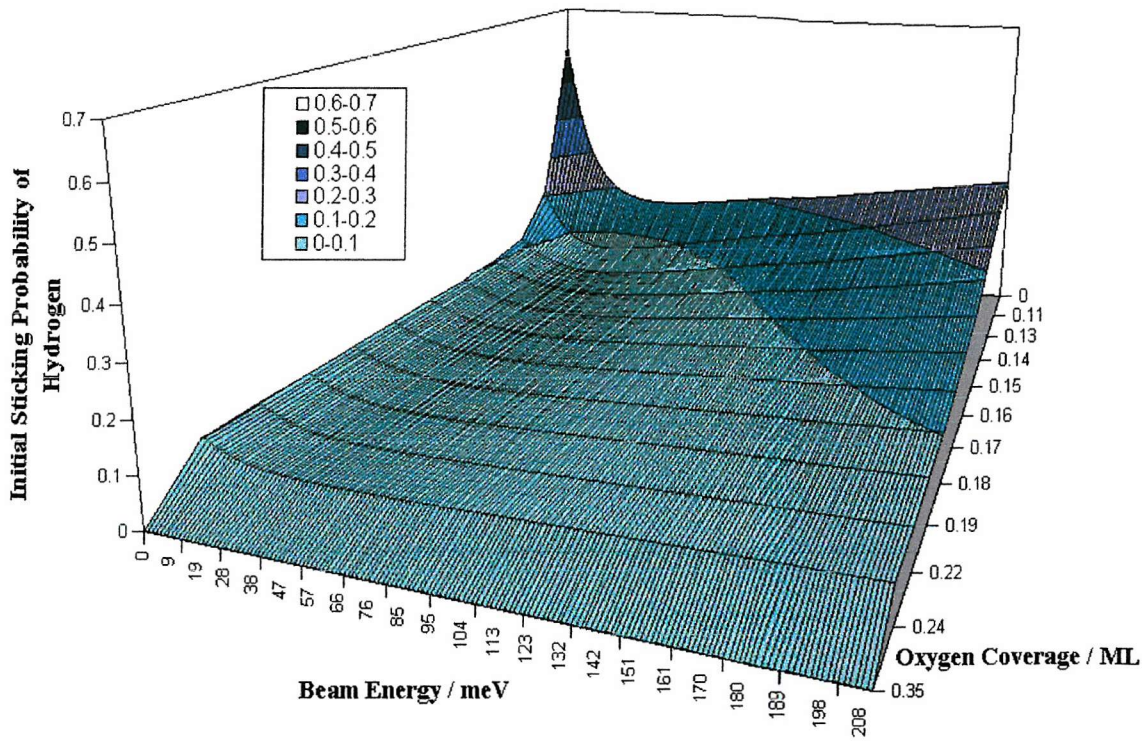

Figure V.11: Initial sticking probability of hydrogen on Pt(533), as a function of E_i, covered with variable O_2-coverage at $T_S = 307$ K and $\Theta_I = 0°$.

The initial sticking of hydrogen decreases with the oxygen coverage, thus after a 0.133 ML O_2-coverage, $S_0(H_2)$ is of the order of 0.05 in the whole energy range, which value is at the limit of validity given by the King and Wells method. However it is not insignificant, as previous results [29] have shown, complete oxygen saturation on the Pt(533) surface does not occur until 0.35 ML.

On **figure V.12**, the oxygen coverage dependence of the initial sticking probability of H_2 is shown at two energies: $E_i = 3.3$ meV, which corresponds to dissociative adsorption through the indirect channel, and $E_i = 190.3$ meV which corresponds to dissociative adsorption through the direct channel. At low energy the sticking trend appears exponential, demonstrating the strong influence of the steps on $S_0(H_2)$. When the oxygen has saturated the steps ($\theta_O = 0.12$ ML) and starts to fill the terraces no noticeable change is observed which is expected because the terraces do not have an essential role in the hydrogen sticking at low energy. At high energy, the sticking (within experimental error) is quasi-independent of the oxygen coverage from 0 to 0.12 ML of O. However as soon as the terraces start to be filled with oxygen the hydrogen sticking decreases drastically showing the importance of the terraces.

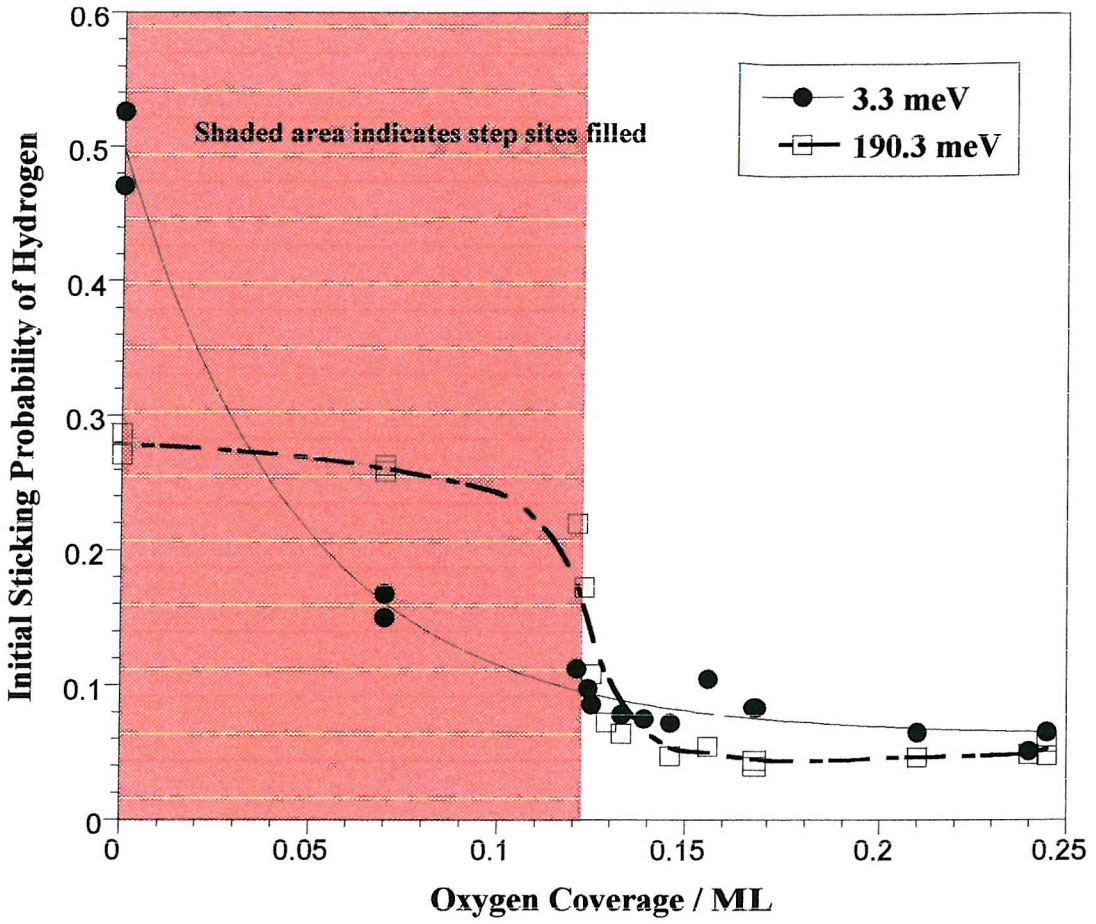

Figure V.12: Initial sticking probability of hydrogen on Pt(533) at $E_i = 3.3$ meV and $E_i = 190.3$ meV covered with variable O_2-exposure, $T_s = 307$ K and $\Theta_I = 0°$. Lines of best fit for each set of data are shown.

V.3.5 Maxwell-Boltzmann Distribution

In this study all the experiments were performed using a supersonic molecular beam source. The molecules stream out of the nozzle with a very narrow velocity distribution, and are then stripped down to a beam by passing through a skimmer (**chapter II**). Thus, the majority of the molecules will have the velocity, or beam energy, selected by the nozzle temperature and the gas mixture.

In catalysis studies, the reacting gas is dosed through an isotropic thermal source, therefore the incident molecules colliding with the surface have a wider range of kinetic energies. Thus it would be interesting to quantify the effect of the steps on the overall dissociation process of hydrogen on platinum for a thermal source.

The thermal source results in a high distribution of the velocities of the molecules (irrespective of their direction of motion) in an assumed perfect gas. Thus, the probability that a molecule has velocity components in the range $\mathbf{V_x}$ to $\mathbf{V_x+dV_x}$, $\mathbf{V_y}$ to $\mathbf{V_y+dV_y}$, and $\mathbf{V_z}$ to $\mathbf{uV_z+duV_z}$ is:

$$P(V_x,V_y,V_z)\, dV_x dV_y dV_z = (m/2\pi k_B T)^{3/2} * \exp(-mV^2/2k_B T)\, dV_x dV_y dV_z \qquad (13)$$

The probability **P(V)dV** that the molecule has a speed in the range **V** to **V+dV** is the sum of the probabilities that it lies in any of the volume elements $\mathbf{dV_x dV_y dV_z}$ in a spherical shell of radius **V**. Therefore,

$$P(V) = 4\pi \left(\frac{m}{2\pi k_B T} \right)^{\frac{3}{2}} V^2 \exp\left(-\frac{mV^2}{2k_B T} \right) \qquad (14)$$

which is known as the Maxwell-Boltzmann distribution of speeds (see **appendix B**).
After conversion into energy and to account for the distribution of energies normal to the surface (for comparison with the beam data) this distribution, MB, is represented in **figure V.13** for a gas temperature of 300 K. Note that the angle of incidence of the molecules θ is also important and therefore the MB distribution of energies is:

$$P(E) = 8\pi^2 \frac{\sin\theta \times E(\vec{u})}{m\cos\theta} \left(\frac{m}{2\pi k_B T} \right)^{\frac{3}{2}} V^2 \exp\left(-\frac{\pi \sin\theta \times E(\vec{u})}{k_B T \cos\theta} \right) \qquad (15)$$

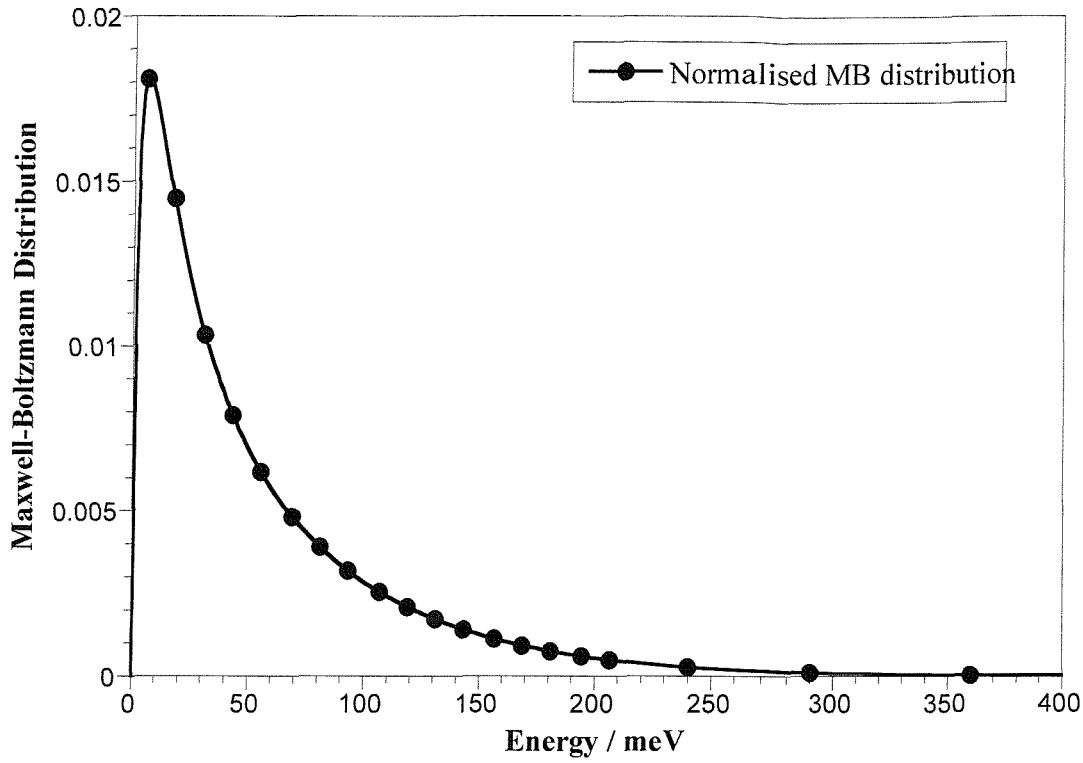

Figure V.13: Normalised Maxwell-Boltzmann distribution of energies MB for all angle θ.

By integrating the product of the data of $S_0(H_2) = f(E_i)$ for each oxygen precoverage performed on Pt(533) by the Maxwell-Boltzmann distribution of molecular energies at a particular temperature, it is possible to obtain a value for the absolute sticking on the surface from an isotropic thermal source, as opposed to the directed supersonic source of hydrogen (see **figure V.14**). Therefore on the clean Pt(533), the absolute sticking probability of H_2, $S(H_2)_{th} \sim 0.24$, while on O decorated Pt(533) this probability is reduced to 0.06 (a 76 % reduction) at saturation oxygen coverage of *ca.* 0.25 ML. Most of this poisoning (~ 81 %) of the surface to hydrogen dissociation clearly takes place as the steps are decorated by the oxygen atoms, at a coverage of *ca.* 0.12 ML. These results demonstrate the importance of the low energy regime to adsorption and reaction in heterogeneous catalytic reactions. This is particularly true for low reaction temperatures, for example those employed in hydrogen fuel cell anode catalysis, where the blocking of steps and defects can strongly influence the dissociation probability.

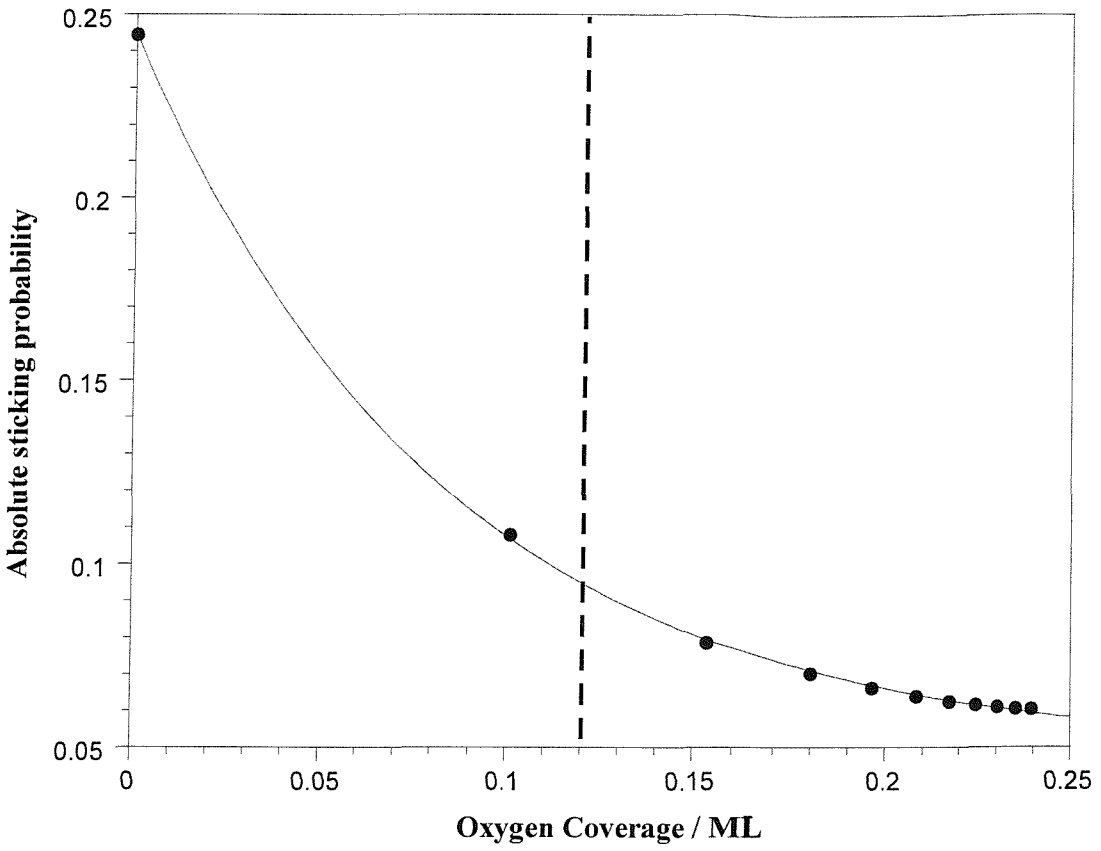

Figure V.14: Absolute sticking probabilities calculated using the curves in **figure V.11** for Pt(533) as a function of oxygen coverage for a thermalised isotropic gas at 300 K. The dotted line indicates the coverage at which the step sites are saturated.

V.3.6 Dependence of $S_0(H_2)$ on Surface Temperature

The initial sticking probability of hydrogen $S_0(H_2)$ has been measured on a Pt(533) surface precovered with 0.12 ML of O_2, as a function of surface temperature in the range $150 < T_s(K) < 500$ at incident energies E_i of 6.6, 18 and 65 meV. This oxygen coverage has been chosen in order to totally cover the (100) steps to block them while leaving the terraces free for hydrogen adsorption. The results are shown in **figure V.15**, with linear fits shown for each set of data. For comparison the results obtained by Gee *et al.* [29] of $S_0(D_2)$ on a clean Pt(533) are displayed in **figure V.16**.

At an energy of 6.6 meV on clean Pt(533) (**figure V.16**), a clear surface temperature dependence is observed, with $dS_0/dT = -4\times10^{-4}$ K^{-1}. This is characteristic of dissociation through an indirect accommodated channel, and has been described earlier. Note that the results on clean Pt(533) [29] concluded the existence of two components to the low energy channel. On the O step-decorated Pt(533), the E_i dependence (**section V.3.4**) indicates that

only one of these components is available and corresponds to dissociation through the accommodated physisorbed precursor. This is consistent with the surface temperature dependence observed in **figureV.15** on the oxygen decorated surface, with $dS_0/dT = -2\times10^{-4}\ K^{-1}$. The potential well of this precursor state is very shallow, therefore increasing T_s will significantly reduce the surface lifetime.

At 180 meV, on clean Pt(533), $S_0(D_2)$ appears independent of surface temperature, with $dS_0/dT = 6\times10^{-6}\ K^{-1}$ [29] (**figure V.16**). This is characteristic of dissociation through a direct channel on the (111) terraces, and is in agreement with the weak temperature dependence ($dS_0/dT < 1\times10^{-4}\ K^{-1}$) observed on Pt(111) for the same channel [6] and what one may expect even with a recoil contribution in view of the mass ratio between H_2 or D_2 and Pt. In fact, for light molecules the influence of recoil of the lattice atoms is always rather small because the collisions are fast and energy transfer ineffective owing to the unfavourable mass ratio [72]. On the O decorated Pt(533), at $E_i = 65$ meV, only a very small T_s dependence ($dS_0/dT < 8\times10^{-6}\ K^{-1}$) is observed, which is indicative of the direct channel to dissociation and in complete agreement with Gee *et al.* results[29].

On clean Pt(533), only a very weak dependence of $S_0(D_2)$ with T_s is observed at 18 meV, with $dS_0/dT = 5\times10^{-5}\ K^{-1}$. This result is difficult to analyse because at 18 meV there are 3 channels competing. The indirect accommodated channel only accounts for 13 % of $S_0(D_2)$ and the direct one for 10 %, while the indirect unaccommodated channel accounts for 77 % of the sticking. Moreover, from previous results it is concluded that the direct channel is independent of the surface temperature and that the very low-energy accommodated channel is dependent on T_s. There is no data available to prove the unaccommodated channel behaviour with T_s which has the main influence at this energy, however it is expected to be independent of T_s (**chapter I**). On O-Pt(533) the step-channel has been blocked by adsorption of atomic oxygen on the (100) steps, therefore the accommodated channel accounts for 58 % of $S_0(H_2)$, while the direct channel accounts for 42 %. The direct channel is independent of T_s, hence the dependence of $S_0(H_2)$ with T_s should be the same than at 6.6 meV, where the accommodated channel is the major route to dissociation. **Figure V.15**, shows in fact that $dS_0/dT = -1\times10^{-4}\ K^{-1}$ at $E_i = 18$ meV which is identical to $dS_0/dT = -2\times10^{-4}\ K^{-1}$ found at 6.6 meV within the experimental error. Notice that in the case of a Pt(111) surface, under conditions it was suspected that the small proportion of defects ($< 10^{-3}$) were significantly contributing to S_0, and a very small increase

($dS_0/dT_s = 6x10^{-5}\ K^{-1}$) in S_0 with T_s was reported for a Maxwellian source with $T_{gas} = 291$ K [34].

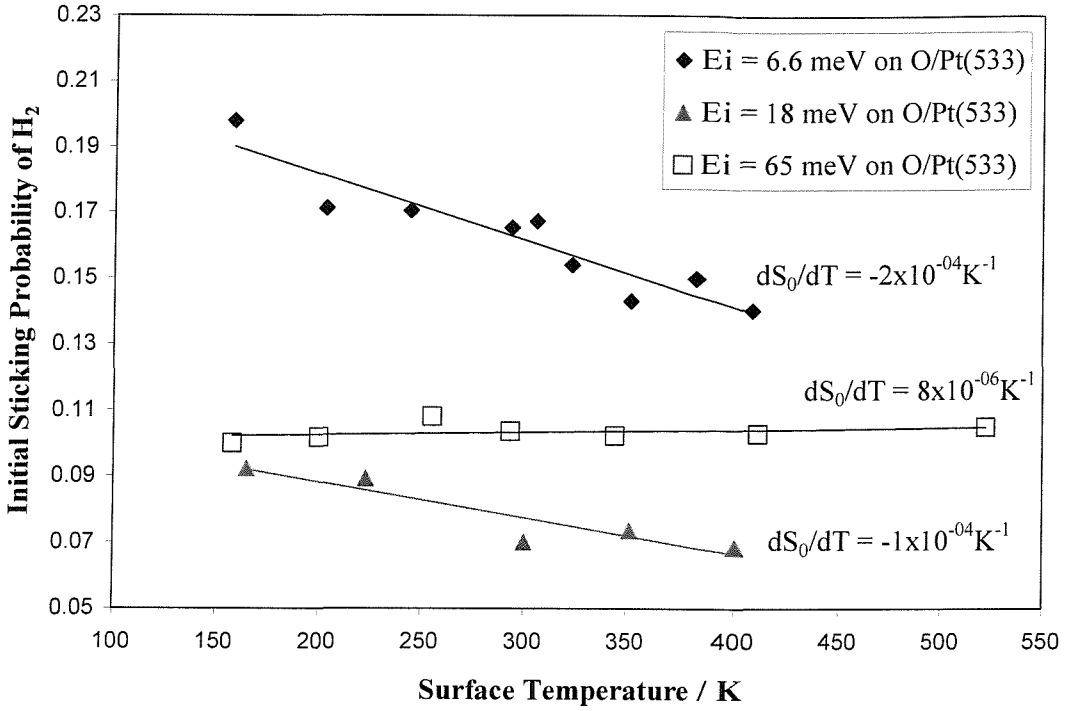

Figure V.15: Initial sticking probability of H_2 on O step-decorated Pt(533) as a function of T_s at E_i = 6.6, 18 and 65 meV. With $\Theta_i = 0°$.

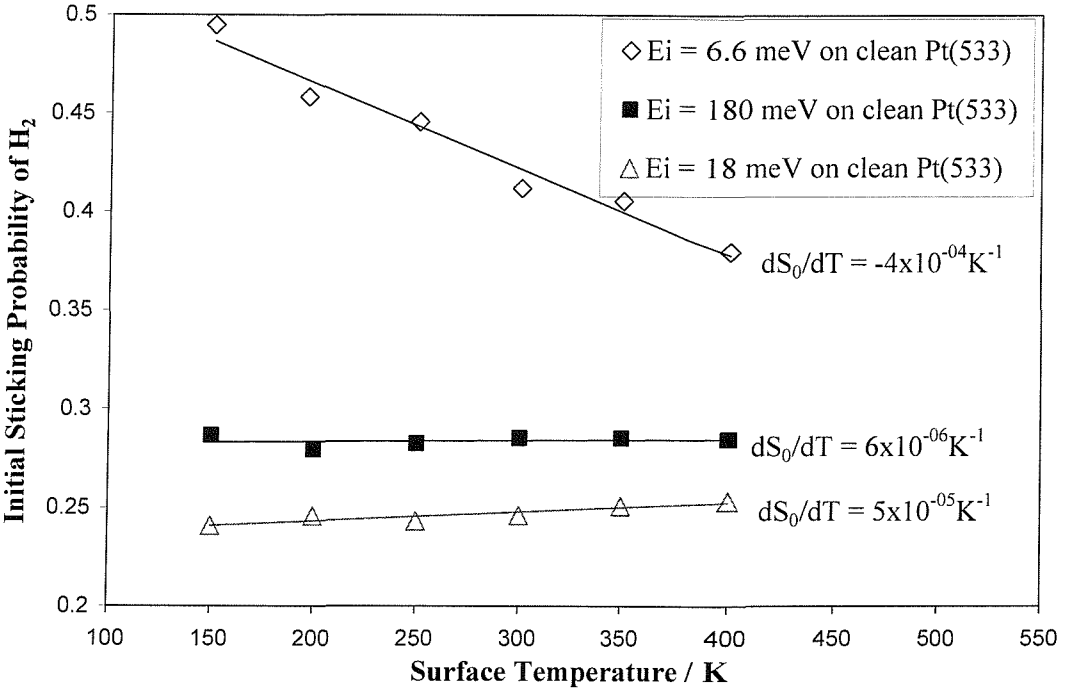

Figure V.16: Initial sticking probability of D_2 on clean Pt(533) as a function of T_s at incident energies 6.6, 18 and 180 meV. With $\Theta_i = 0°$ [29].

It is of interest to compare the temperature dependence of the initial sticking probability observed for H_2 or D_2 on other surfaces that exhibit similar E_i dependent dissociative sticking probabilities specifically in the low energy regime. H_2 dissociation on both Ni(997) and Ni(110) [5] exhibit a negative temperature dependence for a Maxwellian source at T_{gas} = 300 K. No dependence in S_0 with T_s was detectable at energies where the low energy channel was contributing on W(100) [4]. At the same incident energy on W(100)-c(2×2)Cu, where it was suggested that the indirect channel was responsible for all of the dissociative sticking, only a very small negative T_s dependence ($dS_0/dT = -3.2\times10^{-4}K^{-1}$) was observed [15, 28]. Therefore in all cases and conditions where an indirect channel to dissociation has been suggested primarily on the basis of the E_i dependence, and where specific surface sites are implicated in the dissociation, either no, or a very small, negative temperature dependence has been reported.

V.3.7 Dependence of $S_0(H_2)$ on Hydrogen Coverage

The sticking probability of hydrogen $S(H_2)$ has been measured on a O step-decorated Pt(533) surface as a function of hydrogen coverage at several incident kinetic energies, with the molecular beam incident normal to the Pt(533) surface plane, and at a surface temperature T_s = 150 K. The energies 6.6 and 18 meV were specifically chosen because they correspond to the energy regimes where the dissociation dynamics is strongly influenced by the indirect components on the clean surface, while E_i = 66 meV was chosen because the H_2 molecules mainly only adsorb through the direct channel (see **figure V.10**). The saturation coverage at 150 K has been measured earlier on from the H_2 TPD as 0.84 ± 0.05, and therefore this value has been taken as saturation in the reflection detection measurement at the same T_s. Comparison with similar measurements performed on a clean Pt(533) surface by Gee *et al.* [29] were made.

Figure V.17 shows two sets of data at 6.6 meV. On clean Pt(533) a complex coverage dependence is observed, exhibiting a weak decrease of the $S(D_2)$ during the initial adsorption up to 0.4 ML of deuterium (gradient = - 0.34) followed by a stronger dependence from 0.4 ML up to total saturation of deuterium on the surface ($dS/d\theta$ = -0.98). The direct channel accounts for only 5 % of the dissociation, while the indirect channel accounts for

95 %. Gee *et al.* [29] assumed trapping of the molecules into either a conventional molecular precursor and/or into an unaccommodated, short lived and highly mobile molecular precursor which goes on to dissociate at a step site (**figure V.10**).

After a pre-coverage of 0.12 ML of oxygen on the surface, a mixture of 4 % of H_2 in Ne was dosed onto the surface. $S(H_2)$ shows a completely different coverage dependent behaviour (**figure V.17**). On the O-precovered platinum surface, the direct channel only accounts for approximately 12 % of the hydrogen dissociation, therefore the behaviour of $S(H_2)$ is mainly due to the accommodated channel. A similar trend in the coverage dependence of $S(H_2)$ at low E_i was observed on W(110) [4] and on W(100)-c(2×2)Cu [15, 28].

The integration of both sticking measurements leads to 0.84 ML of hydrogen adsorbed on the clean Pt(533) surface while only 0.16 ML adsorb on the oxygen precovered Pt surface due to the unavailability of the unaccommodated channel. As seen earlier, the oxygen coverage performed on the Pt(533) surface to block the steps is equal to 0.12 ML. This rather surprising similarity leads us to propose a mechanism where each incident hydrogen atom must adsorb on top of each oxygen atom, hence forming some OH species at the steps. The rather drastic dependence of the sticking probability with the hydrogen coverage also suggests that the hydrogen atoms adsorbed on the O-step are no longer mobile and cannot diffuse to the terraces. This can also be seen in **figure V.10**, where the unaccommodated channel is no longer available, therefore the $S(H_2)$ trend features the hydrogen adsorption into a conventional precursor at the steps, which appears to be more sensitive to the hydrogen surface coverage. However, this mechanism is rather doubtful in light of the results obtained by other groups. Gdowski and Madix [73], who studied the kinetics and the mechanism of the hydrogen-oxygen reaction on a stepped Pt characterised by 9 atoms wide (111) terraces separated by monoatomic (100) steps and Gland *et al.* [73] who studied the same reaction on a flat Pt(111) surface, both believed that O and H adsorbed are favoured to OH adsorbed at $T_s < 700$ K. There is no significant surface concentration of OH species between 120 and 155 K detected nor by Fisher *et al* [74] and nor by Norton *et al.* [75], while H_2O is detected on Pt(111). However they concluded that the absence of large surface concentrations of OH species does not rule out OH as a reaction intermediate, but does eliminate any mechanism which requires OH to be a stable surface intermediate. Hence we cannot be sure if hydrogen adsorbs on the step-oxygen or on the terraces. It would have been useful to have facilities for HREELS, IRAS or XPS to check the presence (or absence) of

OH species on the surface. Note that the hydroxyl radical production has been studied with both laser-induced fluorescence and matrix isolation experiments that led to an activation energy for desorption of respectively 129.7 and 171.5 kJ mol^{-1} [76].

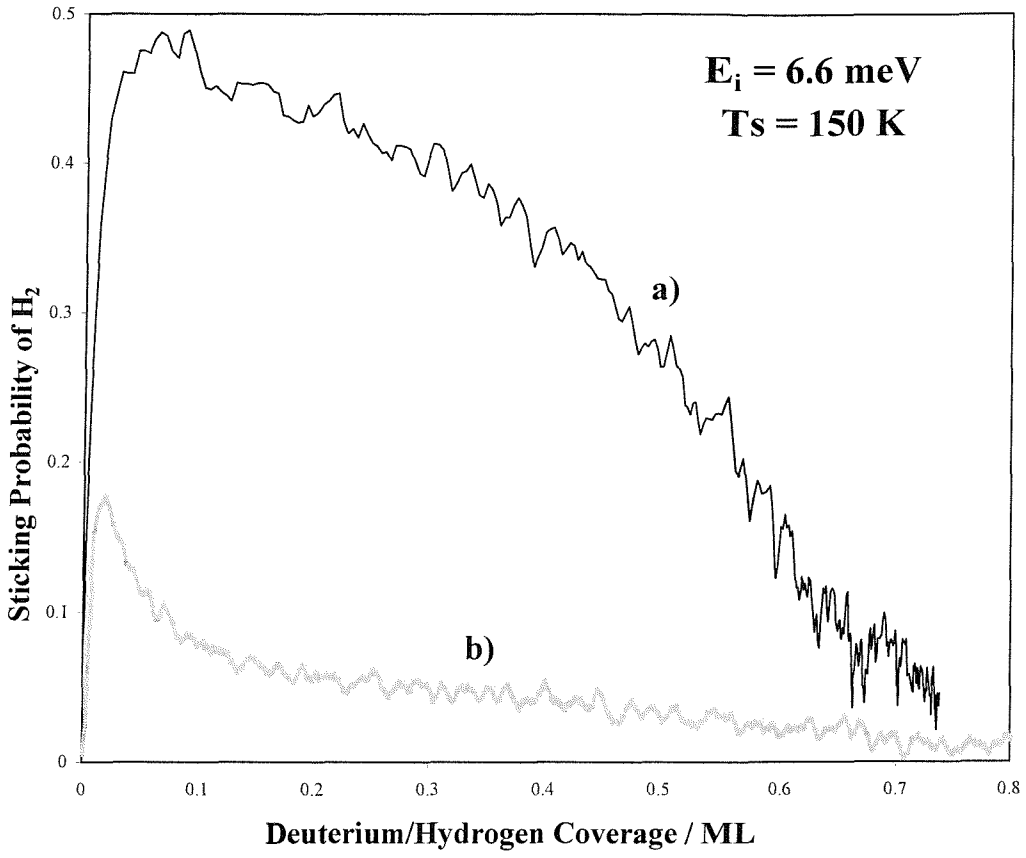

Figure V.17: **a)** $S(D_2)$ on the clean Pt(533) surface against θ_D, at E_i = 6.6 meV, T_s = 150 K and $\Theta_I = 0°$. Reproduced from Gee *et al.* data [29].
b) $S(H_2)$ on the Pt(533) surface pre-covered with 0.12 ML of oxygen against θ_H, at E_i = 6.6 meV, T_s = 150 K and $\Theta_I = 0°$. H_2 was dosed using a beam source (4 % H_2 in Ne).

Figure V.18 shows two sets of data at 18 meV. On clean Pt(533), $S(D_2)$ initially shows a weak dependence on D_2 coverage, but this behaviour is of short duration and above 0.2 ML a stronger coverage dependence is observed. At 18 meV, the direct channel accounts for only 10 % of the deuterium adsorption, and similar remarks to those made at 6.6 meV can be made concerning the behaviour of the $S(D_2)$. The effect of oxygen adsorption at the step sites produces a coverage dependency exhibiting a monotonic decrease from the lowest coverage. At this energy the direct channel accounts for 42 % of the hydrogen dissociation, therefore the trend of $S(H_2)$ is due to both the accommodated indirect and direct channels.

The integration of both sticking measurements leads to 0.84 ML of hydrogen adsorbed on the clean Pt(533) surface while only 0.23 ML adsorb on the oxygen precovered Pt surface due to the unavailability of the unaccommodated channel to adsorption.

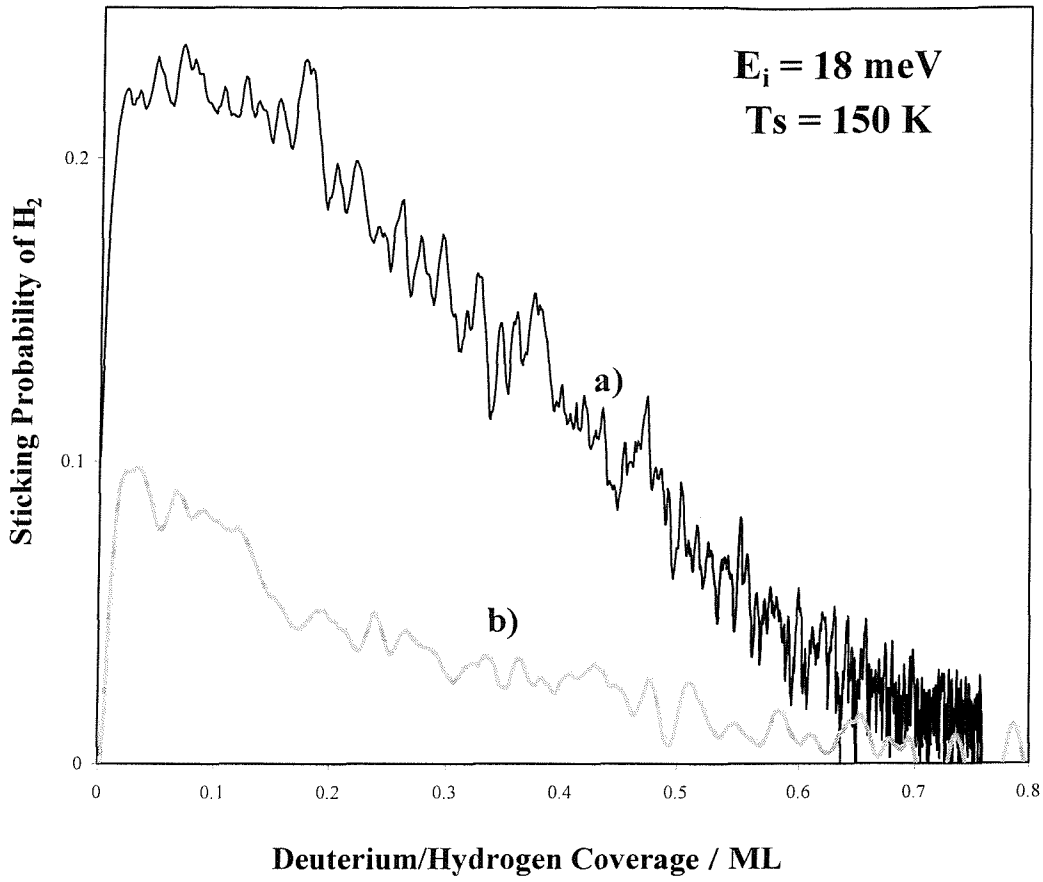

Figure V.18: **a)** $S(D_2)$ on the clean Pt(533) surface against θ_D, at E_i = 18 meV. T_s = 150 K and $\Theta_I = 0^o$. Reproduced from Gee's data [29].
b) $S(H_2)$ on the O-decorated Pt(533) at E_i = 18meV. T_s = 150 K, $\Theta_I = 0^o$. H_2 was dosed using a beam source (4 % H_2 in Ne).

Figure V.19 shows two sets of data at 66 meV. On clean and O-decorated Pt(533), $S(H_2)$ appears to be strongly dependent on H_2 coverage, in fact the sticking shows a non-linear decrease with the hydrogen coverage. The same observation had been made by Gee *et al.* [29] for the coverage dependence of $S(D_2)$ at 180 meV, where 86 % of the sticking is dominated by direct dissociation at the (111) terraces of Pt(533). Gee's data follows a second order Langmurian trend, where the sticking probability is proportional to the square of the number of free surface sites (each impinging molecule requires 2 empty adjacent sites to dissociate), so that:

$$S = S_0 \times (\theta_{sat} - \theta)^2 \qquad (16)$$

where θ_{sat} is the saturation coverage defined as 0.8 ± 0.05 ML.

In the present case, the saturation coverage on clean Pt(533) is $\theta_{sat} = 0.84 \pm 0.05$ ML. The lines of best fit of these data do not exhibit perfect Langmurian behaviour. First, at 66 meV on the clean surface, only 47 % of the sticking is attributed to the direct channel while the rest is attributed to the unaccommodated channel which can explain the observed behaviour. Secondly, at 66 meV on the O/Pt(533) surface the direct channel accounts for 100 % of $S(H_2)$ (note that the oxygen precoverage on the surface ($\theta_O = 0.12$ ML) is not taken into account in equation (16) because the oxygen only adsorbs on the (100) steps, hence theoretically it should not influence the sticking of hydrogen at 66 meV which only occurs through the direct channel on the (111) terraces). However it has been observed (see **figure V.10**) that θ_O slightly influences $S_0(H_2)$, though the effect on $S(H_2)$ cannot be quantified easily as the interaction of the adsorbed oxygen with hydrogen might not be constant as the θ_H increases. Hence it is not surprising to have a non-Langmurian behaviour.

The integration of both sticking measurements leads to ~ 0.84 ML of hydrogen adsorbed on the clean Pt(533) surface while 0.46 ML adsorb on the oxygen precovered Pt surface through direct dissociation.

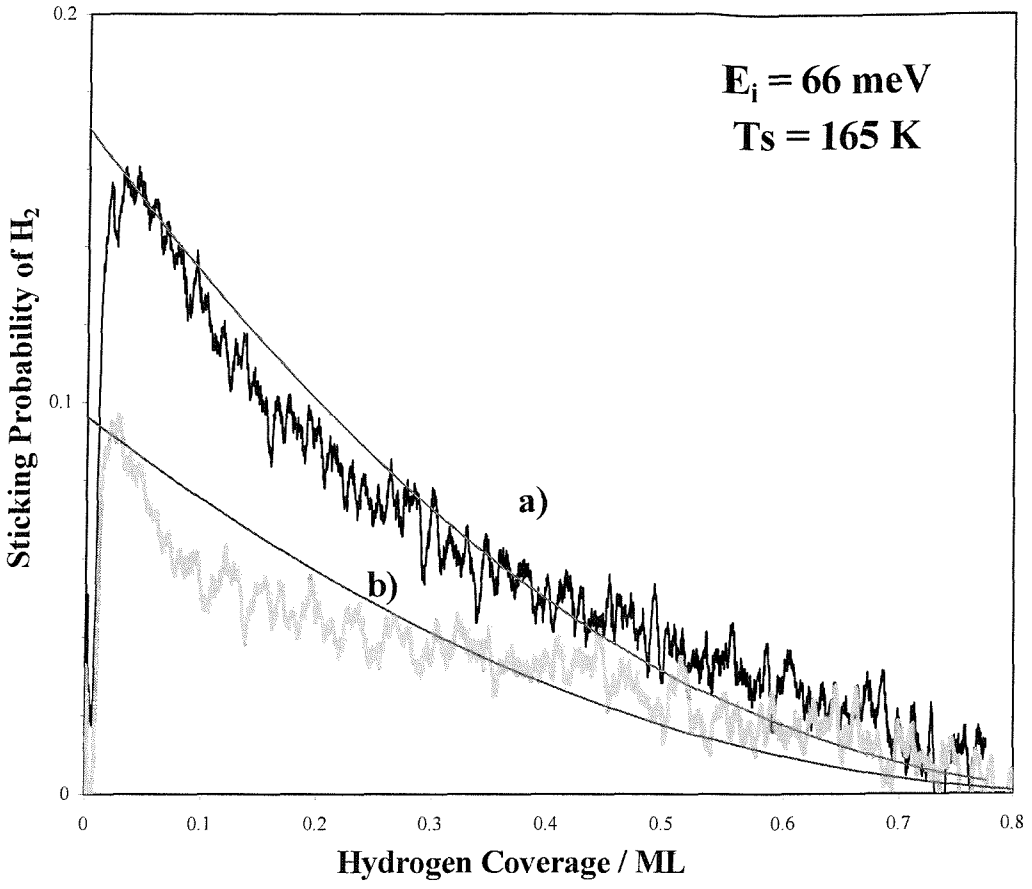

Figure V.19: **a)** $S(H_2)$ on the clean Pt(533) surface against θ_H, at $E_i = 66$ meV, $T_s = 175$ K and $\Theta_l = 0°$.
b) $S(H_2)$ on the Pt(533) surface pre-covered with 0.12 ML of oxygen against θ_H, at $E_i = 66$ meV. $T_s = 158$ K and $\Theta_l = 0°$. In both case H_2 was dosed using a beam source (1 % H_2 in He).

Notice that in the case of hydrogen sticking on W(100) [4] and W(100)-c(2×2)Cu [15] the coverage dependence of $S(H_2)$ was found approximately linear in the direct channel regime. In the case of Ni(997) [5] no coverage dependence is reported, however on Ni(111), a monotonic decrease in $S(H_2)$ with the coverage is reported [59] consistent with the dominance of a direct channel on this surface. In contrast, a more complex dependence of $S(H_2)$ with the coverage was observed on Ni(110) and rationalised on the basis of precursor kinetics [59].

V.3.8 Water Formation on Platinum

Because of the simplicity of the reactants, the hydrogen-oxygen reaction on platinum surfaces has been extensively studied by the past. As seen earlier on, the adsorption and

desorption of oxygen [46-47, 58, 61] and hydrogen [6-7, 29, 33, 43-45] on platinum have already been extensively studied. The hydrogen-oxygen reaction has been studied on Pt(111) on a wide range of surface temperature ($120 < T_s$ (K)< 1200) and with a variety of techniques. Some FEM measurements obtained at low temperature (< 170 K) show the existence of a reaction front between reacted and unreacted oxygen on Pt(111) [77]. With other techniques, such as SIMS [78, 79] and EELS [80, 81], the kinetics of the reaction and the nature of the reaction intermediate were investigated. Some molecular beam techniques [35, 82-84], helium diffraction [84] and TPD were also used [78, 85]. Water formation occurs at 120 K [78, 81], but desorption of water does not take place below 180 K [86]. Moreover the isotope reaction results performed by Gland *et al.* [85] suggest that water formation proceeds via sequential addition of hydrogen first to adsorbed atomic oxygen, then to adsorbed hydroxyl. Note that the energy of an O-H bond formed from the reaction between an H atom and an O atom both adsorbed on a Pt(111) surface has been observed around 12 kJ mol^{-1} by several methods [86].

Gland and Fisher [87] concluded that at temperatures below ~ 250 K, the O atoms are immobile on a Pt(111) surface, thus the O atoms which are not adsorbed at a reactive site cannot react directly with atomic hydrogen, moreover there was no water desorption observed. In the present case, the O atoms are adsorbed specifically at the (100) step sites of the Pt(533) surface, and these have been suggested to be the reactive sites [62], hence we will assume at least reactivity of these atoms, the mobility of the oxygen atoms will be unimportant, and the water formation is expected to take place at the steps.

Figure V.20 shows the dissociative sticking probability of hydrogen on an O-step decorated Pt(533) surface as a function of time, at different surface temperatures, for an incident beam energy of 6.6 meV. $S_0(H_2)$ was observed to slightly decrease with increasing T_s (**figure V.15**). This behaviour is attributed to the decreasing amount of hydrogen being trapped into the accommodated indirect channel as the surface warms up.

At 158 K, the initial sticking $S_0(H_2)$ is equal to 0.19, and the $S(H_2)$ clearly appears strongly dependent on the hydrogen coverage (**figure V.20**). The formation of water occurs at this low temperature [81], but no desorption is expected.

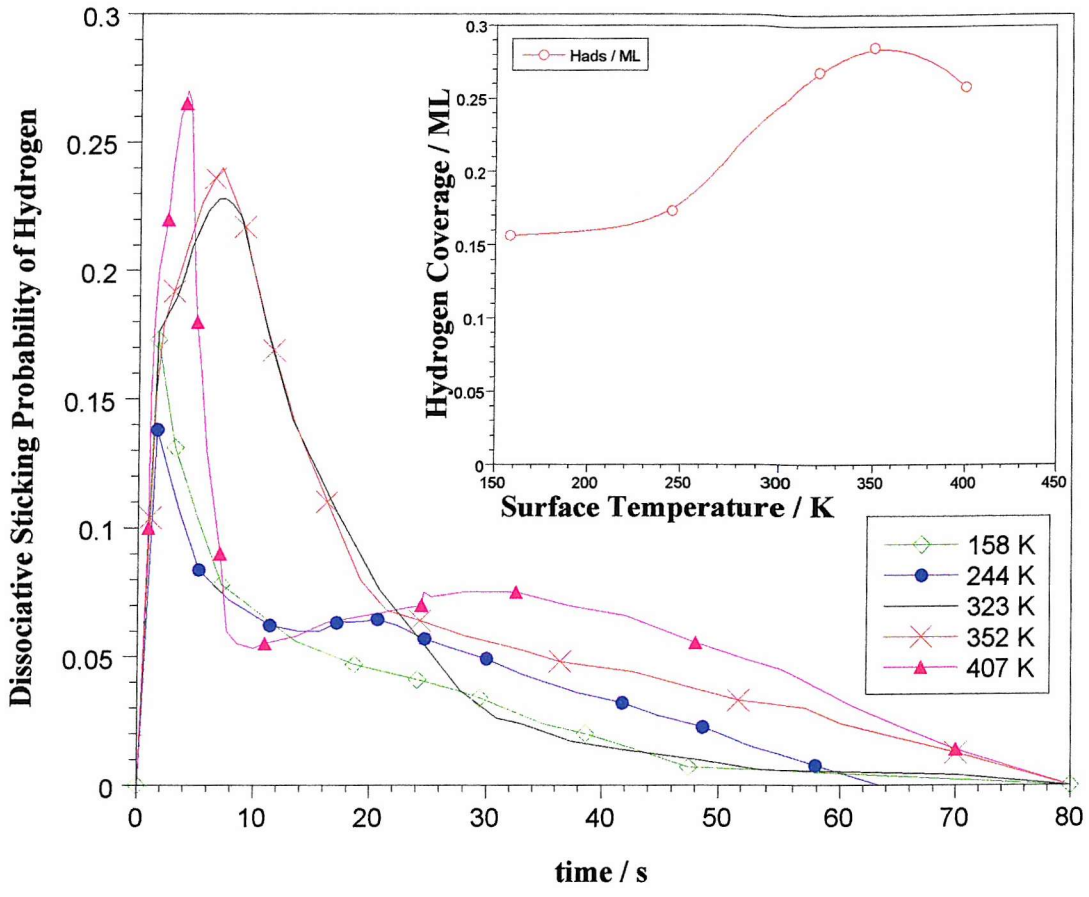

Figure V.20: $S(H_2)$ on the O-decorated Pt(533) surface against the time of dose of hydrogen, at $E_i = 6.6$ meV (4 % H_2 in Ne) and $158 < T_s(K) < 407$. With $\Theta_i = 0°$. The insert corresponds to the integration of the present sticking probability data versus the T_s.

The onset of water formation is observed in the gas phase at $T_s \sim 250$ K (**figure V.22**) with a maximum production at ~ 28 s, which is well after the maximum in $S_0(H_2)$ (max ~ 3 s for $T_s = 244$ K in **figure V.20**). However, a concomitant secondary maximum in $S(H_2)$ is observed (**figure V.20**) which almost coincides with the maximum in the water desorption. This maximum occurs earlier as T_s increases, as seen in **figure V.22** (10 s for 344 K) but is quite difficult to follow in **figure V.20**. In fact, it seems to go down in temperature for $244 < T_s(K) < 352$ (*e.g.* 10 s for 323 K), however for $T_s = 407$ K it appears around 30 s. This maximum corresponds to the freeing up of step sites favourable to hydrogen dissociation as the water desorbs.

Sticking data were particularly difficult to analyse at high temperature hence we tentatively propose the following explanation. The first maximum in hydrogen dissociative sticking probability at 407 K is related to the rapid desorption of H_2O as was the second maximum defined earlier for smaller T_s. Hence it leads to numerous free sites on the steps

for hydrogen to adsorb, which is characterised by an increase in sticking up to a new maximum at 30 s. When most of the oxygen has been consumed, the water production is decreasing fast, therefore the hydrogen adsorbed stays on the surface and rapidly fills the whole (100) steps which is characterised by a decrease of the sticking after ~ 30 s.

Note that we also observed the same phenomena when dosing hydrogen in helium at E_i = 66 meV (**figure V.21**). In this later case, the secondary maximum clearly shifts from 18 to 12 s as T_s increases from 255 to 293 K. And appears around 30 s at T_s = 522 K.

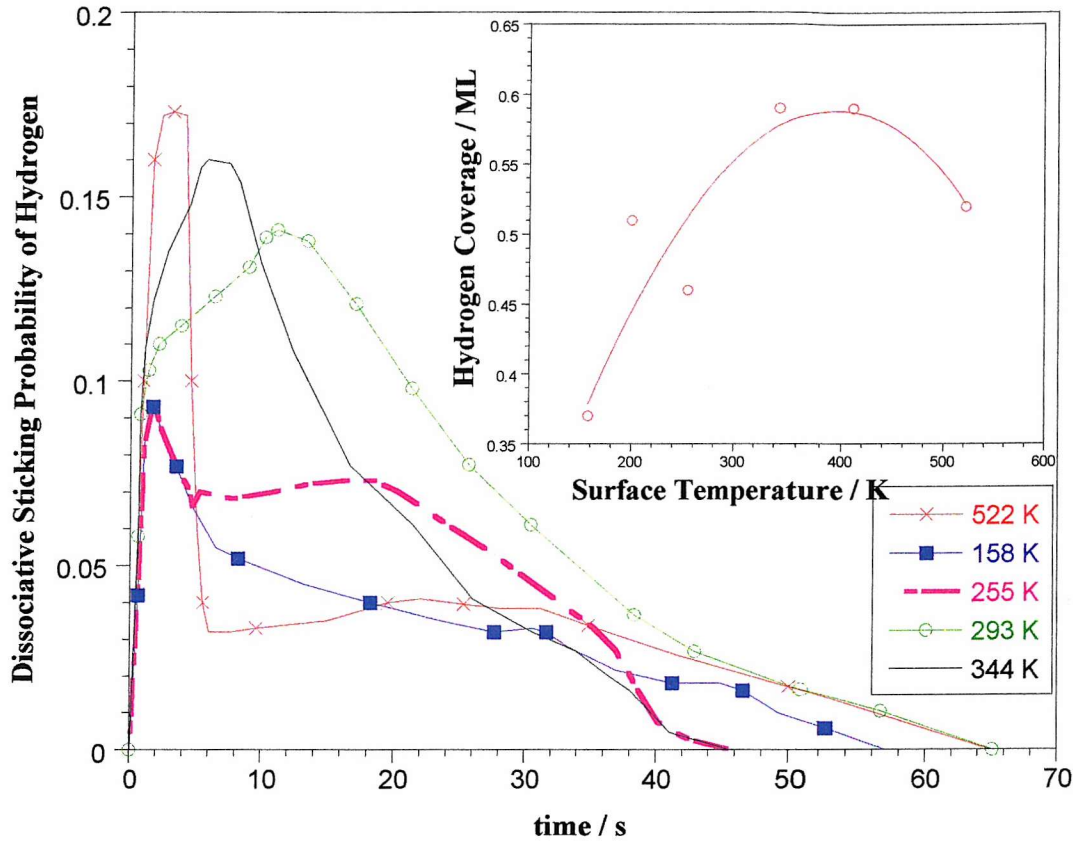

Figure V.21: $S(H_2)$ on the O-decorated Pt(533) surface against the time of dose of hydrogen, at E_i = 66 meV (1 % H_2 in He). With 158 < T_s(K) < 522. With Θ_I = 0°. The insert corresponds to the integration of the present sticking probability data versus the T_s.

On the oxygen precovered surface at E_i = 6.6 meV, the trend of $S(H_2)$ undergoes some drastic changes. In **figure V.22**, when T_s = 255 K, the water desorption starts slowly after 10 s, liberating some sites for further hydrogen adsorption. The maximum water production is reached around 25 s. Saturating the steps with atomic O might lead to some repulsion between the adsorbates, weakening their bonds to the surface. Hence it increases the reactivity between the adsorbed O and the incoming hydrogen to form OH and further H_2O. When the amount of O is gone down enough for the repulsion not to occur, the oxygen

atoms bond more strongly to the surface and the reaction with the hydrogen does not occur anymore. Note however that all the H_2O production profiles follow a similar trend after they reached their maximum, which makes us think that the same mechanism to produce water then takes place independently of the surface temperature. It would have been interesting to calculate the remaining amount of oxygen desorbing from the surface.

As T_s increases more water molecules are produced (see **figure V.22**) liberating more reactive sites on the steps for further hydrogen adsorption, hence the total coverage of hydrogen is expected to increase. The integration of the sticking data is shown in the insert of **figures V.20** and **V.21**.

We conclude that there probably are two different mechanisms for water production. A relatively low temperature mechanism which limits the production of H_2O molecules under ~ 320 K, and a second mechanism independent of T_s.

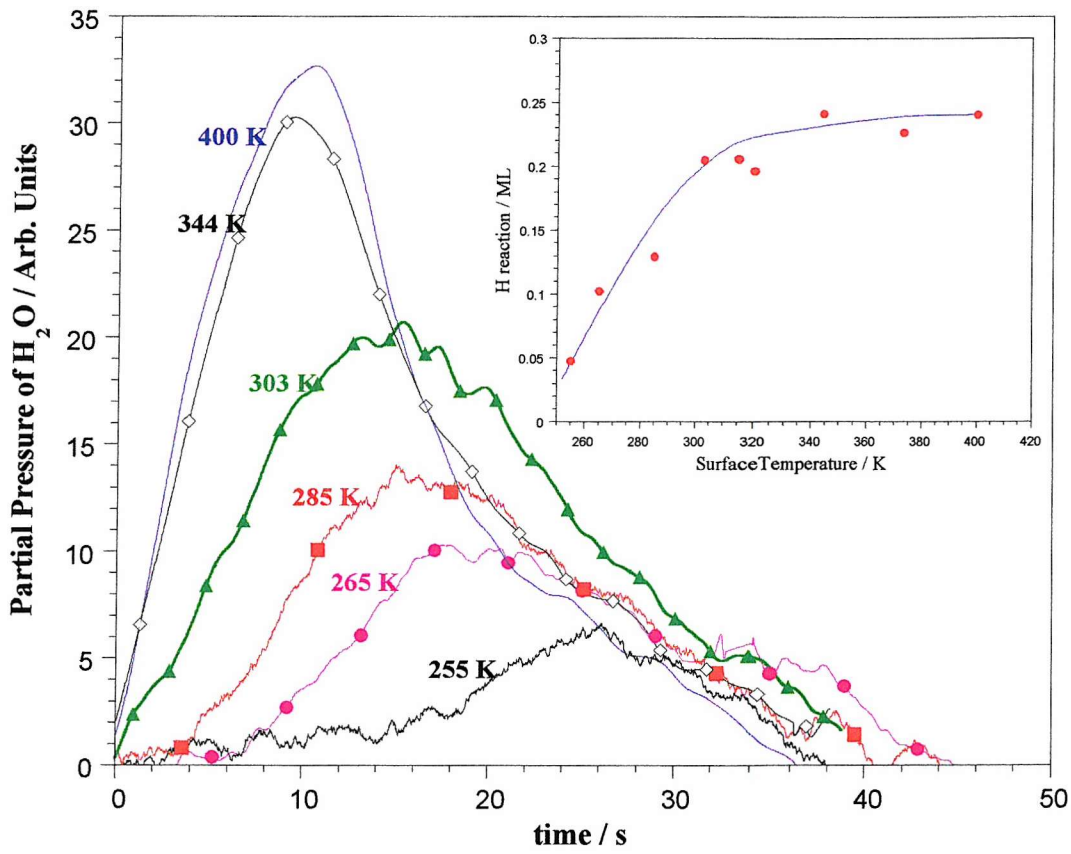

Figure V.22: Water desorption following the titration of the atomic oxygen decorating the (100) steps of the Pt(533) surface by hydrogen. E_i = 6.6 meV (4 % H_2 in Ne) and $\Theta_I = 0°$.

The water production is limited by the number of oxygen atoms on the surface available to form OH groups. Hence the integration of the water desorption data is shown in

the insert of **figure V.22**, which clearly shows that the water production reaches a maximum around 340 K when all the oxygen adsorbed on the surface has been used. The saturation coverage of atomic oxygen on a Pt(533) surface has been obtained by TPD measurements and found to be $\theta_O \sim 0.35$ ML, with 0.12 ML corresponding to the saturation of the (100) steps. Hence, to form H_2O molecules on the whole steps, $2 \times 0.12 = 0.24$ ML of atomic hydrogen are necessary. Notice that from the hydrogen TPD performed in **figure V.1** one would expect that at 400 K the lifetime of adsorbed hydrogen is very small. However this does not seem to influence the production of water which is constant for $340 < T_s\,(K) < 400$, *i.e.* the adsorbed H atoms are available for reaction with O.

Several reaction schemes have been proposed in the past, which were able to explain some of the observed phenomena [73, 78, 85], but a description of the reaction, consistent with all reported data, has not yet been provided. The two fundamentally different reasons for this are:

1) The sticking probability of both O_2 and H_2 is known to depend in a complicated way on surface coverage, surface temperature and quality of the surface (defect density).
2) Adsorbed O or H atoms may exist on the surface in different binding states, due to the presence of defects or to the specific distribution of the adsorbates on the surface (islanding).

In the present case, the conditions are simplified because adsorption of oxygen has been limited to the step sites of a defect free Pt(533) surface.

Gland *et al.* [74, 85] postulated as did Engel and Kuipers [88] and Gdowski and Madix [73] that the formation of adsorbed hydroxyl is rate limiting. This reaction sequence causes low surface hydroxyl concentrations under all reaction conditions. Moreover Gdowski and Madix [73] concluded that the disproportionation involving two OH groups leading to H_2O formation cannot exist, as well as the reaction model involving the fast formation of OH groups from O and H adsorbed atoms on a stepped Pt surface.

The following surface reaction mechanisms (**figure V.23**) can describe the hydrogen-oxygen reaction. For $120 < T_s(K) < 220$, steps (1) to (5) are believed to take place, while for $T_s \geq 220$ K step (5) is replaced by step (6).

$$H_{2(gas)} \underset{k_1}{\overset{k_{-1}}{\rightleftharpoons}} H_{2(ads)} \qquad (1) \quad \textit{fast}$$

$$H_{2(ads)} \underset{k_2}{\overset{k_{-2}}{\rightleftharpoons}} 2H_{(ads)} \qquad (2) \quad \textit{fast}$$

$$H_{(ads)} + O_{(ads)} \xrightarrow{k_3} (OH)_{(ads)} \qquad (3) \quad \textit{(RLS)}$$

$$H_{(ads)} + (OH)_{(ads)} \xrightarrow{k_4} (H_2O)_{(ads)} \qquad (4) \quad \textit{fast}$$

$$(H_2O)_{(ads)} + O_{(ads)} \xrightarrow{k_5} 2OH_{(ads)} \qquad (5) \quad \textit{fast}$$

$$(H_2O)_{(ads)} \xrightarrow{k_6} (H_2O)_{(gas)} \qquad (6) \quad \textit{fast}$$

Figure V.23: surface reaction mechanism for hydrogen adsorbed on a precovered atomic oxygen Pt(533). Mechanism (3) is the rate limiting step (RLS).

Steps (1) and (2) of these mechanisms are fast as has been seen earlier.

The formation of water has been shown to occur above 120 K, hence at the temperature studied here reactions (3) and (4) can occur leading to some H_2O formation. Below ~ 220 K a cyclic reaction sequence is believed to occur (see step (5)) [89]. Water has been observed to desorb above ~ 220 K (see step (6)), hence above this temperature the rate constant k_6 is also relatively high. Note that we concluded in two different mechanisms for water production earlier, which are both included in step (6). More experiments would need to be performed to define each of them and their respective rate constant k_{6A} and k_{6B}.

At temperature above 120 K the rate limiting step **RLS** is (3).

At $T_s = 244$ K, the sticking data from **figure V.20** shows a separation between the hydrogen sticking and the hydrogen reacting to form water (after 20 s there is enhancement of the sticking). This reaction depends on the number of free adsorption sites for hydrogen in the near neighbourhood of the O atoms. As the number of oxygen atoms adsorbed

decreases when water is produced, more hydrogen can dissociatively adsorb on the steps, hence reaction (2) goes faster and k_2 increases.

The hydrogen coverage remaining on the platinum surface after production of water, θ_{Hsurf}, is obtained by:

$$\theta_{Hsurf} = \theta_{Hads} - \theta_{Hreact} \qquad (16)$$

With θ_{Hads} the total coverage of hydrogen obtained at $E_i = 6.6$ meV with the sticking measurements from **figure V.20**, and θ_{Hreact} the coverage of hydrogen which participated in the water formation, obtained at 6.6 meV with the water desorption measurements from **figure V.22**. The results are shown in **figure V.24**.

All the hydrogen atoms reacting to form water are theoretically included in θ_{Hads}. Hence, within the experimental errors and the difficulties in extracting results from the sticking data (*i.e.* the base line for each set of data was particularly difficult to obtain at high surface temperature), the coverage of hydrogen remaining on the surface tends to zero as T_s increases to 407 K.

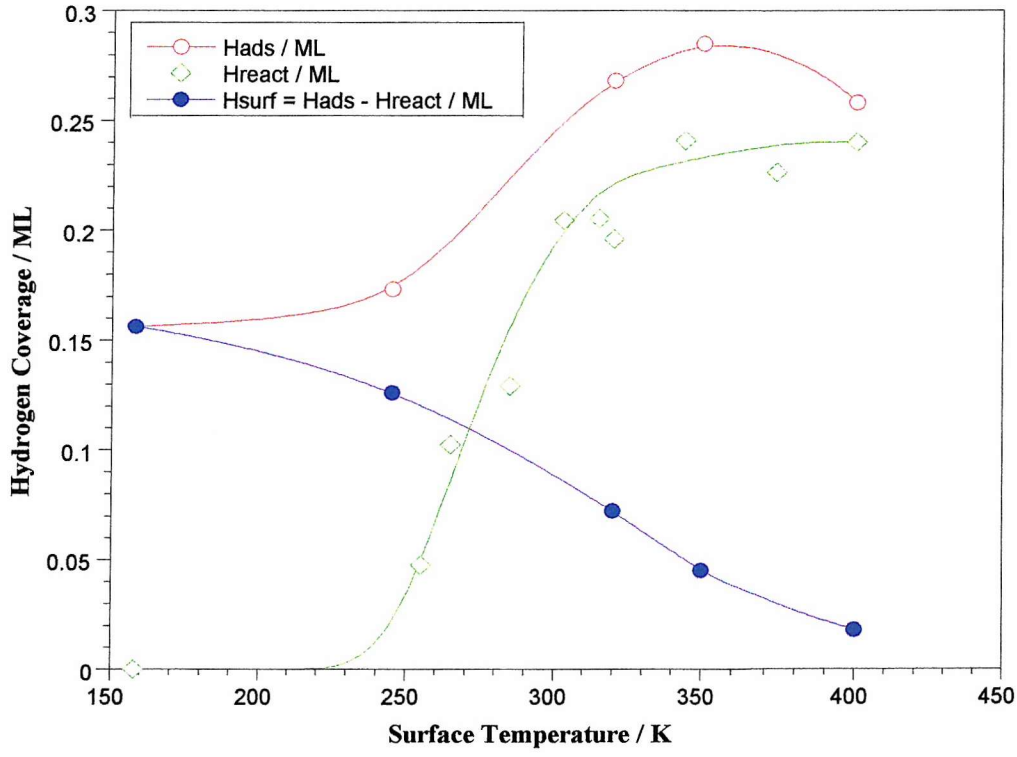

Figure V.24: Hydrogen coverage remaining on the surface after reaction with oxygen versus surface temperature.

Figure V.25 shows the production of H_2O versus the oxygen coverage on the surface, at various T_s. While **figure V.26** shows the logarithm of H_2O production versus $1/T_s$ for short times of hydrogen exposure.

Figure V.26 reveals that ln(H_2O production) decay with $1/T_s$ seems always first order in oxygen coverage, in other words the H_2O production decays exponentially with $1/T_s$ showing that the constant k_6 is independent of the coverage for $0.100 < \theta_O(ML) < 0.118$ for $265 < T_s(K) < 400$. The energy of water desorption has been calculated to be ~ 5.7 kJ mol^{-1}, which means that the activation barrier to desorption is very small, as expected.

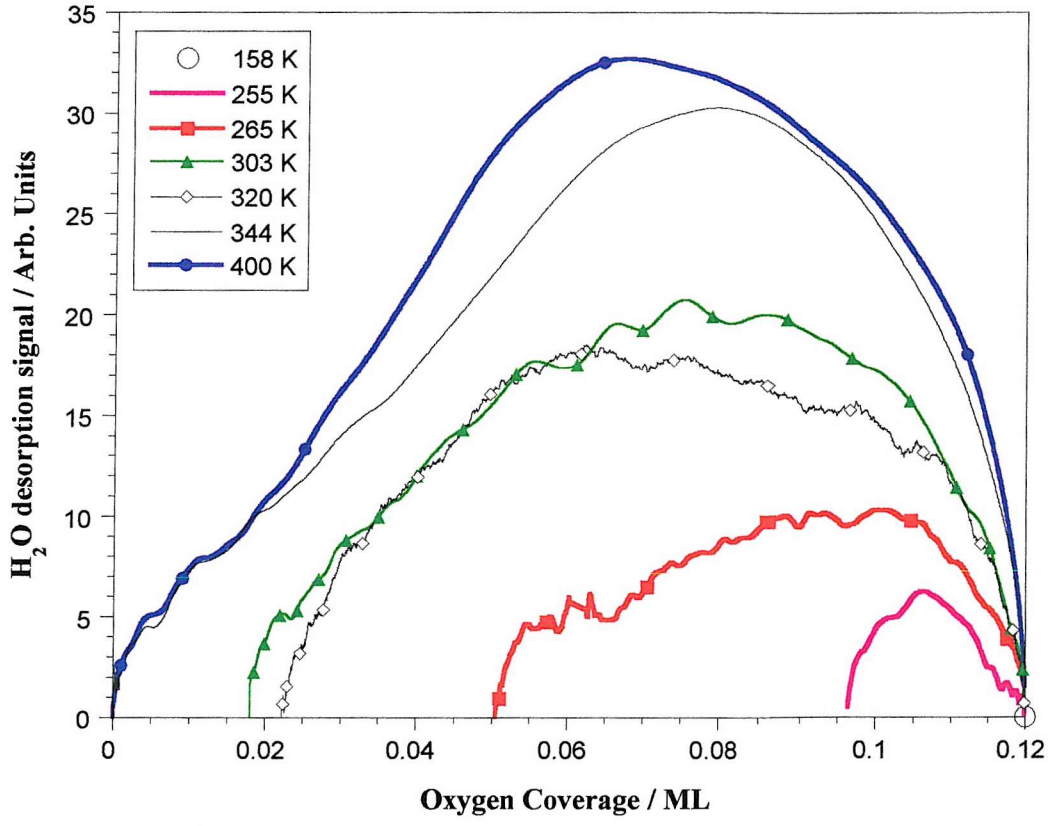

Figure V.25: Production of H_2O versus the oxygen coverage on the surface, for $158 < T_s(K) < 400$.

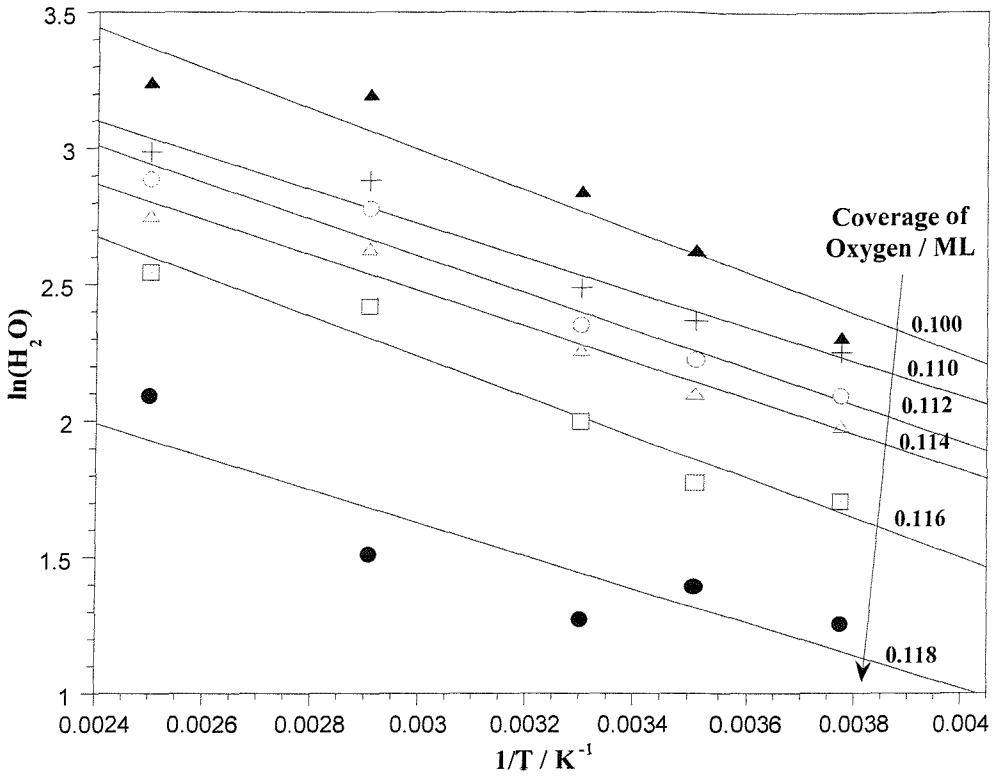

Figure V.26: Production of H_2O versus the oxygen coverage on the surface, for $266 < T_s(K) < 400$.

V.3.9 Consequences of Pre-Adsorbed Carbon Monoxide on $S_0(H_2)$

To establish the role of the step sites on the overall dissociation dynamics of hydrogen on platinum, $S_0(H_2)$ was studied on a stepped Pt(533) surface. In the previous section, the (100) steps of the Pt(533) surface were decorated with 0.12 ± 0.02 ML of oxygen in order to be blocked for any hydrogen adsorption. The following measurements of the hydrogen sticking probability on this virtual Pt(111) surface were compared with previous data obtained on clean Pt(533) [29] and clean Pt(111) [6, 45]. Here the same set of experiments are performed by decorating the steps sites with carbon monoxide instead of oxygen.

The adsorption and desorption of CO has been studied on numerous metal surfaces. It has been shown to chemisorb molecularly on Ni(100) [90], Ni(111) [91], Fe(110) [92], Fe(100) [93], Fe(111) [94], Pd(111) [95], Rh(111) [96], Ru(001) [97], Cu(110) [98, 99], Pt(100) [100, 101], Pt(110) [102, 103], and Pt(111) [104-108]. CO bonds through its carbon end to the surface, with the C-O axis perpendicular to the surface. There is no indication that

CO dissociates on the stepped or kinked [109] surfaces of Pt such as Pt(533) [110], Pt{6(111)×(100)} and Pt{6(111)×(111)} [106], and polycrystalline Pt [111-113].

On Pt(111) CO was found to occupy mainly one fold coordinated on-top sites at low coverage, while at higher coverage two-fold coordinated bridge sites start to appear [104]. CO on Pt(111) is characterised by a series of ordered adsorbate structures, evidenced by LEED [107, 114]. The desorption peak of CO on Pt(111) shifts downward in temperature with increasing coverage in a manner consistent with repulsive adsorbate-adsorbate interactions.

The behaviour of CO adsorbed on Pt(100) is not relevant here because of the nature of the (100) steps of the Pt(533) surface. Being monoatomic, these steps are not expected to react like (100) planes but more individually.

The adsorption of CO on Pt(112) has also been studied [115]. This surface is vicinal to (111) and only differs in terrace width from the Pt(533) surface. Pt(112) is defined by 3 atoms wide (111) terraces separated by (100) monoatomic steps. Henderson *et al.* [115] concluded that at low coverage, CO is situated on every other atop step site with a (-20°, 0°) Pt-CO orientation. When the coverage increases, CO molecules begin filling every other vacant step sites with an orientation of (-24°, ±13°). Then increasing the coverage even more leads to CO molecules filling the terrace sites and the vacant step sites at the same time.

After reviewing some experiments performed earlier on Pt(110) [102], Pt(111) [108], Pt(111) and Pt6(111)×(111) [109], Brandt *et al.* [116], Xu *et al.* [117] as well as Hayden *et al.* [110] proposed a model for the arrangement of CO adsorbed on Pt(533) from low coverage up to saturation. The saturation of the steps leads to CO molecules adsorbed on atop and also bridge sites, with only 50% of CO molecules adsorbed compared to the number of step Pt atoms. When the whole surface is saturated, only on-top CO persist on the steps with 1 CO molecule per Pt atom, while the terraces are occupied by a layer of CO that forms a localised c(4×2) structure and contains an equal amount of top- and bridge- bonded CO molecules, with only one CO molecule per 2 Pt atoms. However no evidence for ordered overlayer was found on stepped and kinked Pt surface [109, 118, 119].

Figure V.27 shows a series of TPD of CO adsorbed on clean Pt(533). Two desorption peaks appear clearly. At low coverage, θ_{CO}, only the 540 K peak is present. When θ_{CO} increases a low temperature component emerges. The position of the highest peak remains constant when θ_{CO} increases while the lowest one shifts from 450 to 410 K. By comparing these TPD spectra with those obtained for CO on Pt(111) [107, 114, 120] and on Pt(533) [110, 121, 122], the 540 K peak is associated with CO adsorbed at the step edges and the lower peak corresponds to CO adsorbed on the terraces.

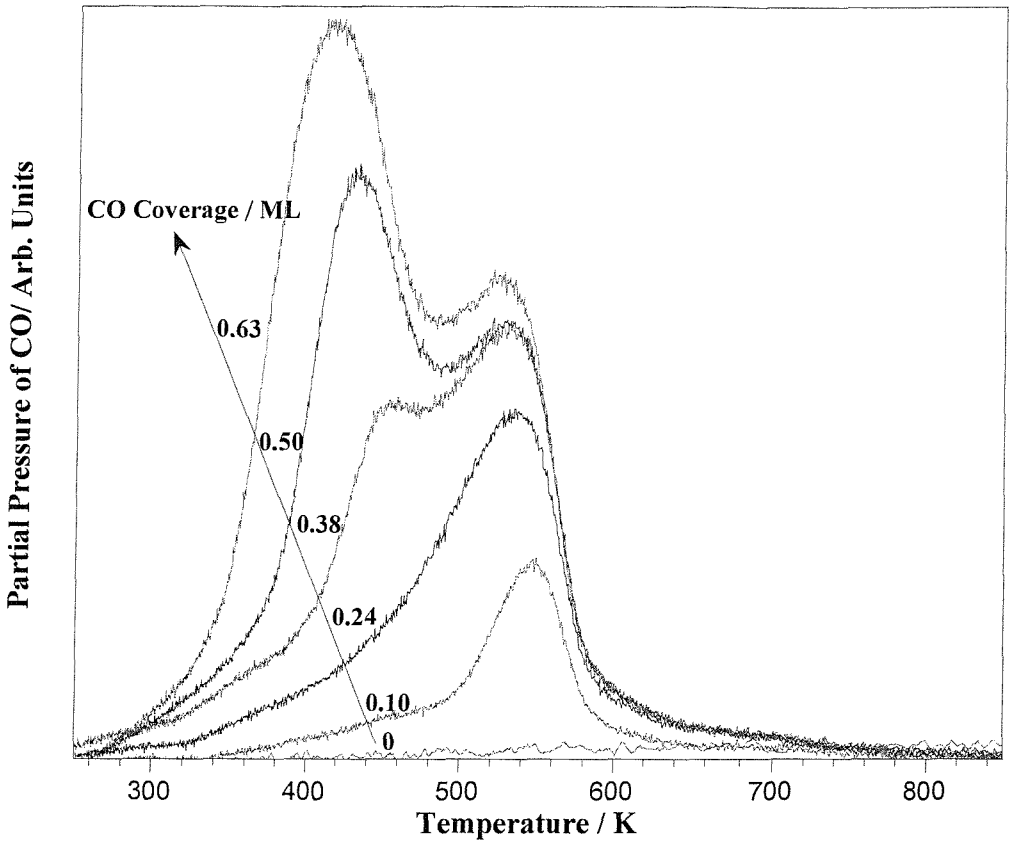

Figure V.27: CO temperature programmed desorption spectra from the Pt(533) surface at $0 < \theta_{CO}(ML) < 0.63$, obtained at $T_s = 147$ K, with CO dosed through a capillary source. The heating rate was $dT/dt = 7$ K s^{-1}.

The interaction of hydrogen and CO has been studied on several metal surfaces, such as Ni(100) [123], Ni(110) [60], Ir(110) [124], Ru(001) [125], Rh(111) [126], Fe(100) [127], polycrystalline Pt [128], Pt(111) [129], Pt(112) [130], Pt(997) [131] and Pt(533) [121, 132].

The experimental evidence from previous studies of CO and H coadsorption on Pt surfaces points convincingly toward a strongly repulsive CO-H interaction [60, 129, 130,

131, 133] despite early studies claim the contrary [129, 134]. Thus, it is also expected to observe a repulsive interaction between the CO adsorbates and the incoming hydrogen molecules, which could affect the initial dissociative sticking probability of hydrogen expected on the terraces. On Pt(533) we expect that each CO molecule adsorbed does not only block one step Pt atom for hydrogen adsorption, but could block one more adsorption site if the CO molecule is bridge-bonded or could just forbid adsorption on a neighbouring Pt atom physically free, but strongly experiencing the CO influence [60, 125]. Notice however that it seems that this repulsion decreases as one proceeds from the close packed to the more open crystal surfaces [135].

Thus, in order to block the steps, the surface was exposed at $T_s = 300$ K to 0.19 ± 0.02 ML of CO. This coverage, which is expected to correspond to the filling of the steps without any significant CO deposition on the terraces, was determined by looking at the CO TPD on Pt(533) (see **figure V.27**). Luo *et al.* [122] calculated the CO saturation coverage to be 0.63 ML on Pt(533) and the saturation of the steps corresponds to $\sim 0.19 \pm 0.01$ ML for $85 < T_s(K) < 105$ [110, 122] which is in complete agreement with our data.

A series of dissociative sticking measurements for hydrogen were made on the CO-predecorated Pt(533) surface. These results were performed with the same method as for $S_0(H_2)$ on O-predecorated Pt(533), selecting the incident energy of the H_2 molecules by varying the nozzle temperature and the seeding.

Figure V.28 presents the variation of $S_0(H_2)$ with E_i on the CO/Pt(533) surface, along with $S_0(H_2)$ on clean Pt(533) and O/Pt(533) [44]. Beam energies were varied between 3 and 130 meV. The H_2 was seeded in argon, neon or helium. Unfortunately some problems of nozzle heating prevented measurement of $S_0(H_2)$ in the energy range $10 < Ei\ (meV) < 30$ and above 130 meV.

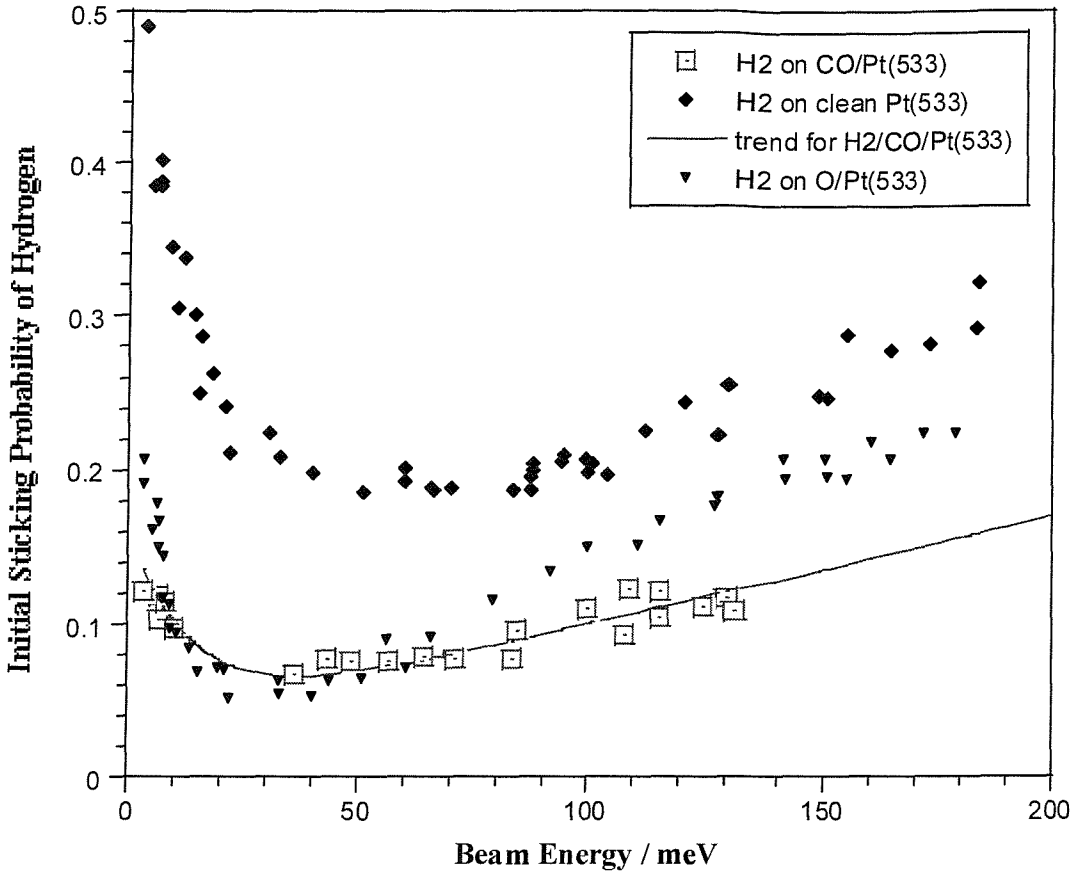

Figure V.28: $S_0(H_2/D_2)$ on clean Pt(533) at $T_s = 300$ K and $\Theta_i = 0°$ [29] and $S_0(H_2)$ on O and CO-predecorated Pt(533) at $T_s = 300$ K and $\Theta_i = 0°$.

These results show two different energetic regions for $S_0(H_2)$ on the CO step-decorated Pt(533) surface, similar to $S_0(H_2)$ on O/Pt(533) [see **section V.3.4**]. Above 30 meV $S_0(H_2)$ increases steadily with E_i and is characteristic of dissociative adsorption on the (111) terraces through a direct channel. Note however that $S_0(H_2)$ is lower on the CO/Pt(533) surface than on the O/Pt(533) surface, illustrating an activation energy to adsorption more likely to be higher due to the CO adsorbates on the steps. Below 30 meV $S_0(H_2)$ seems to be inhibited by E_i. As seen for H_2 on O/Pt(533), when O (here CO) block the steps, the indirect channel component associated with the steps [29] is no longer available. However there is still a non-negligible sticking at low energy which we suggested to be an accommodated precursor. As stated earlier, there is no data available on Pt(111) at these low energies, therefore we do not know if there is an indirect channel which would take in account any dissociative adsorption of H_2 on the whole (111) surface through an accommodated physisorption precursor state. Thus the indirect channel evidenced for $S_0(H_2)$ on O/Pt(533) could be due to the steps only or may be to the whole surface. In the present

case, covering the steps with CO leads to a much larger decrease of the initial sticking probability of H_2 under 10 meV, compared to $S_0(H_2)$ on O/Pt(533). At $E_i \sim 3$ meV $S_0(H_2) = 0.2$ on O/Pt(533), supposing that this value was the result of H_2 adsorbing on the whole surface, it is surprising that on CO/Pt(533) at $E_i \sim 3$ meV $S_0(H_2)$ is reduced by 50 %, meaning that CO adsorbed on the steps is strongly influencing the accommodated precursor route of hydrogen sticking, probably due to the strong repulsive interactions between CO and H as stated earlier. At $E_i \sim 130$ meV, $S_0(H_2) = 0.18$ ML on O/Pt(533) while $S_0(H_2) = 0.11$ ML on CO/Pt(533), which can also be explained as above. Hence the activation energy for hydrogen adsorption through the accommodated precursor channel is more likely to be higher, while the energy well will be shallower, on the CO/Pt(533) surface than on the O/Pt(533) surface, due to the destabilisation of the hydrogen adsorbates by the CO repulsion.

V.3.10 Dependence of $S_0(H_2)$ on Surface Temperature

$S_0(H_2)$ has been measured on a Pt(533) surface precovered with 0.19 ± 0.02 ML of CO, as a function of T_s in the range $160 < T_s(K) < 370$ at $E_i = 6.6$ and 65 meV. The results are shown in **figure V.29**, with linear fits shown for each set of data. These data will be compared to the results obtained previously for $S_0(H_2)$ on O/Pt(533) (see **figure V.15**) and to Gee *et al.* data [29] of $S_0(D_2)$ on a clean Pt(533) (see **figure V.16**).

At 6.6 meV, the same weak surface temperature dependence on clean Pt(533), O/Pt(533) and CO/Pt(533) is observed. The slope for $S_0(H_2)$ on CO/Pt(533) is $dS_0/dT = -4\times10^{-4}$ K^{-1}. This is characteristic of dissociation through an indirect accommodated channel.

At 66 meV, on CO/Pt(533) a very small surface temperature dependence is observed with $dS_0/dT = 1\times10^{-5}$ K^{-1} (note that due to the limited number of points and the error on each measurement we cannot give any meaningful error bar). This is in agreement with previous results (see **figures V.15** and **V.16**) and is characteristic of dissociation through a direct channel on the (111) terraces of Pt(533).

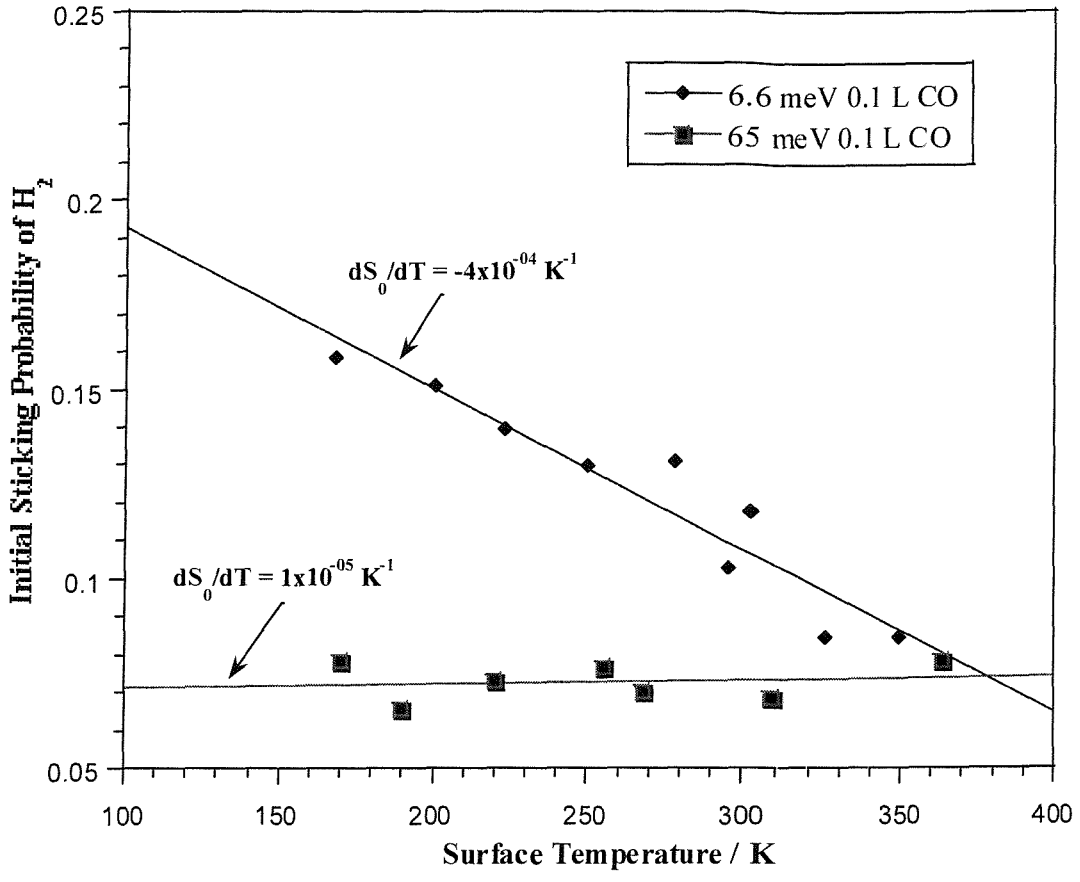

Figure V.29: $S_0(H_2)$ on CO pre-decorated Pt(533) as a function of T_s at E_i = 6.6 and 65 meV. With $\Theta_i = 0°$.

V.3.11 Dependence of $S_0(H_2)$ on Hydrogen Coverage

The sticking probability of hydrogen $S(H_2)$ has been measured on a CO step-decorated Pt(533) surface as a function of hydrogen coverage at 6.6 and 65 meV, with the molecular beam incident normal to the Pt(533) surface plane, at T_s = 170 K. The hydrogen saturation coverage at 150 K has been measured earlier on from the H_2 TPD as 0.84 ± 0.05 ML (this value has been taken as saturation in the reflection detection measurement at 170 K). Comparison with similar measurements on a clean Pt(533) surface by Gee *et al.* [29] are performed.

Figure V.30 shows two sets of $S(H_2)$ data at 6.6 meV on clean and CO precovered Pt(533). The same conclusions as for $S(H_2)$ on O/Pt(533) (see **V.3.7** and **figure V.17**) can be drawn, where the trend of $S(H_2)$ on CO/Pt(533) is mainly due to the accommodated channel (**figure V.28**) as the direct channel has no influence at this low energy, while on

clean Pt(533) the trend of $S(H_2)$ is more complex due to the main influence of the unaccommodated and accommodated indirect channels. The integration of these sticking measurements leads to $\theta_H = 0.84$ ML on the clean surface while $\theta_H = 0.11$ ML on the CO/Pt(533) surface. This latter value is similar to the 0.19 ML of CO adsorbed on the steps. However due to the repulsive interactions between the CO and H species there is no formation of CO-H complex. Henderson and Yates [130] who studied the adsorption of hydrogen on CO-precovered Pt(112) (3 atoms wide (111) terraces separated by monoatomic (100) steps) propose that the CO present on the steps is compressed by H_2 adsorption into islands which contains up and down titled species, while no displacement to the terrace is observed. Hence we propose that, some H_2 molecules are still able to adsorb on the steps via the accommodated channel. As for H_2 on O/Pt(533) the unaccommodated channel has been blocked, but there is probably a small proportion of molecules being able to directly dissociate on the surface.

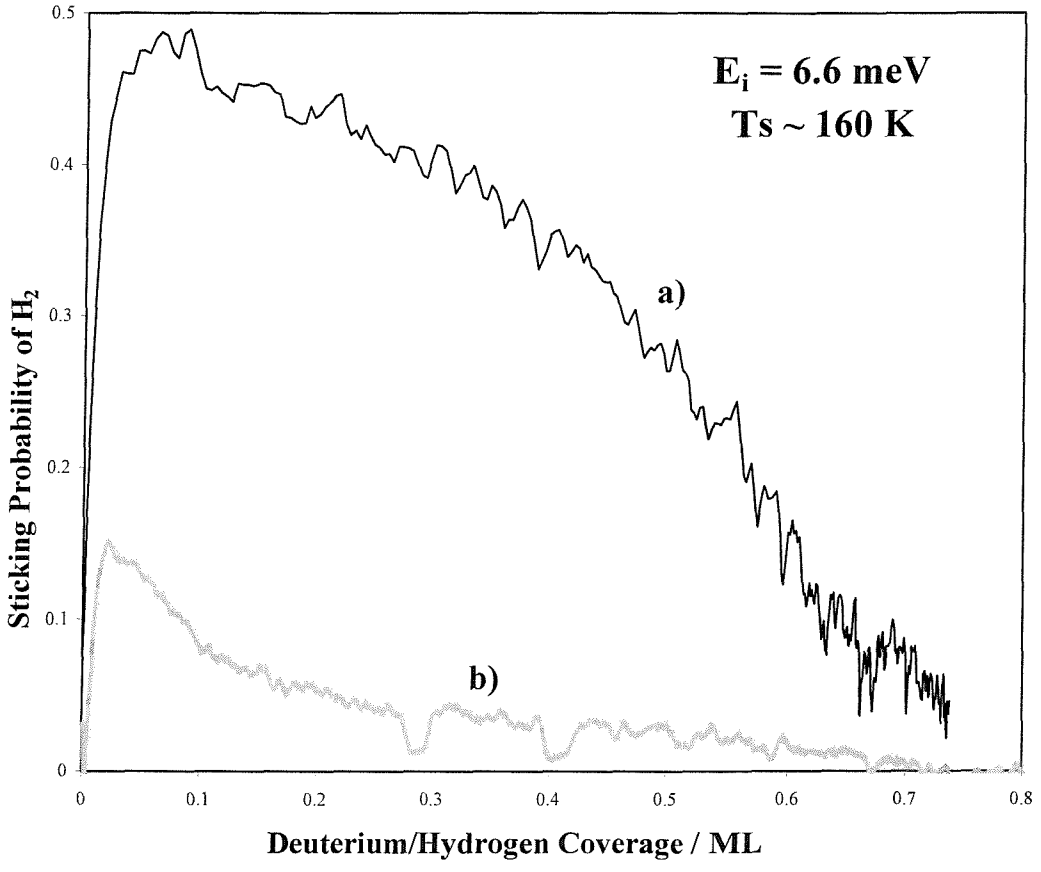

Figure V.30: **a)** $S(D_2)$ on the clean Pt(533) surface against θ_D, at $E_i = 6.6$ meV, $T_s = 150$ K and $\Theta_I = 0°$ [29].
b) $S(H_2)$ on the Pt(533) surface precovered with 0.19 ML of CO, at $E_i = 6.6$ meV, $T_s = 170$ K and $\Theta_I = 0°$. H_2 was dosed using a beam source (4 % H_2 in Ne).

Figure V.31 shows two set of data at 66 meV on clean and CO-precovered Pt(533). At this energy, the hydrogen adsorption is believed to occur through a direct channel and shows a near second-order Langmurian adsorption behaviour in $S(H_2)$ as seen previously in **figure V.19** for $S(H_2)$ on clean Pt(533) and O/Pt(533). The integration of these sticking measurements leads to $\theta_H = 0.84$ ML on the clean surface, and $\theta_H = 0.37$ ML on the CO/Pt(533) surface which is lower than $\theta_H = 0.46$ ML on the O/Pt(533) surface, due to the strong CO-H repulsive interactions.

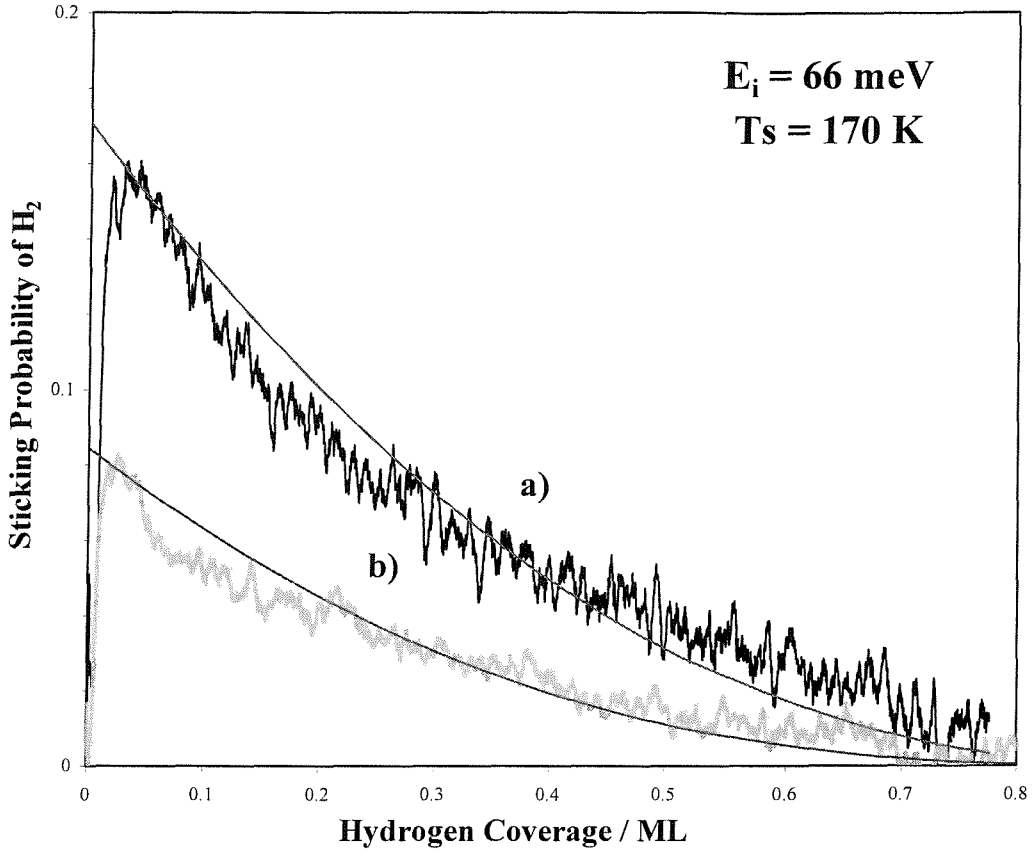

Figure V.31: **a)** $S(D_2)$ on the clean Pt(533) surface against θ_D, at $E_i = 66$ meV, $T_s = 175$ K and $\Theta_I = 0°$.
b) $S(H_2)$ on the Pt(533) surface precovered with 0.19 ML of CO, at $E_i = 66$ meV, $T_s = 170$ K and $\Theta_I = 0°$. In both cases H_2 was dosed with a beam source (1 % H_2 in He).

Hydrogen adsorption on O/Pt(533) results in the formation of H_2O (see **part V.3.8**). The production of water increases with T_s (when beaming the hydrogen molecules) until it reaches a maximum when all the adsorbed oxygen has been used. In the case of hydrogen adsorbing on CO/Pt(533) there is no reaction at the surface because CO adsorbs molecularly on platinum and does not dissociate, hence there are no free oxygen atoms to react with H_2.

Figure V.32 shows $S(H_2)$ versus the time for $168 < T_s(K) < 349$, at $E_i = 6.6$ meV. When T_s increases $S(H_2)$ is clearly decreasing, but the trend of the sticking is not influenced by T_s. The same remark can be made at $E_i = 66$ meV in **figure V.33**.

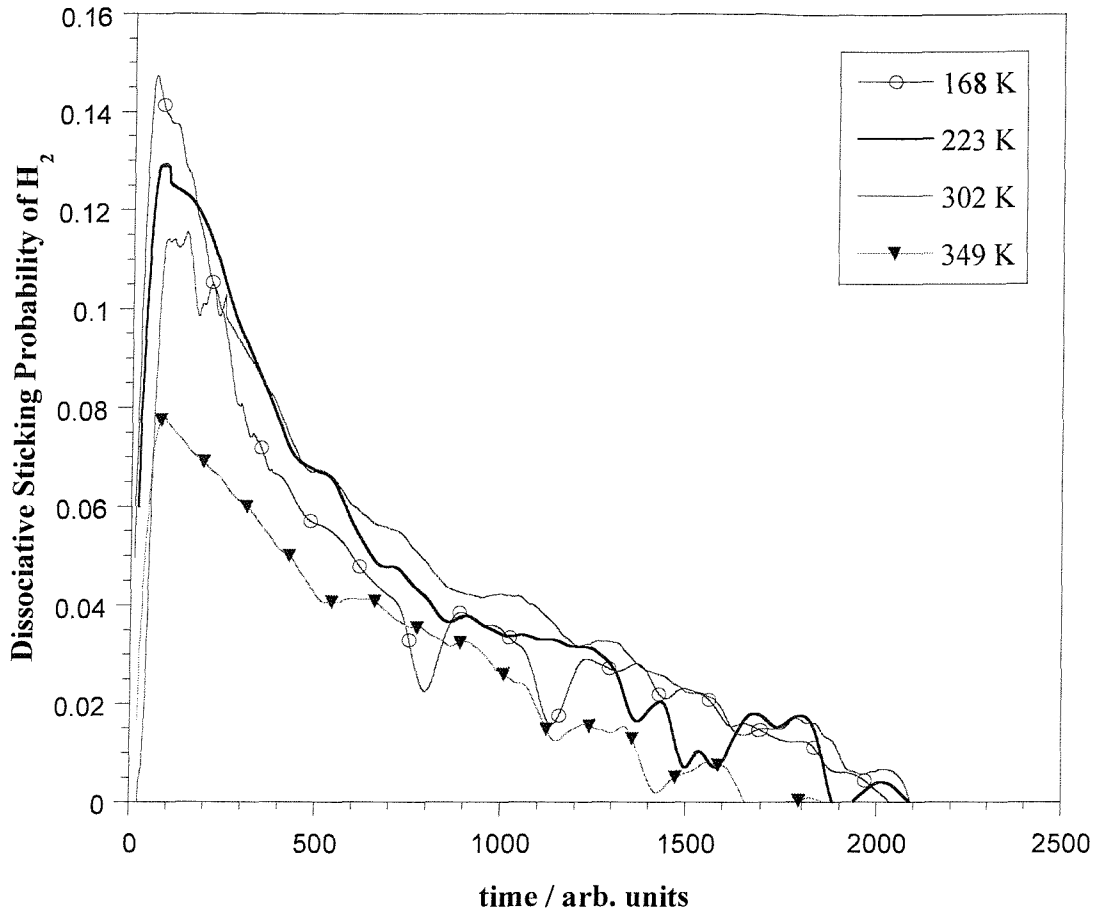

Figure V.32: $S(H_2)$ on the CO/Pt(533) surface against the time of dose of hydrogen, at $E_i = 6.6$ meV, with $168 < T_s(K) < 349$ and $\Theta_I = 0°$.

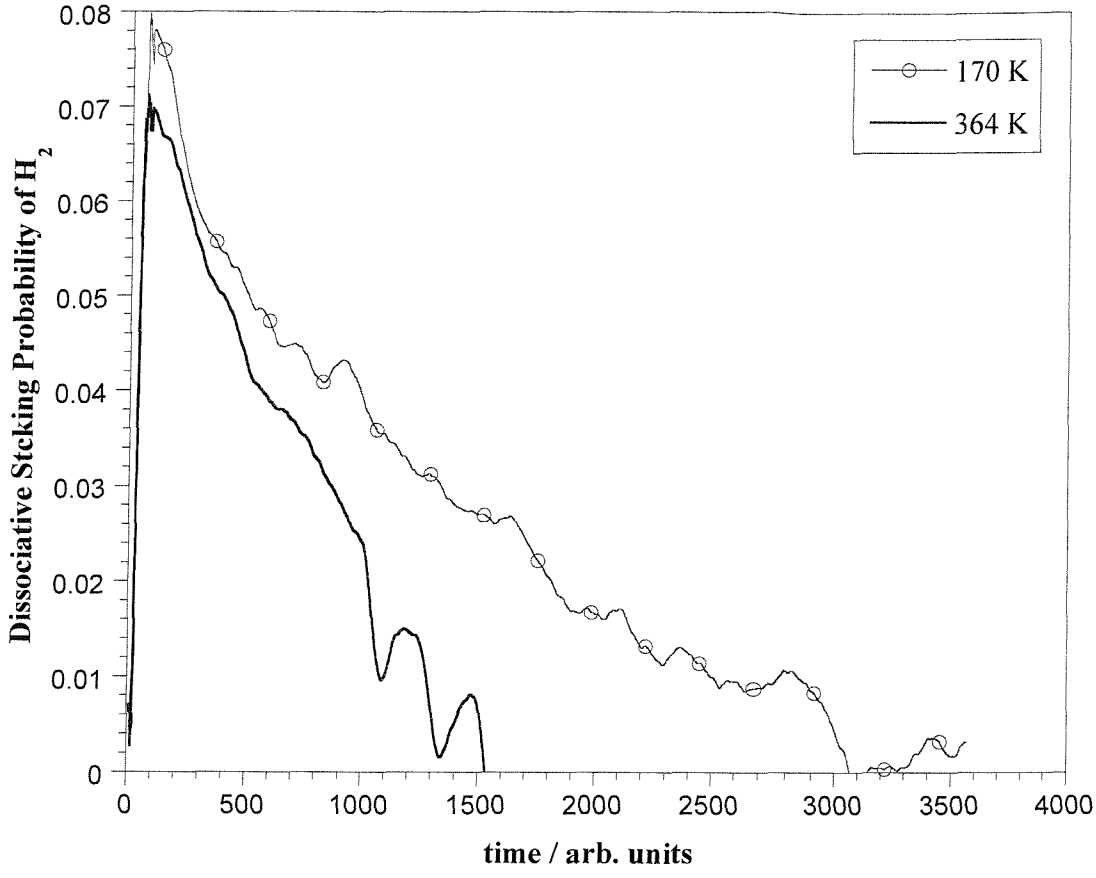

Figure V.33: $S(H_2)$ on the CO/Pt(533) surface against the time of dose of hydrogen, $E_i = 66$ meV, with $170 < T_s(K) < 364$ and $\Theta_I = 0°$.

V.4 CONCLUSION

Temperature programmed desorption measurements indicate that associative desorption of H_2 from the (100) step sites on Pt(533) is observed around 380 K with an activation energy of 94 kJ mol^{-1}. Saturation of the peak assigned to desorption from the steps takes place at 0.18 ± 0.02 ML, corresponding to the filling of half of the four-fold sites at the (100) step edge. The associative desorption of H_2 from the (111) terraces occurs below 310 K and is a second order desorption kinetics process, with an activation energy of 70 kJ mol^{-1}, which is similar to Lu and Rye results for H_2 on Pt(111) [52].

The initial dissociative sticking probability of H_2, $S_0(H_2)$, has been measured in the energy range $3 < E_i(meV) < 180$ on oxygen and CO decorated Pt(533) surfaces. At oxygen coverage greater than 0.12 ML, corresponding to the saturation of the (100) step sites, $S_0(H_2)$ exhibits a rapid decrease from 3 to 30 meV, and a linear increase above 30 meV. By removing the contribution of the step sites responsible for the low energy component of

$S_0(H_2)$ through decoration of step sites, and creating a "virtual" (111) surface, the dynamics of H_2 dissociation on the Pt(533) mimic that of Pt(111). Decorating the step sites with 0.19 ML of CO instead of O has a stronger influence on $S_0(H_2)$ due to a strongly repulsive CO-H interaction [60, 130, 131, 133], therefore the initial sticking is lower across the whole energy range studied.

The probability of dissociation through the direct channel on Pt(533), O/Pt(533) and CO/Pt(533) is found to exhibit a negligible surface temperature dependence as seen on clean Pt(533) [29] and on Pt(111) [6], moreover the $S(H_2)$ trend is near to second order Langmurian.

At 18 meV on clean Pt(533) the 3 channels are available and a very small T_s dependence is observed, while on O/Pt(533) only the direct and the accommodated indirect channels are available, hence the T_s dependence observed is characteristic of the indirect channel component.

Only at the smallest energy values (E_i = 6.6 meV) does $S_0(H_2)$ exhibit a more significant T_s dependence (on the three surfaces) which is associated with the accommodated indirect channel component. It is the partition between desorption and dissociation which is likely to be responsible for the T_s dependence of this channel at low incident energy.

At 6.6 meV, on clean Pt(533) Gee *et al.* [29] showed that the dependence of $S(H_2/D_2)$ on the hydrogen/deuterium coverage, $\theta_{H/D}$, exhibits characteristics of two different precursor mediated channel components to dissociation. Whilst on O/Pt(533) and CO/Pt(533) the trend of the sticking of H_2 is mainly due to the accommodated indirect channel.

The dominance of the indirect channels to dissociation in the overall dissociation process in the presence of step sites on Pt(533) is highlighted by demonstrating that, for a simulated isotropic thermal source, 81 % of the sticking is blocked by oxygen adsorbed at the (100) step sites (a similar result is expected for CO).

At 6.6 meV, the production of water from hydrogen adsorption on the step sites of the O/Pt(533) surface is observed above 244 K, and reaches a maximum at $T_s \sim 340$ K, while on CO/Pt(533) there is no water formation due to the lack of free oxygen adsorbates.

V.5 REFERENCES

[1] Sneed M. C. and Brasted R. C., "*Comprehensive Inorganic Chemistry*", D. Van Nostrand Company, INC. (USA), v. VI, chap. 2, p. 221, **1957**.

[2] Hayden B. E. and Lamont C. L. A., *Phys. Rev. Lett.*, 63: 1823, **1989**.

[3] Hodgson A., Wight A., Worthy G., Butler D. A., Hayden B. E., *Faraday Disc.*, 96: 161,**1993**.

[4] Butler D. A., Hayden B. E. and Jones J. D., *Chem. Phys. Lett.*, 217: 423, **1994**.

[5] Steinrück H. P., Luger M., Winkler A. and Rendulic K. D., *Phys. Rev. B*, 32: 5032, **1985**.

[6] Luntz A. C., Brown J. K. and Williams M. D., *J. Chem. Phys.*, 93: 5240, **1990**.

[7] Christmann K., Ertl G. and Pignet T., *Surf. Sci.*, 54: 365, **1976**.

[8] Harris J. and Andersson S., *Phys. Rev. Lett.*, 48: 545, **1982**.

[9] Hammer B. and Norskov J. K., *Surf. Sci.*, 343: 211, **1995**.

[10] Brivio G. P. and Grimley T. B., *Surf. Sci.*, 89: 226, **1979**.

[11] Norskov J. K. and Lundqvist B. I., *Surf. Sci.*, 89: 251, **1979**.

[12] Hayden B. E. and Lamont C. L. A., *Surf. Sci.*, 243: 31, **1991**.

[13] Hand M. and Holloway S., *Surf. Sci.*, 211/212: 940, **1989**.

[14] Steinrück R. and Winkler A., *Surf. Sci.*, 154: 99, **1985**.

[15] Butler D. A. and Hayden B. E., *Surf. Sci.*, 337: 67, **1995**.

[16] Rendulic K. D., Anger G., and Winkler A., *Surf. Sci.*, 208: 404, **1989**.

[17] Resch C., Berger H. F., Rendulic K. D., and Bertel E., *Surf. Sci. Lett.*, 316: L1105, **1994**.

[18] Berger H. F., Resch C., and Rendulic K. D., *Surf. Sci. Lett.*, 275: L627, **1992**.

[19] Alnot P., Cassuto A., and King D. A., *Surf. Sci.*, 215: 29, **1989**.

[20] Kay M., Darling G. R., Holloway S., White J. A., and D. M. Bird, *Chem. Phys. Lett.*, 245: 311, **1995**.

[21] Holloway S., Kay M., Darling G. R., *Faraday Disc.*, 105: 209, **1996**.

[22] White J. A., Bird D. M., Payne M. C., *Phys. Rev. B-Condensed Matt.*, 53: 1667, **1996**.

[23] Kay M., Darling G. R., Holloway S., *J. Chem. Phys.*, 108: 4614, **1998**.

[24] Gross A., *Surf. Sci.*, 363: 1, **1996**.

[25] Gross A. and Scheffler M., *Phys. Rev. Lett.*, 77: 405, **1996**.

[26] Gross A., and Scheffler M., *Phys. Rev. B-Condensed Matt.*, 57: 2493, **1998**.

[27] Gross A., *J. Chem. Phys.*, 110: 8696, **1999**.

[28] Butler D. A. and Hayden B. E., *Chem. Phys. Lett.*, 232: 542, **1995**.

[29] Gee A. T., Hayden B. E., Mormiche C., Nunney T. S., *J. Chem. Phys.*, 112: 7660, **2000**.

[30] Bernasek S. L., Siekhaus W. J., Somorjai G. A., *Phys. Rev. Lett.*,30: 1202, **1973**.

[31] Taylor H. S., *Proc. R. Soc. London A*, 108: 105, **1925**.

[32] Schonhammer K., and Gunnarsson O., *Phys. Rev. B-Cond. Matt.*, 24: 7084, **1981**.

[33] Christmann K. and Ertl G., *Surf. Sci.*, 60: 365, **1976**.

[34] Poelsema B., Verheij L. K. and Comsa G., *Surf. Sci.*, 152: 496, **1985**.

[35] Verheij L. K., Hugenschmidt M. B., Poelsema B., and Comsa G., *Catal. Lett.*, 9: 195, **1991**.

[36] Bernasek S. L., and Somorjai G. A., *J. Chem. Phys.*, 62: 3149, **1975**.

[37] Gale R. J., Salmeron M., and Somorjai G. A., *Phys. Rev. Lett.*, 38: 1027, **1977**.

[38] Salmeron M., Gale R. J., and Somorjai G. A., *J. Chem. Phys.*, 67: 5324, **1977**.

[39] Salmeron M., Gale R. J., and Somorjai G. A., *J. Chem. Phys.*, 70: 2807, **1979**.

[40] Verheij L.K., Hugenschmidt M. B., Anton A. B., Poelsema B., and Comsa G., *Surf. Sci.*, 210: 1, **1989**.

[41] Nyberg C., Svensson K., Martensson A. S., and Andersson S., *J. Electr. Spectr. Relat. Phen.*, 64/65: 51, **1993**.

[42] Rendulic K. D. and Winkler A., and Steinruck H. P., *Surf. Sci.*, 185: 469, **1987**.

[43] Rendulic K. D. and Winkler A., *Int. J. Modern Phys. B.*, 7: 941, **1989**.

[44] Gee A.T., Hayden B. E., Mormiche C., Nunney T.S., *Surf. Sci.*, 512: 165, **2002**.

[45] Samson P., Nesbitt A., Koel B. E. and Hodgson A., *J. Chem. Phys.*, 109: 3255, **1998**.

[46] McClellan M. R., McFeely F. R., and Gland J. L., *Surf. Sci.*, 123: 188, **1983**.

[47] Wang H., Tobin R. G., Lambert D. K., DiMaggio C. L., and Fisher G. B., *Surf. Sci.*, 372: 267, **1997**.

[48] King D. A. and Wells M. G., *Surf. Sci.*, 29: 454, **1972**.

[49] Redhead P. A., *Vacuum*, 12: 203, **1962**.

[50] Hatzikos G. H., Ph. D. dissertation, University of Illinois at Urbana-Champaign, **1987**.

[51] Thomas P. A., M. S. thesis, University of Illinois at Urbana-Champaign, **1987**.

[52] Lu K. E. and Rye R. R., *Surf. Sci.*, 45: 677, **1974**.

[53] Evans M. G., and Polanyi M., *Trans. Faraday. Soc.*, 34: 11, **1938**.

[54] Brønsted N., *Chem. Rev.*, 5: 231, **1928**.

[55] Hammer B., *Faraday Disc. Chem. Soc.*, 110: 323, **1998**.

[56] Dahl S., Logadottir A., Jacobsen C. J. H. and Nørskov J. K., *Appl. Catal. A*, 222: 19, **2001**.

[57] Baro A. M., Ibach H., and Bruchmann H. D., *Surf. Sci.*, 88: 384, **1979**.

[58] Michelsen H. A. and Luntz A. C., *Chem. Phys. Lett.*, 187: 555, **1991**.

[59] Winkler A. and Rendulic K. D., *Surf. Sci.*, 118: 19, **1982**.

[60] Rangelov G., Bischler U., Memmel N., Bertel E., Dose V., Pabst M. and Rösch N., *Surf. Sci.*, 273: 61, **1992**.

[61] Norton P. R., Davies J. A., and Jackman T. E., *Surf. Sci. Lett.*, 122: L593, **1982**.

[62] Gee A. T., Hayden B. E., *J. Chem. Phys.*, 113: 10333, **2000**.

[63] Mortensen K., Klink C., Jensen F., Besenbacher F. and Stensgaard I., *Surf. Sci. Lett.*, 220: L701, **1989**.

[64] Puglia C., Nilsson A., Hernnäs B., Karis O., Bennich P., and Mårtensson N., *Surf. Sci.*, 342: 119, **1995**.

[65] Björneholm O., Nilsson A., Tillborg H., Bennich P., Sandell A., Hernnäs B., Puglia C., and Mårtensson N., *Surf. Sci. Lett.*, 315: L983, **1994**.

[66] Materer N., Starke U., Barbieri A., Döll R., Heinz K., Van Hove M. A., and Somorjai G. A., *Surf. Sci.*, 325: 207, **1995**.

[67] Feibelman P. J., Esch S., and Michely T., *Phys. Rev. Lett.*, 77: 2257, **1996**.

[68] McClellan M. R., McFeely F. R., Gland J. L., *Surf. Sci.*, 123: 188, **1983**.

[69] Gland J. L., *Surf. Sci.*, 93: 487, **1980**.

[70] Gland J. L., Sexton B. A., and Fisher G. B., *Surf. Sci.*, 95: 587, **1980**.

[71] Gee A. T., PhD thesis, University of Southampton, **1999**.

[72] Hand M., and Harris J., *J. Chem. Phys.*, 92: 7610, **1990**.

[73] Gdowski G. E. and Madix R. J., *Surf. Sci.*, 119: 184, **1982**.

[74] Fisher G. B., Gland J. L. and Schmieg S. J., *J. Vac. Sci. Technol.*, 20: 518, **1982**.

[75] Norton P. R., "*The chemical physics of solid surfaces and heterogeneous catalysis*", King D. A. and Woodruff D. P., ed. Elsevier, v. 4, chap. 2, p. 38, **1982**.

[76] Tevault D. E., Talley L. D. and Lin M. C., *J. Chem. Phys.*, 72:3314, **1980**.

[77] Gorodetskii V. V., Sobyanin V. A., Cholach A. R. and Smirnov M. Y., *Proc. 8th Int.* Congr. Catal. W. Berlin, chap. III, p. 323, **1986**.

[78] Ogle K. M., and White J. M., *Surf. Sci.*, 139: 43, **1984**.

[79] Mitchell G. E., Akhter S., and White J. M., *Surf. Sci.*, 166: 283, **1986**.

[80] Mitchell G. E., and White J. M., *Chem. Phys. Lett.*, 135: 84, **1987**.

[81] Germer T. A., and Ho W., *Chem. Phys. Lett.*, 163: 449, **1989**.

[82] Anton A., Cadogan D. C., *Surf. Sci. Lett.*, 239: L548, **1990**.

[83] Verheij L.K., Hugenschmidt M. B., Cölln L., Poelsema B., and Comsa G., *Phys. Lett.*, 166: 523, **1990**.

[84] Verheij L.K., Freitag M., Hugenschmidt M. B., Kempf I., Poelsema B., and Comsa G., *Surf. Sci.*, 272: 276, **1992**.

[85] Gland J. L., Fisher G. B., and Kollin E. B., *J. Catal.*, 77: 263, **1982**.

[86] Kwasniewski V. J. and Schmidt L. D., *J. Phys. Chem.*, 96: 5931, **1992**.

[87] Gland J. L., and Fisher G. B., *Proc. Am. Chem. Soc. Div. Of Petroleum Chem.*, Las Vegas, p. 410, **1982**.

[88] Engel T. and Kuipers H., *Surf. Sci.*, 90: 181, **1979**.

[89] Sachs C., Hildebrand M., Völkening S., Wintterlin J., and Ertl G., *Science*, 293: 1635, **2201**.

[90] Batra, I.B., Bagus P. S., *Sol. Stat. Comm.*, 16: 1097, **1975**.

[91] Bertolini J. C., Dalmai-Imelik G., Rousseau J., *Surf. Sci.*, 68: 539, **1977**.

[92] Brodén G., Gafner G., Bonzel H. P., *Appl. Phys.*, 13: 333, **1977**.

[93] Rhodin T. N., Brucker C. F., *Sol. St. Comm.*, 23: 275, **1977**.

[94] Mason R. and Textor M., *Proc. R. Soc. London A*, 356: 47, **1977**.

[95] Bradshaw A. M., Hoffmann F. M., *Surf. Sci.*, 72: 513, **1978**.

[96] Castner D. G., Sexton B. A., Somorjai G. A., *Surf. Sci.*, 71: 519, **1978**.

[97] Williams E. D., Weinberg W. H., *Surf. Sci.*, 82: 93, **1979**.

[98] Horn K., Hussain M., Pritchard J., *Surf. Sci.*, 63: 244, **1977**.

[99] Hayden B. E., Godfrey D. C., *Surf. Sci.*, 232: 24, **1990**.

[100] Kneringer G., and Netzer F. P., *Surf. Sci.*, 49: 125, **1975**.

[101] Guo X.-C., King D. A., *Surf. Sci. Lett.*, 302: L251, **1994**.

[102] Bonzel H. P., and Ku R., *J. Chem. Phys.*, 58: 4617, **1973**.

[103] McCabe R. W., and Schmidt L. D., *Surf. Sci.*, 60: 85, **1976**.

[104] Kwasniewski V. J., Schmidt L. D., *Surf. Sci.*, 274: 329, **1992**.

[105] Campbell C. T., Ertl G., Kuipers H., and Segner J., *Surf. Sci.*, 107: 207, **1981**.

[106] Collins D. M., and Spicer W. E., *Surf. Sci.*, 69: 85, **1977**.

[107] Ertl G., Newmann M., Streit K. M., *Surf. Sci.*, 64: 393, **1977**.

[108] McCabe R. W., Schmidt L. D., *Surf. Sci.*, 65: 189, **1977**.

[109] Hopster H., and Ibach H., *Surf. Sci.*, 77: 109, **1978**.

[110] Hayden B. E., Kretzschmar K., Bradshaw A. M., and Greenler R. G., *Surf. Sci.*, 149: 394, **1985**.

[111] Winterbottom W. L., *Surf. Sci.*, 37: 195, **1973**.

[112] Collins D. M., Lee J. B., and Spicer W. E., *Surf. Sci.*, 55: 389, **1976**.

[113] Lambert R. M., and Comrie C. M., *Surf. Sci.*, 46: 61, **1974**.

[114] Hayden B. E., and Bradshaw A. M., *Surf. Sci.*, 125: 787, **1983**.

[115] Henderson M. A., Szabó A., and Yates J. T., *J. Chem. Phys.*, 91: 7245, **1989**.

[116] Brandt R. K., and Greenler R. G., *Chem. Phys. Lett.*, 221: 219, **1994**.

[117] Xu J., Henriksen P. N., and Yates J. T., *Langmuir*, 10: 3663, **1994**.

[118] McClellan M. R., Gland J. L., and McFeeley F. R., *Surf. Sci.*, 112: 63, **1981**.

[119] Lang B., Joyner R. W., and Somorjai G. A., *Surf. Sci.*, 30: 440, **1972.**

[120] Steininger H., Lehwald S., Ibach H., *Surf. Sci.*, 123: 264, **1982**.

[121] Wang H., Tobin R. G., and Lambert D. K., *J. Chem. Phys.*, 101: 4277, **1994**.

[122] Luo J. S., Tobin R. G., Lambert D. K., Fisher G. B., and DiMaggio C. L., *Surf. Sci.*, 274: 53, **1992**.

[123] Koel B., Peebles D.E., and White J.M., *Surf. Sci. Lett.*, 107: L367, **1981**.

[124] Ibbotson D.E., Wittrig T.S., and Weinberg W.H., *Surf. Sci.*, 97: 297, **1980**.

[125] Peebles D. E., Schreifels J. A., and White J. M., *Surf. Sci.*, 116: 117, **1982**.

[126] Williams E. D., Thiel P.A., Weinberg W. H., Yates, J. T., *J. Chem. Phys.*, 72: 3496, **1980**.

[127] Benziger J. B., and Madix R. J., *Surf. Sci.*, 115: 279, **1982**.

[128] Thrush K. A., and White J. M., *Appl. Surf. Sci.*, 24: 108, **1985**.

[129] Baldwin, V.H., and J.B. Hudson, *J.Vac.Sci.Technol.*, 8: 49, **1971**.

[130] Henderson M. A., and Yates J. T., *Surf. Sci.*, 268: 189, **1992**.

[131] Hahn E., Frike A., Röder H., and Kern K., *Surf. Sci.*, 297: 19, **1993**.

[132] Wang H., Tobin R. G., Lamberg D. K., Fisher G. B., Dimaggio C. L., *Surf. Sci.*, 330: 173, **1995**.

[133] Parker D. H., Fisher D. H., Colbert J., Koel B. E., and Gland J. L., *Surf. Sci.*, 258: 75, **1991**.

[134] Craig J. H., *Surf. Sci. Lett.*, 111: L695, **1981**.

[135] J. M. White and S. Akhter, *Crit. Rev. Solid State Mater. Sci.*, 14: 131, **1988**.

CHAPTER VI: DYNAMICS AND KINETICS OF ADSORPTION OF AMMONIA ON Pt(533)

VI.1 INTRODUCTION

VI.1.1 Ammonia Production

In terms of scale of production, ammonia is one of the five most important products in the chemical industry [1]. It is widely used as an industrial chemical and in agriculture, in fact 85 % is used to produce fertilisers. Its chief uses include the production of other compounds of nitrogen, particularly nitric acid (Ostwald process) and ammonium salts; among the latter the sulphate, nitrate, chloride and sodium carbonate (Solvay process) are especially important. Ammonia is also used in the production of a variety of organic chemicals, including various dyes, drugs and plastics. The mild alkalinity of aqueous NH_3 enables it to be used as a household-cleansing agent. Due to its high heat of vaporisation and the ease with which NH_3 gas is liquefied under pressure, NH_3 is widely used as a refrigerant.

Because of this industrial relevance, a minor improvement in the efficiency of the production or decomposition of ammonia results in large economic benefits.

Physicals methods, in particular microwave and infrared spectroscopy, have established in detail the structure of ammonia (in the gas phase) which is formally the simplest amine. The molecule forms a somewhat flattened trigonal pyramid. The H-N-H angles, all equal, are close to 107°, and the N-H bond length is close to 1.01 Å. The height of the pyramid is about 0.3 Å. The bonding energy of each N-H bond for gaseous ammonia is -386 kJ mol^{-1}.

VI.1.2 Ammonia Adsorption on Transition Metals

The interaction of NH_3 with metal surfaces has become a classical problem in the field of heterogeneous catalysis. In particular the catalytic action of transition metals permits a more rapid attainment of the chemical equilibrium for certain chemical reactions involving

NH_3 formation, adsorption and decomposition. Platinum [2-11], palladium [12, 13] and nickel [12] represent good catalysts for ammonia adsorption and decomposition, while iron [14] represents a good catalyst for NH_3 formation:

$$3\ H_2 + N_2 \rightarrow 2\ NH_3 \qquad (1)$$

This synthesis requires the activation of the N-N (and H-H) bond by the surface. The nitrogen atoms that then form must react with hydrogen atoms to produce NH_3. The very large dissociation energy of N_2 ($\Delta E = 1120$ kJ mol^{-1}) makes it virtually impossible for this reaction to occur in the gas phase. However, N_2 dissociates on a properly structured iron surface with a small activation energy ($\Delta E = 12$ kJ mol^{-1}). This is the key initiation step for the catalytic reaction. Iron also readily atomises the hydrogen molecules. The chemisorbed nitrogen atoms then react with hydrogen atoms on the surface to produce NH, NH_2, and finally NH_3 molecules that desorb into the gas phase [14]. This process developed by Fritz Haber in 1909, known as the Haber-Bosch process [15], was the first commercially important high-pressure (~ 1000 atm) chemical process and is still the major method of production of NH_3. It requires a high temperature (between 720 and 870 K). The collaboration between Haber, Bosch and Mittash from the Oppau and Leuna Ammonia Works enabled Germany to prolong the First World War when in 1914 the supplies of nitrates for making explosives had failed. N_2 dissociation is also the rate-limiting step to NH_3 synthesis over Ru [16].

Thus, great interest was found in studying the interaction of NH_3 with metal surfaces and the elementary steps leading to its synthesis and its decomposition, in order to elucidate the mechanistics of NH_3 behaviour in catalytic reactions. Therefore, it is of primary importance to know the stoichiometry, structure, bonding and stability both of the initial adsorbed species and the intermediates formed by the process of dissociation. Studies of the ammonia decomposition probe the properties of the N-H bonds of ammonia.

As stated in **chapter IV**, platinum is one of the most versatile, heterogeneous metal catalysts and therefore is used in many different reactions, but it is a relatively poor ammonia synthesis catalyst. Ammonia thermal desorption and oxidation on platinum were studied in the late 1970s. Additionally, several surface science techniques have been

employed to gain an understanding of the catalytic processes that occur with NH_3 as probe molecule and platinum as a substrate. These include TPD [2,3], work function measurements, ultraviolet and X-ray photoelectron spectroscopy (UPS and XPS) [2], electron energy loss spectroscopy (EELS) [3], collision induced desorption (CID) experiments [4], electron stimulated desorption ion angular distribution (ESDIAD) [5-9] and molecular beam techniques [10]. However, relatively few basic studies concerning the dynamics of ammonia adsorption have been carried out, therefore the present study will concentrate on NH_3 on the Pt(533) surface in order to elucidate the dynamics of NH_3 adsorption and decomposition over platinum.

VI.1.3 Molecular Orbitals of NH_3 and Energy Diagram Correlation with Pt

A wide range of surface science techniques and theoretical treatments have been used to interpret the surface interaction between the platinum atoms and the NH_3 molecules. After studying the NH_3/Pt(111) system by photoemission, work function and thermal desorption measurements, Fisher [2] proposed that, for a low coverage, NH_3 adsorbs on Pt(111) in a threefold fcc hollow site which has a vacancy underneath. Sexton and Mitchell [3] studied ammonia chemisorption on Pt(111) by EELS and TPD, and came to the same conclusion. However, the molecular orbital calculations performed by Fierro [17] on NH_3 adsorbing on a hollow and on a bridge site reveals that there is repulsion from the Pt surface; and this was also confirmed by Garcia-Hernandez *et al.* 11 years later [1]. In fact, there is only a weak interaction between the d_{z2}, d_{xz} and d_{yz} orbitals of the metal atom and the $2a_1$ MO of the ammonia molecule adsorbed on a hollow site, therefore the $2a_1^*$ combination orbitals are not destabilised above the Fermi level and consequently remain occupied by electrons leading to a destabilisation of the adsorbed ammonia.

The molecular orbital approach developed by Fierro clearly implies that the N-H bonds are weakened, suggesting that there is opening of a decomposition pathway for NH_3 on a cluster model Pt(111) surface, proceeding via the N-H bond scission. The energy molecular orbital correlation diagram for NH_3 directly above a Pt surface atom is shown in **figure VI.1** [17].

The $1s^1$ atomic orbitals of the three H atoms and the $1s^2\ 2s^2\ 2p^3$ atomic orbitals of the N interact together. They give three bonding orbitals $1a_1^2$, $1e_x^2$ and $1e_y^2$, corresponding to the N-H bonds, and the non–bonding orbital $2a_1^2$ which has a slight N-H bonding character, and corresponds to the N lone pair.

The most stable Pt-N distance of 2.05 Å was optimised to the nearest 0.05 Å. The unoccupied s-p and occupied s-d bands of the Pt are located on the left side of the diagram, with the darker areas indicating single occupied levels. On the right side of the figure the ammonia MOs are shown before the interaction with the surface [17].

The MO 1e is lower in energy than the $2a_1$. It has a high contribution at the N end of the molecule, and thus it is well suited for π interactions with the d_{xz} and d_{yz} metal orbitals. However, the large energy gap between this MO and the Pt s-d band and the large bond length lead to negligible interaction.

The lone pair $2a_1$ orbital corresponds to the highest occupied MO (HOMO). It is ideally polarised for a σ interaction at the N end of the molecule. For NH_3 on top of a Pt atom, the $2a_1$ orbital is close to the s-d band and interacts with the appropriate orbitals of the metal d_{z2} by transferring charge to form a strong chemisorbed bond. In fact, this interaction will produce two bonding combinations: $2a_1$ (formally assigned to the lone pair of chemisorbed NH_3) and a_1 (mainly metal character). The rehybridisation of the d_{z2} orbital with the p band also interacts with the $2a_1$ orbital of the ammonia to produce an antibonding combination, $2a_1^*$. This latter MO is pushed up in energy above the Fermi level hence the electrons from the $2a_1$(HOMO) orbital of the NH_3 in gas phase will not fill the $2a_1^*$ orbital of the NH_3 above the Pt atom. These electrons will drop to lower empty energy levels, *i.e.* available metal states. Thus, as found experimentally by surface core-level photoemission, the d_{z2} orbital of the platinum atom underneath the chemisorbed ammonia (entering in the MO $2a_1^*$) has been electron depleted in favour of the surrounding Pt atoms. Hence the N-H bonds are destabilised and the polarisation of the molecule is increased.

$3a_1$ is the lowest unoccupied MO (LUMO) and is N-H antibonding and more localised at the H atoms. Moreover the energy gap between this orbital and the Pt s-d is

rather large. Therefore, this particular orbital was found to play a negligible role when NH_3 is adsorbed on top of a Pt atom.

Fierro's approach is relevant to the present study of NH_3 on the Pt(533) surface, because it helps understanding how the ammonia molecules stick on the (111) terraces of this surface, and how they might decompose. Moreover it gives an idea on the NH_3-Pt bond likely to occur at the (100) steps. Each platinum (111) terrace atom has 6 nearest neighbours in the first layer, and another 3 in the layer immediately below; a total of 9. Each (100) step atom has 4 nearest neighbours in the surface layer of terrace atoms which terminates at the step, and another 3 in the layer immediately below; a total of 7. As the number of coordination is smaller at the step, the electron density is lower, hence the Fermi level of the d band goes down, leading to a stronger bond with the adsorbate than on the terrace. Hence for NH_3 adsorbed on a step Pt atom we expect the $2a_1$ MO, which correspond to the σ interaction, to be even lower in energy, and the $2a_{1*}$ MO, to be even higher in energy, in order to stabilise even more the Pt-N bond on the surface. Hence the N-H bonds are also expected to be weaker than for NH_3 adsorbed on the terraces, meaning that the decomposition of ammonia is likely to be more activated on the steps.

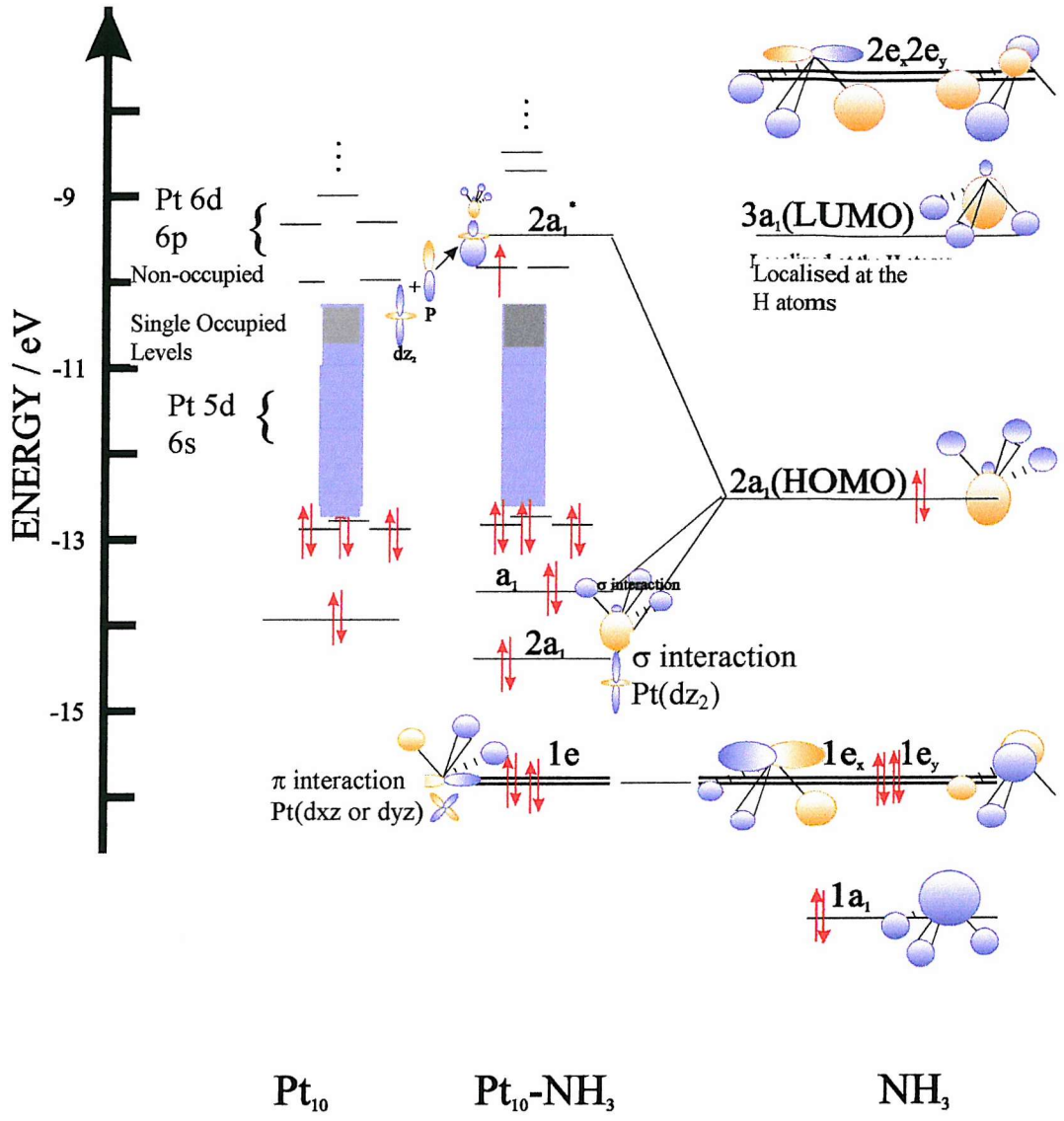

Figure VI.1: Energy MO correlation diagram for NH_3 directly on top of a Pt surface atom [18,19].

VI.1.4 NH_3 Adsorption on Platinum Surfaces

A study led by Löffler and Schmidt [11] on the ammonia dissociation over several single-crystal planes of platinum near atmospheric pressure, showed that the most open planes, such as Pt(210) and Pt(110) are the most effective for dissociation, while Pt(111) or Pt(100) give a poor rate of decomposition of NH_3. This early work drove others to study the structural effects of platinum on ammonia adsorption, desorption and dissociation.

Several studies have been performed on the adsorption of ammonia on supported Pt [20, 21], polycrystalline Pt [22-26] and single crystal Pt planes [2,3,10,11,27] under vacuum. Fisher [2] performed some NH_3 TPD experiments over a Pt(111) single crystal

surface as shown in **figure VI.2**, but did not see any evidence of any structural effects. Gohndrone *et al.* [28] also obtained some TPD data on several platinum surfaces (**figures VI.3 and VI.4**), as well as some EELS data for NH_3 adsorption on Pt(210), which led them to conclude that the binding of ammonia does not vary significantly with crystal plane.

Figure VI.2 shows a first low narrow temperature peak, called γ, at 120 K representing the desorption of multilayers of ammonia. There are two phases of NH_3 in the first monolayer, called α and β ammonia. At low coverage, less than a quarter monolayer, the TPD spectra of ammonia on Pt(111) shows the broad, low coverage α peak centred between 300 and 400 K that implies the presence of a high binding energy adsorbate. This has previously been assigned to NH_3 molecules directly interacting with the metal surface (the α ammonia is thought to be bound through the lone pair on the nitrogen). This peak is so broad, suggesting strong interactions within the adsorbed layer, that no estimation of the adsorption energy can be deduced. However, complementary information is provided by CID measurements performed by Szulczewski and Levis [4] led to an estimate of 107 kJ mol^{-1} for the absolute value of the adsorption energy at low coverage [1]. Moreover this is in good agreement with the prediction of 112 kJ mol^{-1} from Garcia-Hernandez ab-initio calculations carried out in the frame work of the hybrid B3LYP DFT based method. Fahmi and van Santen [29] also calculated this energy to be around 114 kJ mol^{-1} (depending on the size of the Pt-cluster) with a GGA method, while Jennison *et al.* [30] used the LDA method with a much larger Pt-cluster to find a value around 121 kJ mol^{-1}. The β ammonia desorbs between 120 and 180 K and is thought to be held with a hydrogen bond to the α ammonia and is a first order kinetics process with a heat of desorption around 36 ± 3 kJ mol^{-1} calculated by Gland [27]. It is quite clear that the β-phase is almost entirely electrostatically bound, and involves lateral interactions and direct interactions with the metal surface [30], whereas it is likely that the α-species corresponds to isolated chemisorbed molecules. The following layers γ are all held by hydrogen bonding too. This type of bond only represents 5 % of the strength of a covalent bond but it is a fairly strong dipole-dipole interaction typically between 4 and 30 kJ mol^{-1}.

Sexton and Mitchell [3] studied the NH_3/Pt(111) system by EELS. The vibrational spectrum of ammonia obtained leads to conclude that the α-NH_3 directly chemisorbed on the Pt surface via the N-atom with the C_3 molecular axis normal to the surface. This model

for α-NH_3 is in agreement with the model proposed by Purtell *et al.* for NH_3 on Ir(111) [31]. However, there is no direct determination of the active site. According to the common interpretation of EELS the NH_3 molecules should lie on a three-fold-hollow open, or fcc, site of Pt(111) [2]. However this prediction is against the theoretical calculations based on the DFT formalism [29, 30]. Therefore at present there is still no information concerning the geometry of molecularly adsorbed NH_3 on Pt(111) or any other metal surface. It is clear that chemisorbed NH_3 preserves its C_{3v} symmetry, but the extent of deformation from the gas-phase structure remains essentially unknown except for preliminary work by Garcia-Hernandez *et al.* [1]. In fact, they concluded in a small distortion of the gas phase molecular geometry and no azimuthal preference for the on-top chemisorption and found that there is a net charge transfer from NH_3 to the surface with N closer to the surface. Moreover, ESDIAD experiments on different transition metal surfaces show that chemisorbed NH_3 seems to be freely rotating around its C_3 molecular axis [5-9] which can explain the difficulties of studying the position of H atoms from adsorbed NH_3 by LEED [3].

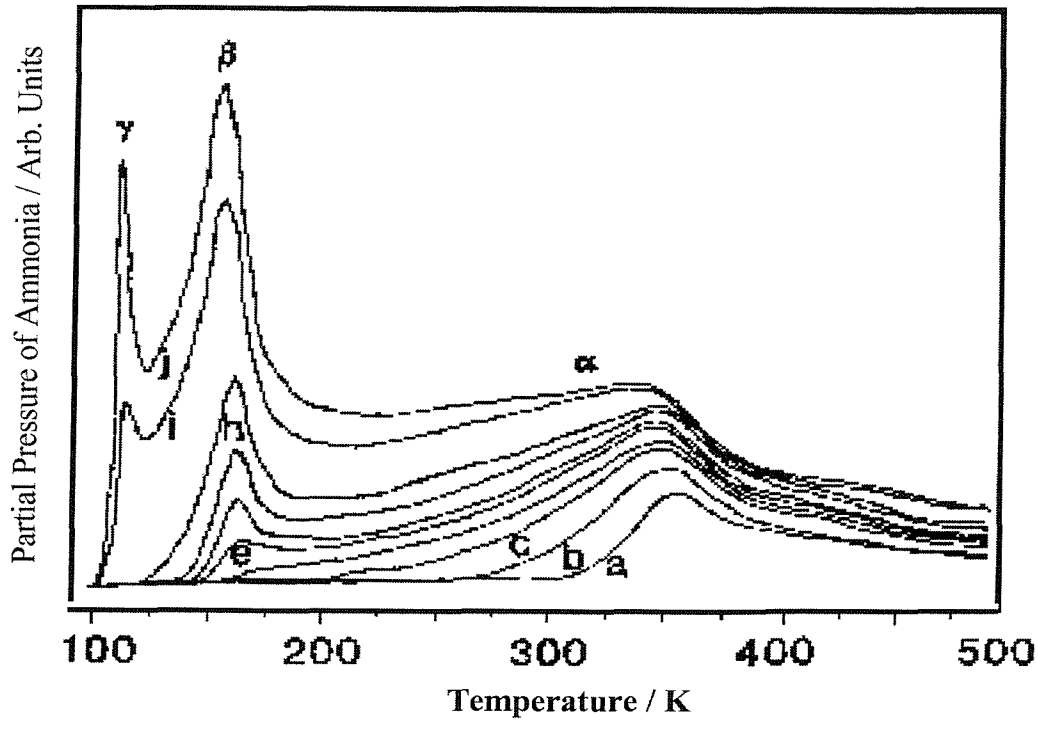

Figure VI.2: Reproduction of ammonia temperature programmed desorption spectra from the Pt(111) surface obtained after exposure at 100 K with a heating rate of 9 K s^{-1} from Fisher [2].

Figures VI.3 and VI.4, show some ammonia thermal desorption data from the (111), (100)-hex, (110), (210) and (211) Pt single crystal planes. All of the spectra show a

multilayer peak γ at 120 K, a high coverage peak or series of peaks β at 170 K and a broad low coverage feature α between 300 and 380 K. Therefore there is no discernible effect of the platinum surface structure.

While Fisher [2] and Gohndrone [28] observed only 3 peaks on Pt(111), Ranney *et al.* [32] observed an additional peak around 220-240 K on this surface. It is quite probable that the samples used by Fisher and Gohndrone had surfaces relatively defect free, while the one used by Ranney was not, hence contributing in a fourth feature. It should be noticed that Gohdrone also observed this last feature, β', for ammonia desorbing from Pt(110) and Pt(211). Thus the defected Pt(111) surface as well as the Pt(110) and Pt(211) surfaces have some identical adsorption sites.

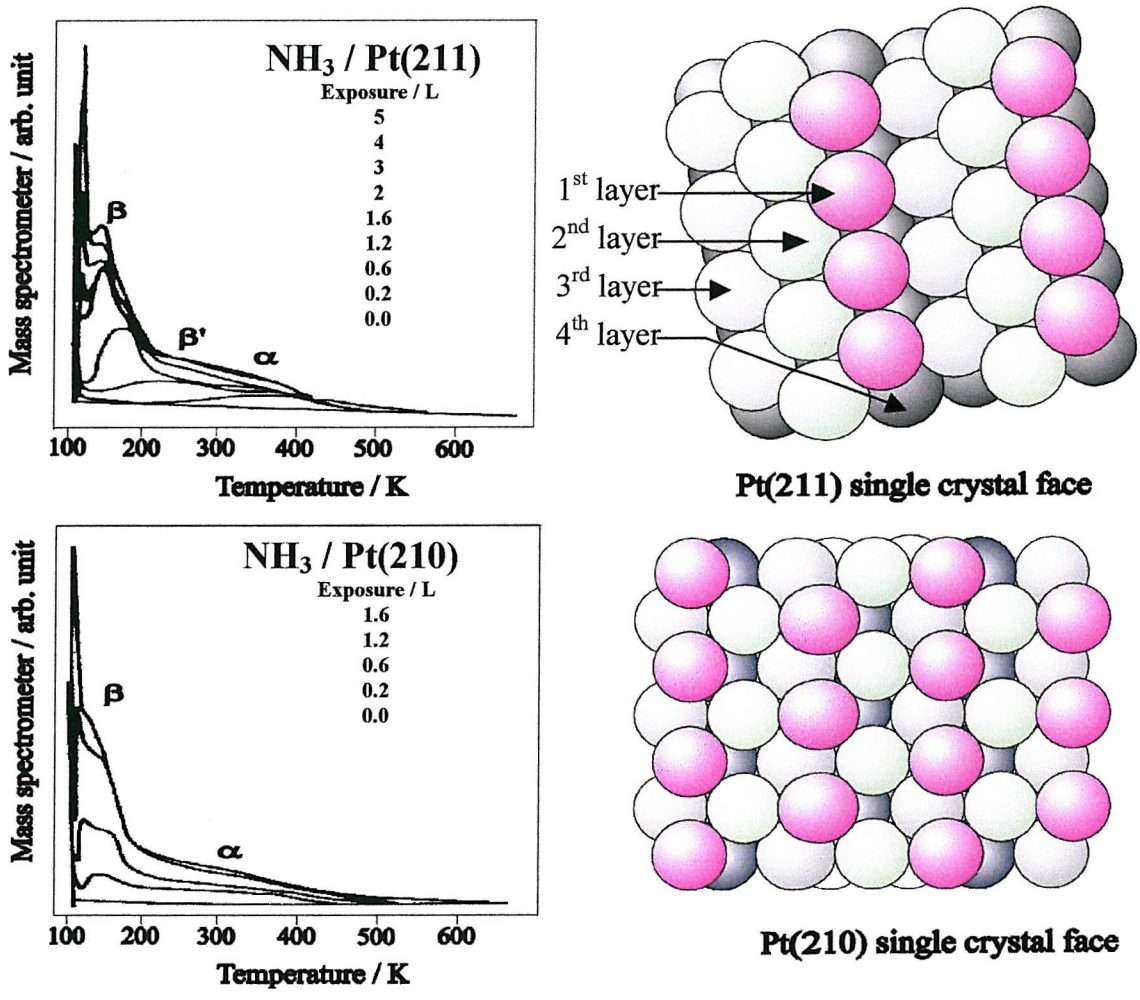

Figure VI.3: Reproduction of a set of TPD spectra taken by adsorbing varying amounts of ammonia onto a 100 K Pt(210), and Pt(211) samples then heating at 14 K s^{-1} from Gohndrone *et al.* [28].

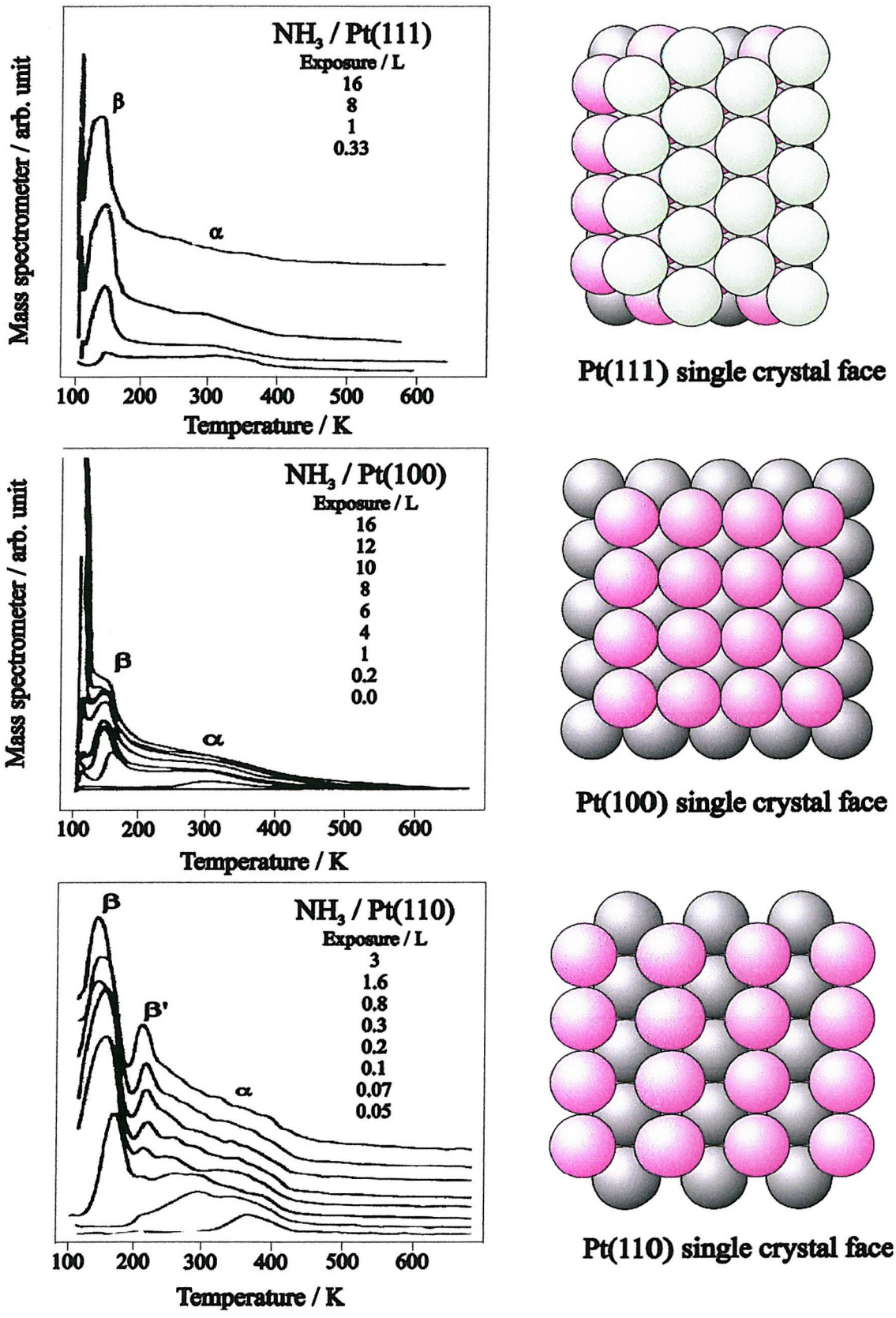

Figure VI.4: Reproduction of a set of TPD spectra taken by adsorbing varying amounts of ammonia onto a 100 K Pt(111), Pt(100) and Pt(110) samples then heating at 14 K s^{-1} from Gohndrone *et al.* [28].

These data lead to conclude that ammonia adsorption is molecular under 400 K and does not seem to depend on the platinum surface plane. This observation was also made for other metal catalysts, for example the presence of steps on a Rh(100) surface has very little influence on the NH_3 heat of adsorption [33].

VI.1.5 Decomposition of NH_3

While all the research groups who worked on the NH_3/Pt system since the 80's agree on the fact that ammonia does not decompose under 400–450 K, they did not always agree on the ammonia behaviour at higher temperatures.

Gohndrone *et al.* [28] searched for hydrogen and nitrogen production from Pt(111), Pt(100), Pt(110), Pt(210), and Pt(211) using TPD but did not see anything. However, using molecular-beam techniques, H_2 and N_2 are detected above 500 K. Still they conclude that Pt(210) is at least 100 times as active as Pt(111) for ammonia decomposition. Guthrie *et al.* [10] also performed some molecular beam surface scattering experiments which led to observe N_2 and H_2 desorption following NH_3 adsorption on Pt(557) and Pt(111). In a UHV molecular beam surface scattering apparatus, a pure beam of ammonia was formed under nearly effusive conditions in the source chamber, then it was chopped when entering the differential chamber by a slotted disk chopper then it impinged on the crystal surface in the reaction chamber. A mass spectrometer positioned out of line-of-sight of the crystal surface allowed to measure the modulation in partial pressure of the species emitted from the surface. The amplitude and phase lag vary as a function of chopping frequency of the beam because the emitted molecules have a finite residence time in the UHV chamber before being pumped away. Both were obtained by measuring the filtered ion current detected by a channeltron multiplier and processed using a lock-in amplifier (to measure the component of the mass spectrometer signal at the incident beam chopping frequency). The major difference is the amplitude of the hydrogen signal which was found to be 16 times greater for the stepped Pt surface, demonstrating that the Pt(557) surface is 16 times more active than the flat surface, which was concluded to be due to the higher density of steps. Notice that the Pt(210) surface has roughly 6 times more steps than the Pt(557) surface, therefore it

was expected to be (16x6 = 96) a 100 times more active than the Pt(111) surface which is confirmed by Gohndrone results [28].

Earlier work by Gland in 1978 [34] showed that NH_3 dissociates over a Pt(566) surface (which is defined by 12 atoms wide (111) terraces separated by (111) monoatomic steps) after exposure to NH_3 at 200 K and gives rise to N_2 and H_2 desorption. Gland observed a main N_2 peak above 500 K. The same author [27] later published a series of isotope exchange thermal desorption experiments with adsorbed deuterium and ammonia on a Pt(111) and a stepped Pt(466) surface (which is defined by 6 atoms wide (111) terraces separated by (111) monoatomic steps). They concluded that NH_3 dissociative adsorption does not occur below 400 K on either surface. Moreover, there is a noticeable effect of the (111) type steps as shown by the large desorption of N_2 around 500 K compared to the small N_2 peak on the flat Pt(111). Results from Guthrie *et al.* [10] show no decomposition of NH_3 on a clean Pt(111) surface under 600 K, which together with Gonhdrone's [28] experiments on Pt(111) lead us to the conclusion that Gland's Pt(111) sample contained a high density of defects which consequently allowed NH_3 dissociation below 500 K.

This last suggestion was reinforced in 1995, by Mieher *et al.* [35] who observed no decomposition of NH_3 on Pt(111) whatsoever.

The desorption of N_2 following NO adsorption on platinum (111) also occurs around 525 K as observed by Lee *et al.* [36] with a shoulder at 610 K and a large feature above 700 K, suggesting that the recombination of atomic nitrogen on Pt occurs in this temperature range. Gland *et al.* also observed this phenomenon around 500 K following NO adsorption [34,37], reduction [38] and shows it to be independent on the amount desorbed. Gohndrone and Masel [39] observed the production of N_2 after decomposition of NO dosed on to a Pt(211) = [3(111)×(100)] at 450-500 K.
However there is no recombinative desorption of N_2 at 500 K when dosing N_2H_4 on Pt(111) because N_2 is formed intramolecularly [40].

In summary, a defect free Pt(111) surface as well as Pt (111) terraces do not dissociate NH_3 to produce N_2 and H_2, while Pt steps may be more active.

VI.2 EXPERIMENTAL

The experiments were carried out in an UHV chamber. The platinum single crystal used in this study is a stepped Pt(533) crystal. The crystal was cleaned by annealing between runs to 1120 K for 5 to 20 minutes depending on its degree of cleanliness, but required other sort of treatments before a series of measurements as described previously in **chapter II.**

In order to obtain the initial dissociative sticking coefficient of NH_3 on the platinum surface, $S_0(NH_3)$, the gas-mixture was varied depending on the energy required. Thus argon, helium and neon, each with a purity of 99.9995 %, were used as seeding gases (**chapter II**), and NH_3 had a purity of 99.99 % too (all BOC Gases).

The nozzle temperature was varied from 300 K to an upper limit of 900 K. For the TPD experiments $130 < T_s(K) < 180$ (depending on the efficiency of the cooling) during the NH_3 exposure. T_s was held at 400 K during the King and Wells measurements of initial dissociative sticking probability of NH_3, which corresponds to the first maximum of H_2 desorption after NH_3 adsorption, therefore ensuring that NH_3 has already undergone some decomposition at this specific temperature. Moreover **figure VI.5** shows that NH_3 is not adsorbed molecularly at this temperature.

VI.3 RESULTS AND DISCUSSION

VI.3.1 Ammonia Temperature Programmed Desorption

Some attempts to run thermal desorption spectra following NH_3 exposures from a pure or seeded NH_3 supersonic molecular beam on a platinum (533) crystal surface resulted in spectra dominated by background desorption, apparently arising from the sample holder. This was due to the poor efficiency of the sample heating, thus a new design of the sample mounting was favoured as it necessitates a much lower current to reach the same temperatures. As a result, the heat drawn in the W wires is minor leading to a minor heat through the sample holder thus noticeably less desorption from the holder was observed (it has a very low resistance), however we were still highly limited in the exposition time due to this rising background. Therefore the maximum exposure performed giving a trustworthy

TPD spectrum was only of 0.1 L. In the present work, using a molecular beam technique, a mixture varying from 4 % to 100 % of ammonia in helium was dosed on to the Pt(533) surface. The dosing was carried out with $T_n = 300$ K, using a 1,3 mm aperture leading to a beam of 3 mm diameter on the sample surface, and at $T_s = 135$ K obtained by liquid nitrogen cooling of the sample holder. Subsequent thermal desorption was monitored by a fixed quadrupole mass spectrometer measuring the resulting background pressure rise in the reaction chamber.

Figure VI.5 shows the desorption of NH_3 obtained for increasing NH_3 exposures. The limitation of the sample cooling to 135 K did not allow to observe the multilayer peak γ previously described by Gland [27], Gohndrone [28] and Fisher [2]. However the relatively sharp β at 165 K and the large α feature, peaking between 250 and 300 K and corresponding to the first monolayer of NH_3 on the surface, are clearly present.

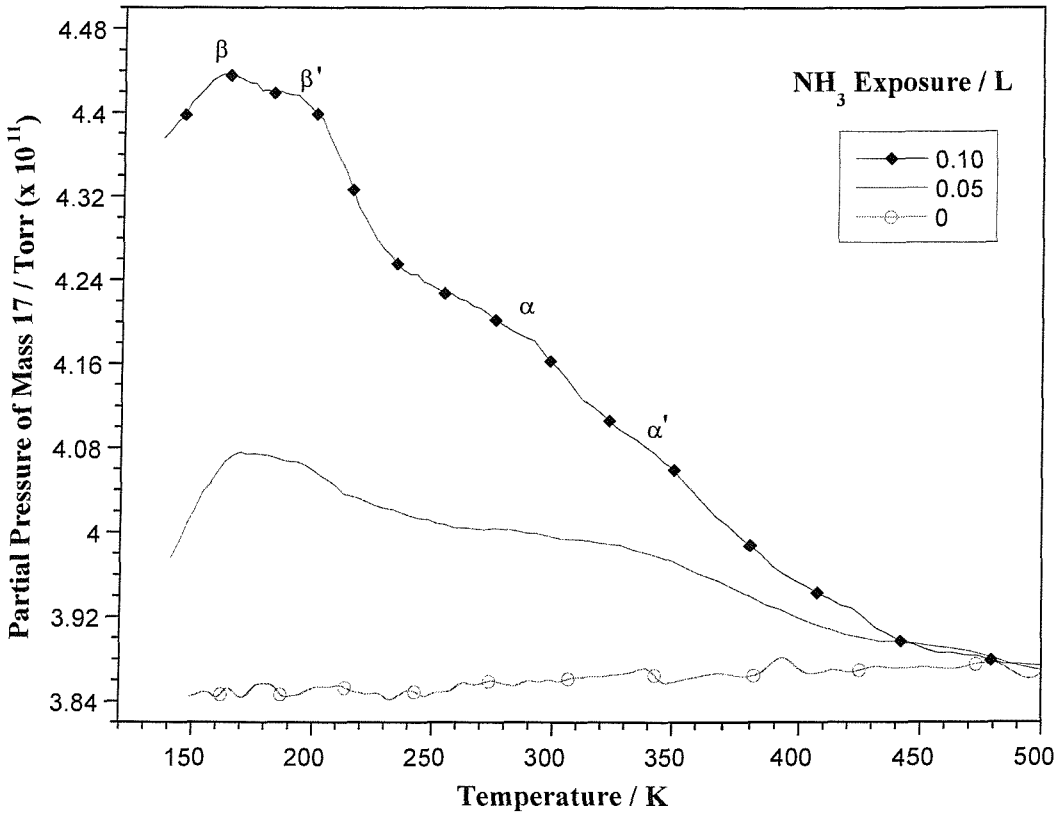

Figure VI.5: TPD of NH_3 following exposure of Pt(533) to NH_3. NH_3 was dosed using the beam source (4-100 % NH_3 in He), at $T_s = 135$ K, $T_n = 295$ K, $E_i = 108$ meV. The heating rate was 3.4-4.4 K s^{-1}. Exposures are shown in Langmuir.

Moreover, there is a third feature β' appearing around 190-210 K, which has also been observed previously on Pt(110) and Pt(211) by Gohndrone [28] and on Pt(111) by Ranney [32] firstly associated with surface defects. The experiments performed in **chapter V** have shown that the present Pt(533) sample surface is of high quality and therefore it is more likely that the β' peak refers to the presence of the (100) steps. Notice also a very weak shoulder at 330 K, α', which will be attributed later.

Figure VI.6 shows the deconvolution of the TPD feature corresponding to the highest NH_3 dose performed earlier in **figure VI.5**. The 2 first features peak at 156 and 184 K respectively for β and β', and correspond to a binding energy of respectively 39 kJ mol^{-1} and 46 kJ mol^{-1}. The values for the β and β' peaks are in the same range as the data obtained by Gland [27].

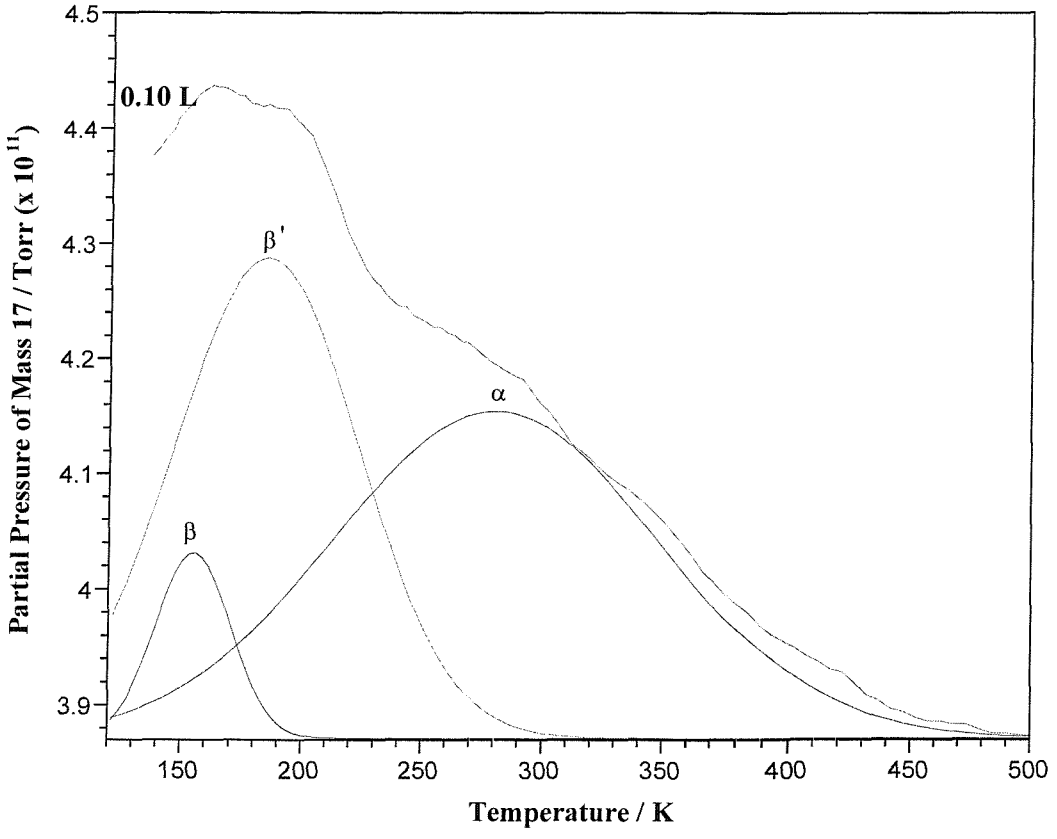

Figure VI.6: TPD of NH_3 following an exposure of Pt(533) to 0.1 L NH_3. NH_3 was dosed using a beam source (100 % of NH_3) at T_s = 136 K, T_n = 294 K and E_i = 108 meV. The heating rate was 3.9 K s^{-1}. The exposure is shown in Langmuir.

The position of the α peak maximum is uncertain, therefore its heat of desorption could not be estimated reliably using the heating rate and the temperature of the maximum desorption, however the present deconvolution shows it to be at 281 K, which correspond to a desorption energy of 72 kJ mol^{-1} rather different from the values obtained earlier on [4]. There was no attempt to extract the α' shoulder from the spectrum.

VI.3.2 Temperature Programmed Desorption (TPD) of N_2 and H_2

While no decomposition of NH_3 was observed on Pt(111) [10, 28, 35], the present study clearly reveals the production of N_2 and H_2 by dosing NH_3 on a clean Pt(533) surface. **Figure VI.7** shows the production of N_2 after NH_3 was dosed in a He beam (2-50 % NH_3), at $T_s = 135$ K, $T_n = 295$ K and $138 < E_i$ (meV) < 256. The TPD exhibits clearly a single peak around 530-540 K and a feature around 950 K.

The 530 K feature is in complete agreement with the literature results obtained dosing NH_3 on Pt(466) and on Pt(566) [27, 34], and dosing NO on Pt(111) and on Pt(211) [36, 39]. It correspond to the recombinative desorption of nitrogen atoms. This is supported by the observation that when atomic nitrogen is dosed at low temperature (< 200 K), N_2 recombinative desorption takes place between 450 and 650 K [41, 42]. Hence the rate controlling step of N_2 desorption on Pt(533) the associative desorption of nitrogen adatoms, and not NH_x decomposition which must take place at $T_s < 530$ K. Moreover given the fact that molecular N_2 does not stick on stepped Pt surfaces at $T_s > 150$ K [43], N_2 is not expected to reside on the surface after its formation. N atom recombination also occurs at relatively high temperature on other metal surface, such as Rh(111) at 670 K [44], Rh(100) at 775 K [45], and Fe at 800 K [46]. The inactivity of Pt(111) to dissociate NH_3 leads us to conclude that the N_2 desorbing at 530-540 K is due to NH_3 dissociating at the (100) steps.

The feature around 950 K was also observed by Gland *et al.* on Pt(111) and Pt(466) surfaces [27] and was associated with nitrogen desorbing from a nitrogen containing near-surface compound (surface platinum "nitride"). Mieher and Ho [35] in their EELS experiments also observed a feature on clean Pt(111), O/Pt(111) and O_2/Pt(111) at 98 meV that they assigned with the latter nitride species (Pt-N stretch mode). A second feature at

132 meV on both oxygen precovered surfaces was also assigned to nitride species experiencing the influence of the oxygen adsorbates. In fact they observed that after building up a huge coverage of ammonia, atomic nitrogen is still present for annealing temperatures up to 650 K but is not present after annealing to 1050 K. Therefore we attributed the present 950 K-N_2 feature to N_2 resulting from the recombination of atomic N occurring after dissociation of NH_3 on Pt(533). Noticed that the mass 14 signal (**figure VI.8**) present a large background desorption above 800 K which conceal the probable cracking patterns of N_2 at 950 K from the mass 28 signal (**figure VI.7**). Moreover, no trace of carbon at these high temperatures was detected.

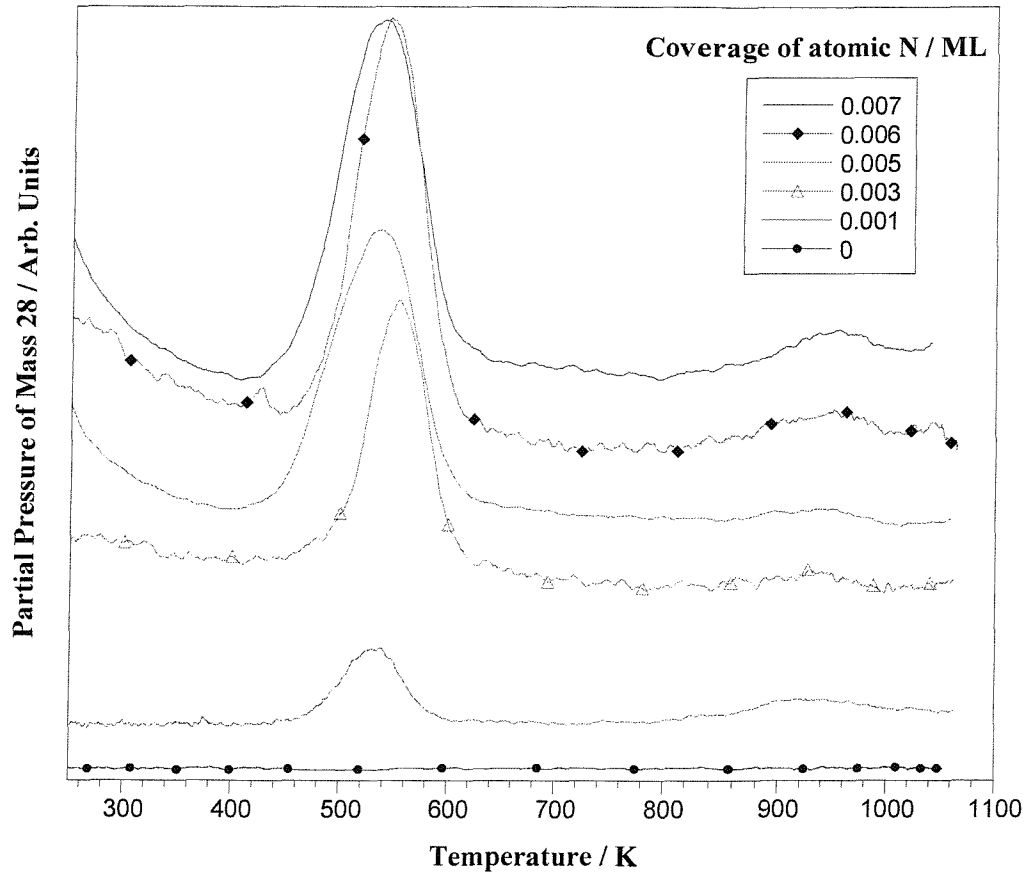

Figure VI.7: TPD of N_2 following exposure of Pt(533) to NH_3. NH_3 was dosed using the beam source (2-50 % NH_3 in He) at T_s = 135 K, T_n = 300 K. The heating rate was 15-16 K s^{-1}.

A comparison of mass 28 and mass 14 and 12 fragments (**figures VI.7, VI.8** and **VI.9**) confirms that the 530 K peak from mass 28 signal is mainly from N_2, and any influence of CO (from the background CO in the chamber) in the mass 28 amu TPD is very small (**figure VI.10**).

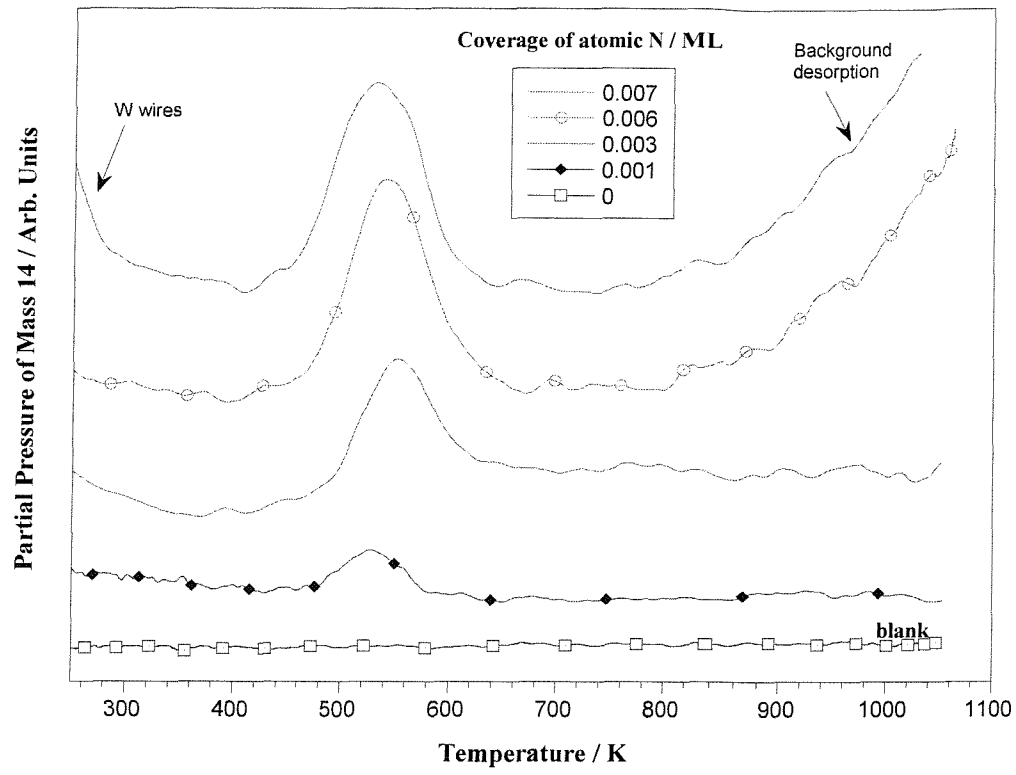

Figure VI.8: TPD of mass 14 following exposure of Pt(533) to NH_3. NH_3 was dosed using the beam source (2-50 % NH_3 in He) at T_s = 135 K, T_n = 300 K. The heating rate was 15-16 K s^{-1}.

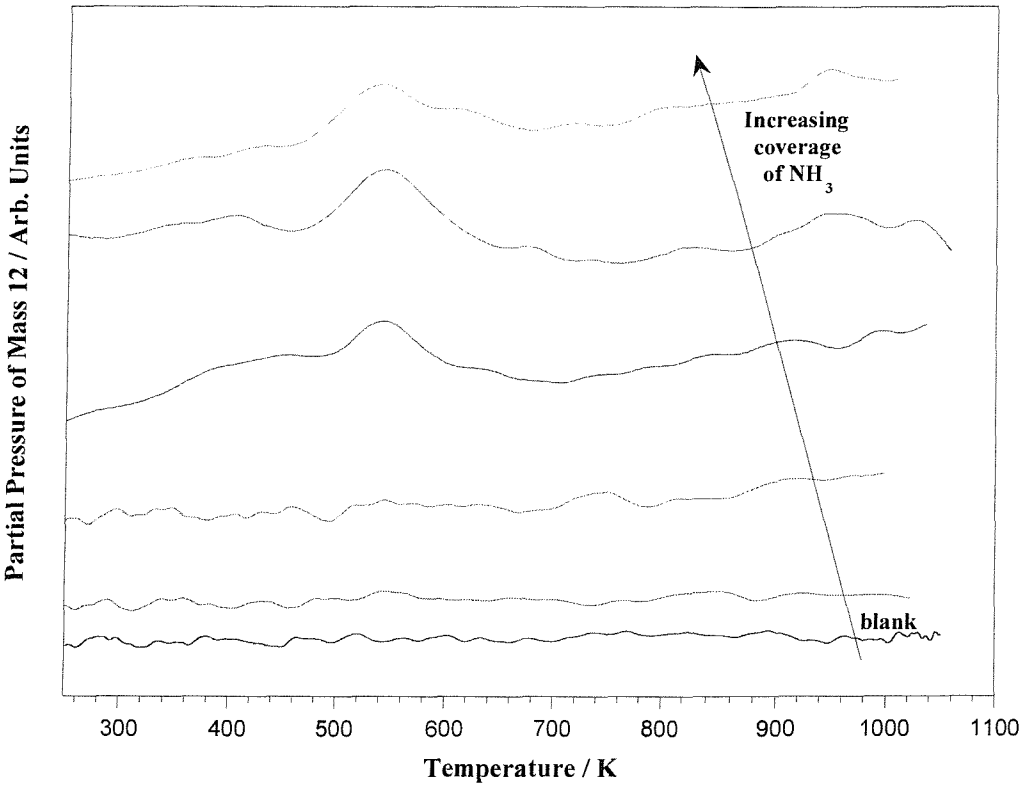

Figure VI.9: TPD of mass 12 following exposure of Pt(533) to NH_3. NH_3 was dosed using the beam source (2-50 % NH_3 in He) at T_s = 135 K, T_n = 300 K. The heating rate was 15-16 K s^{-1}.

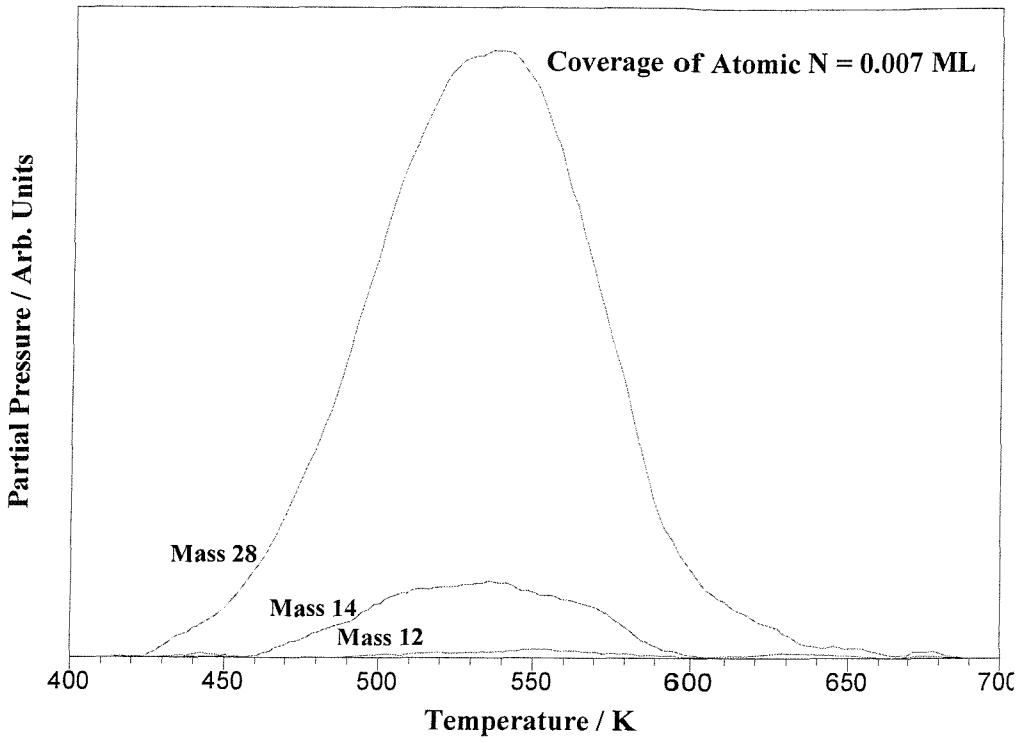

Figure VI.10: TPD of masses 28, 14 and 12 following exposure of Pt(533) to NH_3. NH_3 was dosed using the beam source (50 % NH_3 in He) at $T_s = 135$ K, $T_n = 300$ K, $E_i = 138$ meV. The heating rate was 15-16 K s^{-1}.

Figure VI.11 shows the production of H_2 after dosing NH_3 on clean Pt(533) at $T_s = 135$ K. A "blank" run corresponding to no NH_3 adsorption shows a small H_2 desorption at 400 K resulting from the adsorption of background hydrogen on the (100) Pt steps (**figure V.1 chapter V**).

With a small NH_3 exposure, two main peaks are observed. The lowest one at 400 K is similar to the recombinative desorption of atomic hydrogen preferentially adsorbed on the (100) steps of the Pt(533) surface as observed in our earlier work (**chapter V**). Previous results have led to conclude that there is no NH_3 decomposition on the (111) terraces, which means that NH_3 must undergo dissociation directly on the steps were atomic H will recombine to desorb as H_2.

A second H_2 peak is observed with a maximum at 530-540 K. This feature does not appear on H_2-TPD spectra from the clean Pt(533) surface (see bold line in **figure VI.11**). Since the desorption temperature is above that of the associated desorption of hydrogen

from Pt(533), the origin of this peak must be the rate limited decomposition of an NH_x species. The 530-540 K peak coincides with the N_2 desorption (**figure VI.7**). We conclude that both the H_2 and N_2 peaks result from reaction limited decomposition of an NH_x surface species.

Notice that all the H_2-TPD obtained after ammonia exposure present an underlying background from 260 to 700 K, which we associate with decomposition of ammonia from the sample holder (Cu support, W wires, Ni bars...). The heating rate differed slightly from one spectrum to the other resulting in a small variation of the maximum temperature of the peaks.

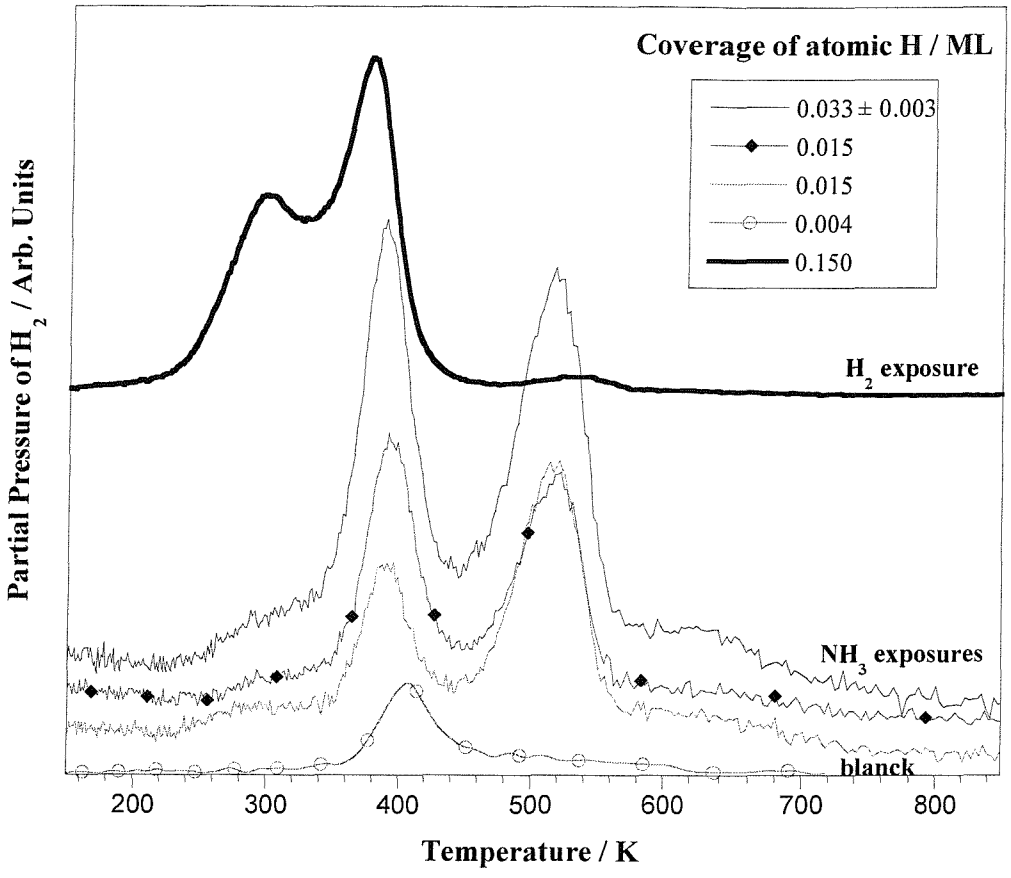

Figure VL11: TPD of H_2 following exposure of Pt(533) to NH_3. NH_3 was dosed using the beam source (pure flow) at $T_s = 135$ K, $T_n = 300$ K. For comparison, a H_2-TPD spectrum following exposure of Pt(533) to H_2 (pure flow) is shown (bold line). The heating rate was 4.5 K s^{-1}.

The coverage of hydrogen obtained after decomposition of NH_3 dosed on the clean Pt(533) surface has been estimated by comparing the integration of the TPD signals with the one from pure hydrogen dosed on the same Pt(533) surface (see **figure V.1 chapter V**). The

maximum production of hydrogen from NH_3 decomposition is reached at 0.030 ± 0.003 ML. Hence the maximum coverage of ammonia undergoing decomposition is approximately 0.010 ± 0.001 ML. The amount of NH_3 which dissociates is really small compared to the saturation coverage of the first layer of ammonia on Pt(533) which is expected to be around 0.25 ML (estimated by Fisher for NH_3 on Pt(111) [2]).

Moreover, the integration of the first production of hydrogen at 400 K corresponds to 50 % of the integration of the second production of hydrogen at 530 K meaning that the 400 K peak represents the production of hydrogen via:

$$2NH_3 \rightarrow 2NH_2 + 2H \qquad (2)$$

$$2H \rightarrow H_2 \qquad (3)$$

While the 530 K peak represents:

$$2NH_2 \rightarrow 2N + 4H \qquad (4)$$

$$4H \rightarrow 2H_2 \qquad (5)$$

This second process produces twice more hydrogen.

A detailed search for N_2H_2 and N_2H_4 at masses 30 and 32 respectively, as well as other possible desorption products, was undertaken but none were detected. Note that early results by Gland [34] on NH_3 adsorption and decomposition over a step platinum surface showed evidence of N_2 and H_2 production, but there was no NH_2 desorption observed.

It is concluded than above 400 K the open surfaces (such as step surfaces) are more active for ammonia decomposition than flat surfaces.

VI.3.3 Summary

- NH_3 desorbs at $T_s < 400$ K.
- NH_3 adsorbs at the steps (α' peak at ~ 350 K and β' peak at 200 K) and on the terraces (α peak at ~280 K and β peak at 165 K).

- NH_2 must be formed at $T_s < 350$ K due to the first desorption of H_2 starting at ~ 350 K.
- NH_3 has been shown not to decompose on the (111) terraces, hence the formation of NH_x (x = 0, 1, 2) species occurs only at the steps.
- The coverages of atomic H and atomic N have been estimated to be respectively around 0.03 and 0.01 ML at saturation, hence the coverage of NH_3 undergoing decomposition, $\theta(NH_3)_{diss}$, is of the order of 0.01 ML, which only represents ~ 4 % of the total amount of NH_3 expected to adsorb on the Pt(533) surface if we assume it to be ~ 0.25 ML at saturation [2].

Moroever, if the NH_x species formed at the steps were able to move towards the terraces the steps would be free for further dissociation which would lead to a much larger value for $\theta(NH_3)_{diss}$ than observed. Hence we conclude that the NH_x species are only present at the steps and not mobile.

- NH_x (x = 1, 2) has decomposed at $T_s < 460$ K and leads to the second hydrogen desorption starting at ~ 460 K. Since no NH_3 is stable at $T_s > 400$ K, hence this must be the result of NH_2 and/or NH dissolution.
- At $\theta(NH_3)_{diss}$ = 0.01 ML, the first H_2 production represents 50 % of the secondary H_2 production, hence:

at $T_s < 350$ K the first decomposition of ammonia starts at the steps: $NH_3 \rightarrow NH_2 + H$ and finishes at $T_s \leq 450$ K leading to the production of H_2.

at $T_s \sim 460$ K the second decomposition of ammonia starts: $NH_2 \rightarrow N + 2H$ and finishes at $T_s \leq 580$ K leading to the production of H_2 and N_2.

- NH_3 decomposes below ~ 600 K, giving rise to H_2 and N_2 desorption. However some N atoms appears to recombine and desorb much later at 950 K, which implies that there are two types of nitrogen adsorbates. We denote N^I (atoms recombining in N_2^I and desorbing at $T_s < 600$ K) and more strongly bound atom N^{II} (recombining in N_2^{II} and desorbing at $T_s \sim 950$ K).

Van Hardeveld and Van Montfoort [47] studied high surface-area dispersed Pt, Ni and Pd catalysts by nitrogen adsorption, with a combination of infrared spectroscopy of the adsorbed nitrogen and of electron-microscopy to determine the metal size distribution. They proposed a special surface defect site, designated as the B_5 site, where molecular N_2 adsorbed. B_5 means that the adsorbate will be in contact with 5 surface atoms. The observed

absorption band (Raman band) is at 2230 cm^{-1} for Pt. These B_5 sites are not expected to exist on flat surfaces such as Pt(111), where only B_3 sites exist. However Shigeishi and King [48] observed a strong IR band at 2238 cm^{-1} for nitrogen adsorbed on Pt(111) foil at 120 K which discredited the existence of special sites for IR-active nitrogen adsorption since it was assumed that the surface had an ideal Pt(111) structure. Nevertheless, the results obtained by Arumainayagam *et al.* [49] clearly show that no IR signal is observed for a fully annealed Pt(111) surface, while a strong band at 2222 cm^{-1} (N-N stretching mode) is detected only when nitrogen is adsorbed on special defect sites (the most highly coordinated surface Pt atoms at the base of monovacancy sites) created by Ar^+ bombardment of Pt(111). Hence the B_5 site can exist on defect/stepped surface but not on flat Pt(111).

When atomic nitrogen is dosed at low temperature (< 200 K), N_2 recombines and then desorbs between 450 and 650 K on Pt(111) [41] but this cannot be due to B_5 sites. The same desorption is observed for N_2 desorbing after dosing NH_3 on Pt(533) hence we believe that it is not the result of adsorption in a B_5 site.

The B_5 sites do exist on stepped Pt(533) and are likely to lead to much more stable nitrogen than B_4 and B_3 sites hence it might account for the 950 K-N_2 species.

The following scheme (**figures VI.12a** and **VI.12b**) of the ammonia adsorption, dissociation and desorption on a step platinum surface sum-up the previous results.

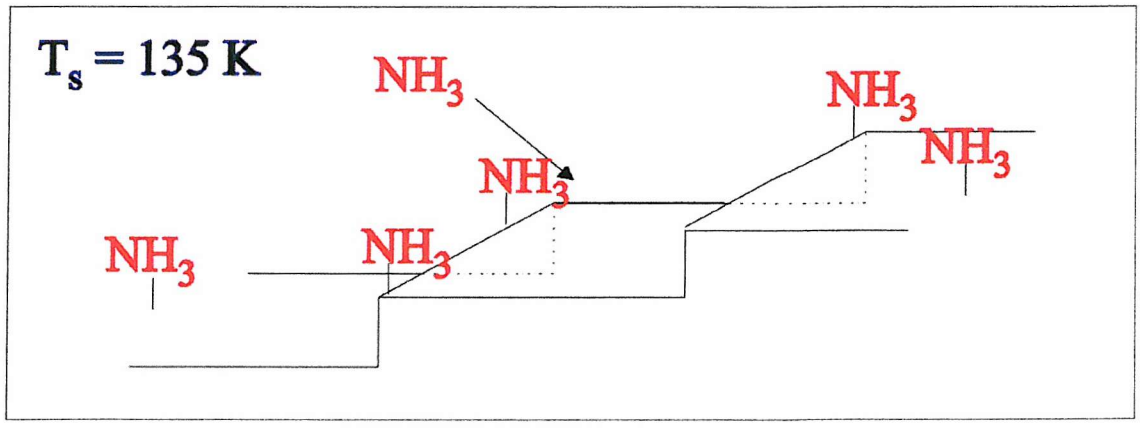

Figure VI.12a: Scheme of NH_3 adsorption, dissociation and decomposition on clean Pt(533).

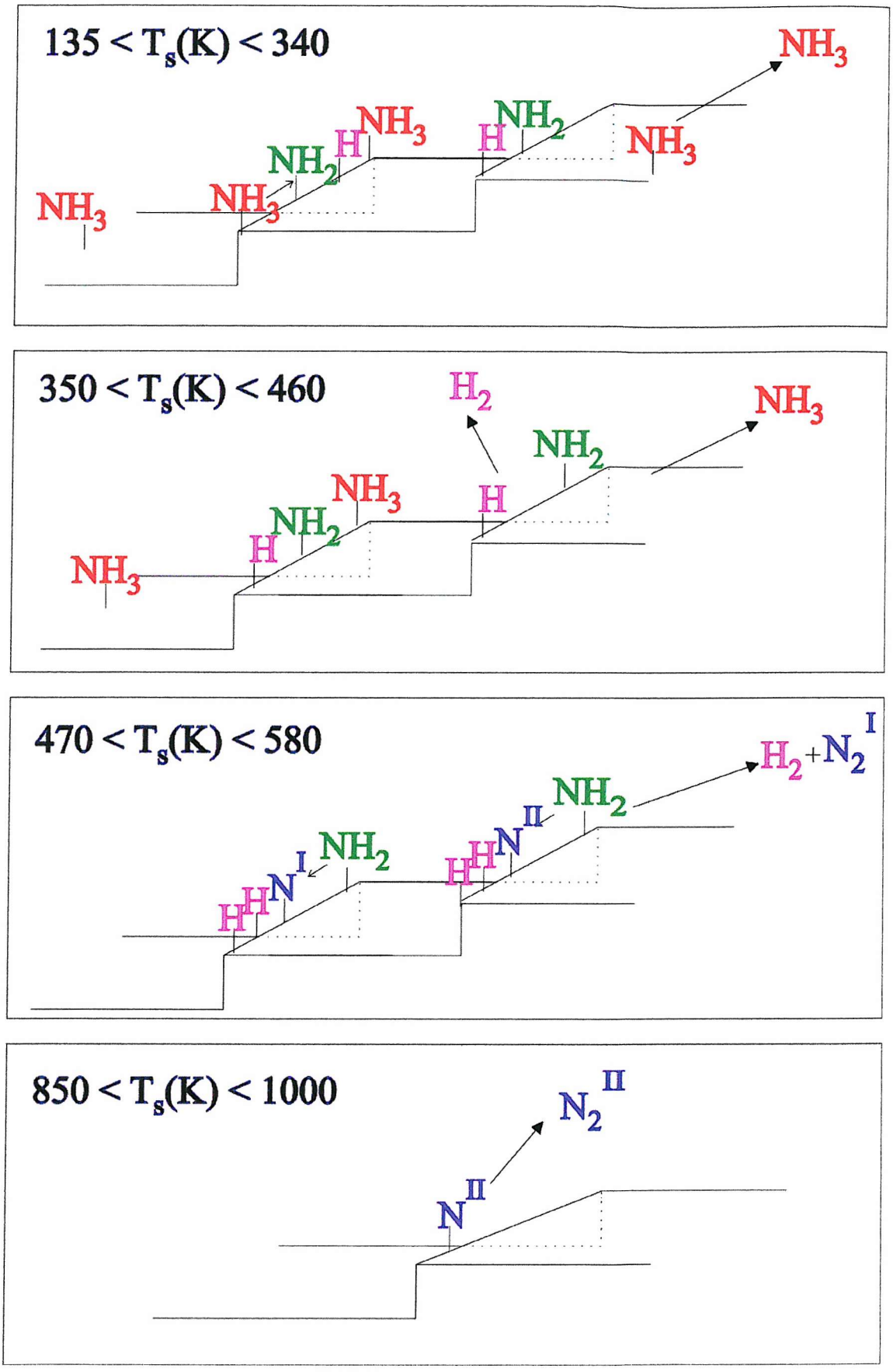

Figure VI.12b: Scheme of NH_3 adsorption, dissociation and decomposition on clean Pt(533).

VI.3.4 King & Wells Method

This method, which has already been described in **chapter III**, permits a direct measurement of the initial dissociative sticking probability S_0.

Figure VI.13 shows two pressure-time profiles for NH_3 using the King & Wells method. The mixtures used were (a) 1 ml min^{-1} of NH_3 in 29.5 ml min^{-1} of Ar, at T_n = 500 K hence E_i = 45.813 meV, at T_s = 396 K. Spectrum (b) has been performed with a 0.5 ml min^{-1} of H_2 in 49.5 ml min^{-1} of He at E_i = 269 meV and T_s = 400 K.

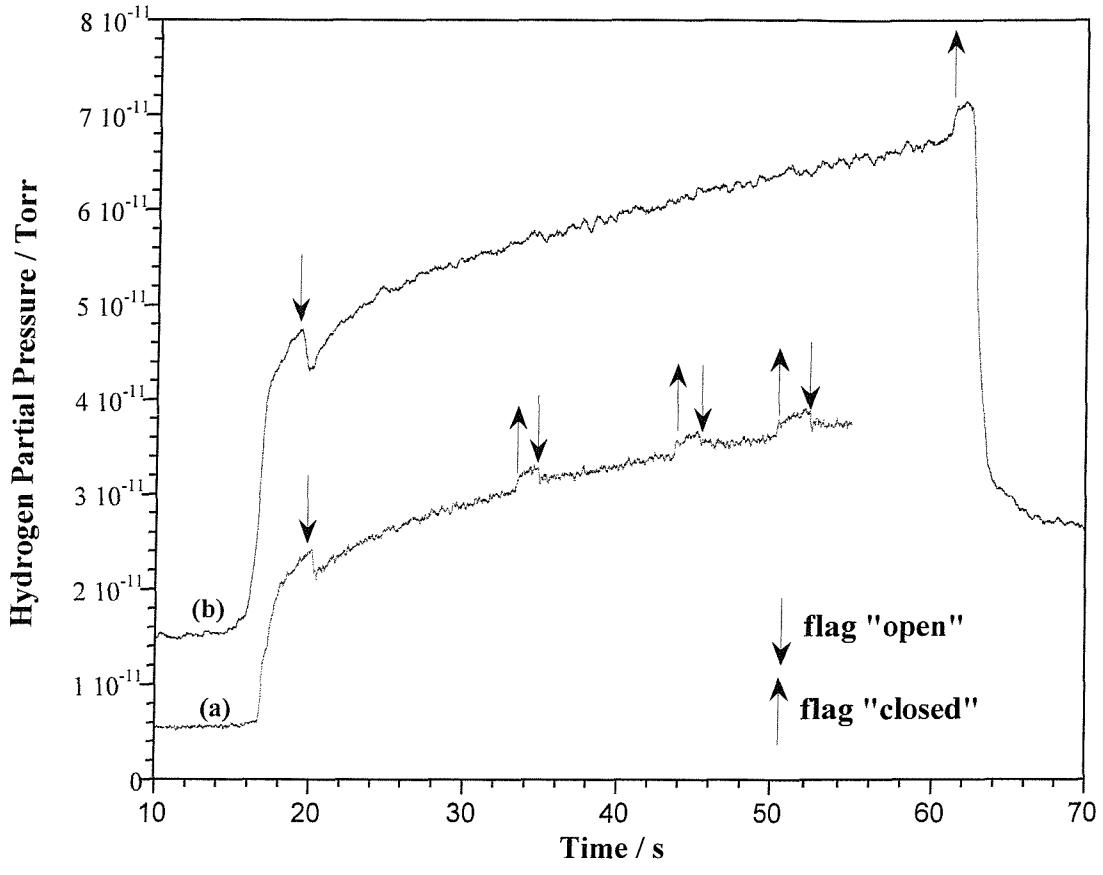

Figure VI.14: Typical mass spectrometer responses during $S_0(NH_3)$. In spectrum (a) NH_3 was seeded in Ar, at T_s = 396 K and E_i = 45.813 meV. Spectrum (b) correspond to NH_3 seeded in He, at T_s = 400 K, and E_i = 269 meV.

VI.3.5 Dependence of $S_0(NH_3)$ on Incident Energy

As seen previously, ammonia undergoes dissociation on the clean platinum (533) surface into H_2 and N_2, while there was no dissociation observed on Pt(111) [10, 28]. This

decomposition, which is believed to occur at the steps, starts at 340 K as shown by the hydrogen temperature programmed desorption spectra. At 400 K the desorption of N_2 starts while the first production of hydrogen from the steps is maximal. Note that H_2 was produced in two steps, first H_2 desorbs around 400 K after NH_3 decomposition on the (100) steps (primary production), then H_2 is produced from NH_x species on these steps and desorbs at 530 K (secondary production). **From these results, it was decided to study the initial dissociative sticking probability of ammonia, $S_0(NH_3)$ at 400 K.**

No molecular beam study of ammonia dissociative adsorption on platinum single crystal has been performed yet. Only Bradley *et al.* [50] have studied the ammonia adsorption on Pt(100) with a molecular beam, however they performed experiments at 150 K where no dissociation of ammonia has ever been observed hence it is not relevant in the present case.

Figure VI.14 displays the $S_0(NH_3)$ as a function of beam energy for the Pt(533) surface at $T_s = 400$ K, with the beam at normal incidence to the crystal. The results of $S_0(NH_3)$ were measured in the E_i energy range $27 - 825$ meV. Beam energies were controlled by a combination of nozzle temperature and seeding. At lowest energy, 27 meV, the sticking is equal to 0.38 ± 0.02, which proves the dissociative adsorption of NH_3 to be clearly non-activated. The falling of $S_0(NH_3)$ on Pt(533) with increasing E_i is probably a sign of ammonia molecules losing their translational energy on impact, hence trapping into a precursor state (weakly bound) during the initial collision. The increase of the incident energy of the molecules will lead to less and less molecules being able to stay in a shallow, precursor state potential before finding a proper site to dissociate, while more and more will directly go back to the gas phase. This is an indirect channel and it requires a precursor with sufficient lifetime and mobility to locate such step sites.

An estimate of the accommodated channel is performed using a hard cube calculation (see **appendix A**) of a chemisorbed NH_3 species with a deep well depth of 747 meV (corresponding to the energy of desorption of the first layer of NH_3 on clean Pt(533) obtained in **part VI.3**). This model assumes that the NH_3 molecule is a rigid spherical elastic particle which collides with one cube of Pt atoms. These Pt atoms are also

assumed to be elastic particles and their cube moves like an oscillator only in the direction normal to the assumed perfectly smooth surface [51].

At low energies the sticking suggested by the model is around 0.9, which is much higher than the experimental results. The hard cube model assumes that all the NH_3 molecules impinging on the surface have the right geometry to trap. Hence if some of them are not in this geometry they will not be able to trap in the precursor well hence the initial sticking probability will be lower than expected as shown by the experimental data.

Above 130 meV, the experimental results are higher than the model predicted. The hard cube model assumes that all the NH_3 molecules are rigid sphere, however ammonia is a rather flexible molecule, in fact the energy of the umbrella mode is 127 meV, hence instead of balancing back to the gas phase as expected with the hard-cube model, they will probably be able to exchange energy with the Pt surface atoms during their deformation and therefore adsorb.

Note that no attempt of estimating the accommodated channel with a soft cube model was made due to its complexicity.

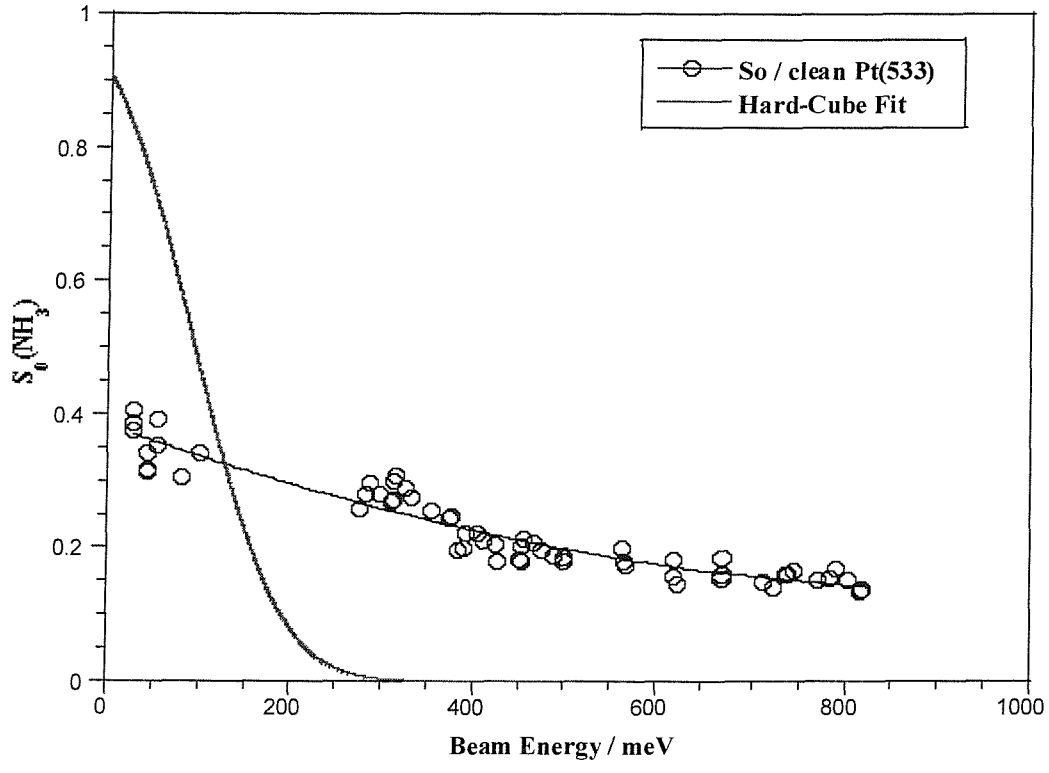

Figure VI.14: Initial sticking probability of ammonia on clean Pt(533), $T_s = 400$ K, $\theta_i = 0°$ and an estimate of an accommodated channel obtained using a hard cube calculation of a physisorbed species with a 747 meV well depth. The line of best fit of the set of data is also shown.

VI.3.6 Dependence of $S_0(NH_3)$ on Ammonia Coverage

The sticking probability of NH_3, $S(NH_3)$, has been measured on a clean Pt(533) surface as a function of NH_3 coverage at several incident kinetic energies, with the molecular beam incident normal to the Pt(533) surface plane, and at $T_s = 400$ K.

Figures VI.15 to**VI.18** seem to present a rather low initial sticking probability followed by a maximum in $S(H_2)$ at $\theta_H < 0.02$ ML. However we believe it to be due to the time lag of the quadrupole mass spectrometer, hence we obtain $S_0(H_2)$ by extrapolating the trend of $S(H_2)$ at $\theta_H = 0$. There is no obvious change of $S(NH_3)$ behavior with NH_3 coverage when the energy varies from 28 to 770 meV (**figures VI.15** to **VI.18**), hence it is tempting to say that there is a unique channel of ammonia dissociative adsorption over the whole range of energies studied: the accommodated precursor channel evidenced previously.

The trend of the sticking versus NH_3 coverage was quite difficult to extract from the data due to the poor signal-to-noise ratio, nevertheless the $S(NH_3)$ clearly decreases as the ammonia coverage goes up. This suggests that the blocking of the dissociation sites quickly enhances desorption of the precursor rather than dissociation. This is indicative of a very short precursor lifetime, or a pre-exponential factor in the partition between dissociation and desorption largely in favor of desorption.

Notice that the coverage of NH_3 which will undergo dissociation has been calculated to be 0.01 ML at saturation, which is very small.

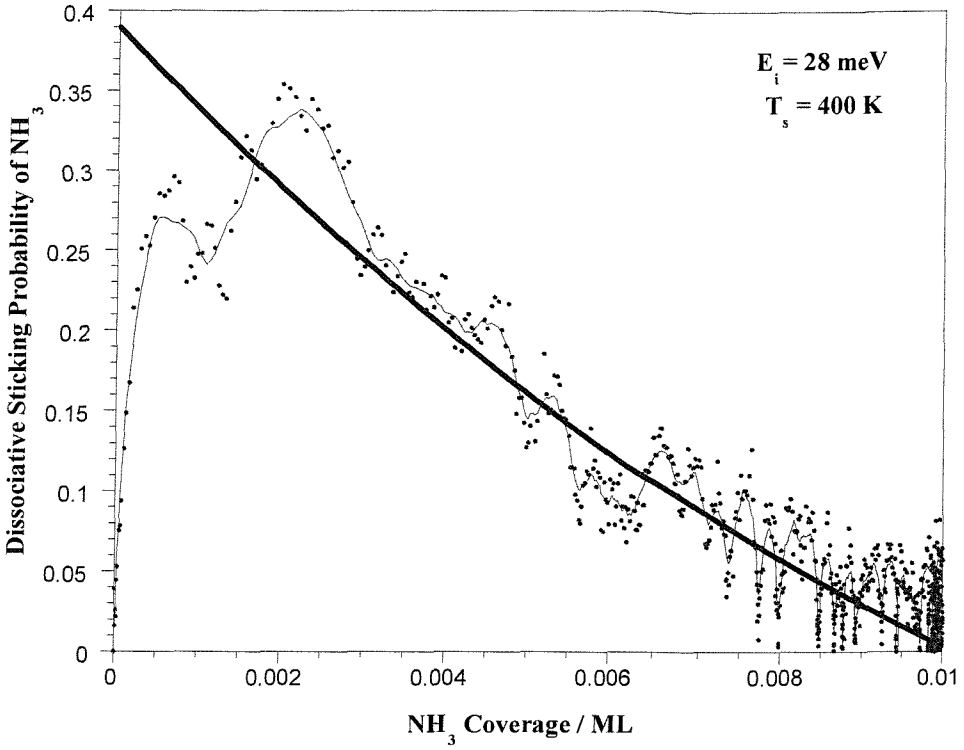

Figure VI.15: $S(NH_3)$ on the clean Pt(533) surface against the ammonia coverage, at $E_i = 28$ meV, $T_s = 400$ K and $\Theta_I = 0°$ (4 % NH_3 Ar). $S_0(NH_3) = 0.39$. A line to guide the eye on the sticking trend is also present.

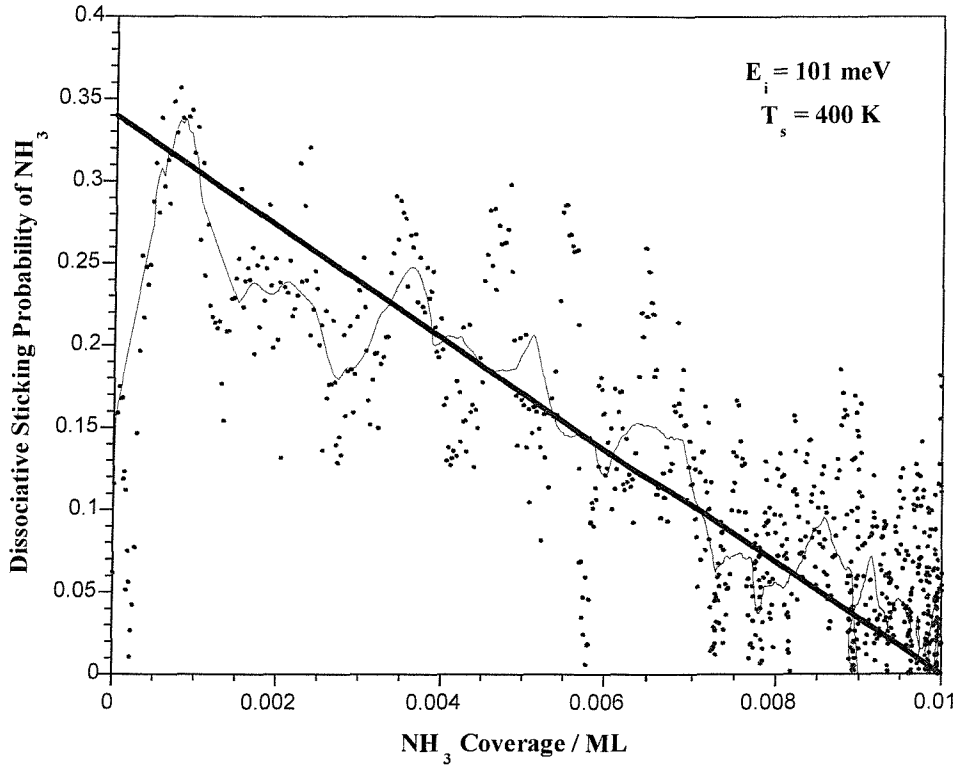

Figure VI.16: $S(NH_3)$ on clean Pt(533) surface against the ammonia coverage, at $E_i = 101$ meV, $T_s = 400$ K and $\Theta_I = 0°$ (2 % NH_3 in Ne). $S_0(NH_3) = 0.34$. A line to guide the eye on the sticking trend is also present.

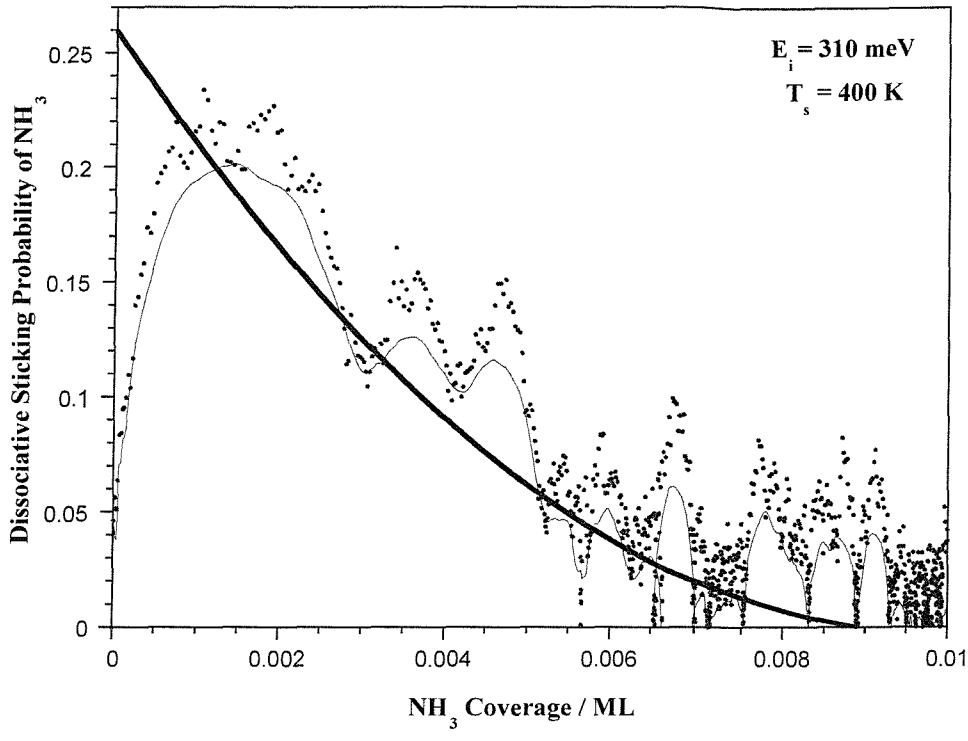

Figure VI.17: $S(NH_3)$ on clean Pt(533) surface against the ammonia coverage, at $E_i = 310$ meV, $T_s = 400$ K and $\Theta_I = 0°$ (2 % NH_3 in He). $S_0(NH_3) = 0.25$. A line to guide the eye on the sticking trend is also present.

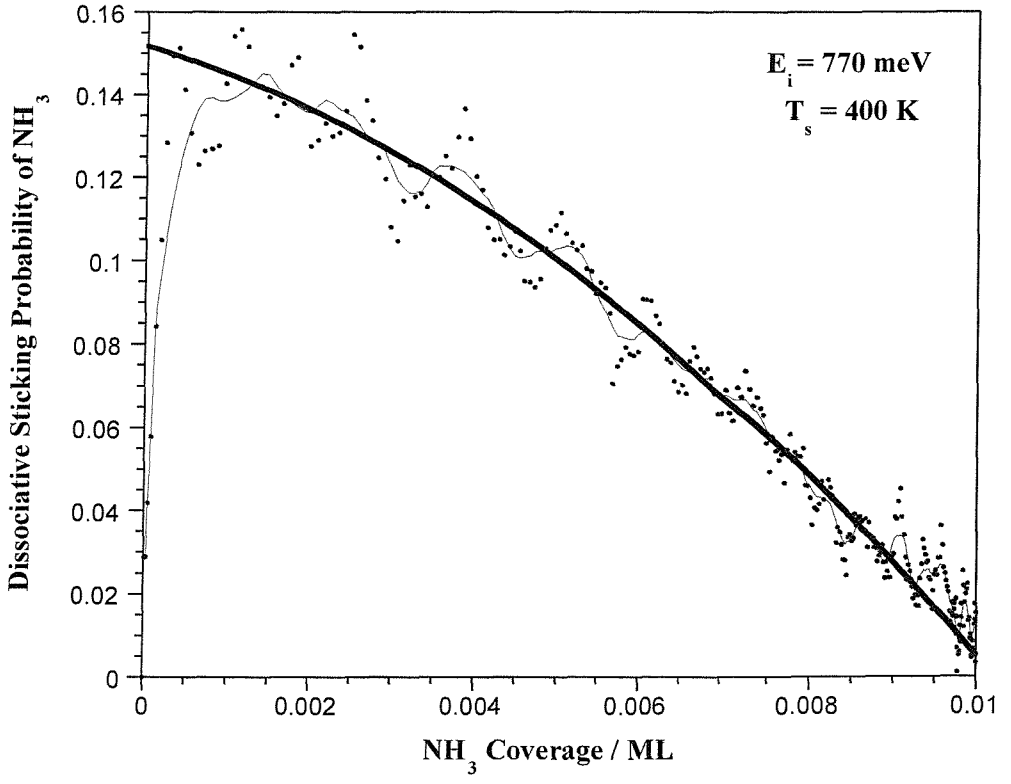

Figure VI.18: $S(NH_3)$ on the clean Pt(533) surface against the number of cycles, at $E_i = 770$ meV, $T_s = 400$ K and $\Theta_I = 0°$ (1 % NH_3 in He). $S_0(NH_3) = 0.15$. A line to guide the eye on the sticking trend is also present.

VI.3.7 Dependence of $S_0(NH_3)$ on Surface Temperature

In order to investigate the partition between the desorption of NH_3 and the first dissociation step to produce NH_2, the initial sticking probability was measured as a function of T_s for $T_s > 400$ K and for $T_s < 400$ K.

$$NH_{3gas} \longleftarrow NH_{3ads} \longrightarrow NH_2 + H \qquad (6)$$

For any form of precursor-mediated chemisorption, the dissociative probability S_0 can be expressed as the product of an adsorption probability into the precursor state $\alpha_{mc}=f(E_i, \theta_i, T_s)$, by a kinetic term representing the fraction of precursors that go on to dissociate, $\mathbf{k_{ca}}$, rather than desorb. If we neglect the kinetic effect of the weakly bound physisorbed species, we can write:

$$S_0 = \frac{\alpha_{mc} k_{ca}}{k_{ca} + k_{des}} \qquad (7)$$

Where $\mathbf{k_{des}}$ is the overall rate coefficient for desorption of these molecules, which may include both direct desorption from the molecular chemisorption state and desorption via the precursor state.

Figure VI.19 shows $S_0(NH_3)$ measured at 275 meV for $220 < T_s(K) < 450$. From 220 to 350 K there is no surface temperature dependence observed. The spread of the data is in agreement with the error limit of the King and Wells method of ± 0.02. At $T_s < 350$ K there is partition between NH_3 desorption (**figure VI.5**) and decomposition of NH_3 (see **part VI.3.2**) following adsorption. $T_s = 350$ K corresponds to the start of the hydrogen desorption feature coming from NH_3 decomposition (**figure VI.11**). At $T_s \geq 400$ K there is nearly no NH_3 desorption observed (**figure VI.5**) thus $S_0(NH_3)$ observed only corresponds to NH_3 trapping into the precursor well before dissociation occurs. These trapped molecules are expected to be in equilibrium with T_s and they should desorb or adsorb in the ratio depending on T_s, this is a so-called trapping desorption scattering. At $T_s = 450$ K $S_0(NH_3)$ drops drastically to zero which shows that desorption is much more likely to occur than dissociation.

In fact it is most likely that very few trapped NH_3 molecules find a site to dissociate due to an unfavorable preexponential factor or that the activation barrier to dissociation is too high to be overcome.

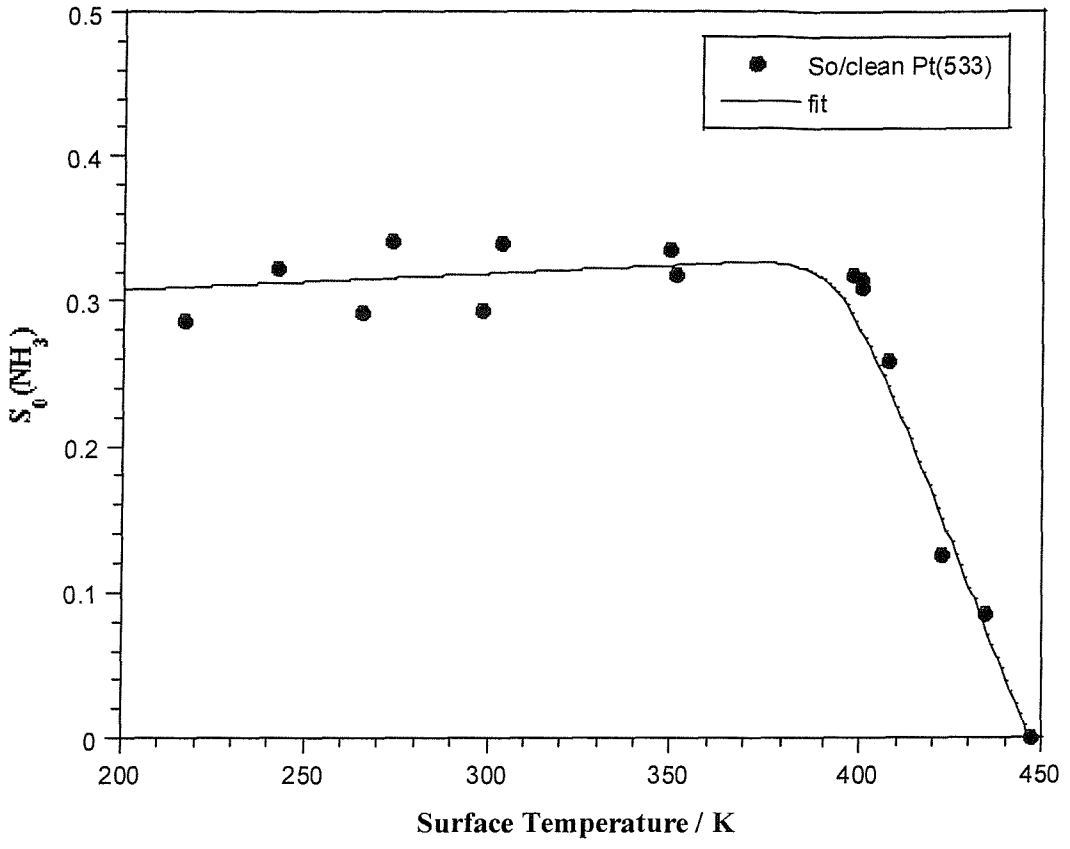

Figure VI.19: Initial sticking probability of ammonia on a clean and CO-precovered Pt(533) surface, at E_i = 275 meV and $\Theta_I = 0°$, for 220 < T_s(K)< 450 K. The line of best fit of the set of data is also shown.

Assuming that the two rates (dissociative adsorption and desorption) can be expressed in an Arrhenius form [52]:

$$k_{des} = \nu_{des} \exp\left(-\frac{E_{des}}{RT_s}\right) \qquad (8)$$

With $\mathbf{k_{des}}$ the overall rate coefficient for desorption of NH_3, ν_{des} is the preexponential factor and is of the order of the vibrational frequency of the bond broken in the reaction coordinate ~ 10^{13} Hz. $\mathbf{E_{des}}$ is the energy of desorption of NH_3 in the first monolayer and has been calculated earlier E_{des} = 72 kJ mol^{-1}. T_s is the temperature of the surface.

And:

$$k_{ca} = \nu_{ca} \exp\left(-\frac{E_{ca}}{RT_s}\right) \qquad (9)$$

With $\mathbf{k_{ca}}$ the rate coefficient for the evolution of the molecularly chemisorbed precursor species into the dissociative chemisorbed state, ν_{ca} is the preexponential factor, and $\mathbf{E_{ca}}$ is the energy of activation for NH_3 dissociation in the first monolayer.

Hence:

$$\frac{k_{des}}{k_{ca}} = \frac{\nu_{des}}{\nu_{ca}} \exp\left(\frac{E_{ca} - E_{des}}{RT_s}\right) \qquad (10)$$

$$\frac{k_{des}}{k_{ca}} = \frac{\nu_{des}}{\nu_{ca}} \exp\left(-\frac{\Delta E}{RT_s}\right) \qquad (11)$$

with:

$$\Delta E = E_{des} - E_{ca} \qquad (12)$$

Hence:

$$\ln\left(\frac{k_{des}}{k_{ca}}\right) = \ln\left(\frac{\nu_{des}}{\nu_{ca}}\right) - \frac{\Delta E}{RT_s} \qquad (13)$$

Assuming that α_{mc} is independent of T_s, equation (7) can be written in terms of the ratio of preexponentials ν_{des}/ν_{ca}, hence:

$$\frac{\alpha_{mc}}{S_0} = \frac{k_{ca} + k_{des}}{k_{ca}} \qquad (14)$$

$$\frac{k_{d}es}{k_{ca}} = \frac{\alpha_{mc}}{S_0} - 1 \qquad (15)$$

Hence:

$$\ln\left(\frac{\alpha_{mc}}{S_0} - 1\right) = \ln\left(\frac{\nu_{des}}{\nu_{ca}}\right) - \frac{\Delta E}{RT_s} \qquad (16)$$

Assuming that the initial sticking probability of NH_3 is 1 when the overall rate coefficient for desorption $k_{des} = 0$, hence $\alpha_{mc} = 1$.

For $400 < T_s(K) < 450$ the sticking probability $S_0(NH_3)$ falls rapidly with increasing T_s which reflects the kinetic competition between conversion to a more stable state

(dissociative chemisorption: $NH_3 \rightarrow NH_2$) corresponding to the rate k_{ca} and desorption corresponding to k_{des}.

The plot of $\ln\left(\frac{\alpha_{mc}}{S_0}-1\right)$ versus $\frac{1}{T_s}$ is shown in **figure VI.20**.

$$\Delta E = 67 \pm 35 \text{ kJ mol}^{-1}.$$

Therefore the energy of activation for dissociative adsorption is:

$$E_{ca} = 72\text{-}67 = 5 \text{ kJ mol}^{-1}.$$

The error on the intercept is rather large: $\ln(\nu_d/\nu_{ca}) = 21 \pm 11$, hence the error on the ratio ν_{des}/ν_{ca} is enormous and will not be given here.

$$\frac{\nu_{des}}{\nu_{ca}} = 1.2\times10^{9} \quad \text{with} \quad \nu_a = 8456 \text{ Hz}.$$

The activation barrier to dissociation is very small but the ratio of preexponential factors ν_{des}/ν_{ca} is largely in favour of the desorption rather than the dissociative adsorption, which explains the trend of $S_0(NH_3)$ versus T_s.

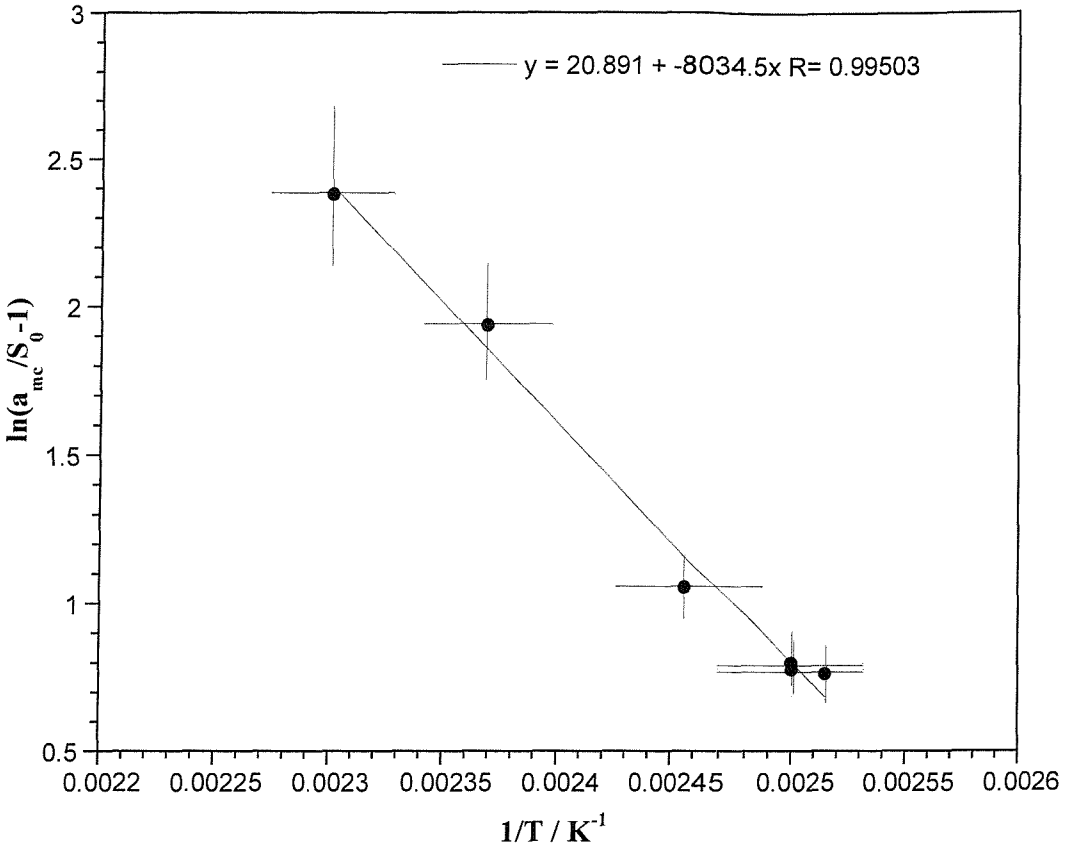

Figure VI.20: $\ln\left(\frac{\alpha_{mc}}{S_0(NH_3)}-1\right)$ versus $\frac{1}{T_s}$, at $E_i = 275$ meV and $\Theta_I = 0°$, for $400 < T_s(K) < 450$.

Other authors have studied the sticking of ammonia on different metal surfaces and similar phenomena were observed. Takaoka and Kusunoki [53] studied the sticking probability of NH_3 on a Si(100) surface. NH_3 is known to dissociate as NH_2 and H above 90 K [54], while around 600 K NH_2 begin to decompose into N and H atoms [55]. Hence they measured the initial dissociative probability of NH_3 into NH_2 for $300 < T_s(K) < 600$. $S_0(NH_3)$ decreases as T_s increases which conclude that NH_3 obey the trapping-mediated mechanism, where molecules lose their translational energy on impact. Masson *et al.* [56] studied the sticking probability of NH_3 on a W(110) surface. Production of hydrogen coming from NH_3 decomposition is observed around 500 K and corresponds to NH_3 dissociating into N_2 and H_2. Hence from 500 K to 700 K they observed decrease of $S_0(NH_3)$ as T_s increases, which corresponds to NH_3 trapping into a shallow potential well.

The sticking probability of NH_3 versus NH_3 coverage has been measured at several surface temperatures, from 213 to 363 K at $E_i = 275$ meV. These data cannot be directly compared to each other because the NH_3 coverage at saturation depends strongly on the

surface temperature. At 135 K the sticking of ammonia corresponds to non-dissociative NH_3 and has been shown to be ~ 0.25 ML at saturation [2]. At 400 K ammonia has been seen not to desorb from the Pt(533) surface (see **figure VI.5**), hence the observed sticking corresponds in fact to dissociative NH_3, which has been found to be ~ 0.01 ML at saturation. For $135 < T_s(K) < 400$ the saturation coverage is unknown, therefore in **figure VI.21** θ_{NH3} is in arbitrary units, and the integration of the sets of data cannot be compared. However we can discuss the shape of each set of data. From **figure VI.19**, the initial sticking probability is 0.31 ± 0.02 at $T_s = 400$ K which corresponds to NH_3 dissociatively adsorbing on the (100) steps and the sticking profile is similar at 363 K one. As the surface temperature decreases S_0 stays constant at 0.31 ± 0.02 while the trend of the sticking varies strongly. In fact, at low temperature, *i.e.* 213 K, the sticking seems to be enhanced by the presence of ammonia adsorbed on the steps until it reaches a maximum, then the sticking decreases with a very steep gradient down to zero. When the temperature of the surface increases, *i.e.* 243 or 300 K, the same behaviour is observed, however the maximum of the sticking is reached more rapidly and it is noticeably smaller than for a colder surface. At 363 K the initial sticking probability correspond to the maximum of the sticking with a steep decrease of $S(NH_3)$ occurring straight after.

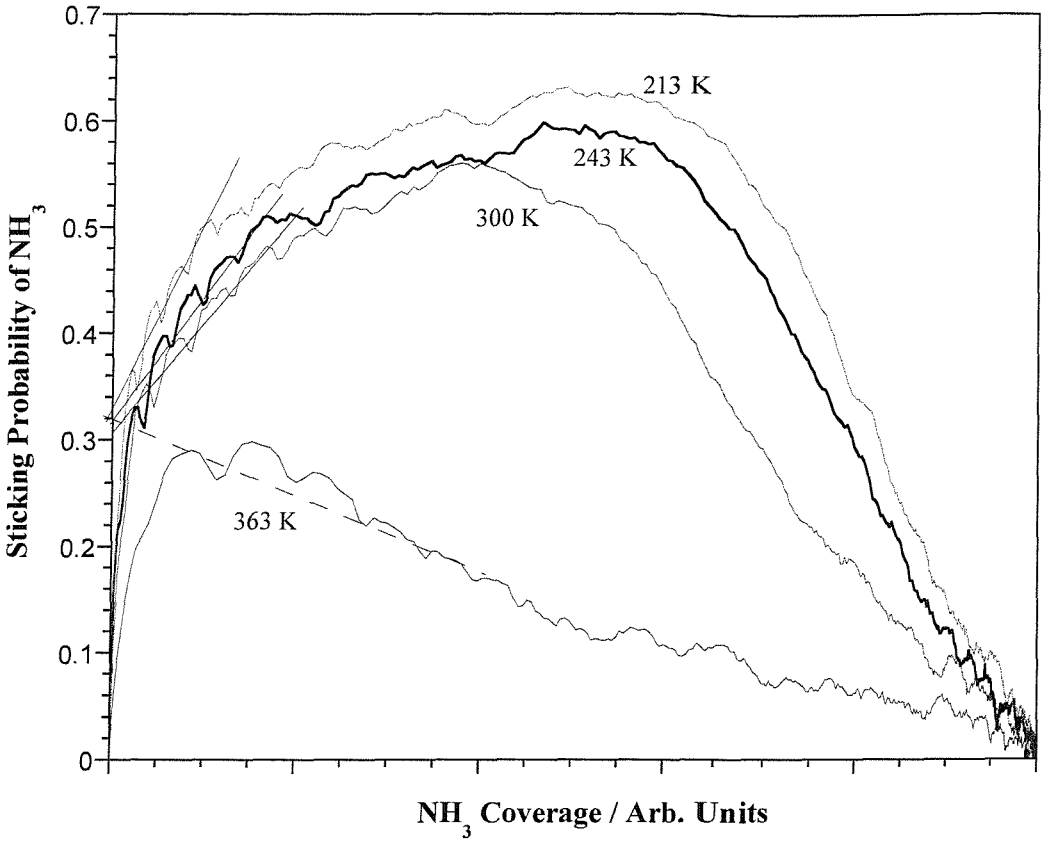

Figure VI.21: $S(NH_3)$ on the clean Pt(533) surface versus the θ_{NH3}, at $213 < T_s(K) < 363$, $E_i = 275$ meV, and $\Theta_I = 0°$. NH_3 was dosed using the beam source (1 % NH_3 in He). $S_0(NH_3) \sim 0.31$. $\theta Max_{NH3} = 0.01$ ML for Ts = 363 K, $\theta Max_{NH3} >> 0.01$ ML for $213 < T_s(K) < 300$.

From these results it is believed that the α'-NH_3 molecules adsorbed on the steps are precursors for NH_3 adsorption on the whole surface, under the present conditions ($E_i = 275$ meV), or they represent favorable adsorption sites for further molecules: β'-NH_3 molecules. These newly adsorbed β'-NH_3 molecules most likely move to α sites on the terraces liberating the β' sites. Then more NH_3 molecules adsorb on top of the α' and α sites in β' and β forms which results in a further increase of the sticking. These molecules move again on the surface to more tightly bound sites α. When all the available α sites have been filled the sticking decreases steeply. If the surface temperature is low enough a second layer of NH_3 molecules could adsorb via hydrogen bonding to the first layer therefore increasing $S(NH_3)$.

VI.3.8 Consequences of Pre-adsorbed CO on NH_3 Adsorption/Desorption

In order to further elucidate the influence of the (100) steps of the Pt(533) surface on NH_3 dissociation, carbon monoxide (CO) was dosed prior to NH_3, so as to block any ammonia adsorption on the steps, whilst leaving the terraces free to react. This should lead to a "virtual" Pt(111) surface which is expected to react as a real Pt(111) surface with NH_3. Hence no dissociation of ammonia is expected on this CO-blocked Pt(533) surface.

The saturation CO coverage produced by dosing CO on Pt(533) at ~ 105 K was found to be 0.63 ML [57], while the saturation of the steps corresponds to ~ 0.19 ± 0.01 ML for $85 < T_s(K) < 105$ [57, 58]. Hence in the present case a series of exposures was performed at $T_s = 135$ K in order to identify the exposure corresponding to the blocking of the steps by $\theta_{CO} = 0.19 \pm 0.01$ ML (see **figure VI.22**).

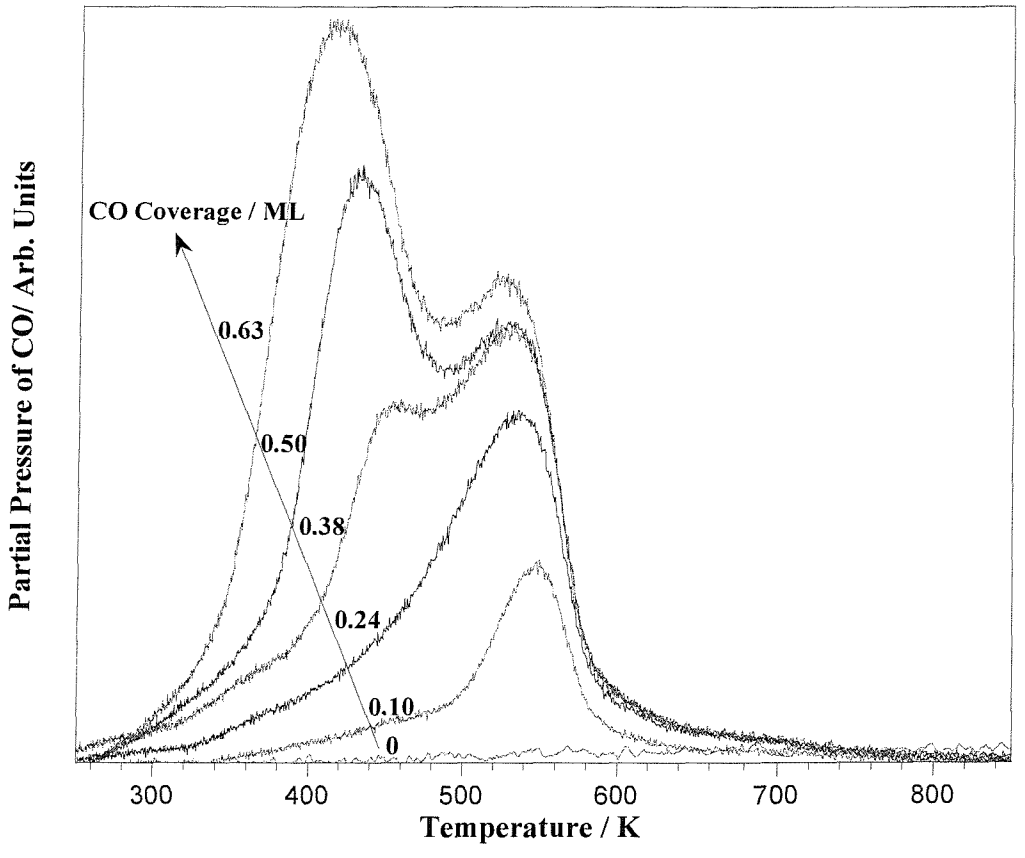

Figure VI.22: TPD of CO following exposure of Pt(533) to CO. CO was dosed with an isotropic thermal source at $T_s = 135$ K. The coverage was 0-0.63 ML, and the heating rate was 7 K s^{-1}.

CO is known to adsorb molecularly on platinum and does not undergo dissociation [57, 58, 59]. The CO TPD data on clean Pt(533) (see **figure VI.22**) show two desorption peaks at 417-450 K and 528-546 K corresponding respectively to CO desorbing from the terraces and from the steps. This is in agreement with the CO data on clean Pt(533) from Wang *et al.* [57] which shows two desorption peaks at 416 and 518 K, from Hayden *et al.* [58] which shows two peaks at about 400 and 550 K and from Luo *et al.* [59] which shows two CO desorption at 410-430 K and 520-550 K (for more details on CO adsorption refer to **chapter V section V.3.9**).

Dosing NH_3 on the clean surface, **figure VI.23** results in 4 peaks: α corresponding to NH_3 molecules sticking directly onto the platinum atoms, β from the NH_3 molecules of the bilayer sticking on the (111) terraces. The weak shoulders α' around 330-350 K and β' around 200 K are believed to correspond to NH_3 adsorbing on the clean Pt (100) steps and on the NH_3-covered (100) steps respectively.

By increasing slightly the CO precoverage (0.07 ML), the number of ammonia molecules adsorbed on the surface will decrease. Ranney *et al.* have shown that CO and NH_3 molecules compete for adsorption sites on Pt(111) [32], however their behaviour on stepped platinum is not known. Based on infrared reflection absorption spectroscopy (IRAS), Hayden *et al.* [58] showed that CO is located only at atop sites on Pt(533), with its C-end closer to the surface. Hammer *et al.* performed some density-functional calculations that led to the same conclusion [60].

The interaction of CO and NH_3 molecules has already been investigated on Ni(111) [61, 62], Ru(001) [63] and Re(0001) [64], where both direct and long-range interactions are found. Moreover the binding energy of NH_3 to Ni(111) is weaker than the binding energy of NH_3 when CO is present. This may be due to an attractive CO-NH_3 interaction, or to a modification of the electronic properties of the surface caused by the presence of CO. The coadsorption of molecules which donates electrons to the surface (NH_3) with molecules which accept electrons from the surface (CO, O) often leads to stronger binding of the donor [62]. Ranney *et al.* [32] observed no such change in the TPD spectrum of NH_3 on Pt(111) because of the weaker effect of CO on the work function of platinum. However, the broadness of the desorption of NH_3 over Pt(111) surface may be altered by the CO adsorbate, which may inhibit the ammonia-ammonia interactions, possibly acting as an

electron acceptor as it does on Ni(111) [62]. In fact, Ranney *et al.* [32] concluded that CO seems to modify the ammonia desorption through long-range metal-mediated interaction and direct interaction. This is supported by the fact that the NH_3 desorption following exposure of Pt(111) to a NH_3/CO mixture is substantially different to that from clean Pt(111). On the clean Pt(111) surface, the β phase of NH_3 desorbs in a sharp feature at 150 K, and NH_3 from the α state desorbs in a broad plateau from 200 to 375 K probably due to through-metal interactions. When coadsorbed with subsaturation CO coverage, NH_3 desorbs in two sharp peaks at 150 and 295 K (α'). On the CO presaturated surface, four distinct NH_3 desorption features are resolved at 150, 200, 260 (α_1) and 325 K (α_2). The α_1 and α_2 states fall within the envelope of the NH_3 α' desorption peak, therefore regardless of CO coverage, two separate high-temperature low-coverage NH_3 states probably desorb from the CO/Pt(111) surface. These observations seem to corroborate with the inhibition of NH_3-NH_3 interactions by CO.

Substantial changes in the NH_3 TPD from a CO precovered Pt(533) surface are also observed (see **figure VI.23**), however due to the poor signal to background ratio our following interpretations would need to be confirmed by further experiments. The α-peak is wide on the clean surface due to lateral and long-range interactions and is narrowing very fast peaking around 295 K when the surface is precovered with CO. As seen by Ranney *et al.* [32] we observed two peaks α_1 and α_2 within the envelope of the α peak suggesting the inhibition of some NH_3-NH_3 interactions.

The behaviour of the α' and β' features is quite difficult to follow, however notice that the β, α' and β' peaks like the α peak are still present when the surface is believed to be saturated by CO which implies that the ammonia molecules are still finding some (100) step sites and (111) terrace sites to adsorb.

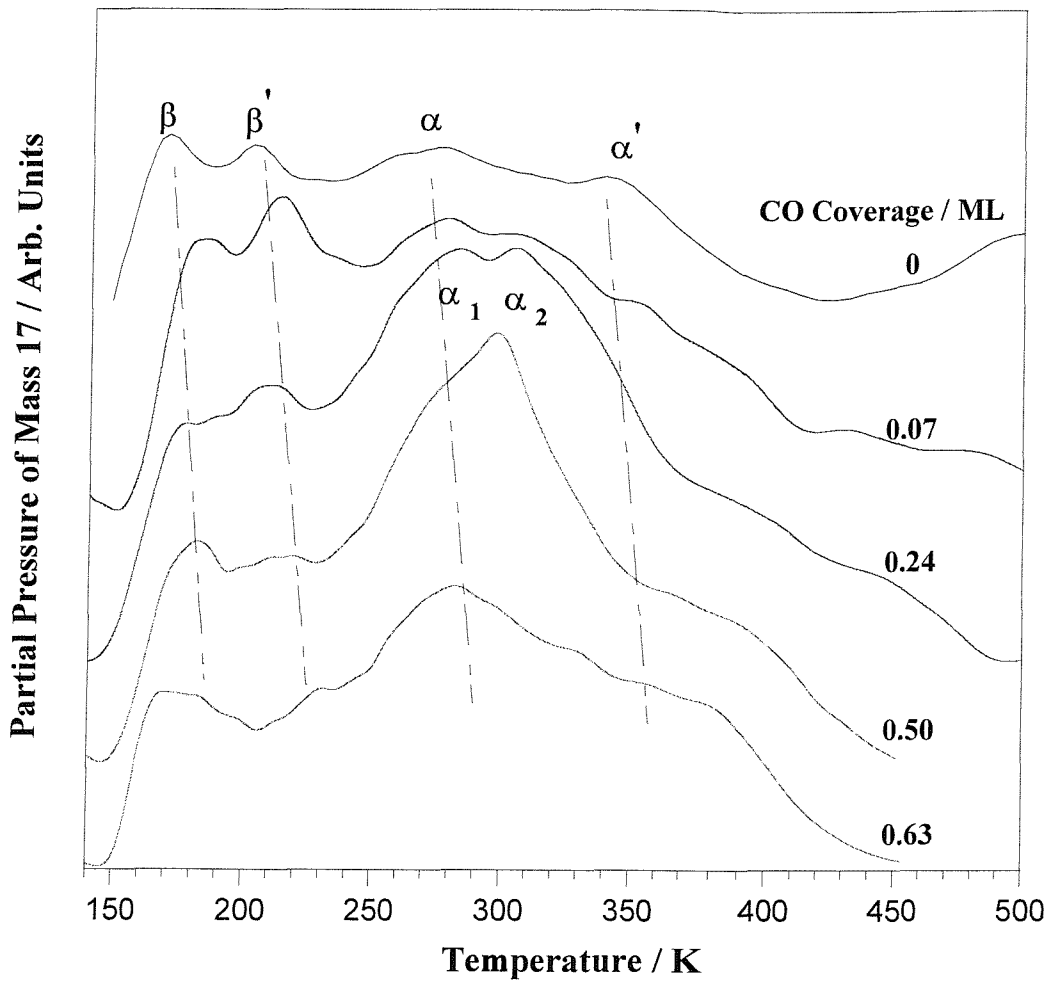

Figure VI.23: TPD of NH_3 following exposure of CO/Pt(533) to NH_3. NH_3 was dosed using the beam source (pure NH_3 beam) at $T_s = 135$ K, $T_n = 295$ K, $E_i = 108$ meV. The heating rate was 4 K s^{-1}. The Pt(533) was preexposed to a CO coverage of 0-0.63 ML.

Figure VI.24, shows the mass 28 TPD spectra after dosing ammonia on a CO-precovered Pt(533) surface. First of all, some TPD data have been performed for masses 12 and 16 to allow the assignment of the mass 28 signals. **From figures VI.25** and **VI.26** it is clear that the TPD peaks of mass 16 and mass 12 track well the mass 28 desorption signal therefore attributed to CO. The features from **figures VI.25** and **VI.26** correspond to the fragmentation of CO in the mass spectrometer analyser. Several attempts to record the mass 14 signal, which should correspond to the decomposition of N_2 in the mass spectrometer, were performed, however the signal was much too weak to be trustworthy, thus it is not presented here. Moreover it could not be compared to the mass 28 signal, because the amplitude of the TPD peaks in **figure VI.24** corresponding to CO are very large and overlap any possible N_2 signal. To give an idea of the amplitude difference between the CO and N_2

features, NH_3 was dosed on the clean Pt(533) surface which leads to the production of N_2 on the (100) steps around 510-520 K (as seen by the insert in **figure VI.24**).

There is no obvious displacement of the CO desorption peaks by ammonia, as also observed on Pt(111) by Ranney *et al.* [32] since ammonia desorption is complete when CO desorption begins.

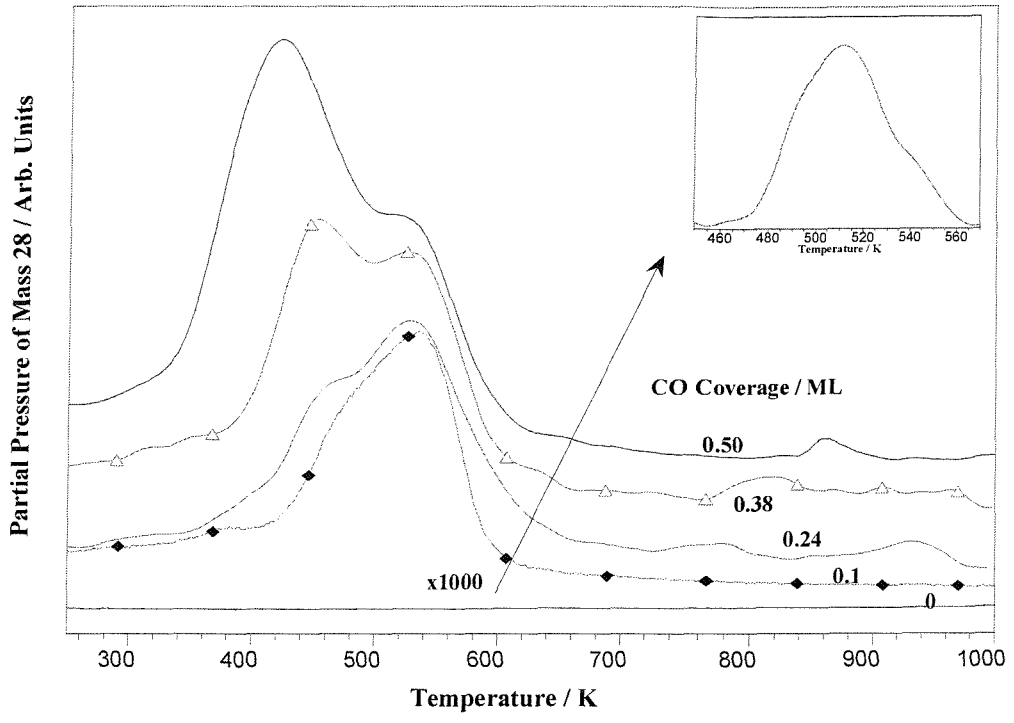

Figure VI.24: TPD of mass 28 following exposure of CO/Pt(533) to NH_3. NH_3 was dosed using the beam source (50 % NH_3 in He) at T_s = 135 K, T_n = 300 K, E_i = 138 meV. The heating rate was 17.25 K s^{-1}. The Pt(533) was preexposed to a CO coverage of 0-0.5 ML.

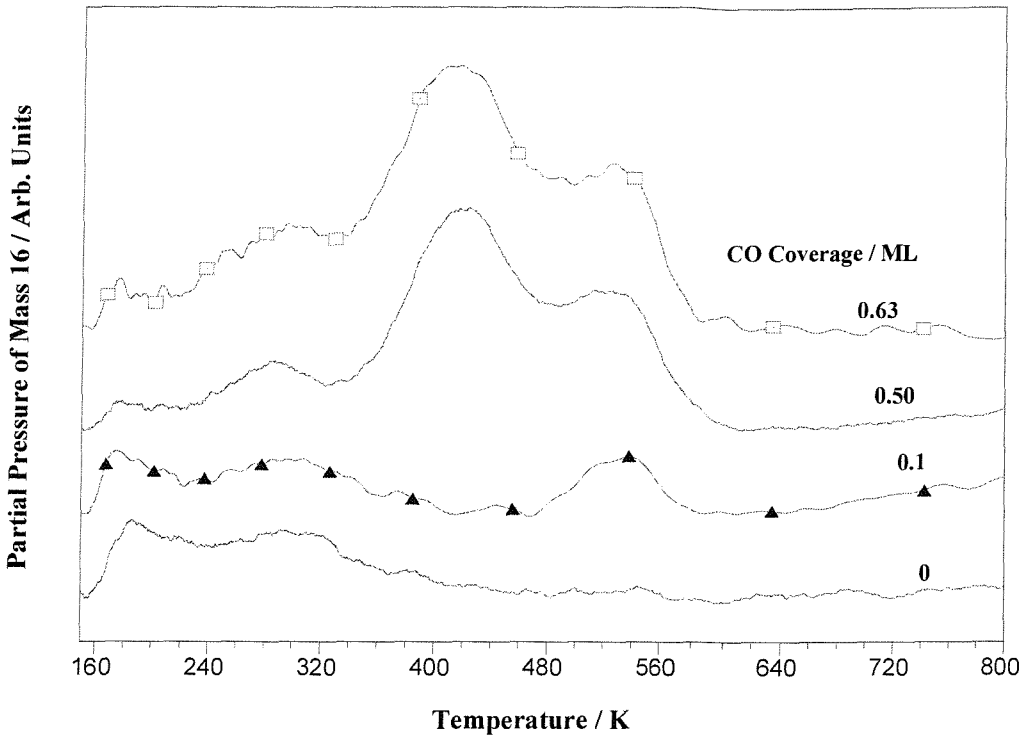

Figure VI.25: TPD of atomic O following exposure of CO/Pt(533) to NH_3. NH_3 was dosed using the beam source (50 % NH_3 in He) at T_s = 135 K, T_n = 300 K, E_i = 138 meV. The heating rate was 7-17.25 K s^{-1}. The Pt(533) was preexposed to a CO coverage of 0-0.63 ML.

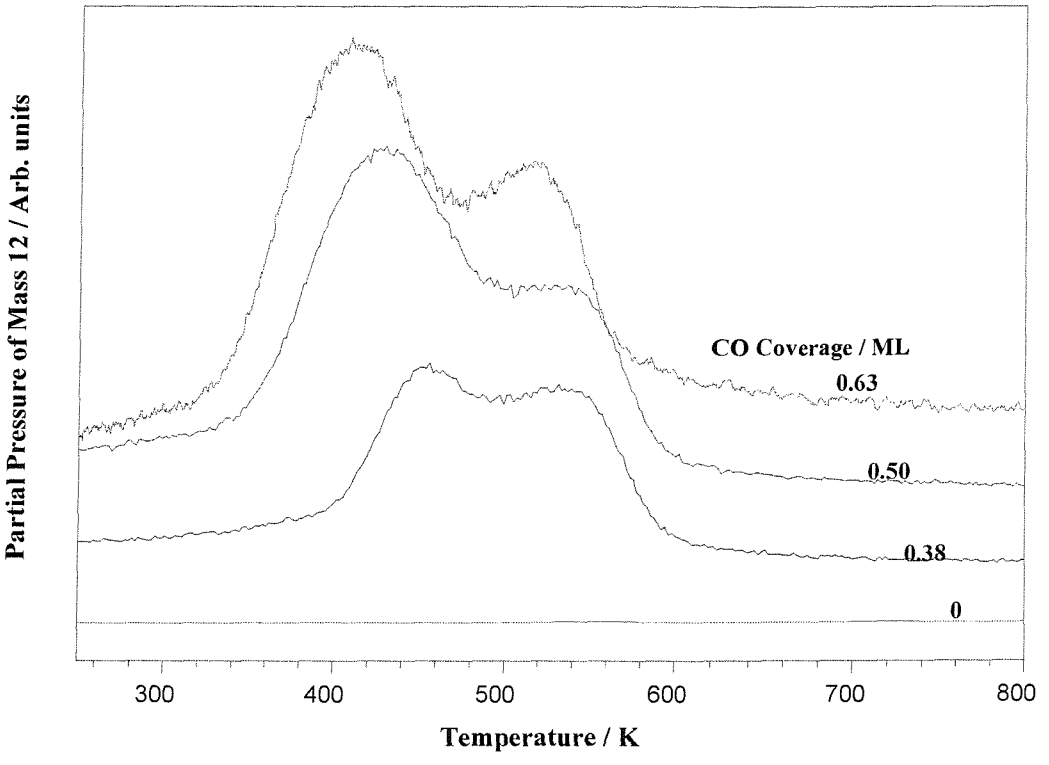

Figure VI.26: TPD of atomic C following exposure of CO/Pt(533) to NH_3. NH_3 was dosed using the beam source (50 % NH_3 in He) at T_s = 135 K, T_n = 295 K, E_i = 138 meV. The heating rate was 17.3 K s^{-1}. The Pt(533) was preexposed to a CO coverage of 0-0.63 ML. The C spectra on 0.63 ML CO/Pt(533) was performed with a heating rate of 5.2 K s^{-1} to clearly separate the two peaks.

As seen earlier, NH_3 adsorbed on the clean Pt(533) starts to decompose under 350 K due to the presence of the (100) steps and gives rise to N_2 and H_2 production. Atomic hydrogen will recombine on the (100) steps and desorb around 400 K while some NH_x species still present on the steps will be responsible for some H_2 desorbing later around 530 K (see **figure VI.27**).

When covering the steps with CO, the NH_3 adsorption is expected to be partially or even totally blocked at these step sites depending on the CO precoverage. Hence the decomposition of NH_3 leading to H_2 and N_2, which has been shown to only occur at the steps, is also expected to decrease until complete disappearance.

As seen in **figure VI.27**, the 400 K hydrogen desorption peak, related to the first decomposition of NH_3 in NH_2 (see **part VI.3.3**), and the 530 K hydrogen peak, corresponding to the decomposition of NH_2, both decrease.

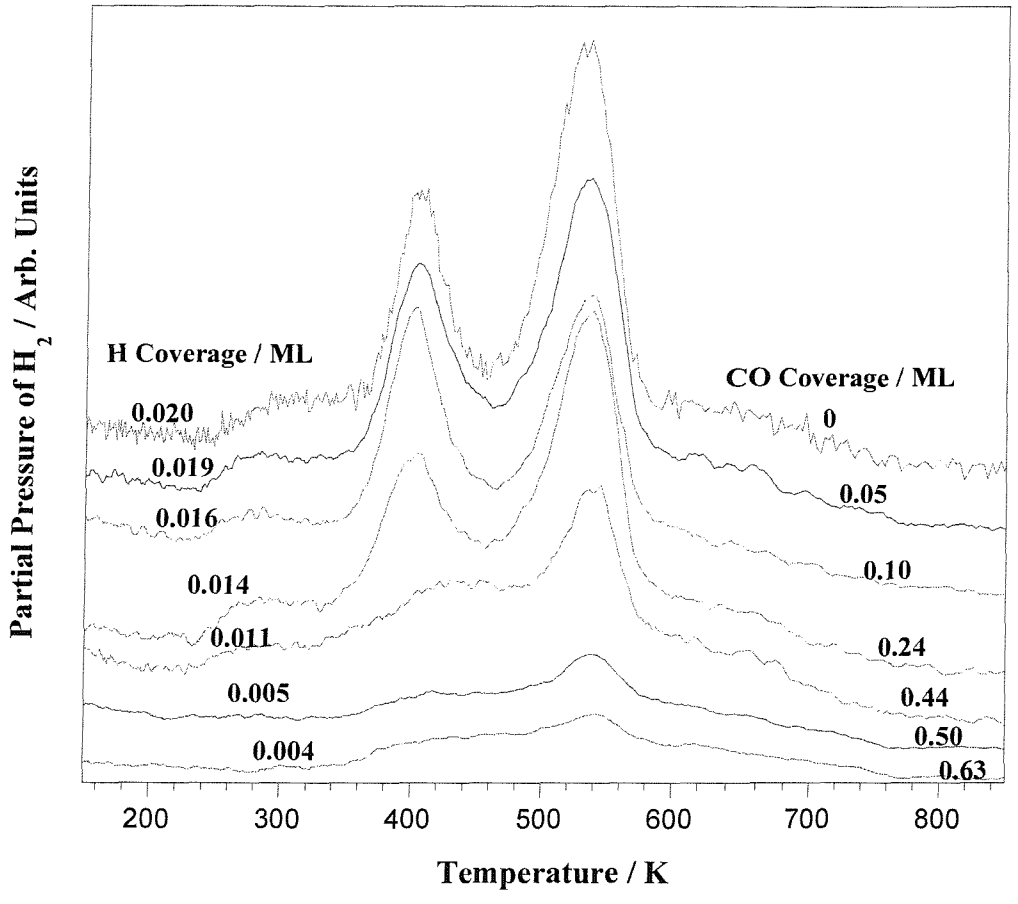

Figure VI.27: TPD of H_2 following exposure of CO/Pt(533) to NH_3. NH_3 was dosed using the beam source (pure NH_3 beam) at $T_s = 135$ K, $T_n = 300$ K, $E_i = 108$ meV. The heating rate was 4.2 K s^{-1}. The Pt(533) was preexposed to a CO coverage of 0-0.63 ML.

However with 0.24 ML of CO (*i.e.* complete blocking of the steps and partly filled terraces), hydrogen is still being produced at 400 K and at 530 K, which confirm that some ammonia can still find some step sites to dissociate. The second production of H_2 corresponds to approximately twice the amount of the first hydrogen production, hence we believe that N_2 must also be produced during the complete dissociation of NH_2.

Notice that from 0.24 to 0.44 ML of CO the hydrogen production on the steps is decreasing, meaning that the CO adsorbing on the terraces seems to influence the NH_3 molecules decomposing on the steps. Hayden *et al.* [58] concluded that at coverage below 0.19 ML, there is evidence of a one-dimensional array of CO molecules adsorbed along the outside edges of the steps, while at coverage above 0.19 ML CO begins to adsorb on the terraces and two-dimensional islands including both step and terrace molecules form. Hence from the present results it appears quite clear that these islands inhibit ammonia adsorption and as a direct consequence the dissociation decreases too.

Increasing the CO precoverage further will lead to the slow decrease of the two hydrogen peaks. At CO saturation, there is still a clear hydrogen background from 360 to 740 K which we associate with the decomposition of the ammonia from the sample holder (W wires, Cu support, Ni bars...) or the back of the crystal.

It is concluded that preadsorbed CO molecules do not totally block NH_3 adsorption and dissociation.

Figure VI.28 shows the coverage of hydrogen corresponding to NH_2 decomposition (second H_2 peak in **figure VI.27**) versus the CO precoverage on the surface. Due to the difficulty to extract these informations from the data the error bars on the present results are around 25 %. Moreover due to the large background we did not perform the same calculations for the first hydrogen peak.

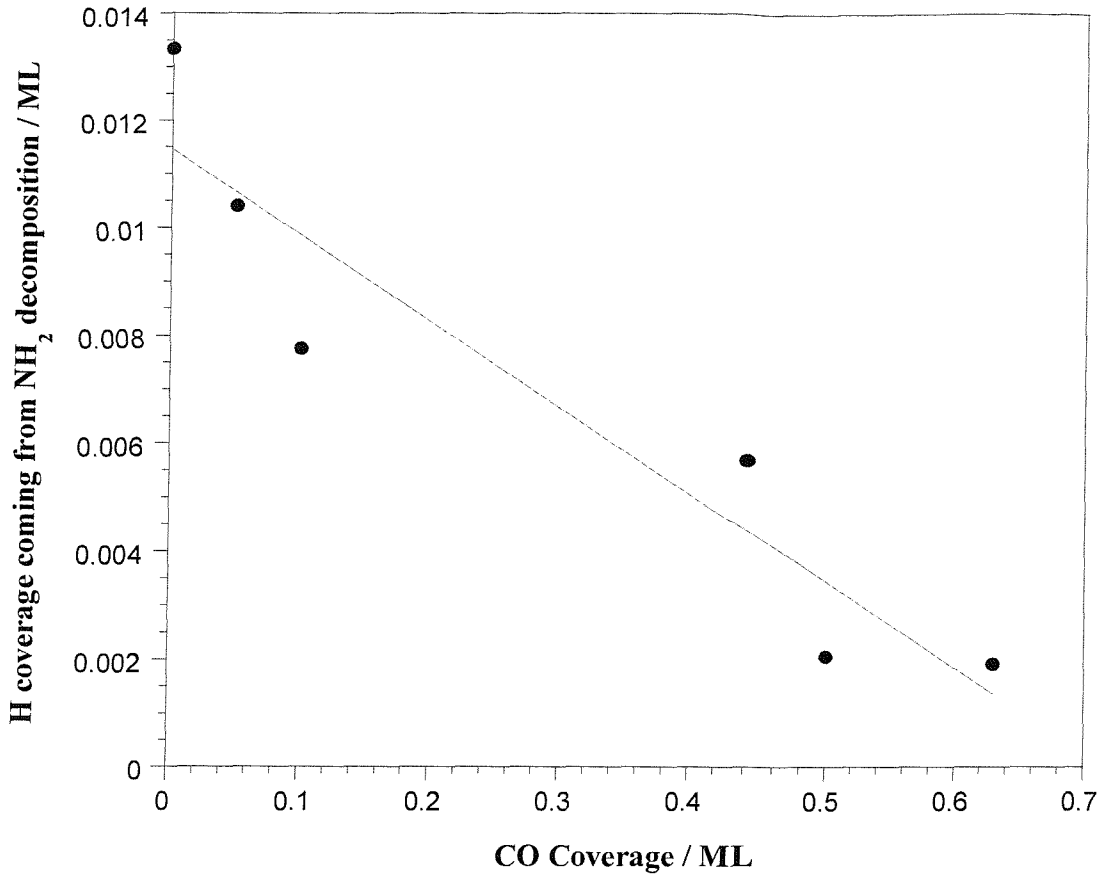

Figure VI.28: H_2 coverage coming from NH_2 decomposition versus CO precoverage. From **figure VI.27** data.

VI.3.9 Summary

- NH_3 and CO adsorbed on Pt(111) have been shown to compete for adsorption sites (*i.e.* on top of Pt atoms) [32].
- NH_3 and CO adsorbed on (100) steps are also believed to compete for the on-top Pt atoms sites, however NH_3 still finds some adsorption sites when the steps are supposedly saturated by CO molecules.
- CO desorption is not displaced by NH_3 post-adsorption.
- The two following reactions do not seem to be blocked by CO adsorption but slowly reduce until reaching a minimum of hydrogen production.

$$\text{At } T_s < 350 \text{ K } NH_3 \rightarrow NH_2 + H$$

$$\text{and at } Ts > 460 \text{ K } NH_2 \rightarrow N + 2H$$

The two next schemes illustrate the adsorption, dissociation and desorption of ammonia, on a CO precovered Pt(533) surface. **Figure VI.29a** and **VI.29b** correspond to a

low CO precoverage, while **figure VI.30a** and **VI.30b** corresponds to a large CO precoverage.

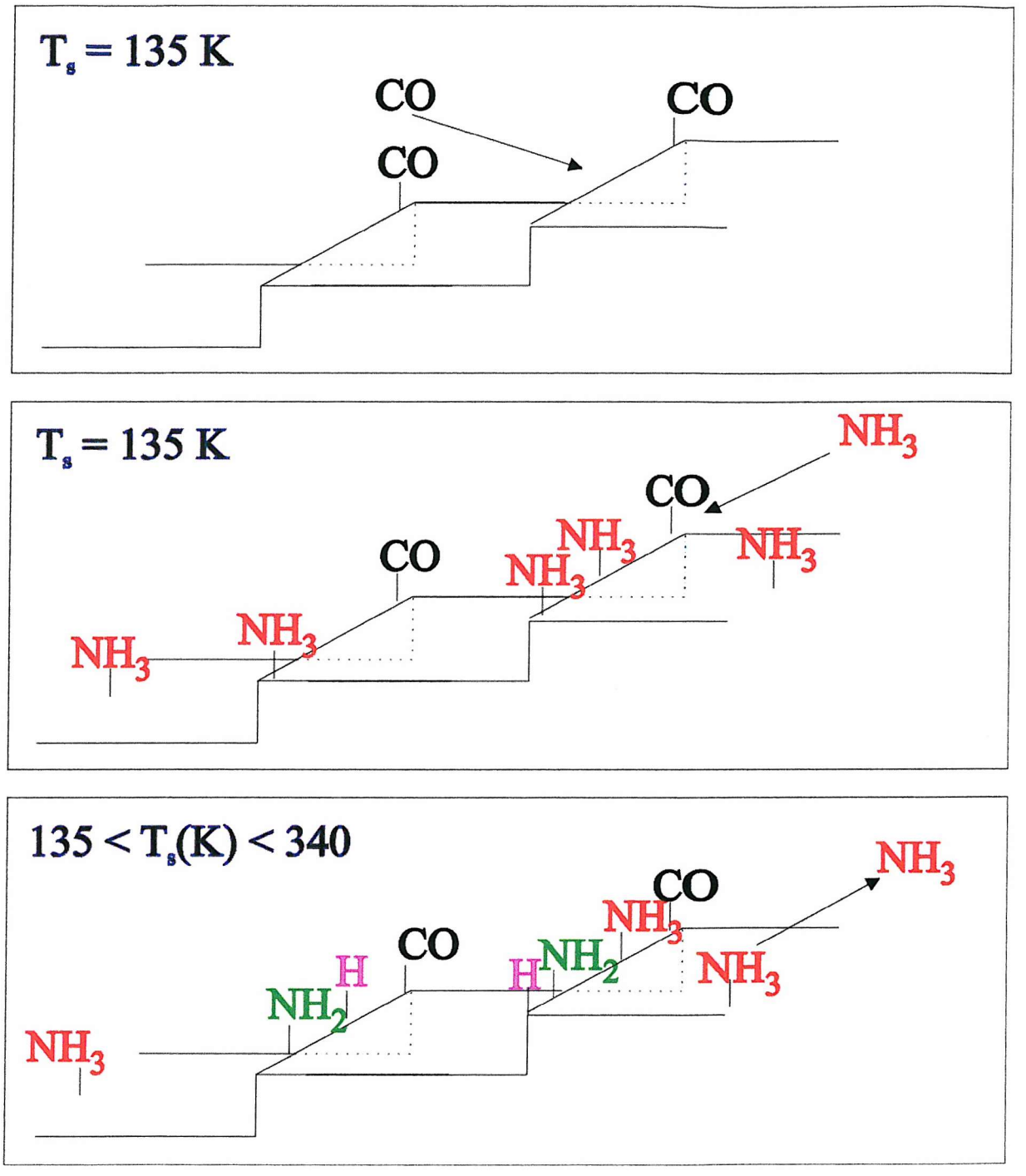

Figure VI.29a: Scheme of NH_3 adsorption and decomposition on a CO precovered Pt(533) surface with $\theta_{CO} < 0.19$ ML.

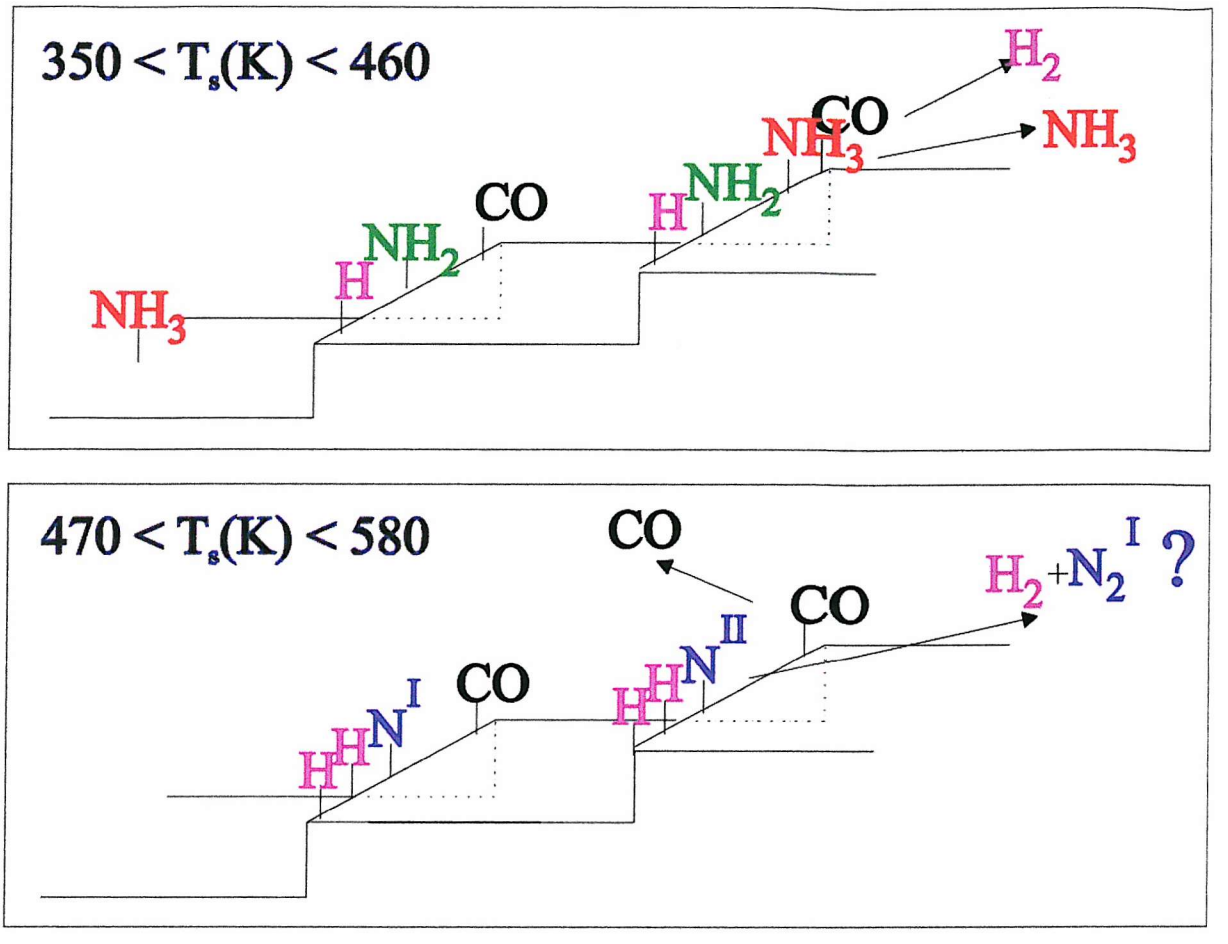

Figure VI.29b: Scheme of NH_3 adsorption and decomposition on a CO precovered Pt(533) surface with $\theta_{CO} < 0.19$ ML.

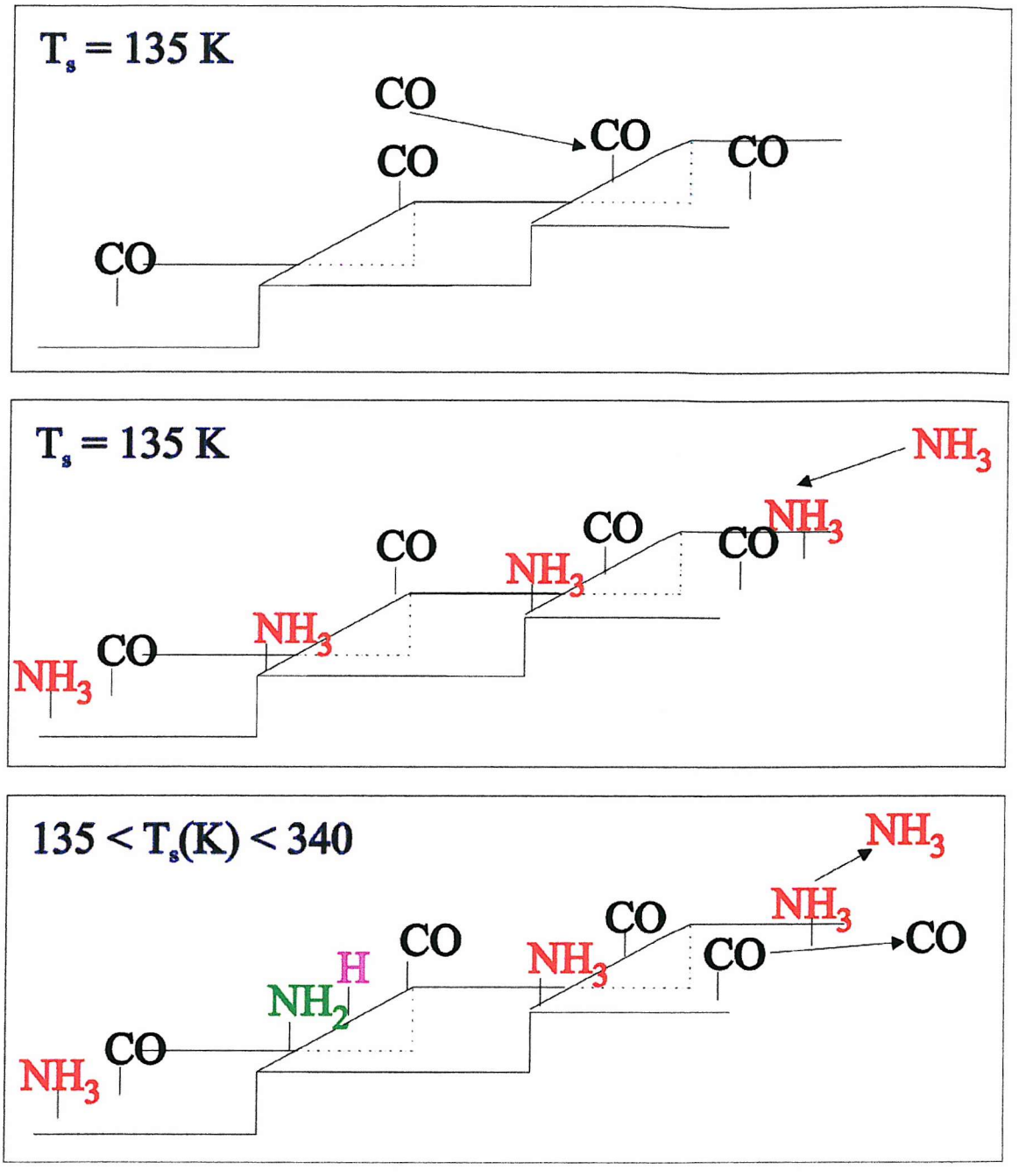

Figure VI.30a: Scheme of NH_3 adsorption and decomposition on a high CO precovered Pt(533) surface with $\theta_{CO} > 0.19$ ML.

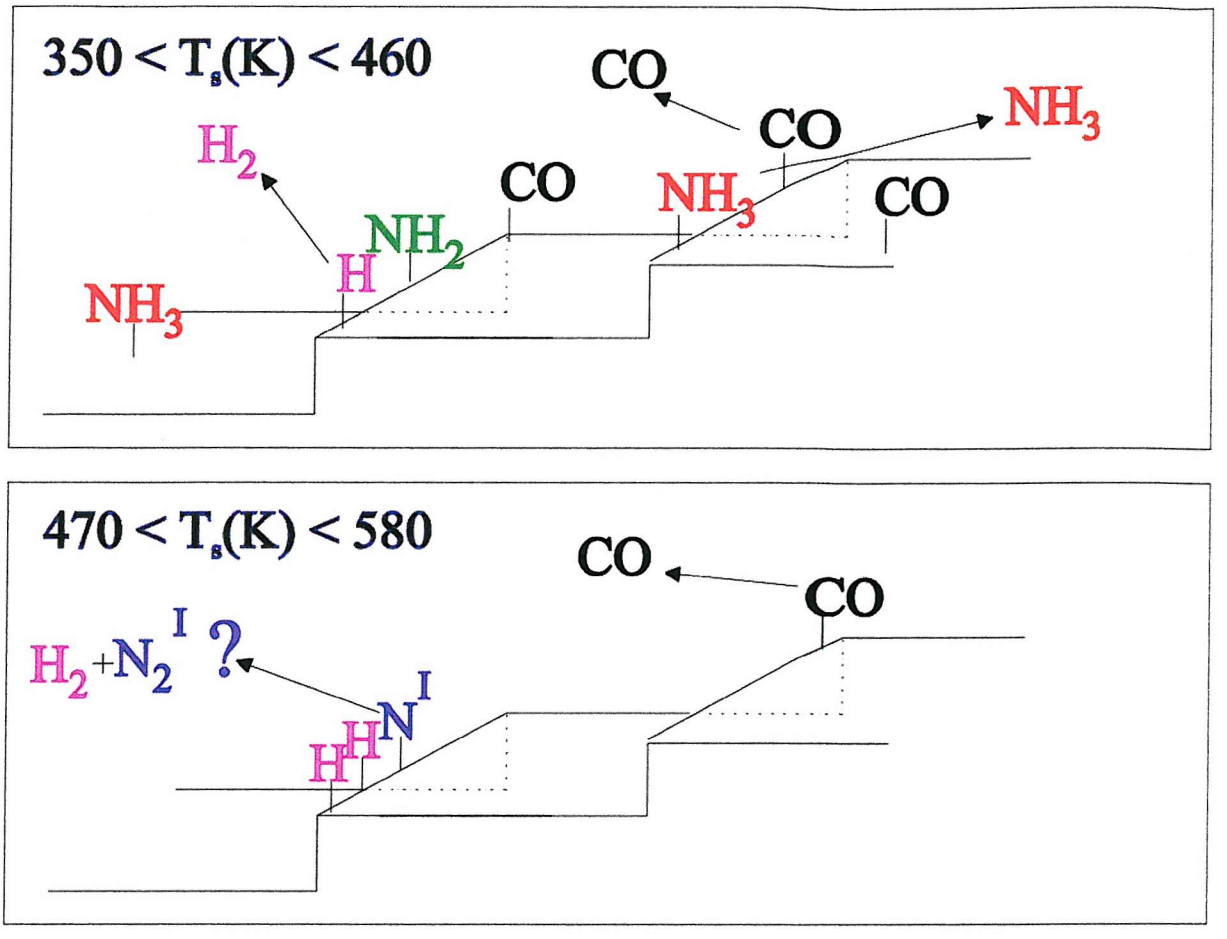

Figure VI.30b: Scheme of NH_3 adsorption and decomposition on a high CO precovered Pt(533) surface with $\theta_{CO} > 0.19$ ML.

VI.3.10 King & Wells Method

From previous experiments it was concluded that dissociation of NH_3 occurs only at the (100) steps of the Pt(533) surface. The saturation of these steps by 0.19 ML CO does not block ammonia adsorption and dissociation at these steps. However we decided to study the dissociative sticking probability of NH_3 on this CO-blocked Pt(533) surface at $T_s = 400$ K and to compare it with $S(NH_3)$ on the clean Pt(533) surface (see **parts VI.3.4-VI.3.7**).

VI.3.11 Dependence of $S_0(NH_3)$ on Incident Energy

As seen in **part VI.3.5**, it was decided to study the initial dissociative sticking probability of NH_3 at 400 K because H_2 has been identified to desorb around 400 K signalling the initial decomposition of ammonia into NH_2 on the (100) steps.

Figure VI.31 displays the $S_0(NH_3)$ as a function of beam energy for the CO step-decorated Pt(533) surface with $\theta_{CO} = 0.19$ ML at $T_s = 400$ K, with the beam at normal incidence to the crystal. The results of $S_0(NH_3)$ were measured in the energy range 27-500 meV. Beam energies were controlled by a combination of T_n and seeding (*i.e.* NH_3 was seeded in argon, neon or helium). Unfortunately, at the time of these experiments, the nozzle heating was not working properly, therefore it was not possible to complete the set of data at energies above 500 meV and between 70 and 270 meV.

The $S_0(NH_3)$ is lower on the precovered surface than on the clean one, which implies that CO has partly blocked the NH_3 adsorption step sites.

On the CO/Pt(533) surface, at lowest energy, 27 meV, the sticking is equal to 0.29±0.01, which proves the dissociative adsorption of NH_3 to be non-activated as seen on clean Pt(533). The falling of $S_0(NH_3)$ with increasing E_i is similar to the trend on the clean surface, and is a sign of NH_3 trapping into a precursor state during the initial collision. Hence as E_i increases, less molecules will be able to stay in the shallow precursor state potential before finding a proper site to dissociate, while more will go back directly to the gas phase.

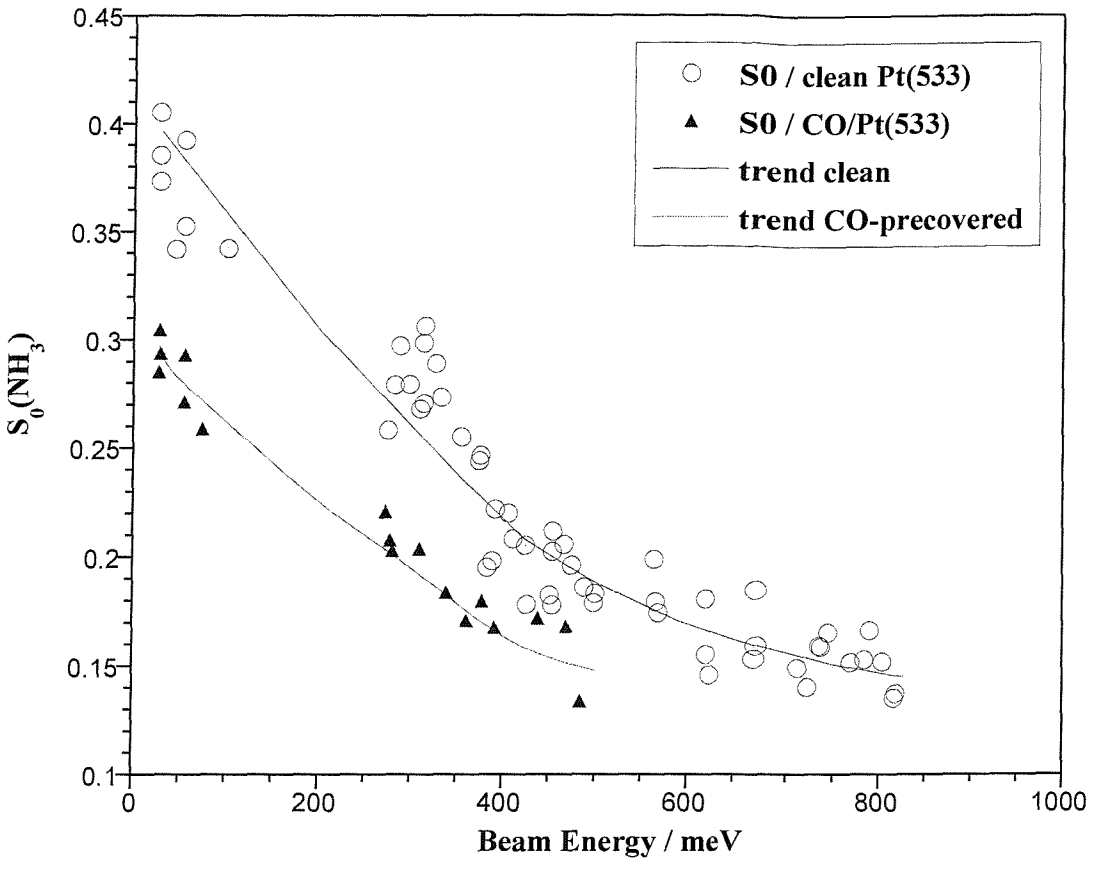

Figure VI.31: Initial sticking probability of ammonia on a clean and CO-precovered Pt(533) surface with $\theta_{CO} = 0.19$ ML, $T_s = 400$ K, $\Theta_i = 0°$. The line of best fit of the sets of data is also shown.

It would be interesting to measure the sticking at higher energies on both clean and precovered surfaces, to highlight the existence or non-existence of a direct route to dissociation.

The profiles of $S(NH_3)$ with the ammonia coverage on CO/Pt(533) at $T_s = 400$ K (not shown here) are identical to the ones on the clean Pt(533) surface (see **part VI.3.6**), thus the trend of $S(NH_3)$ with θ_{NH3} on CO/Pt(533) does not depends on the energy of the beam and is not influenced by the CO step-coverage.

VI.3.12 Consequences of Pre-adsorbed Oxygen on NH_3 Adsorption/Desorption

NH_3, in presence of oxygen, is well-known to undergo oxidation; in fact this oxidation is important in industrial processes such as the synthesis of nitric acid (HNO_3) which is an essential chemical used in the manufacture of fertilisers and explosives such as TNT. The oxidation of ammonia, also called nitrification, is also relevant to the control of pollution. Therefore, it is interesting to study the O_2 influence on the NH_3 decomposition. Moreover, the interaction of NH_3 with O_2 on a flat Pt(111) has already been studied [35], therefore the present experiment performed on Pt(533) will highlight the effect of the steps. This has been performed using TPD and molecular beam techniques. The rate of ammonia decomposition increases in presence of oxygen, leading to many desorption products such as N_2, H_2 but also H_2O. There is also evidence of masses 30 and 32 desorption that will be attributed later.

Prior to NH_3 dosing, the Pt surface was exposed with 0-0.35 ML of oxygen. The ammonia coverage was kept identical for each of these experiments as to only highlight the effect of oxygen.

O_2 was dosed through a capillary source on to the Pt(533) surface, at $T_s = 135$ K. **Figure VI.32** shows a series of O_2 TPD spectra performed to identify the amount of oxygen necessitated to cover the steps without any significant coverage on the terraces (~ 0.12 ML). The molecular desorption of oxygen appears between 110 and 170 K and corresponds to oxygen adsorbed on both step and terrace sites. At 680 and at 780 K appears the desorption of atomic oxygen initially adsorbed respectively on the terraces and on the steps.

Several studies have already been performed on the adsorption of oxygen molecules on Pt(111) [65-70], Pt(100) [71, 72] and Pt(533) [73, 74], showing that adsorbed oxygen can exist either in molecular state or atomic state on the surface depending on the surface temperature. Wang *et al.* [73] studied the adsorption of oxygen on Pt(533) with HREELS and TPD, they conclude that the binding site for oxygen at steps (both atomic and molecular) is on the exposed step edge, consistent with recent theoretical predictions and scanning tunnelling micrographs [75]. It has been shown that on Pt(111) atomic O is formed upon dosing O_2 gas at temperature above ~ 150 K [35, 76], on Pt(533) it appears (**figure VI.32**) that dosing O_2 above 170 K will lead to adsorbed atomic oxygen. In the

present experiments, the pre-exposure of oxygen was performed around 135 K therefore it is more likely that the Pt(533) surface exhibit some molecular oxygen adsorbates. Moreover, at a surface temperature of 135 K, the O_2 adsorption state has been identified to be a peroxo-like configuration. In this configuration the oxygen molecules are more affected by the interaction and hybridisation with the platinum surface. The bond length has been determined to be 1.43 Å [67]. The oxygen molecule seems to be adsorbed in a hollow or more complex adsorption site.

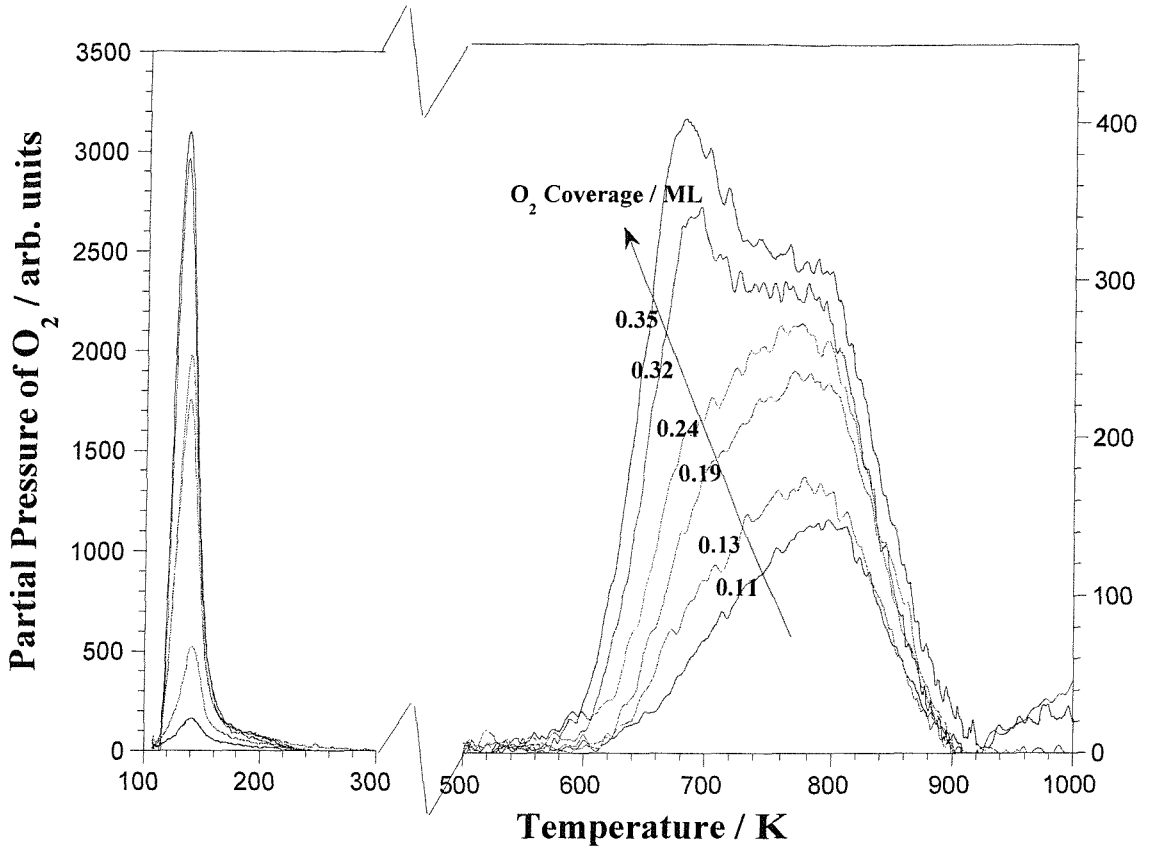

Figure VI.32: TPD of O_2 following exposure of Pt(533) to O_2. O_2 was dosed using a capillary source at T_s = 110 K. With $0.11 < \theta_O < 0.35$ ML and the heating rate was 1-1.3 K s^{-1}.

Figure VI.33 shows some NH_3 thermal desorption spectra following NH_3 exposures from a pure NH_3 supersonic molecular beam (T_n = 295 K and E_i = 108 meV) on the Pt(533) surface modified by increasing coverage of oxygen. The 4 features for ammonia desorbing from a clean Pt(533) surface defined as: β around 160 K, β' around 210 K, α around 270 K and the α' shoulder (**figure VI.5**). Increasing the oxygen coverage results in the decrease in intensity of the four previous features. When the steps are saturated with molecular oxygen

(dosed at 135 K), $\theta_{O2} > 0.12$ ML, the TPD data still show some NH_3 molecules desorbing from the steps in α' phase and even from the second step-layer β'.

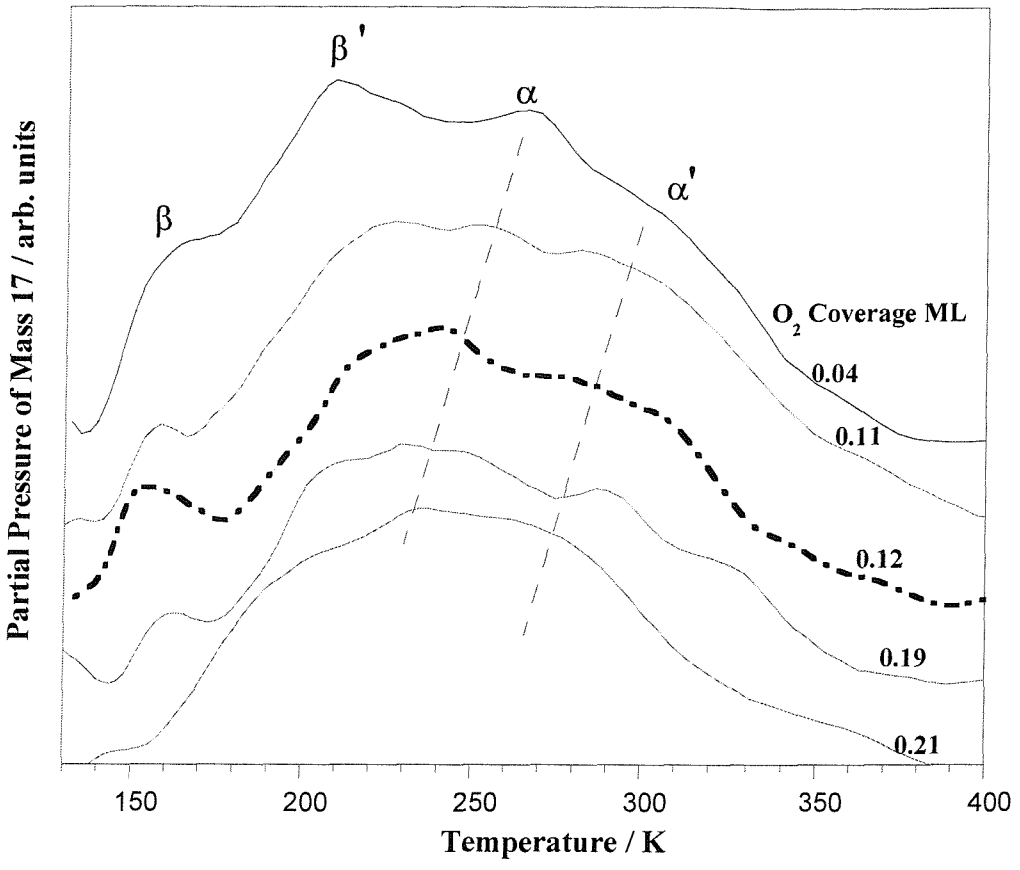

Figure VI.33: TPD of NH_3 following exposure of O_2/Pt(533) to NH_3. NH_3 was dosed using a beam source (pure NH_3) at $T_s = 135$ K, $T_n = 295$ K and $E_i = 108$ meV on an oxygen precovered Pt(533) surface. The heating rate was 3.8 K s^{-1}. The surface was preexposed to an O_2 coverage of 0-0.21 ML.

As said previously, on Pt(533) the O_2 molecules have been shown to adsorb on hollow or more complex sites, while the NH_3 molecules adsorb on on-top sites. Hence these two adsorbates do not compete for adsorption sites. However the amount of NH_3 desorbing decreases when θ_{O2} increases which could be due to the oxygen partly blocking NH_3 adsorption (steric effect). Still it seems more likely that the reduced amount of ammonia desorption results from its oxidation into N_2 and NO (see later on).

The present NH_3 desorption features were really difficult to extract from the original data and do not present any clear peaks. However there seems to still be some NH_3 adsorbing in the α phase but not in the β phase with 0.21 ML of preadsorbed oxygen.

Figure VI.34 shows the production of mass 28 after dosing a mixture of 10 ml min^{-1} of NH_3 with 10 ml min^{-1} of He on an O_2/Pt(533) surface at 135 K. At 0 ML O_2 coverage, there is only 1 peak at 530 K corresponding to N_2 desorbing from the (100) steps of the Pt(533) surface.

When O_2 is dosed on the surface prior to NH_3 exposure, the peak around 530 K is still present and of constant intensity with $0 < \theta_{O2}(ML) < 0.35$, which implies that the NH_3 molecules decomposing on the steps of the clean surface, are not influenced by the presence of oxygen as thought previously. Note that the heating rate for the NH_3 TPD on O_2/Pt(533) was much more different from the NH_3 TPD on clean Pt(533), resulting in a noticeable displacement of the 530 K peak.

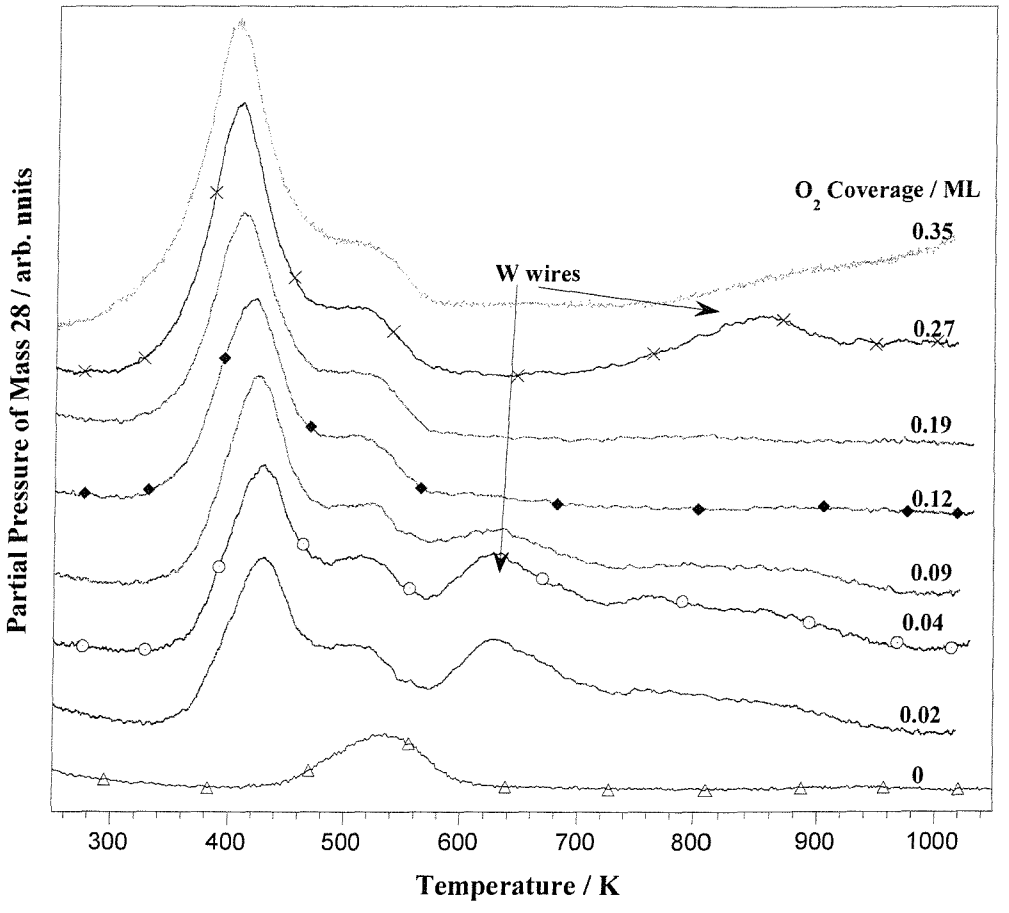

Figure VI.34: TPD of N_2 following exposure of O_2/Pt(533) to NH_3. NH_3 was dosed using the beam source (50 % NH_3 in He) at T_s = 135 K, T_n = 295 K and E_i = 139 meV. The heating rate was 3-15 K s^{-1}. The surface was preexposed to an O_2 coverage of 0-0.35 ML.

In **figure VI.34** a new N_2 desorption feature appears which reaches a maximum at 430 K when the O_2 coverage correspond to 0.02 ML, and then gains in intensity while

moving down to 400 K when the O_2 coverage increases up to 0.35 ML. Mieher *et al.* [35] studied the oxidation of NH_3 on both a molecular and an atomic oxygen presaturated Pt(111) surface. On the O_2/Pt(111) surface they observed N_2 desorbing from 475 K at low NH_3 exposure to 420 K at high NH_3 exposure. Therefore it is tempting to associate the 430 K feature of N_2 to ammonia decomposition enhanced by the oxygen presence on the (111) terraces of the Pt(533) surface. However with an oxygen coverage $\theta_{O2} < 0.12$ ML where oxygen deposition only occurs at the steps, the latter feature is already present, hence we believe that there is a similar path to oxidation of ammonia on the steps and on the terraces.

Notice that a few of these TPD spectra show an other peak around 640 or 840 K. By varying the heating rate from 3 to 15 K s^{-1} it was possible to displace this last feature, therefore proving that it does not correspond to any desorption from the sample surface, but more likely from the tungsten wires. In fact it is well known that tungsten dissociates ammonia into N_2 and H_2 [77].

While on the clean Pt(533) surface there was a peak above 800 K related to N_2 desorbing from a nitrogen containing near-surface compound (nitride), there is no evidence of such a feature here.

Remark: Bradley *et al.* [50] observed the dissociation of NH_3 on the hex-R and (1×1) faces of the Pt(100) surface. A comparison of the data from both clean surfaces and the oxygen-precovered hex-R surface conclude that the latter surface is much more active for ammonia dissociation even though the oxygen exposure performed only covers around 11 % of the exposed surface. The doses were performed at 150 K.

A comparison of mass 28 and masses 14 and 12 fragments (**figure VI.35**) confirms that the 430 and 530 K peaks from mass 28 signal are mainly from N_2, and any influence of CO (from the background CO in the chamber) in the mass 28 TPD is very small.

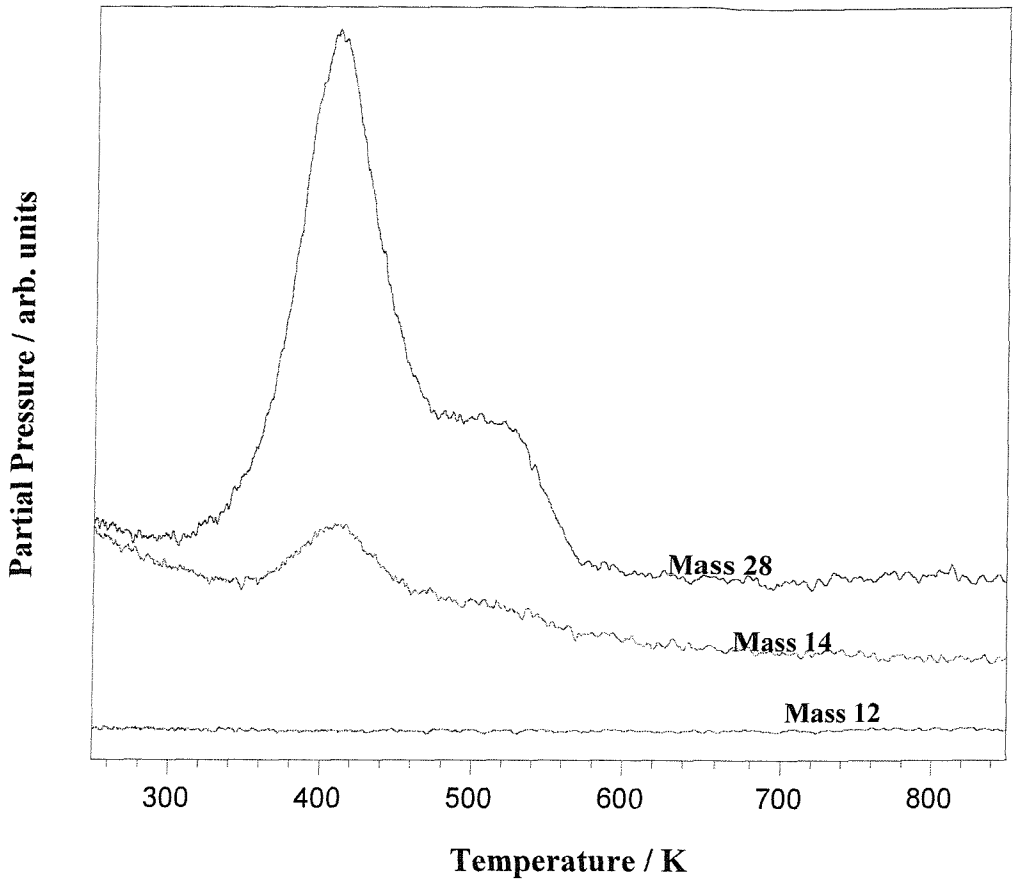

Figure VI.35: TPD of masses 28, 14 and 12 following exposure of O_2/Pt(533) to NH_3. NH_3 was dosed using the beam source (50 % NH_3 in He) at T_s = 136 K, T_n = 295 K and E_i = 139 meV. The heating rate was 2.5 K s^{-1}. The surface was preexposed to an O_2 coverage of 0.19 ML.

Figure VI.36 shows the production of H_2 after dosing a pure beam of NH_3 on an O_2/Pt(533) surface at 135 K.

On the clean Pt(533) surface there are 2 peaks as seen in **paragraph VI.3.2 figure VI.11**. The lowest one at 410 K is similar to the recombinative desorption of atomic hydrogen preferentially adsorbed on the (100) steps of the Pt(533) surface. The second peak appears at 545 K and was earlier on attributed to NH_2 species (originating from the NH_3 decomposition) decomposing into N and 2H on the steps of the clean Pt(533) surface. At 0.04 ML of oxygen, the platinum steps are slightly covered, thus there are less free sites for hydrogen atoms (coming from the NH_3 decomposition) to associatively desorb, which explains the decrease of the intensity of the 410 K peak. When the steps are totally covered with oxygen, the 410 K peak is missing.

As observed for N_2 production, the H_2 peak at 530 K is still present and constant on a O_2 steps saturated surface, which implies that the oxygen does not block the adsorption sites necessary for the NH_2 decomposition leading to H_2 production.

It will become evident why the first hydrogen production is not possible on the O_2 presaturated steps while the second one is.

Notice that all the H_2-TPD obtained after NH_3 exposure present an underlying background from 300 to 800 K as seen on the clean Pt and the CO/Pt surfaces, which is not affected by the oxygen coverage. Earlier experiments have shown that there is no noticeable background hydrogen in the chamber nor decomposition of ammonia into N_2 and H_2 in the nozzle, thus we associate this feature with the decomposition of the ammonia from the sample holder (W wires, Cu support, Ni bars...) or the back of the crystal.

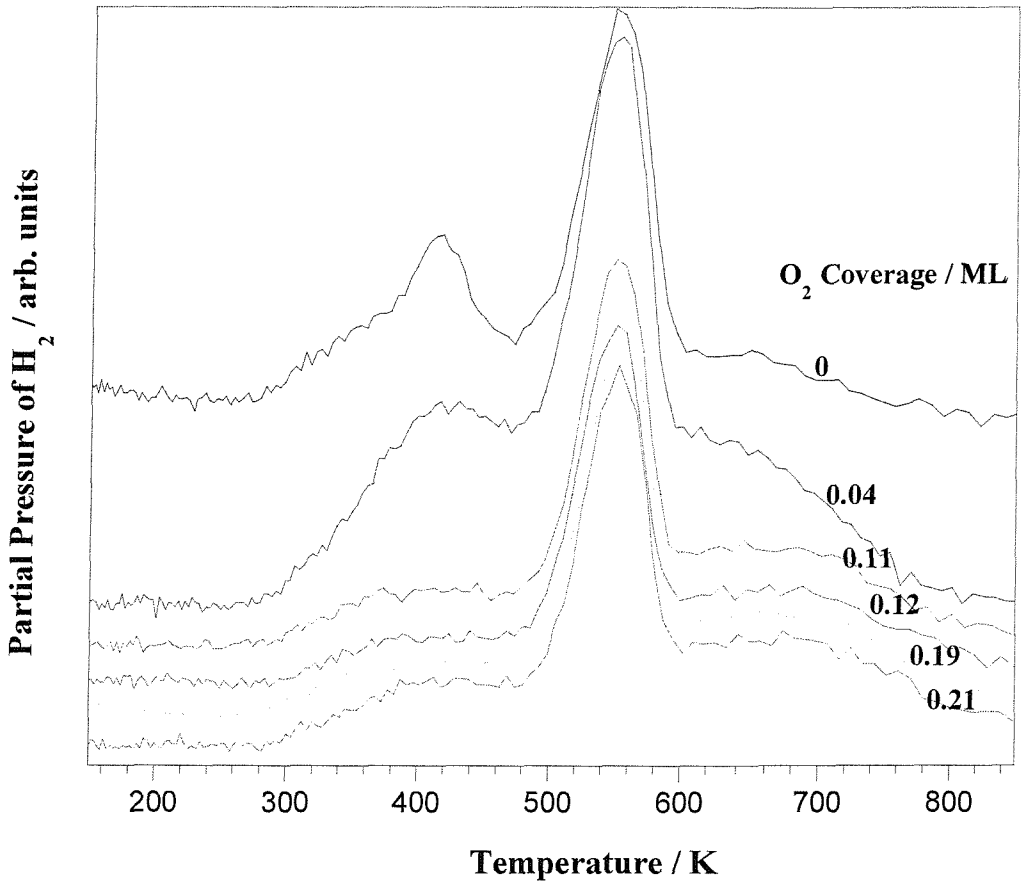

Figure VI.36: TPD of H_2 following exposure of O_2/Pt(533) to NH_3. NH_3 was dosed using the beam source (pure NH_3) at T_s = 135 K, T_n = 295 K and E_i = 108 meV. The heating rate was 6.5-7 K s^{-1}. The surface was preexposed to an O_2 coverage of 0-0.21 ML.

When the oxygen coverage increases from 0 to 0.35 ML, the desorption of N_2 around 400 K clearly increases illustrating the ammonia decomposition enhancement, therefore the hydrogen desorption signal is also expected to increase. However **figure VI.36** shows a rather constant production at 530 K. What happens then with the hydrogen freed from the ammonia decomposition?

Figure VI.37 evidences the formation of H_2O. No water production was detected after dosing ammonia on the clean Pt surface, however on the O_2 precovered surface, water desorption peaks are present around 215-230 K, 350 K and 400 K. In this case, O_2 was dosed at 135 K, leading to adsorbed molecular oxygen. Previous experiments performed by Mieher and Ho [35] also showed some water formation following an NH_3 exposure on an oxygen presaturated-Pt(111). Note that Mieher and Ho studied the oxidation of ammonia on both an atomic and molecular oxygen pre-saturated surfaces. On NH_3/O/Pt(111) surface they observe two well defined peaks at 215 K (β H_2O) and 350 K (α H_2O), while on NH_3/O_2/Pt(111) H_2O production occurs more continuously from ~ 180 to 450 K which appears to be in better agreement with the present data (**figure VI.38**).
In the present data on O_2/Pt(533), the peak at 400 K which appears with 0.35 ML coverage of O_2 was not observed by Mieher and Ho, hence it is tempting to relate it with H_2O produced and desorbed from the (100) steps.
The 350 K feature which appears with 0.36 ML of O_2 is more likely to be due to H_2O desorption initially formed on the (111) terraces as it agrees quite well with the data from Mieher and Ho.

Notice that the adsorption of water on a Pt(111) surface [78] leads to completely different desorption features than the previous ones with H_2O desorbing between 160 and 225 K. On Pt(533) (see insert in **figure VI.38**) Skelton *et al.* [79] observed a first peak at 195 K attributed to the first layer of chemisorbed water directly bonded to the surface. After saturation of this feature, a second peak appears at 155 K attributed to physisorbed water (ice) multilayers. This peak shifts up in temperature when the coverage increases. The form of the TPD spectrum at high H_2O exposure is typical of ice multilayers and has been observed on many metals [80, 81].

Skelton *et al.* [79] also studied the formation of water on Pt(533) when dosing H_2 on a O-precovered surface. They observed some desorption-limited features below 200 K and some reaction-limited processes from 200 to 400 K. Thus, we conclude that the water desorption observed in the present case from 170 to 500 K is a reaction-limited process.

It would be interesting to study the interaction of ammonia with oxygen using other UHV techniques, such as STM and EELS, to confirm our assumptions.

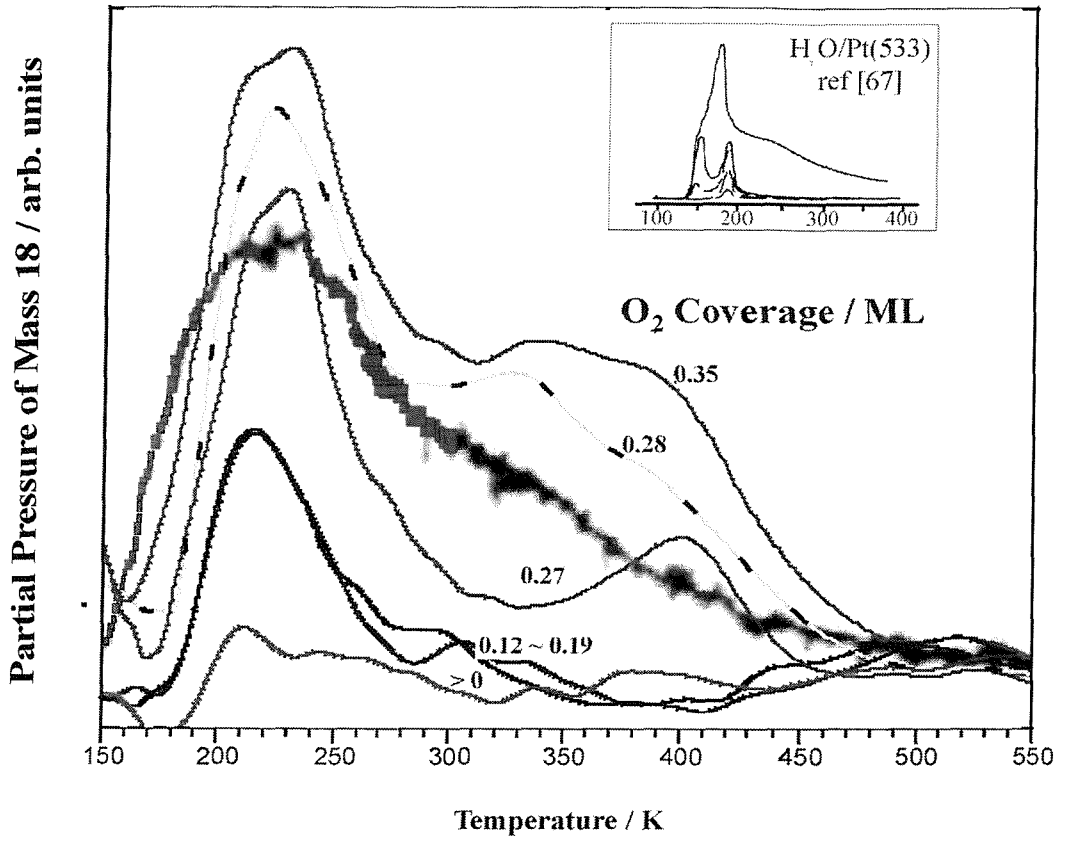

Figure VI.37: TPD of H_2O following exposure of O_2/Pt(533) to NH_3. NH_3 was dosed using the beam source (50 % NH_3 in He) at T_s = 136 K E_i = 138 meV. The heating rate, hard to keep constant, increased from 4 to 9 K s^{-1} when T_s increases from 150 to 500 K. The surface was preexposed to an O_2 coverage of 0-0.35 ML.
Reproduction of a TPD of NH_3 onto a presaturated O_2/Pt(111) surface. T_s = 85 K, and the heating rate was 2 K s^{-1} [35] (large black line). Reproduction of TPD of H_2O on a Pt(533) bare. T_s = 90 K and the heating rate was 10 K s^{-1} [79].

Looking back at **figure VI.35**, we can propose the following mechanism on the steps:

$2NH_3 \rightarrow 2NH_2 + 2H$ at $135 < T_s(K) < 340$

$2H+O \rightarrow H_2O$ at $170 < T_s(K) < 450$

$2H \rightarrow H_2$ at $T_s \sim 400$ K first hydrogen production

$NH_2 \rightarrow N+2H$ at $500 < T_s(K) < 600$ giving rise to second H_2 and N_2 productions

Hence the fourth step of this mechanism can lead to production of N_2 and H_2 on the O-precovered surface because the step sites are freed from the pre-adsorbed oxygen due to production of H_2O in the second step. This mechanism also shows why for $\theta_{O2} > 0.12$ ML the first production of H_2 on the steps was not occurring due to the complete consumption of the initial hydrogen entering water production at the steps. Note that these 2 desorption processes start at ~ 350 K.

Increasing further the oxygen precoverage leads to production of water on the terraces too.

The adsorption of NH_3 on an oxygen precovered surface also leads to the production of nitric oxide, NO. **Figure VI.38** shows only one peak at 480 K which accounts for NO desorbing from NH_3 dosed on a O_2/Pt(533) surface. The energy of desorption of this species is calculated to be around 102 kJ mol^{-1}. Due to the lack of data for NO on a O_2-precovered Pt(533) surface with $\theta_{O2} < 0.12$ ML we do not know if it corresponds to production of NO from the terraces, the steps or on the whole surface.

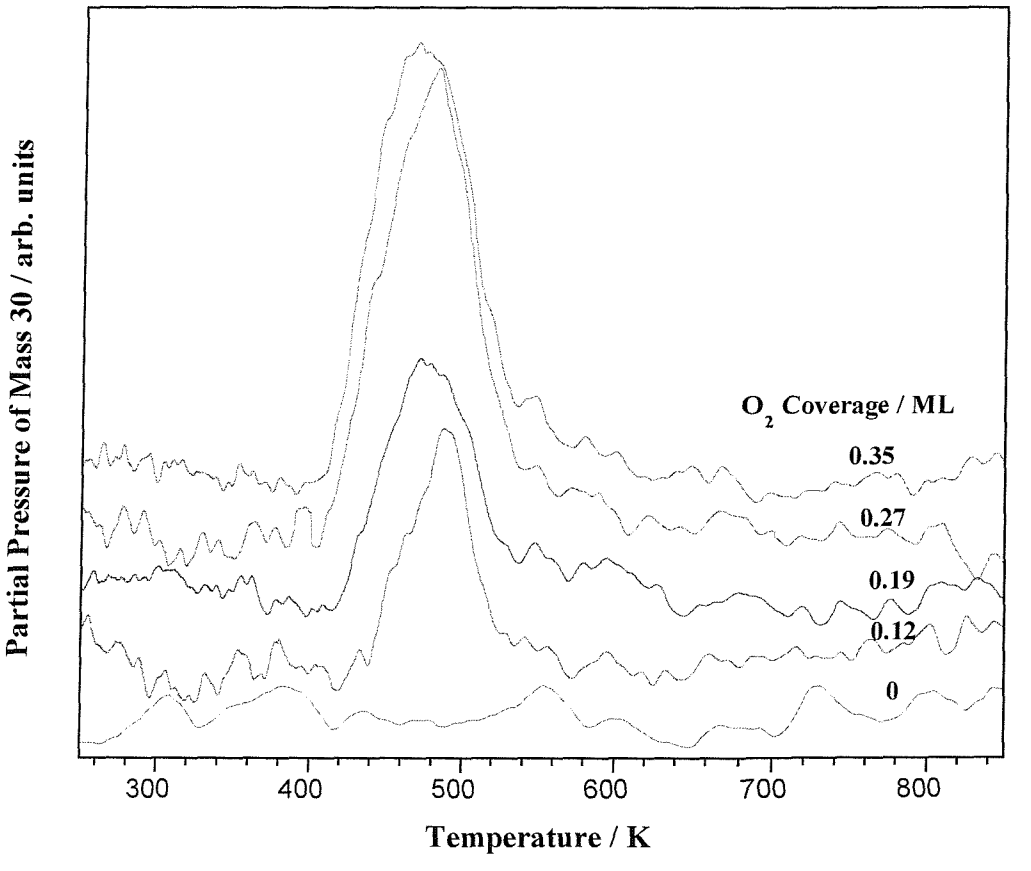

Figure VI.38: TPD of mass 30 following exposure of O_2/Pt(533) to NH_3. NH_3 was dosed using the beam source (50 % NH_3 in He) at T_s = 135 K, T_n = 295 K and E_i = 138 meV. The heating rate was 3-10 K s^{-1}. The surface was preexposed to an O_2 coverage of 0-0.35 ML.

Because of interest in removal of NO as an air pollutant, its adsorption, desorption and decomposition on platinum metals have been extensively studied [87]. Gland *et al.* [37] studied the adsorption of NO on Pt(111) at 100 K; they observed some complex features, with notably a main NO desorption at 335 K which was found to be of first order kinetics (see **figure VI.39** dash line). A high temperature shoulder around 470 K is associated with the presence of surface defects. Gorte *et al.* [87] performed the same experiment on a Pt(111) surface and also observed a main feature at 340 K. No high temperature shoulder was noticed which suggests that the Pt(111) surface studied was defect free. Notice that Gorte (plain line) and Gland (not shown here) both observed a feature around 400 K with a small NO coverage, believed to be of second order kinetics desorption. Campbell *et al.* [88] also performed the same experiment but dosing NO at 284 K on a Pt(111) surface which led to the same observations as Gland, indicating that the dosing temperature does not seem to influence the desorption features [39, 87].

Gohndrone and Masel studied NO adsorption on Pt(211) [39] and also observed a main feature of the same form than Gorte and Gland but at 370 K (marked line). A second main feature believed to correspond to the (100) steps of the Pt(211) appears at 500 K and is also slightly shifted compared to the high temperature shoulder observed by Gland on defected Pt(111). This hypothesis is confirmed by the results obtained by Gorte *et al.* [87] who studied NO adsorption on Pt(100). In fact, for relatively low coverage of NO they observed only one feature around 500 K.

Remark: all these data agree relatively well, and it is our belief that the difference of ~ 30 K observed between Gorte/Gland and Gohndrone data (see **figure VI.39**) is probably due to differences in their temperature measurement (thermocouple problems may be).

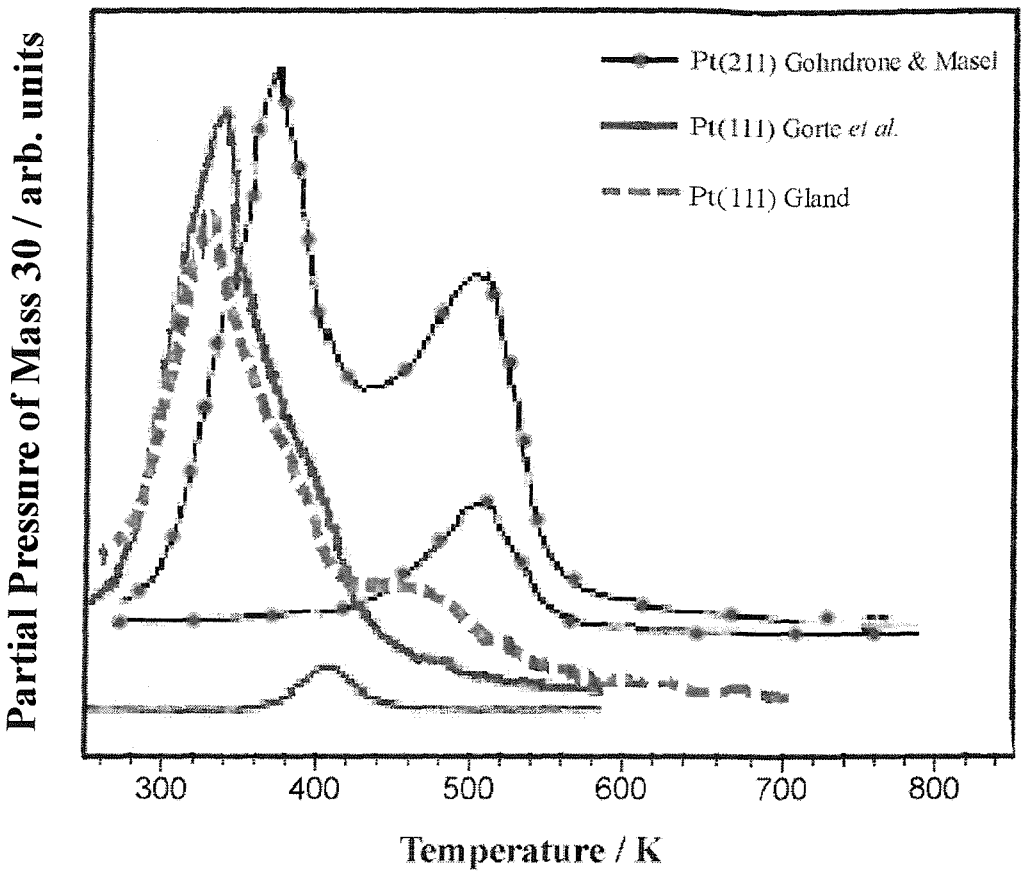

Figure VI.39: Reproduction of TPD of NO following exposure of Pt(111) to 5 L of NO. T_s = 100 K, the heating rate was 4.75 K s^{-1} (dash line) [37]. TPD of NO following exposure of Pt(211) to 0.1 and 5 L of NO. T_s = 300 K and the heating was 28 K s^{-1} (marked line) [39]. TPD of NO following exposure (<10 L) of Pt(111). at T_s = 100 K the heating rate was 10 K s^{-1} (plain line) [88].

Mieher *et al.* [35] found that desorption of NO from NH_3 adsorbed on O/Pt(111) appears around 500 K. For NH_3 adsorbed on O_2/Pt(111), NO desorbs at 486 K when a small amount of NH_3 is dosed on a saturated oxygen surface, while with a higher NH_3 exposure, a second peak appears at 316 K. From their TPD data for N_2, H_2O and NO, we believe that the production of NO at 486 K comes from the defects while the 316 K one comes from the (111) plan.

The feature observed in **figure VI.38** at 480 K is therefore believed to correspond to the desorption of NO from the steps of Pt(533), however it may or may not be formed at the step sites. There is no feature at 320 K hence there is no NO desorption from the (111) terraces. In fact most of the NH_3 oxidised on the terraces will produce N_2.

Increasing the O coverage leads to more N_2 and H_2O production on the whole surface and NO on the steps, until all the ammonia molecules adsorbed on the surface are

decomposed. This probably takes place around θ_{O2} = 0.36-0.4 ML, which explains why the TPD feature areas of these 3 species become relatively constant above this coverage.

Figure VI.40 shows the production of mass 32 after an increasing O_2 precoverage and with a constant NH_3 dose. Two features appear, one small but sharp around 370 K and a large one around 650-700 K. This second feature which keeps increasing with the O_2 coverage is believed to correspond to O_2 desorbing from the (111) terraces of the Pt(533) surface. There is no sign of O_2 desorbing from the steps (above 750 K) because it has been used up in the water formation. In fact it agrees reasonably well with some previous O_2-TPD experiments performed by only dosing O_2 on a clean Pt(533) surface which desorbs around 700 K from the terraces and 800 K from the steps [74]. The peak at 370 K was not observed by Gee and Hayden [74] for O_2 dosed on a clean Pt(533) surface, hence we believe that the oxidation of NH_3 on the surface produces some atomic oxygen which must be weakly bound to the surface, hence it will recombine rapidly in O_2 and desorb at this relatively low temperature.

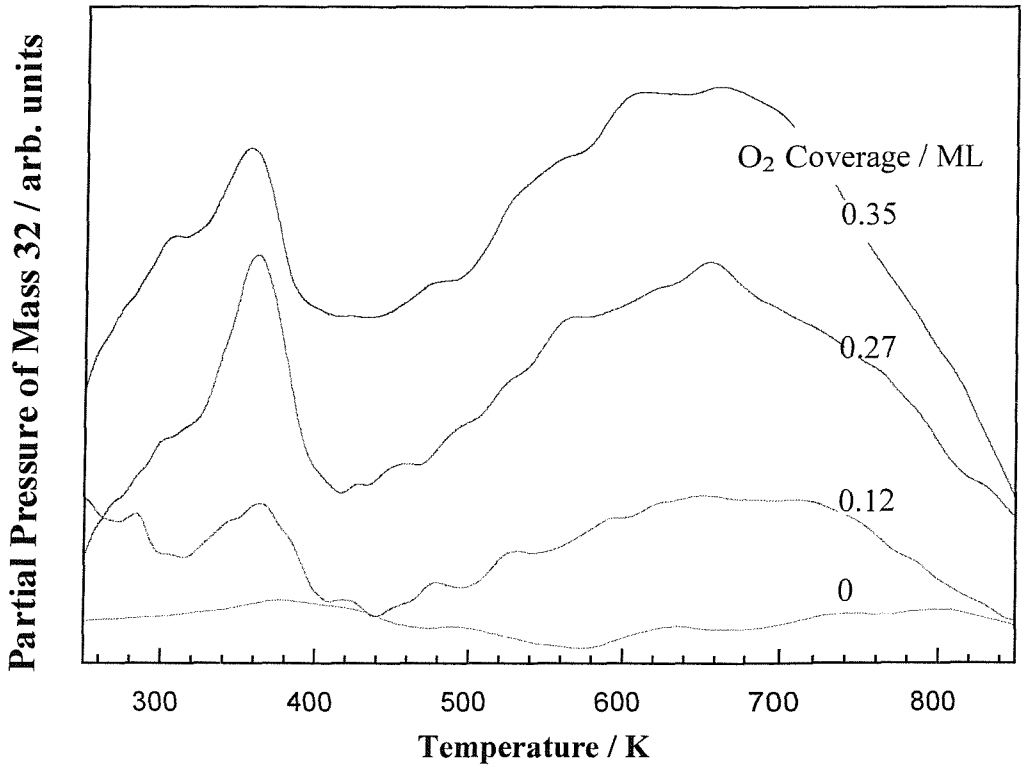

Figure VI.40: TPD of mass 32 following exposure of O_2/Pt(533) to NH_3. NH_3 was dosed using the beam source (50 % NH_3 in He). T_s = 135 K, T_n = 295 K, E_i = 138 meV. The heating rate was 2.5 K s^{-1}. The O_2 coverage was 0-0.35 ML.

VI.3.13 Summary

The two next schemes illustrate the adsorption, dissociation and desorption of ammonia and its products, on a O_2 precovered Pt(533) surface. **Figures VI.41a** and **VI.41b** corresponds to a low O_2 precoverage, while **figures VI.42a** and **VI.42b** corresponds to a large O_2 precoverage.

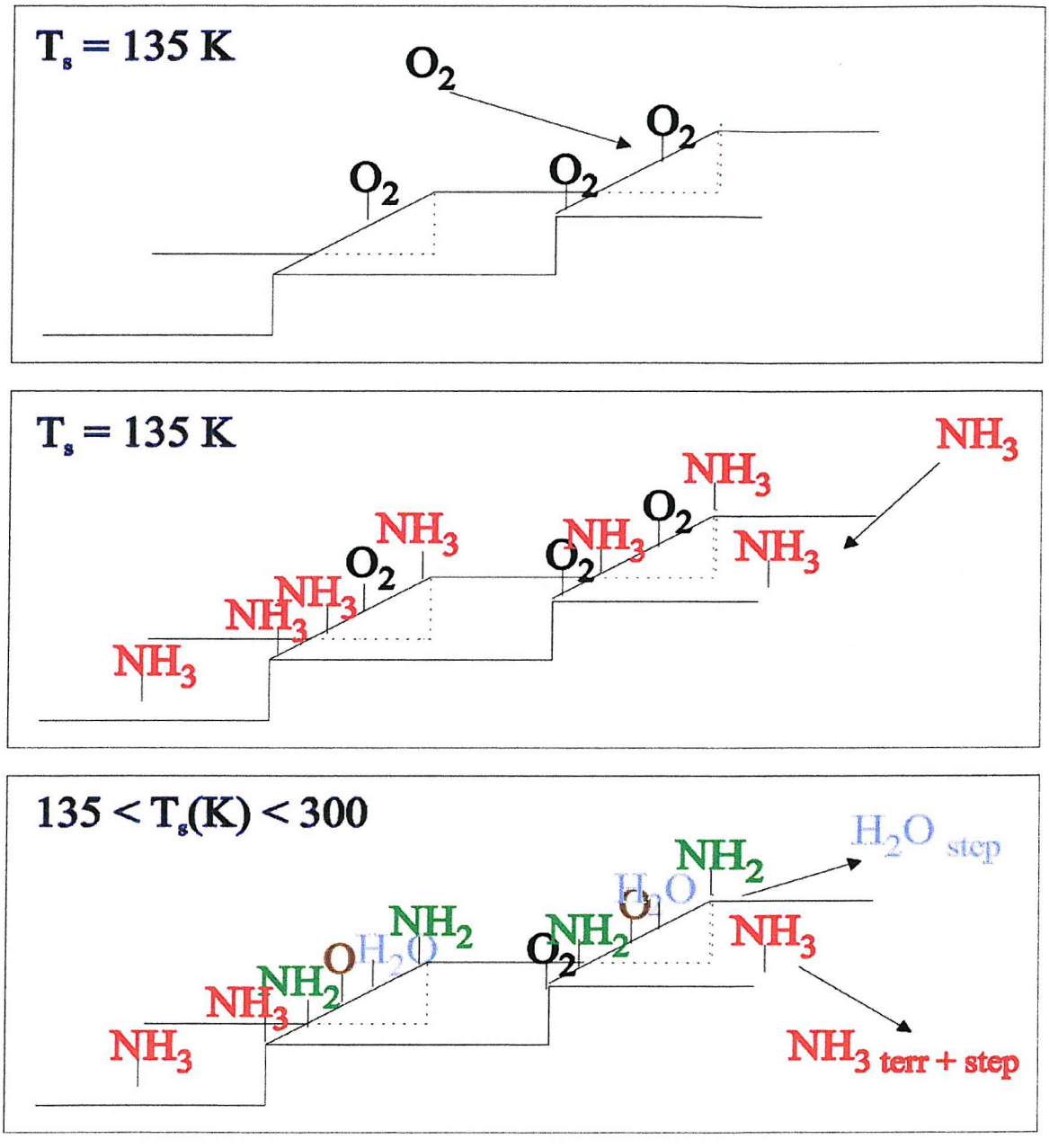

Figure VI.41a: Scheme of NH_3 adsorption and decomposition on a O_2 precovered Pt(533) surface with $\theta_{O2} < 0.12$ ML.

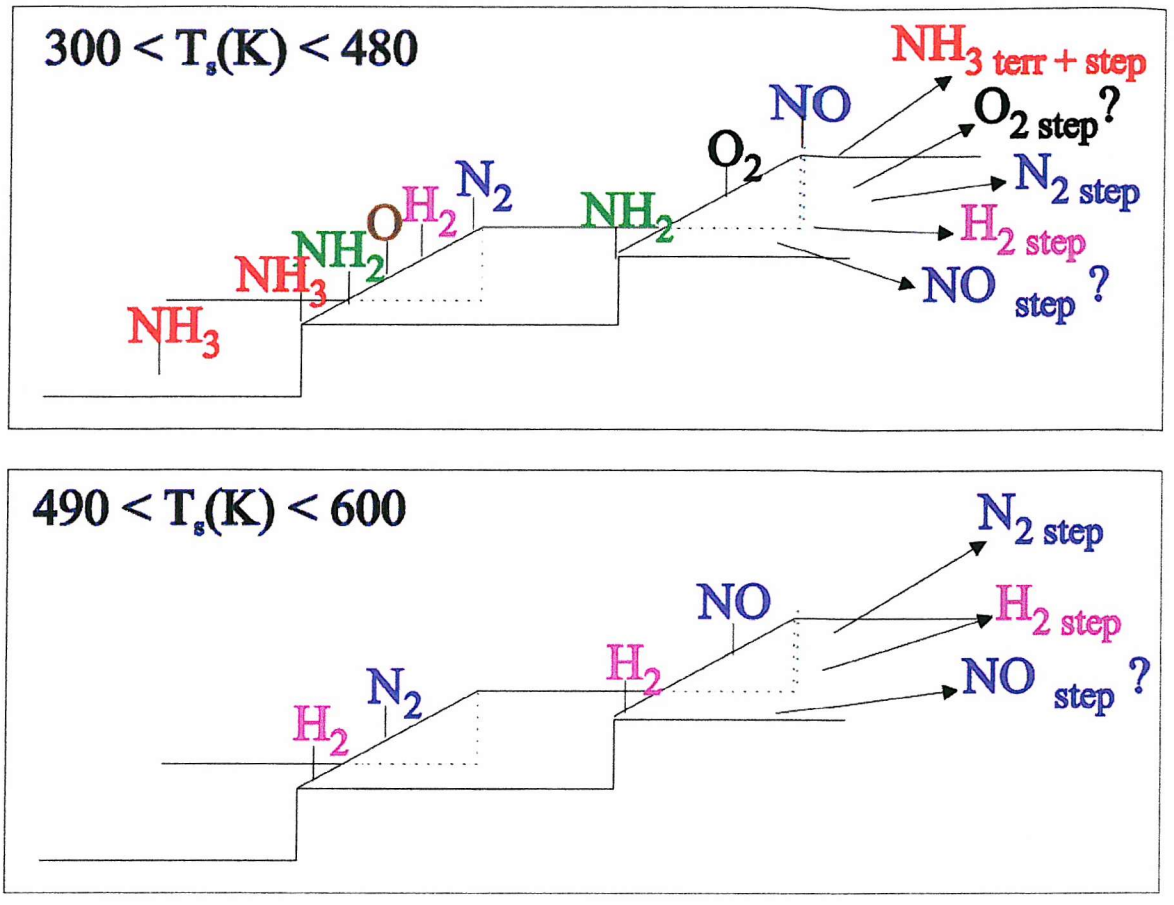

Figure VI.41b: Scheme of NH_3 adsorption and decomposition on a O_2 precovered Pt(533) surface with $\theta_{O2} < 0.12$ ML.

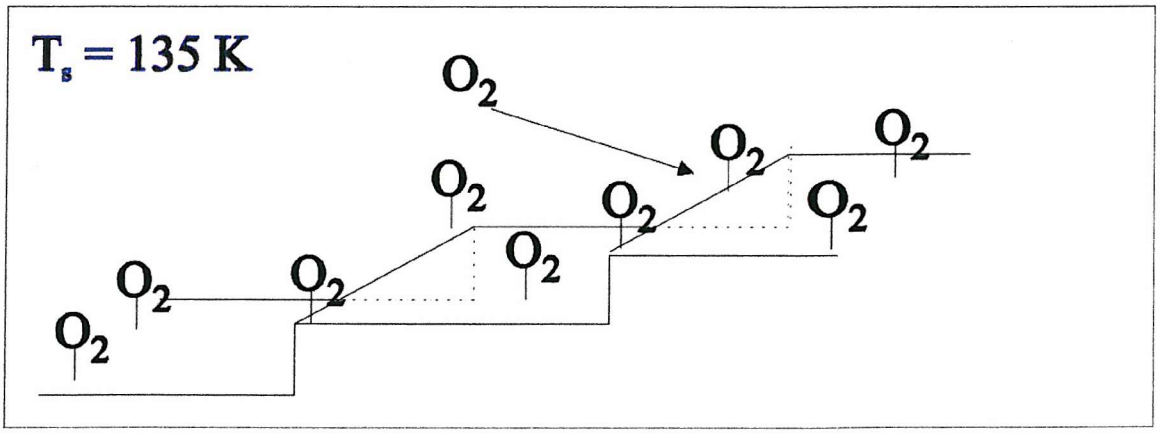

Figure VI.42a: Scheme of NH_3 adsorption and decomposition on a O_2 precovered Pt(533) surface with $\theta_{O2} > 0.12$ ML.

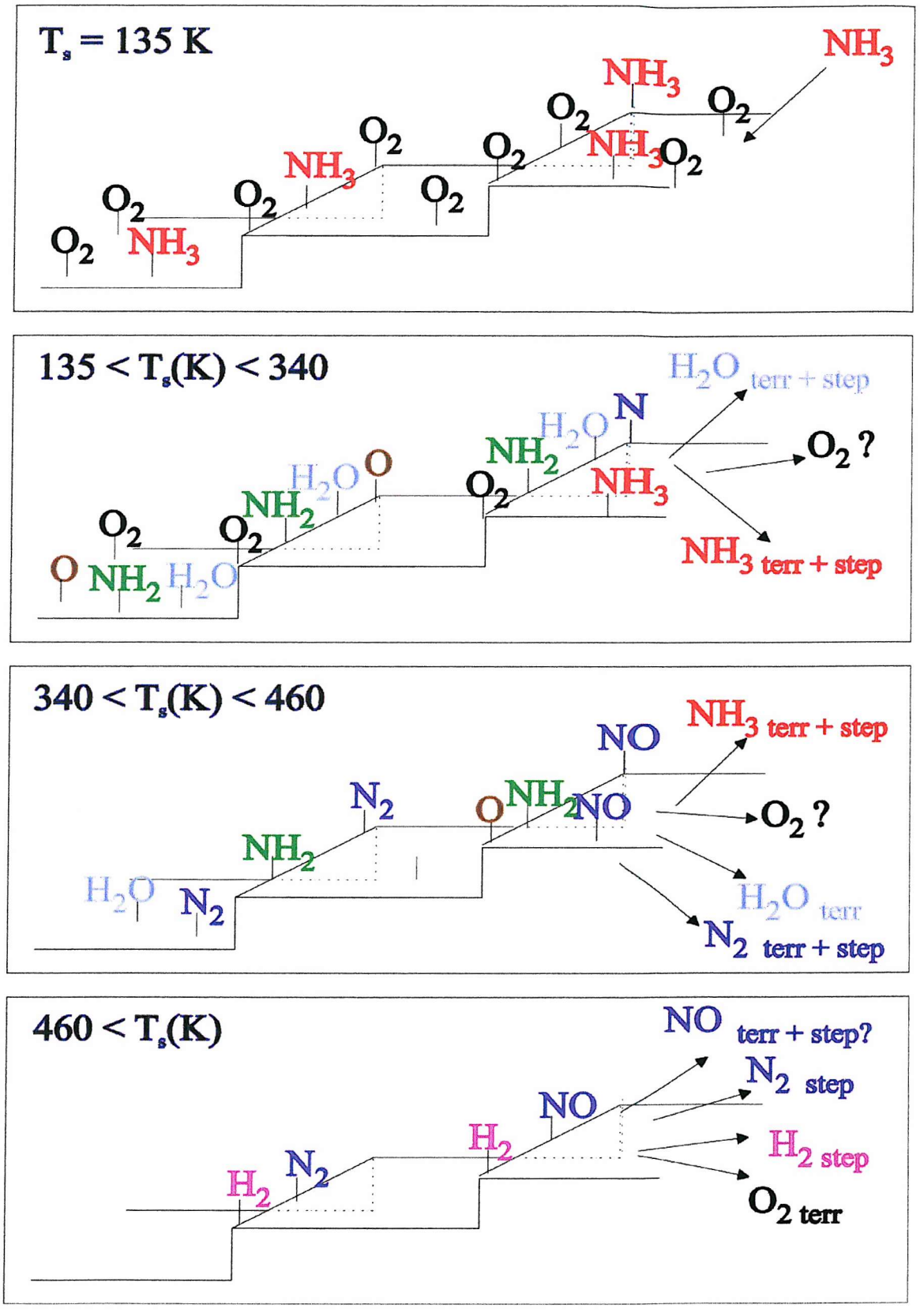

Figure VI.42a: Scheme of NH_3 adsorption and decomposition on a O_2 precovered Pt(533) surface with $\theta_{O2} < 0.12$ ML.

VI.3.14 King & Wells Method

From previous experiments it was concluded that dissociation of NH_3 occurs only at the (100) steps of the clean Pt(533) surface. The saturation of these steps by 0.12 ML O_2 does not block ammonia adsorption and dissociation at these steps, but enhance the decomposition of NH_3 by oxidation on the whole surface. Hence we decided to study the dissociative sticking probability of NH_3 on an oxygen-blocked Pt(533) surface and to compare it with $S(NH_3)$ on the clean Pt(533) surface (see **parts VI.3.4-VI.3.7**). These experiments were performed at $T_s = 400$ K because H_2 has been shown to desorb around 400 K, indicating that the initial decomposition of ammonia into NH_2 on the (100) steps has already taken place.

VI.3.15 Dependence of $S_0(NH_3)$ on Incident Energy

Notice that the previous series of TPD were performed by precovering the Pt(533) surface with O_2 at 135 K in order to adsorb molecularly on the surface, while the present experiments were performed by dosing O_2 at 400 K which leads to atomically adsorbed oxygen. No major difference was observed in the desorption signals of NO, N_2, NH_3 and H_2O on O_2 and O precovered Pt(111) surfaces [35], hence we assume that on O_2 and O precovered Pt(533) there should be no obvious difference either.
As seen in **part VI.3.5**, it was decided to study the initial dissociative sticking probability of NH_3 at 400 K

Figure VI.43 displays the $S_0(NH_3)$ as a function of beam energy for the O step-decorated Pt(533) surface at $T_s = 400$ K, with the beam at normal incidence to the crystal. The results of $S_0(NH_3)$ were measured in the energy range 274-809 meV. Beam energies were controlled by a combination of nozzle temperature and seeding.

The $S_0(NH_3)$ is higher on the precovered surface than on the clean surface, which is consistent with the enhancement in NH_3 dissociative adsorption by oxidation to form NH_2. The falling of $S_0(NH_3)$ with increasing E_i is similar to the trend on the clean surface, and is a sign of NH_3 trapping into a precursor state during the initial collision. Hence as E_i increases,

less molecules will be able to stay in the shallow precursor state potential before finding a proper site to dissociate, while more will go directly back to the gas phase.

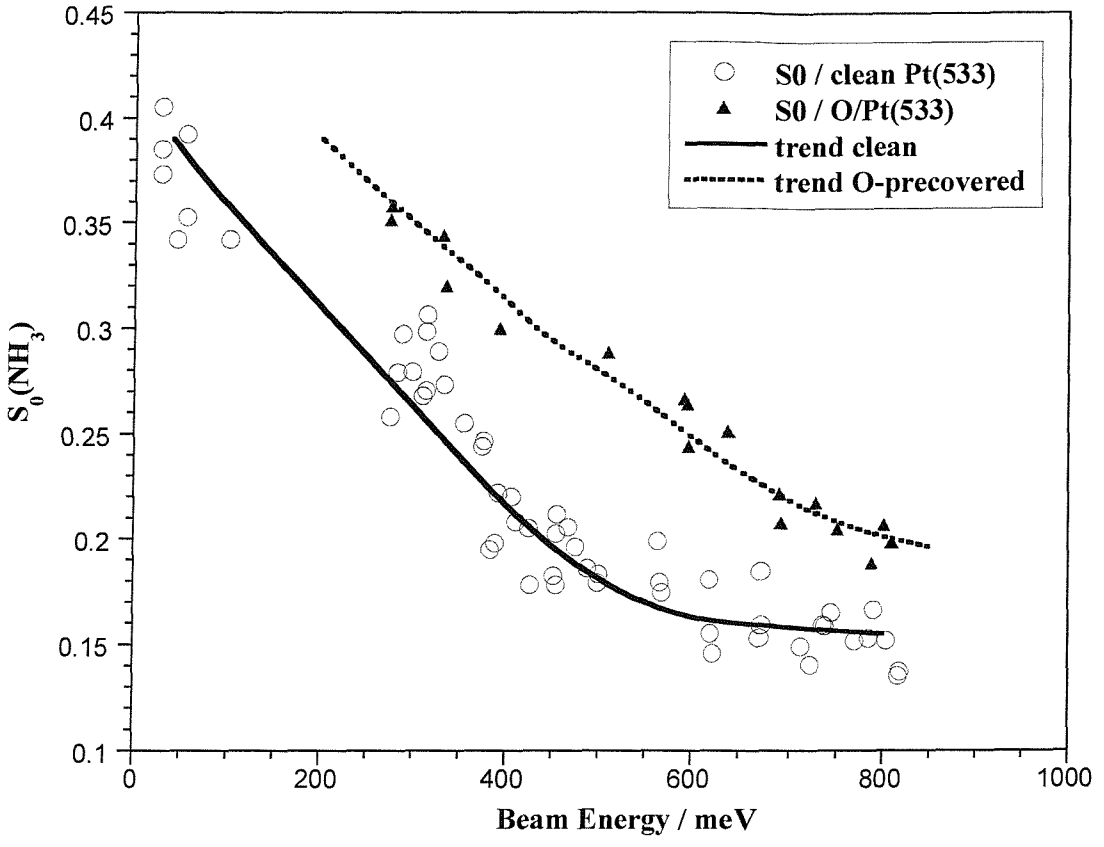

Figure VI.43: Initial sticking probability of ammonia on a clean and O-precovered Pt(533) surface, T_s = 400 K, Θ_I = 0°. The oxygen precoverage performed (0.12 ML) corresponds to the exact filling of the steps by O atoms. The lines of best fit of the sets of data are also shown.

The profiles of $S(NH_3)$ with the ammonia coverage on O/Pt(533) at T_s = 400 K (not shown here) are identical to the ones on the clean Pt(533) surface.

VI.4 CONCLUSION

Temperature programmed desorption measurements indicate that ammonia adsorption is molecular at $T_s < 400$ K and does not seem to depend strongly on the platinum surface plane. Ammonia can adsorb in multilayers, the first layer is made of one phase, α, of NH_3 molecules bound to the metal through the lone pair on the nitrogen, and a second phase, β, of molecules held with a hydrogen bond to the α ammonia. Desorption of ammonia from the (100) steps of Pt(533) appears on the TPD spectra as α' and β'

shoulders. The multilayers of NH_3 desorb around 120 K. Due to the poor resolution during the collection of these TPD spectra, the binding energy values for the α and α' phases contain a large inaccuracy, while the β and β' are in good agreement with the literature [27], at respectively 39 and 46 kJ mol^{-1}. The saturation coverage of ammonia is ~ 0.25 ML on Pt(111) [2] and is believed to be relatively similar on Pt(533).

Ammonia decomposition on Pt(533) was observed at $T_s > 360$ K evidenced by H_2 and N_2 productions, while on defect free Pt(111) NH_3 does not dissociate [12, 27]. N_2 and H_2 were produced on the (100) steps, N_2 desorbing at 530 K, and H_2 at 400 and 530 K. The coverages of atomic H and atomic N coming from NH_3 decomposition have been estimated to saturate around 0.03 and 0.01 ML, hence the coverage of NH_3 undergoing decomposition represents only ~ 4 % of the total amount of NH_3 adsorbed on the Pt(533) surface. The dissociation of NH_3 occurs in two steps:

At $T_s < 450$ K $\quad NH_3 \rightarrow NH_2 + H$ (17)

And for $460 < T_s(K) < 580$ $\quad NH_2 \rightarrow N + 2H$ (18)

The initial dissociative sticking probability of NH_3, $S_0(NH_3)$, has been measured in the energy range $27 < E_i(meV) < 825$, at $T_s = 400$ K a temperature at which ammonia decomposition has already taken place through the reaction: $NH_3 \rightarrow NH_2 + H$. The decrease of $S_0(NH_3)$ observed with increasing E_i is indicative of precursor mediated dissociation of NH_3. The decrease in $S(NH_3)$ as a function of coverage suggests that the blocking of the dissociation sites quickly enhances desorption of the precursor rather than dissociation. This is indicative of a very short precursor lifetime or a pre-exponential factor in the partition between dissociation and desorption largely in favour of desorption. The T_s dependence of $S_0(NH_3)$ indeed indicates that the activation energy for dissociative adsorption is very small ~ 5 kJ mol^{-1}, but the ratio of preexponential factors ν_{des}(desorption)/ν_{ca}(dissociative chemisorption) is strongly in favour of the desorption.

$S_0(NH_3)$ and TPD measurements have also been performed on oxygen and carbon monoxide decorated Pt(533) surfaces. $\theta_{CO} \sim 0.19$ ML or $\theta_{O2} \sim 0.12$ ML were found to correspond to the saturation of the (100) step sites. The NH_3, N_2 and H_2 TPD measurements on both precovered surfaces reveal that dissociation of ammonia is not blocked by the preadsorbed species. On O_2/Pt(533) surface the oxidation of NH_3 molecules on both (100)

steps and (111) terraces is established by the production of H_2, H_2O, N_2 and NO. On CO/Pt(533) the steric effect of CO slowly blocks the adsorption and decomposition of NH_3.

At 400 K, the $S_0(NH_3)$ measurements on the CO/Pt(533) surface show a similar trend with E_i as on the clean surface. However the values are slightly smaller for corresponding values of E_i showing that some of the ammonia adsorption step sites have been blocked by CO.

At 400 K, the oxygen is adsorbed dissociatively and the $S_0(NH_3)$ measurements on the O/Pt(533) surface show a similar trend with E_i as on the clean surface. However the values are slightly higher than on the clean surface for corresponding values of E_i illustrating the enhancement of NH_3 decomposition by oxygen.

The coverage dependencies of $S(NH_3)$ on both precovered surfaces are similar to that found on the clean surface.

VI.5 REFERENCES

[1] Garcia-Hernandez M., Lopez N., de P. R. Moreira I., Paniagua J. C., and Illas F., *Surf. Sci.*, 430: 18, **1999**.

[2] Fisher G. B., *Chem. Phys. Lett.*, 79: 3: 452, **1981**.

[3] Sexton B. A., and Mitchell G. E., *Surf. Sci.*, 99: 523, **1980**.

[4] Szulczewski G., and Levis R. J., *J. Chem. Phys.*, 103: 23: 10238, **1995**.

[5] Mocuta D., Ahner J., and Yates Jr. J. T., *Surf. Sci.*, 383: 299, **1997**.

[6] Klauber C., Alvey M. D., and Yates Jr. J. T., *Surf. Sci.*, 154: 139, **1985**.

[7] Madey T. E., Houston J. E., Seabury C. W., and Rhodin T. N., *J. Vac. Sci. Technol.*, 18: 2: 476, **1981**.

[8] Ceyer S. T., and Yates Jr. J. T., *Surf. Sci.*, 155: 584, **1985**.

[9] Dresser M. J., Lanzillotto A. M., Alvey M. D., and Yates Jr. J. T., *Surf. Sci.*, 191: 1, **1987**.

[10] Guthrie W. L., Sokol J. D., and Somorjai G. A., *Surf. Sci.*, 109: 390, **1981**.

[11] Löffler D. G., and Schmidt L. D., *Surf. Sci.*, 59: 195, **1976**.

[12] Blyholder G., and Sheets R. W., *J. Catal.*, 27: 301, **1972**.

[13] Papapolymerou G. and Bontozoglou V., *J. Molec. Catal. A. Chem.*, 120: 1-3: 165, **1997**.

[14] Somorjai G. A., *"Introduction to surface chemistry and catalysis"*. Wiley-Interscience Publication (New York), chap.7, p.445, **1994**.

[15] http://sis.bris.ac.uk/~cp9610/Project/

[16] Dahl S., Logadottir A., Egeberg R. C., Larsen J. H., Chorkendorff I., Törnqvist E., and Nørskov J. K., *Phys. Rev. Lett.*, 83: 9: 1814, **1999**.

[17] Fierro C., *J. Phys. Chem.*, 92: 4401, **1988**.

[18] Fierro C., and Gimarc B. M., "*molecular structure and bonding: the qualitative molecular orbital approach*" Academic Press, p. 43, **1979**.

[19] Jean Y., and Volatron F., "*Structure electronique des molecules*", Ediscience, International, v. II, p. 42, **1994**.

[20] Morrow B. A., and Cody I. D., *J. Catal.*, 45: 151, **1976**.

[21] Primet M., Basset J. M., Matthieu M. V., and Prettre M., *J. Catal.*, 29: 213, **1973**.

[22] Robertson A. J. B., and Willhoft E. M. A., *Trans. Faraday Soc.*, 63: 476, **1967**.

[23] Loffler D. J., and Schmidt L. D., *J. Catal.*, 41: 440, **1976**.

[24] Mummey M. J., and Schmidt L. D., *Surf. Sci.*, 91: 301, **1980**.

[25] Papapolymerou G. A., and Schmidt L. D., *Langmuir*, 1: 488, **1985**.

[26] Vajo J. J., Tsai W., and Weinberg W. H., *J. Phys. Chem.*, 89: 3243, **1985**.

[27] Gland J. L., and Kollin E. B., *Surf. Sci.*, 104: 478, **1981**.

[28] Gohndrone J. M, Olsen C. W., Backman A. L., Gow T. R., Yagasaki E., and Masel R. I., *J. Vac. Sci. Technol.*, 7: 1986, **1989**.

[29] Fahmi A., and Van Santen R. A., *Z. Phys. Chem.*, 197: 203, **1996**.

[30] Jennison D. R., Schultz P. A., and Sears M. P., *Surf. Sci.*, 368: 253, **1996**.

[31] Purtell R. J., Merrill R. P., Seabury C. W., and Rhodin T. N., *Phys. Rev. Lett.*, 44: 1279, **1980**.

[32] Ranney J. T., Franz A. J. and Gland J. L., *Surf. Sci. Lett.*, 384: L865, **1997**.

[33] Frechard F., Van Santen R. A., Siokou A., Niemantsverdriet J. W., and Hafner J., *J. Chem. Phys.*, 111: 17: 8124, **1999**.

[34] Gland J. L., *Surf. Sci.*, 71: 327, **1978**.

[35] Mieher W.D., and Ho W., *Surf. Sci.*, 322: 151, **1995**.

[36] Lee S. B., Kang D. H., Park C. Y., and Kwak H. T., *Bull. Korean Chem. Soc.*, 16: 2: 157, **1995**.

[37] Gland J. L., and Sexton B. A., *Surf. Sci.*, 94: 355, **1980**.

[38] Gland J. L., Korchak V. N., *J. Catal.*, 55: 324, **1978**.

[39] Gohndrone J. M., and Masel R. I., *Surf. Sci.*, 209: 44, **1989**.

[40] Alberas D. J., Kiss J., Liu Z.-M., and White J. M., *Surf. Sci.*, 278: 51, **1992**.

[41] Schwaha K. and Bechtold E., *Surf. Sci.*, 66: 383, **1977**.

[42] Solymosi F., and Kiss J., *Surf. Sci.*, 108: 641, **1981**.

[43] Tripa C.E., Zubkov T. S., Yates J. T. Jr., Mavrikakis M., and Norskov J. K., *J. Chem. Phys.*, 111: 8651, **1999**.

[44] Kiss J., and Solymosi F., *Surf. Sci.*, 135: 243, **1983**.

[45] Daniel W. M., and White J. M., *Surf. Sci.*, 171: 289, **1986**.

[46] Bozso F., Ertl G., Grunze M., and Weiss M., *J. Catal.*, 49: 18, **1977**.

[47] Van Hardeveld R., and Van Montfoort A., *Surf. Sci.*, 4: 396, **1966**.

[48] Shigeishi R. A., and King D. A., *Surf. Sci.*, 62: 379, **1977**.

[49] Arumainayagam C. R., Tripa C. E., Xu J. and Yates Jr. J. T., *Surf. Sci.*, 360: 121, **1996**.

[50] Bradley J. M., Hopkinson A., King D. A., *Surf. Sci.*, 371: 255, **1997**.

[51] Jones J.D., PhD. thesis, University of Southampton, p.10, **1994**.

[52] Rettner C. T. and Mullins C. B., *J. Chem. Phys.*, 94: 1626, **1991**.

[53] Takanoka T., and Kusunoki I., *Surf. Sci.*, 412/413: 30, **1998**.

[54] Taylor P. A., Wallace R. M., Choyke W. J., Dresser M. J., and Yates J. T. Jr, *Surf. Sci. Lett.*, 215: L286, **1989**.

[55] Zhou X. –L., Flores C. L., and White J. M., *Surf. Sci. Lett.*, 268: L267, **1992**.

[56] Masson D. P., Merrill R. P. and Houston P. L., *Surf. Sci.*, 330: 239, **1995**.

[57] Wang H., Tobin R. G., and Lambert D. K., *J. Chem. Phys.*, 101: 5: 4277, **1994**.

[58] Hayden B.E., Kretzschmar K., Bradshaw A. M., and Greenler R.G., *Surf. Sci.*, 149: 394, **1985**.

[59] Luo J. S., Tobin R. G., Lambert D. K., Fisher G. B., and DiMaggio C. L., *Surf. Sci.*, 274: 53, **1992**.

[60] Hammer B., Nielsen O. H., and Norskov J. K., *Catal. Lett.*, 46: 31, **1997**.

[61] Lanzillotto A. M., Dresser M. J., Alvey M. D., and Yates J. T. Jr., *Surf. Sci.*, 191: 15, **1987**.

[62] Tochihara H., Rocker G., Redding J. D., Yates J. T. Jr., Martin R. M., and Metiu H., *Surf. Sci.*, 176: 1, **1986**.

[63] Sasaki T., Aruga T., Kuroda H., and Iwasawa Y., *Surf. Sci.*, 240: 223, **1990**.

[64] Rosenzweig Z., Asscher M., and Wittenzellner C., *Surf. Sci. Lett.*, 240: L583, **1990**.

[65] Mortensen K., Klink C., Jensen F., Besenbacher F., and Stensgaard I., *Surf. Sci. Lett.*, 220: L701, **1989**.

[66] Norton P. R., Davies J. A., and Jackman T. E., *Surf. Sci. Lett.*, 122: L593, **1982**.

[67] Puglia C., Nilsson A., Hernnäs B., Karis O., Bennich P., and Mårtensson N., *Surf. Sci.*, 342: 119, **1995**.

[68] Björneholm O., Nilsson A., Tillborg H., Bennich P., Sandell A., Hernnäs B., Puglia C., and Mårtensson N., *Surf. Sci. Lett.*, 315: L983, **1994**.

[69] Materer N., Starke U., Barbieri A., Döll R., Heinz K., Van Hove M. A., and Somorjai G. A., *Surf. Sci.*, 325: 207, **1995**.

[70] Gland J. L., Sexton B. A., and Fisher G. B., *Surf. Sci.*, 95: 587, **1980**.

[71] Guo X.-C., Bradley J. M., Hopkinson A., and King D. A., *Surf. Sci.*, 310: 163, **1994**.

[72] Bradley J. M., Guo X.-C., Hopkinson A., and King D. A., *J. Chem. Phys.*, 104: 11: 4283, **1996**.

[73] Wang H., Tobin R. G., Lambert D. K., DiMaggio C. L., and Fisher G. B., *Surf. Sci.*, 372: 267, **1997**.

[74] Gee A. T., Hayden B. E., *J. Chem. Phys.*, 113: 22: 10333, **2000**.

[75] Feibelman P. J., Esch S., and Michely T., *Phys. Rev. Lett.*, 77: 2257, **1996**.

[76] Steininger H., Lehwald S., and Ibach H., *Surf. Sci.*, 123: 1, **1982**.

[77] Reed A.P.C. and Lambert R.M., *J. Phys. Chem.*, 88: 1954, **1984**.

[78] Fisher G. B., and Gland J. L., *Surf. Sci.*, 94: 446, **1980**.

[79] Skelton D. C., Tobin R. G., Fisher G. B., Lambert D. K., and DiMaggio C. L., *J. Phys. Chem. B*, 104: 548, **2000**.

[80] Stuve E. M., Jorgensen S. W. and Madix R. J., *Surf. Sci.*, 146:179, **1984**.

[81] Netzer F. P. and Madey T. E., *Surf. Sci. Lett.*, 127: L102, **1983**.

[82] Madey T. E. and Netzer F. P., *Surf. Sci.*, 117: 549, **1982**.

[83] Doering D. L. and Madey T. E., *Surf. Sci.*, 123: 305, **1982**.

[84] Bange K., Grider D. E., Madey T. E. and Sass J. K., *Surf. Sci.*, 136: 38, **1984**.

[85] Kiss J. and Solymosi F., *Surf. Sci.*, 177: 191, **1986**.

[86] Bange K., Madey T. E., Sass J. K. and Stuve E. M, *Surf. Sci.*, 183: 334, **1987**.

[87] Gorte R., Schmidt L. D., and Gland J. L., *Surf. Sci.*, 109:367, **1981**.

[88] Campbell C. T., Ertl G., and Segner J., *Surf. Sci.*, 115: 309, **1982**.

CHAPTER VII: DYNAMICS AND KINETICS OF DISSOCIATIVE ADSORPTION OF HYDROGEN ON A POLYCRYSTALLINE URANIUM SURFACE

VII.1 INTRODUCTION

Uranium (U) is about 500 times more abundant than gold and about as common as tin, it is present in most rocks and soils as well as in many rivers and in sea water. U was discovered by Martin Klaproth in 1789 after he succeeded in extracting its oxide from pitchblende. Uranium metal itself was first isolated in 1841 by Eugene-Melchoir Peligot, who reduced the anhydrous chloride (UCl_4) with potassium. Uranium is the last and heaviest naturally occurring element present on earth with an atomic weight of 238.089 g mol^{-1} [1].

Uranium is part of the actinide group, characterised by their radioactivity. The radioactive nature of uranium was detected in 1896 by Henri Becquerel [2], who found that U is weakly radioactive, decaying slowly but inexorably at the rate of one milligram per tonne per year (U has a half-life time of 4.46×10^9 years, more than the life of the Earth, which explains why there is "so much" left). It is transformed into inactive lead through a chain of radioelements or daughters (see **figure VII.1**).

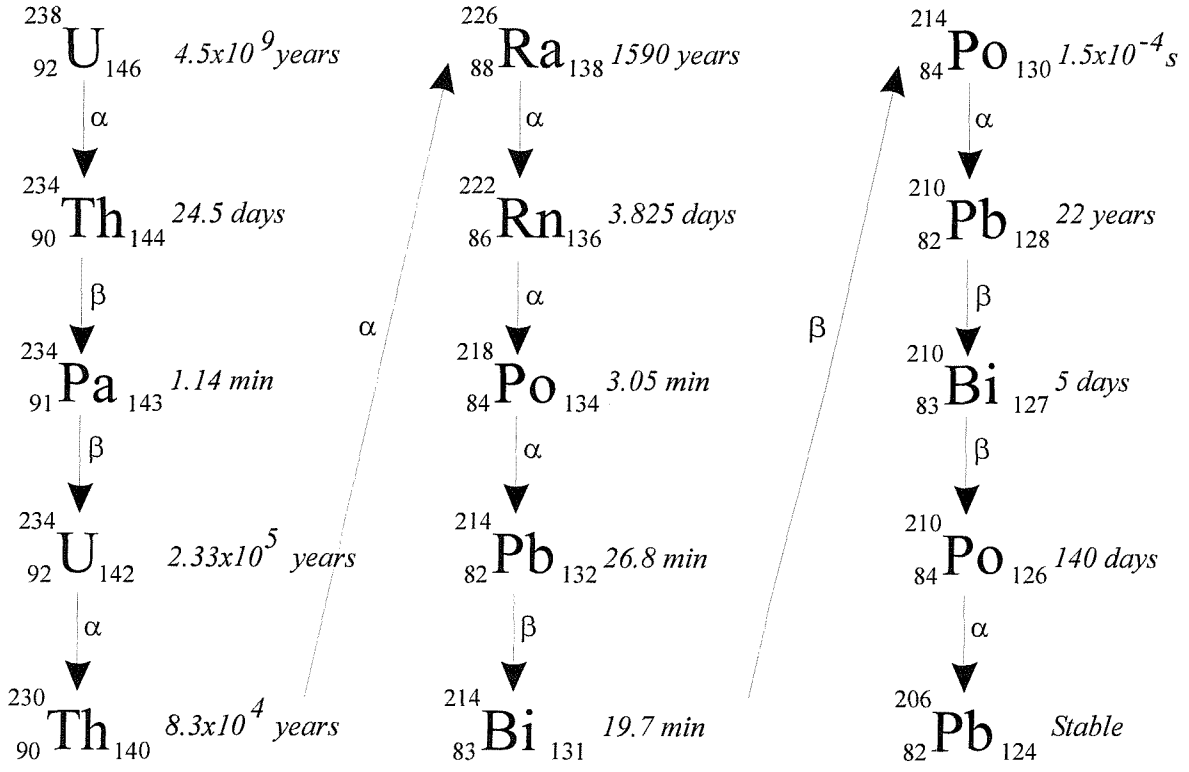

Figure VII.1: Chain of radioelements from ^{238}U to ^{206}Pb and their respective half-life time.

For many years, uranium was used primarily as a colorant for ceramic glazes and as uranium nitrate for tinting in early photography. Nowadays uranium is of great interest because of its numerous uses, such as an X-ray target for production of high-energy X-rays, for the synthesis of its isotopes used for medical, industrial, and defence purposes around the world, and for conversion into plutonium in "breeder" reactors to produce electricity [1, 3]. The most important use is its application to nuclear power as a fuel – the U atom is broken into two when attacked by a neutron. This phenomenon, called fission, releases a lot of energy in the form of heat, and occurs because of the electrostatic repulsion created by the large number of positively charged protons contained in this heavy nucleus. During this fission, two or three additional neutrons are thrown off, and if enough of these expelled neutrons split the nuclei of other U atoms releasing further neutrons, a "chain reaction" can be achieved [4]. Only ^{235}U experiences fission, ^{238}U has the same physical and chemical properties but not the same nuclear ones. Hence due to the weak concentration of ^{235}U in naturally occurring U (0.7 %), a process of enrichment is performed which produces a higher ^{235}U concentration of typically between 3.5 and 4.5 %. This leads to a more efficient fuel for the nuclear reactors [1]. Nuclear power stations produce electricity without emitting

greenhouse gases such as carbon dioxide, thus limiting global warming. The second main application of U is in nuclear weapons as an explosive.

In research most of the studies have been done on depleted uranium, DU. DU consists almost completely of ^{238}U, it is a by-product of U enrichment.

VII.1.1 Oxygen/Uranium and Hydrogen/Uranium Interactions

Chemically, U is highly reactive, oxidising readily in air at relatively low temperatures; the oxides produced (*e.g.* UO_2 and U_3O_8) can continue to react with any water vapour present to produce more oxide, uranium hydride and hydrogen gas [1].

In enclosed volumes, free hydrogen gas can also react, even at room temperature [5], with uranium metal to form large quantities of pyrophoric hydride UH_3 due to the extremely high diffusivity of hydrogen in the metal. The hydride film is non-adherent which means that it does not stay continuous and unfractured during the course of the reaction. In fact the film starts to crack when its thickness exceeds a critical value [6].

The sequence of steps leading to the formation of metal hydrides is very complex, consisting of [6]:

(1) Surface processes: adsorption, chemisorption, surface diffusion, sub-surface penetration,
(2) Transport processes (in surface overlayer, through the bulk, through the hydride film) controlled by bulk diffusion or grain boundaries diffusion,
(3) Nucleation of the hydride phase,
(4) Interface processes occurring at the hydride-metal boundaries: phase transformations.

These processes can evolve during the reaction and change its rate depending on the alterations in the surface cleanliness of the uranium and the purity of the hydrogen. Even small amounts of oxygen impurity [7], or surface oxide [8] extend the induction time (the mean time interval between the initiation of successive reaction sites). In fact, the hydride powder is often coated with an oxide layer that can prevent its spontaneous combustion. But if the oxide layer is disturbed, such as can occur during fuel handling, the hydride will glow

and spark, and possibly ignite the surrounding uranium metal, leading to the release of the radioactivity in the spent fuel element [9].
Consequently, the uranium/hydrogen and uranium/oxygen systems have been of great interest, particularly from a kinetic point of view.

Under ultra high vacuum conditions, there is little previous work in the field of surface dynamics on uranium single crystal surfaces; the majority concerns polycrystalline uranium and oxidised surfaces. Balooch *et al.* have used molecular beam techniques to investigate the interaction of hydrogen and water vapour with clean and partially oxidised U surfaces [10], and also on platinum clusters deposited on uranium films [11]. Mintz *et al.* [12, 13, 14] and Moreno *et al.* [15] have studied the hydride nucleation and growth kinetics dependencies on temperature, pressure and microstructure, on clean and oxidised surfaces using hot stage microscopy, as well as the interaction of H_2 and H_2O using TPD [14]. Swissa *et al.* [16], Muggelberg *et al.* [17] and Allen *et al.* [18] respectively used direct recoil spectroscopy (DRS), STM and XPS to study the interactions of hydrogen and oxygen on U.

Mintz *et al.* observed four different 'families' of hydride nuclei, differing in size, density, and growth rate [13]. The type of nucleation was found to be site dependent, being influenced by the presence of scratches on the pure metal, defect sites in the oxide layer, carbide inclusions in the oxide layer, and unspecified discontinuities in a thicker oxide layer.

In an attempt to clarify the mechanism taking place in the hydrogen-uranium reaction, as well as the influence of an oxide layer on the hydrogen adsorption, the present work will be to investigate the interaction of hydrogen with a polycrystalline uranium surface using TPD and XPS techniques. These techniques only permit a study of the very initial interactions occurring on the uppermost atomic layers (1 to 4 layers wide), thus it will not give any information on bulk diffusion (note that Hayden *et al.* are currently investigating permeation processes for the hydrogen/uranium system). Our second aim will be to quantify the initial dissociative sticking coefficient, S_0, of hydrogen, oxygen and water on polycrystalline uranium by using supersonic molecular beam techniques.

VII.2 EXPERIMENTAL

All the experiments are carried out in an Ultra High Vacuum chamber described in **chapter II.**

The U sample available for these experiments, supplied by the Atomic Weapons Establishment (AWE), was a depleted U sample largely carbon free. It is highly oxidised at the surface, as indicated by its dark colour, most likely due to UO_2 (black-brown), U_3O_8 (dark green) and U_4O_9 (black). Thus the first aim was to observe the progression of its cleanliness up to relatively oxygen-free U metal (metallic grey coloured), by analysing some hydrogen TPD spectra and XPS spectra from the U surface. For this purpose, the surface was cleaned by numerous 60 min argon-bombardment with 1 to 3 keV ions ($\Theta_I = 20°$ from normal incidence) at room temperature and at 675 K. Initially each sputter was followed by 30 to 45 min annealing at 825 K. This temperature is probably insufficient to reform the surface after sputtering, however this does not seem to affect the results since the sample is polycrystalline (*i.e.* rich in defects). Some TPD and XPS experiments were then performed, with a 10 min annealing completed after each experiment (to desorb any hydrogen adsorbed), however after 5-7 experiments the surface seemed too contaminated to go further and sputtering was a necessity.

Note that several obstacles had to be overcome prior to obtaining some data (**chapter II**), in particular the mounting of the thermocouple. In fact due to the thickness of the first samples studied, the spot-welding of the thermocouple was not successful, hence it was decided to wedge it in a small piece of molybdenum foil spot-welded onto the back of the crystal. Therefore the temperature measured by the thermocouple did not correspond to the exact temperature of the sample and a noticeable error was obtained increasing as T_s increases above or decreases under 300 K. Later measurements were performed on thinner and smaller U sample for which the thermocouple was directly spot-welded on to the metal, and gave relatively good agreement with the original data.

Uranium is known to exist in several phases, depending on its temperature and pressure (**figure VII.2**). The phase of interest in our investigation (because of its existence at room temperature and ambient pressure), named α, is known to evolve into the β phase

under atmospheric pressure at a temperature of 935 K thus it was more by care that the anneal was limited to 825 K under UHV. The high temperature phase is the γ-phase (body-centered cubic), stable from 1045 to 1405 K, and the β-phase (tetragonal), the intermediate stage, is stable from 935 to 1045 K, both under atmospheric pressure.

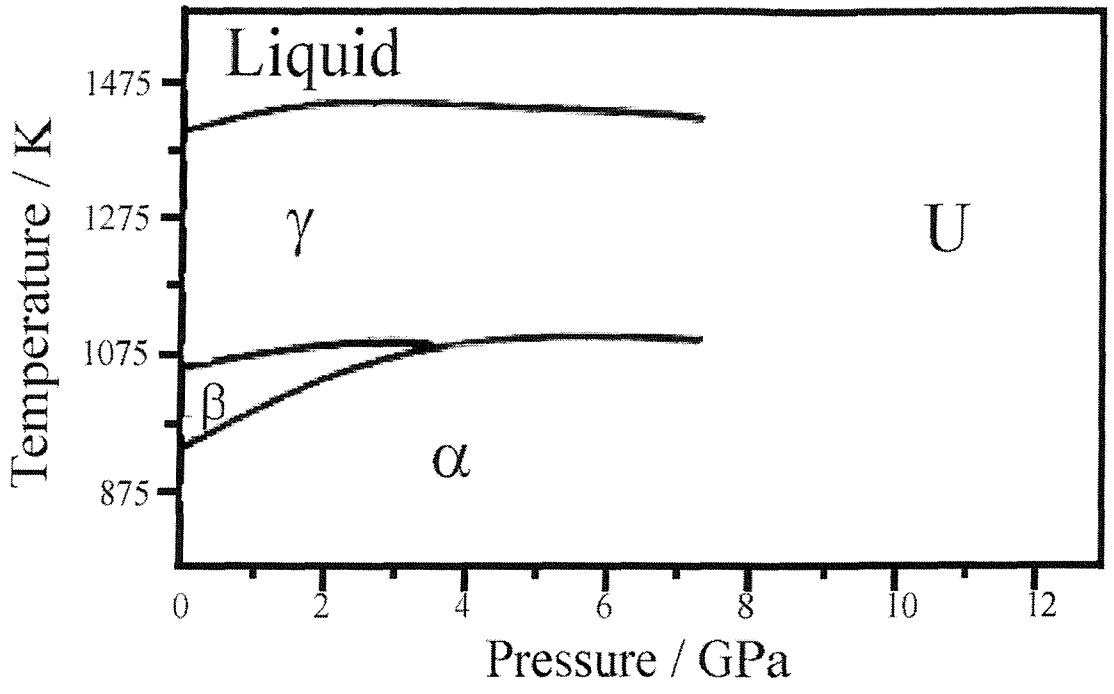

Figure VII.2: Phase diagram of uranium as a function of temperature and pressure from Lander's data, based on Benedict 's results (1985) [19].

The properties of α-uranium have been extensively studied and there exists an abundance of data concerning reaction kinetics [19]. In 1937 Jacob and Warren solved the atomic structure of the U α-phase, which was found to be the most unusual one, being orthorhombic (with parameters a = 285.37 pm, b = 586.95 pm and c = 495.48 pm, with all angles at 90°).

VII.3 RESULTS AND DISCUSSION

VII.3.1 Hydrogen Temperature Programmed Desorption

Using a molecular beam, a pure flow of hydrogen was dosed on to a uranium polycrystalline surface at different stages of cleanliness. Series of thermal desorption

spectra, corresponding to various hydrogen exposures, are reproduced in **figures VII.3** to **VII.5**. The dosing was carried out at T_s = 160 K using a 1.3 mm aperture, with the nozzle at room temperature thus the incident energy of the H_2 molecules is E_i ~66 meV.

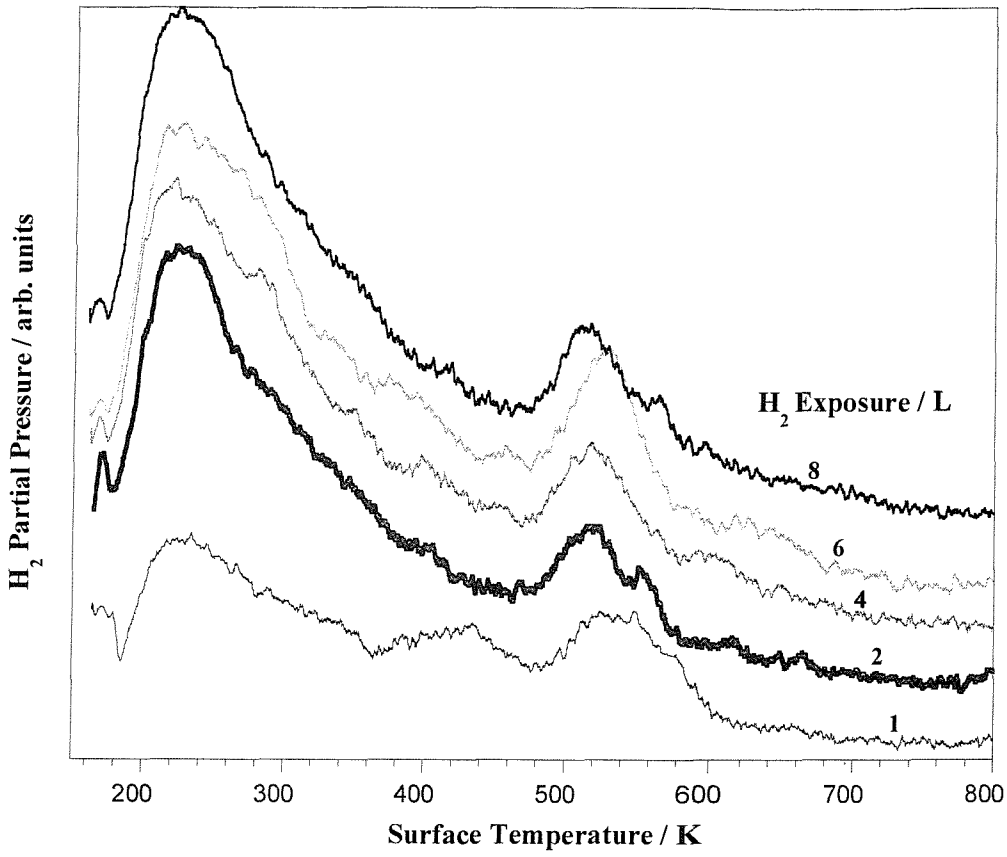

Figure VII.3: TPD of H_2 following exposure of polycrystalline U to a pure H_2 beam. T_s = 160 K, T_n = 300 K and E_i = 66 meV. The heating rate was 2 K s^{-1}. After 3 days of cleaning. The exposures are shown in Langmuir.

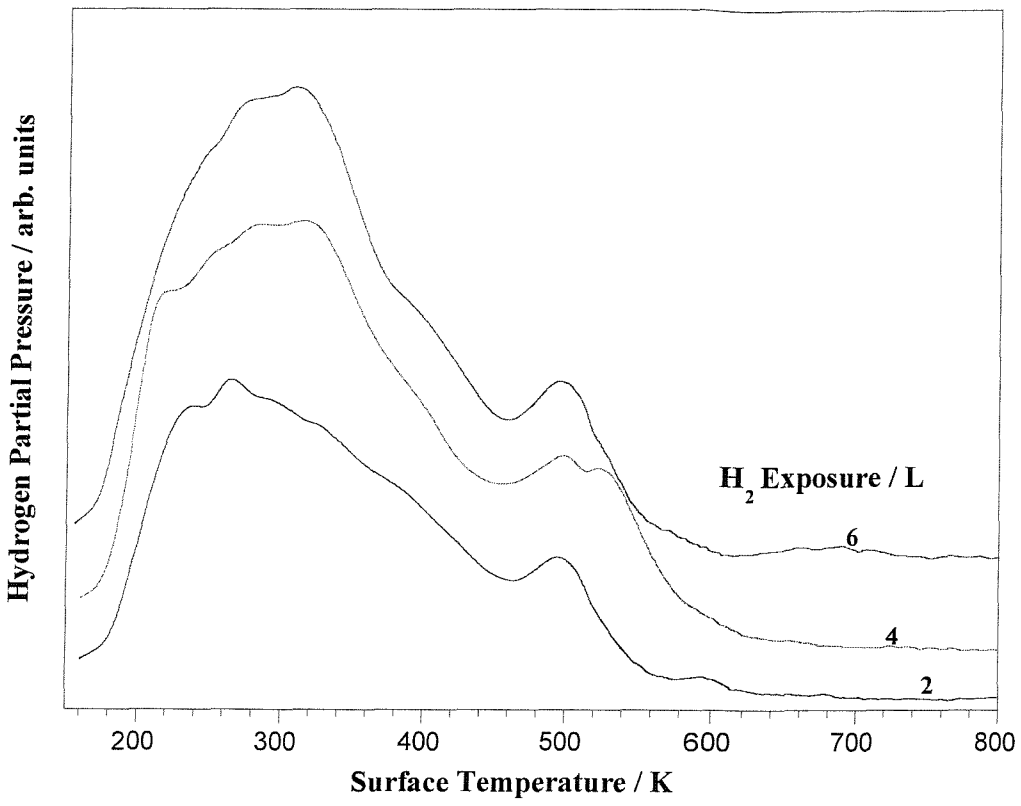

Figure VII.4: TPD of H_2 following exposure of polycrystalline U to a pure H_2 beam. T_s = 160 K, T_n = 300 K and E_i = 66 meV. The heating rate was 2 K s^{-1}. After 5 days of cleaning. The exposures are shown in Langmuir.

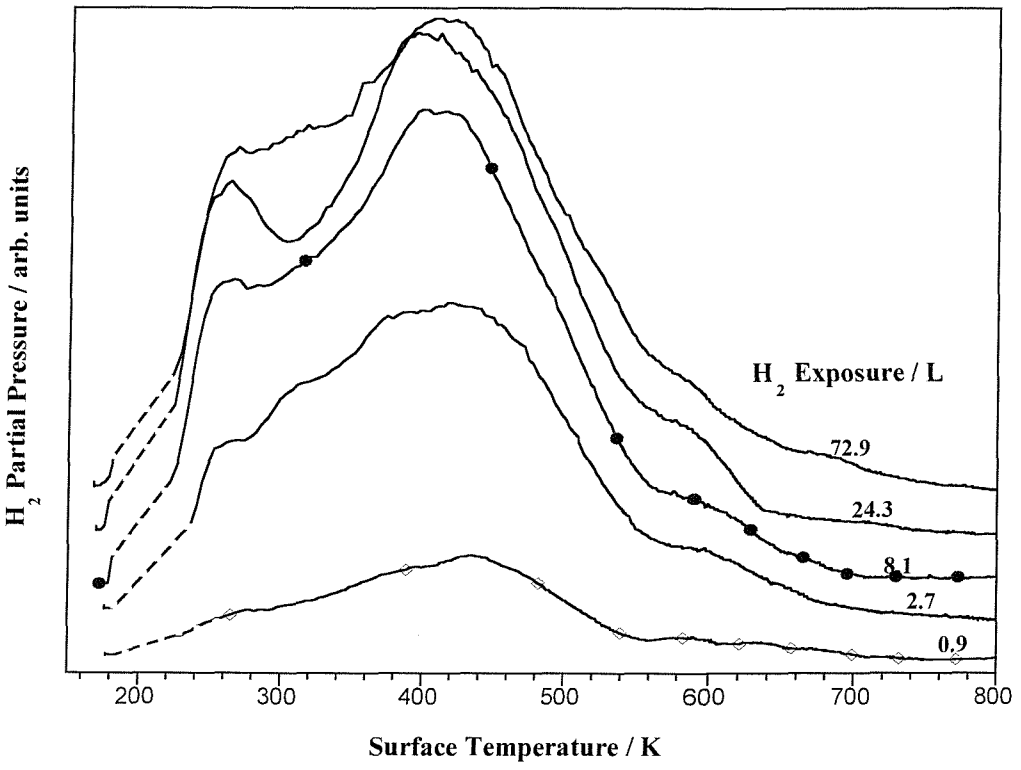

Figure VII.5: TPD of H_2 following exposure of polycrystalline U to a pure H_2 beam. T_s = 170 K, T_n = 300 K and E_i = 66 meV. The heating rate was 5-6 K s^{-1}. After 45 days of cleaning. The exposures are shown in Langmuir.

Because of the polycrystalline nature of the uranium surface, many different type and strength of bonds may exist between the hydrogen atom/molecule and the U/U_xO_y surface. Thus, it is expected to observe some large features (as opposed to well-defined peaks) in the TPD spectra.

Three main features are observed, with the possibility of two others being present.

In **figure VII.3** there is a peak observed around 500-600 K which corresponds to hydrogen desorbing from a highly oxidised surface. This feature is still present after 5 days of cleaning (**figure VII.4**) but seems to have disappeared after 45 days of cleaning (**figure VII.5**). In fact, as seen in **figure VII.6**, Balooch and Hamza [10] did not observe this feature on a clean uranium sample surface. Hence we conclude that it corresponds to hydrogen desorbing from the oxide layer and that an intensive sputtering/annealing treatment of the present surface led to remove the oxide layer originally present on the U sample.

The second feature on the oxidised surface (**figure VII.3**) is observed around 220-270 K. Intensive cleaning does not seem to remove this feature which ruled out the idea of it being related to hydrogen desorption from the oxide layer but might be related to hydroxide formation or H_2 desorbing after atomic absorption into the sample bulk or at the metal-oxide interface.

Figures VII.4 and **VII.5** highlight a third peak around 300-350 K. This peak is believed to be present for hydrogen desorbing from a highly oxidised surface too in **figure VII.3**, however it might be overlapped by the main feature at 220-270 K. Several studies have already been performed concerning the oxide growth using water on clean U samples, and it has been suggested that it requires the cleavage of one H (or D) atom from the H_2O (or D_2O) molecule. The resulting OH (or OD) diffuses through the oxide layer to the metal-oxide interface by an interstitial mechanism where the migrating ion OH^- displaces a lattice anion into an adjacent interstitial site and finally occupies the site of the displaced ion or occupies a vacant anion site [20-23]. The OH species have also been evidenced by Manner *et al.* [24] from the combined information of XPS and SSIMS data after dosing H_2O on a U-Nb alloy. Moreover they observed that as high as 300-350 K there still appears to be a small contribution from hydroxyls on the surface. Hence it seems

reasonable to suggest the formation of OH groups on the present U giving rise to H_2 desorption under 350 K.

Hence we propose that the 300-350 K peak corresponds to recombinative desorption of hydrogen coming from OH adsorbed groups on the metal. Therefore it does not appear clearly on a highly oxidised surface, but it is visibly present on a poorly oxidised surface in **figure VII.4**.

The 220-270 K peak might also correspond to OH species formed on the surface, however we propose here two more likely explanations for this feature. On a highly oxidised U surface, the main type of oxide formed, namely uranium dioxide, does not act as a seal. In fact, this top-layer often cracks due to grain boundaries, discontinuities in the metal structure and inclusions (like carbon atoms) and therefore provides passages to the underlying uranium which could be under appreciable amount of local stress. These are favourite sites for dissociation of incoming H_2 [13]. Thus with or without an oxide layer, the hydrogen atoms could reach the uranium metal and react with it. Then as the surface is heated they recombine and desorb in H_2 gas. In this case, it seems natural not to have any major change in the shape of the TPD peak as the surface gets cleaner.

The second hypothesis would be that after having reached the U metal, the H atoms diffuse into the bulk, which would lead to the same conclusion as before. However, in this case it seems unlikely that the saturation of the bulk can be reached in a sensible time of dose. Dosing H_2 for a very long time would evidence which of these hypothesis is more realistic, however due to the rapid contamination of the surface under the present experimental conditions this experiment was impossible to perform.

The existence of subsurface hydrogen on transition-metal surfaces has already been postulated for hydrogen on Cu and Ru [25-28], but there are still few experimental data to confirm it. Comsa and David [29] evidenced subsurface H atoms for the H_2/Cu(100) system, while Rieder *et al.* evidenced them for H_2/Cu(110) [30] however this last study was contested by Hayden *et al.* who did not find any support for H subsurface species on Cu(110) [31]. Experimental evidence of subsurface species for the H_2/Ru(0001) system was obtained by Behm *et al.* [32]. These results tend to confirm our hypothesis.

In **figureVII.5** both these peaks seem to decrease in intensity in favour of a new peak around 400-430 K. This is consistant with Balooch's results and is associated with recombinative hydrogen desorption of H atoms adsorbed on clean U metal. The peak temperature decreases from 450 to 410 K as the coverage increases in Balooch and Hamza data [10], which led them to conclude in the presence of a second order desorption process. Due to the complexity of the present TPD features, we could not establish the order of the desorption process.

In summary:

- the 220-270 K peak more likely corresponds to subsurface H atoms
- the 300-350 K peak corresponds to OH species formed on the metal surface
- the 400-430 K corresponds to hydrogen adsorbed and desorbing from the clean U metal
- the 500-600 K peak is associated with H_2 species desorbing from the oxide layer

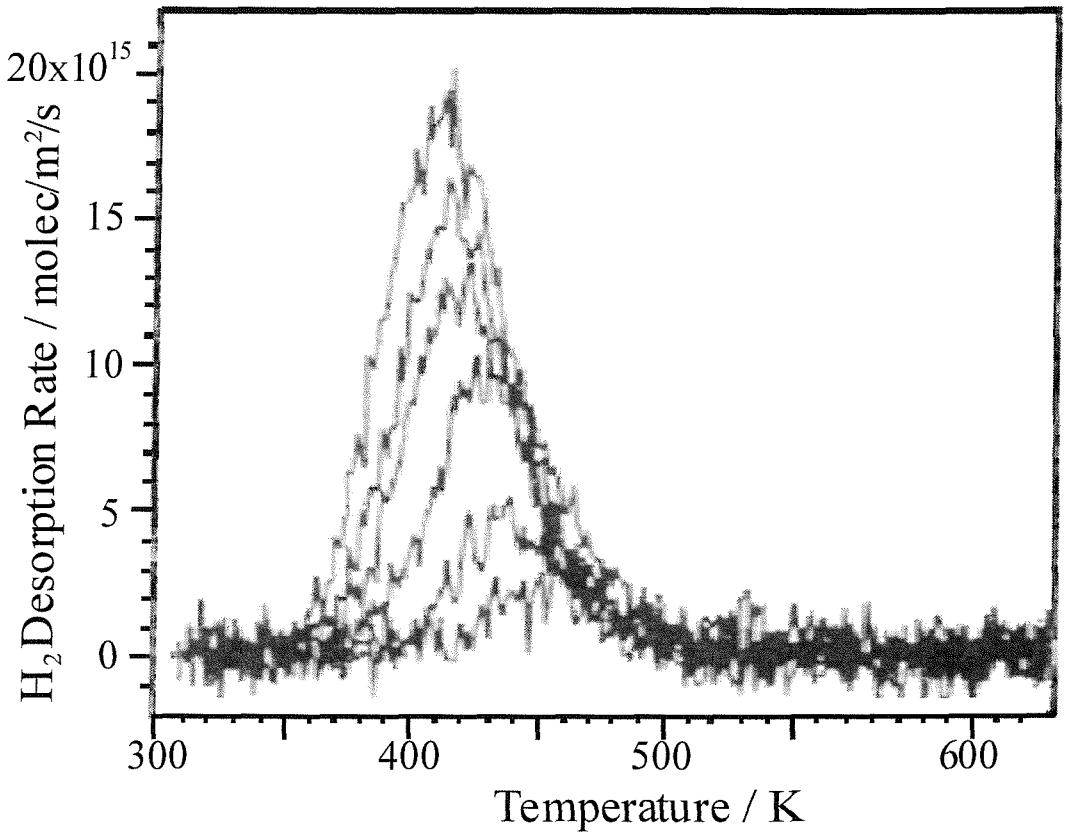

Figure VII.6: Reproduction of H_2 TPD from clean U after exposure to H_2 at room temperature from Balooch data [10]. The coverages were determined by integrating the desorption flux and the heating rate was 3 K s^{-1}.

VII.3.2 XPS Measurements

XPS measurements have been performed using Al $K\alpha$ radiation (the XPS technique and the specificities required for the present analysis are detailed in **chapter III**).

Figure VII.7 depicts a wide scan spectrum of an oxidised uranium surface performed at $T_s = 200$ K. A series of peaks are observed on a background which generally increases to lower kinetic energy (high binding energy) but which also shows step-like increases on the low kinetic energy side of each significant peak. The present peaks can be grouped into three basic types: ones due to photo-emission from core levels and valence levels and others due to X-ray excited Auger emission. The doublets (U4$d_{3/2}$, U4$d_{5/2}$), (U4$f_{7/2}$, U4$f_{5/2}$) and (U5$d_{3/2}$, U5$d_{5/2}$) arise through spin-orbit **(j-j)** coupling. There is no (L-S) coupling for uranium, as it has been found to apply only to elements of low atomic number (i.e. $Z < \sim 20$). The relative intensity of core-level peaks is proportional to the atomic photo-emission cross-section, σ_{ax}, which depends on the energy level (K, L, M) ionised by an electron and his incident beam energy $\mathbf{E_{kin}}$, as well as $\mathbf{E_B}$ the energy of the XPS electrons fom level X of element A in matrix M [33]. The peak width depends on the natural width of the core level, the width of the X-ray line and the analyser resolution [34].

The core levels observed in **figures VII.7** and **VII.8** are listed in **Table VII.1** together with data from Allen *et al.* [18] and Wagner *et al.* [35].

Table VII.1: Core-level energies for uranium, uranium dioxide and oxygen (in eV).

	Uranium Oxide							Oxygen on U_xO_y	
	5$d_{5/2}$	5$d_{3/2}$	4$f_{7/2}$	4$f_{5/2}$	4$d_{5/2}$	4$d_{3/2}$	4$p_{3/2}$	1s	Auger
[19]	96.6	104.6	380.2	391.2	738.4	781.3	1045.5		
[35]	96.0	104.0	380.0	391.0	739.0	781.0	1046.0	531.0	976.0
This work	96.0	104.3	380.5	391.0	739.4	779.6	1044.0	529.7	973.7
Uranium									
[19]	94.2	102.8	377.4	388.2	736.2	778.3	1043.0		
This work			378.0	388.5					

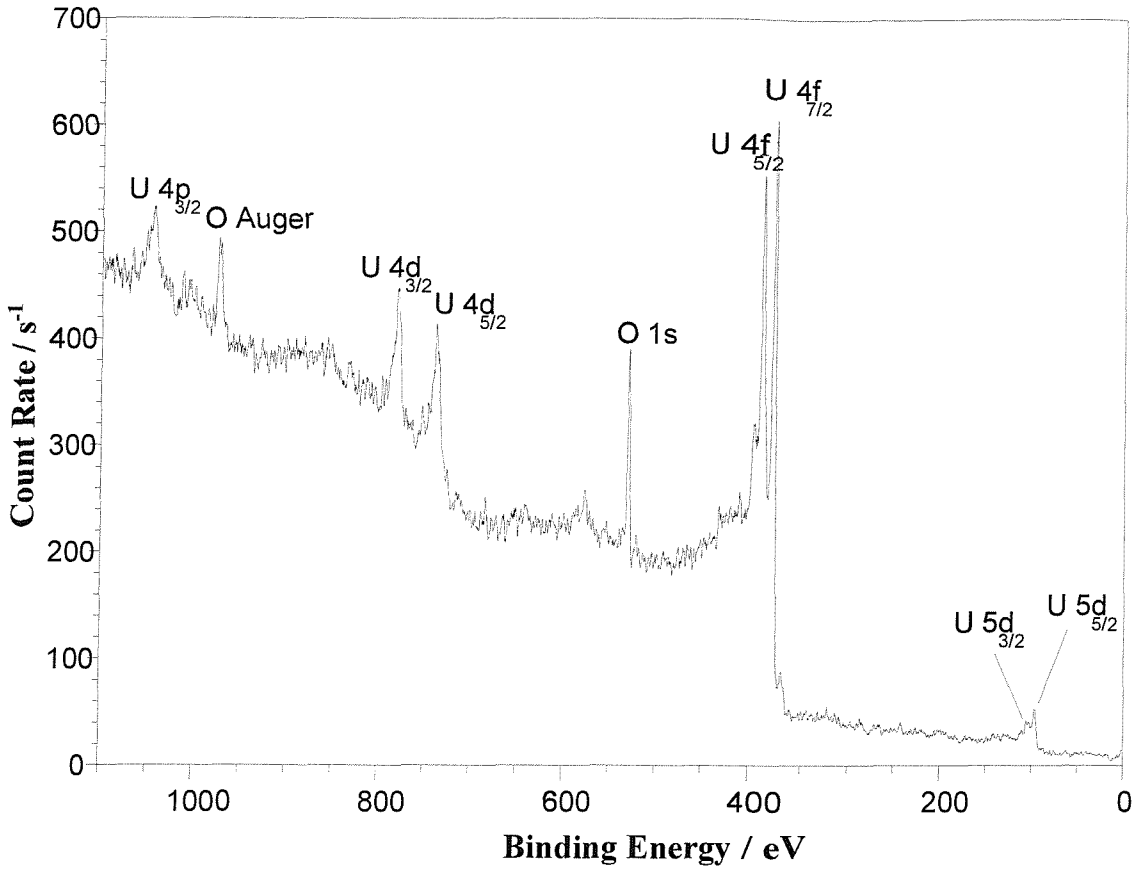

Figure VII.7: X-ray photo-electron spectrum of oxidised uranium excited by Al $K\alpha$. $T_s = 200$ K.

The most intense energy lines are the most suitable in identifying chemical states. **Figure VII.8** confirms the oxide layer on the surface, evidenced by the core level bands $U_{4f(7/2)}$ and $U_{4f(5/2)}$ respectively at 380.5 ± 0.5 and 391.0 ± 0.5 eV. Subsequent cleanings of the surface (mainly sputtering with an argon ion gun) lead to the emergence of the U metal bands at 378.0 and 388.5 eV.

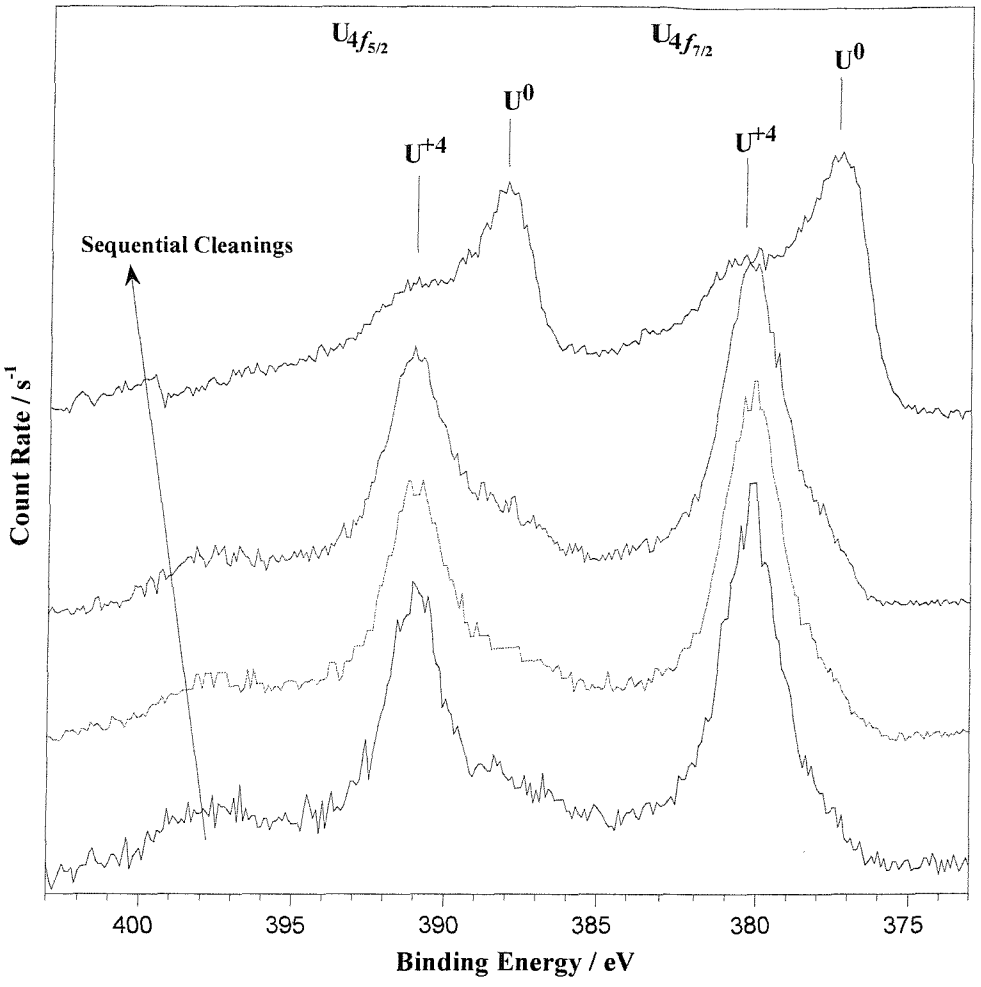

Figure VII.8: X-ray photo-electron spectra of the U 4*f* doublet following sequential cleanings. $T_s = 200$ K.

These results are in complete agreement with Manner *et al.* [36] and Swissa *et al.* data [16, 37]. Moreover Allen *et al.* [18] performed a detailed study of U metal and UO_2 using XPS. They measured the binding energies for core and valence electrons in both U and UO_2. **Table VII.2** presents a comparison between Allen *et al.* results [18], as well as Fuggle *et al.* [38] and the present ones, only for the $4f_{5/2}$ and $4f_{7/2}$ levels of U metal. **Table VII.3** compares the previous authors data and ours for the energies of these levels for uranium oxide.

Table VII.2: Core-level energies for uranium metal (in eV)

Level	Present data	Allen *et al.* [18]	Fuggle *et al.* [38]
$4f_{5/2}$	388.5	388.1(0.1)	388.2(0.1)
$4f_{7/2}$	377.5(0.2)	377.2(0.1)	377.4(0.1)

Table VII.3: Core-level energies for uranium dioxide (in eV).

Level	Present data	Allen *et al.* [18]	Allen *et al.* [39]
$4f_{5/2}$	391.0(0.5)	391.2(0.1)	391.1(0.2)
$4f_{7/2}$	380.5(0.5)	380.2(0.1)	380.3(0.3)

Notice that Swissa *et al.* [16] performed some XPS spectra of O 1s line before and after the hydrogen adsorption on an oxygen precovered polycrystalline U surface, which did not reveal any shift from the oxidic binding energy indicating that no hydroxide was formed and that the hydrogen was probably directly adsorbed on the uranium surface. Moreover the room-temperature accumulation of hydrogen on oxidised U surface progresses via a random two-site chemisorption model mechanism.

To check the cleanliness of the surface more precisely, only the more intense line, U$4f_{7/2}$, was monitored (see **figure VII.9**).

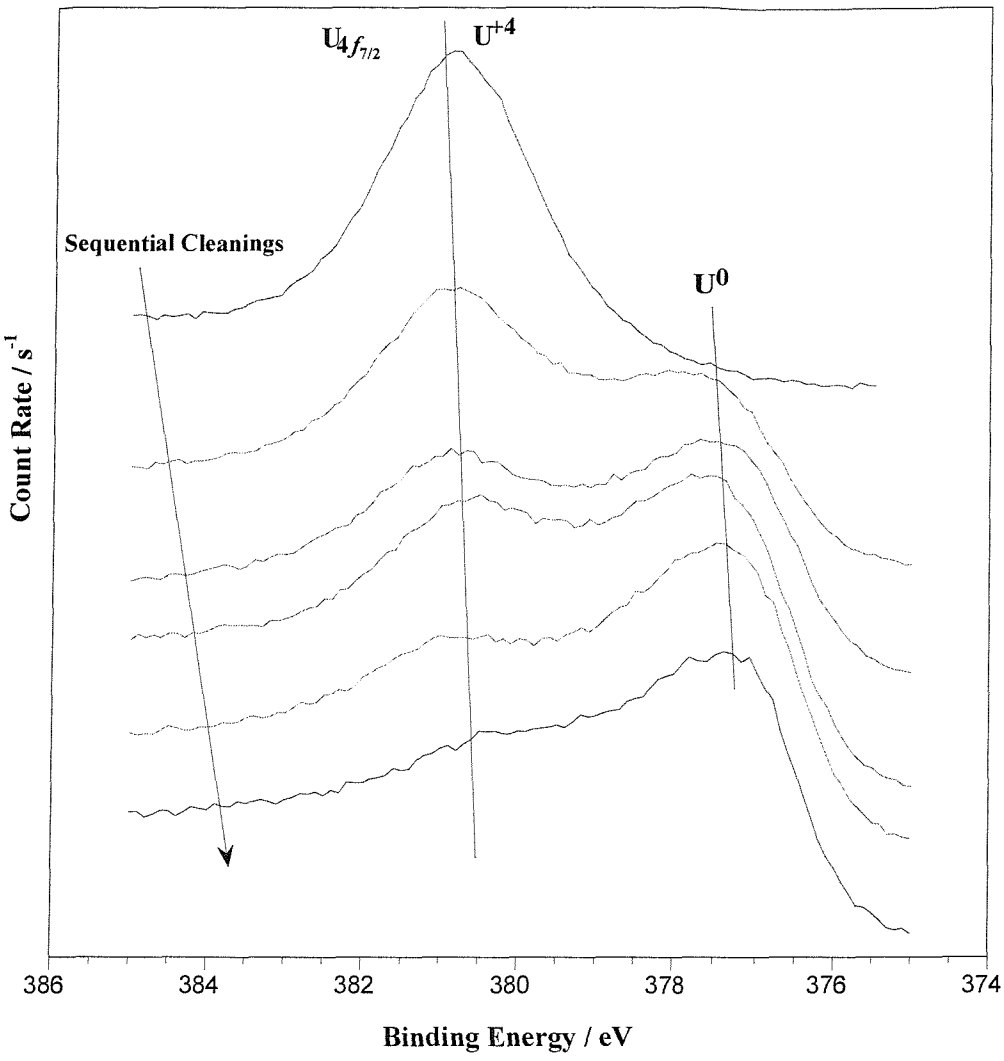

Figure VII.9: X-ray photo-electron spectra of the U $4f_{7/2}$ line following sequential cleanings. $T_s = 200$ K.

VII.3.3 King & Wells Method

This method permits a direct measurement of the initial sticking probability S_0 with a minimum calculable of S_0 being around 5 % [40].

$$S_0 = (P_1-P_2)/((P_1-P_0)\times(1-F_d)) \qquad (1)$$

A typical mass spectrometer response during sticking probability measurements of H_2 on a polycrystalline uranium surface by the King & Wells method is shown on **figure VII.10**. The mixture used was 0.5 ml min^{-1} H_2/49.5 ml min^{-1} He at $T_n = 306$ K, thus an incident energy of 66 meV and $T_s = 180$ K.

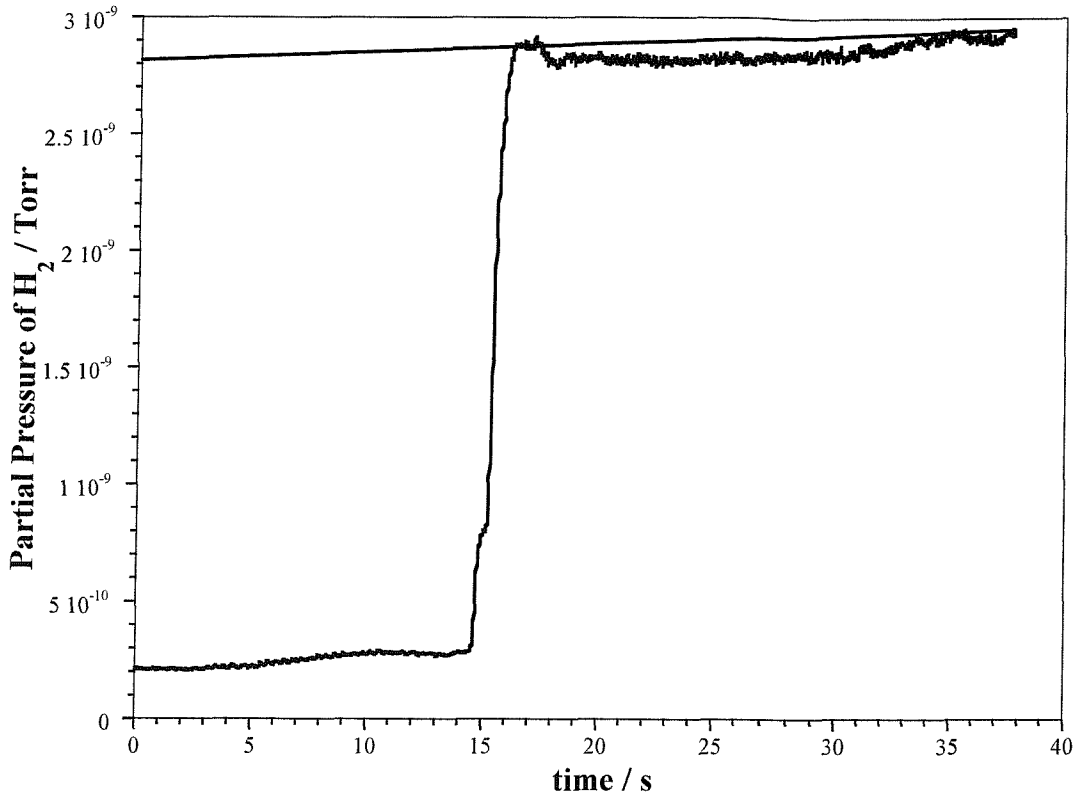

Figure VII.10: Typical mass spectrometer response during sticking probability measurement of hydrogen by the King & Wells method. For T_s = 180 K, E_i = 66 meV and $\Theta_i = 0°$. S_0 = 0.05.

The initial sticking probability for H_2 on clean uranium has been estimated, after one month of intensive cleaning, by the King & Wells method [40] to be 0.04 to 0.05, which has been confirmed using TPD spectroscopy. Due to the small hydrogen sticking on uranium, we worked at the limit of the King & Wells method, however there is no doubt on the drop of the pressure signal observed due to the sticking (**figure VII.10**). Hence the interaction of H_2 with a clean U surface seems weak, and is not even measurable on an oxidised U surface. This result is in perfect agreement with the hydrogen sticking probability measurements from Balooch and Hamza [10] performed on a U surface that was constantly bombarded with argon ions to keep it clean (the base pressure was of 4×10^{-10} Torr) and is in reasonable agreement with Swissa *et al.* [16]. While the King & Wells method gives a direct measure of the sticking, it is not forward to obtain the sticking with the TPD measurements, however by calculating the ratio of the coverage as measured by TPD to the exposure of the surface to H_2, Balooch obtained a trustworthy value of S_0 = 0.04.

The initial sticking probability of hydrogen $S_0(H_2)$ on U surface has been measured as a function of incident beam energy (**figure VII.11**). This experiment necessitated daily three 60 min argon-bombardment with 3 keV ions (*i.e.* to 20° from normal incidence) at room temperature, 575 K and 675 K. Each sputter was followed by 45 to 60 min annealing at 825 K. It was a very long-term job, and only permitted to obtain two sticking data points per set of experiments because of the rapid contamination of the sample surface, in fact even the 10 min annealing at 825 K between the experiments does not permit the surface to stay clean more than 20 min.

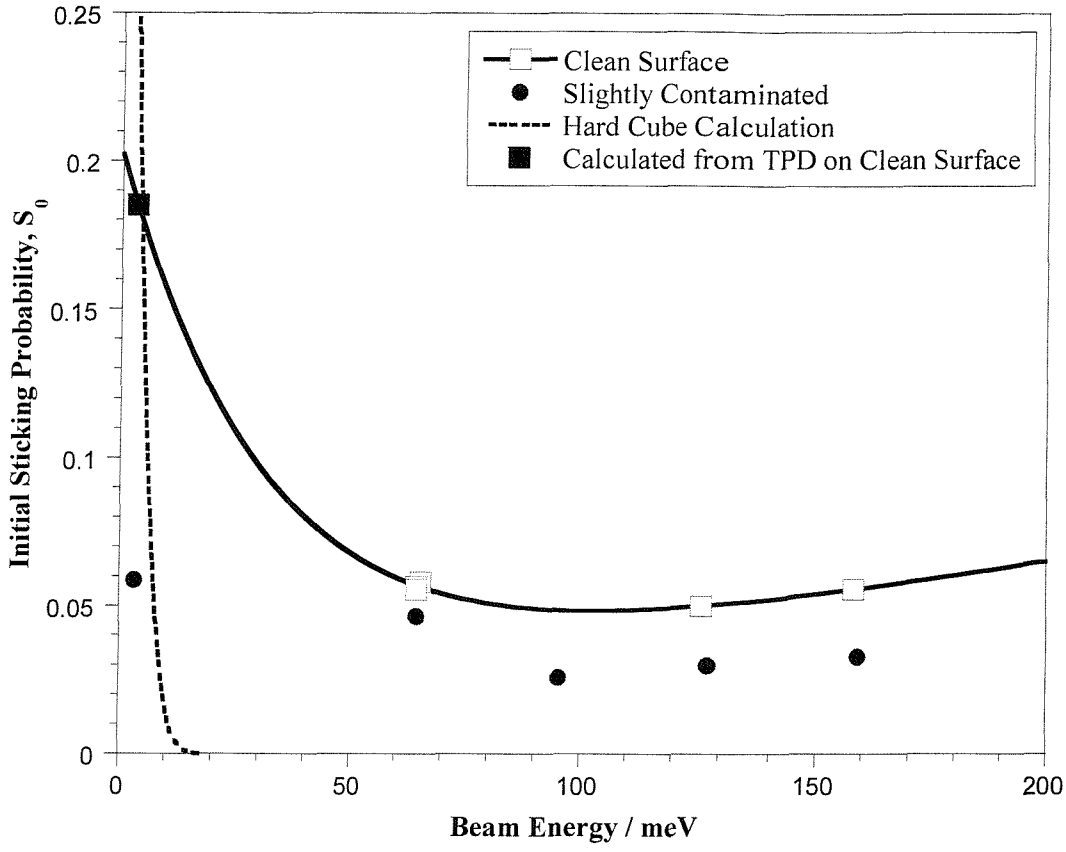

Figure VII.11: Initial sticking probability of H_2 on clean polycrystalline U as a function of incident beam energy, $T_s = 300$ K, $\Theta_I = 0°$.

Hydrogen sticking probability measured with the King & Wells method at an energy below 60 meV was always found to be negligible. This is rather surprising considering the nature of hydrogen dissociation on other metals [41-44], especially ones with surfaces as rich in steps and defects as the polycrystalline U sample is [43]. Hence in order to confirm or disprove these results, some TPD experiments were performed by dosing hydrogen in an

argon beam at T_n = 300 K, which led to an incident kinetic energy of 3.3 meV. The sample was kept at T_s = 300 K during the time of adsorption. These latter data led to conclude that adsorption is occurring at low energy, with an initial sticking probability of 0.185 ±0.03. Therefore it is thought that the oxygen contamination being present in the molecular beam can poison the hydrogen adsorption at low energy [45]. These TPD results are in agreement with our estimate of hydrogen trapping into a molecular potential well (which then dissociate when the appropriate surface site has been encountered) performed using a hard cube calculation (see **appendix A**) of a chemisorbed H_2 species with a well depth of 30 meV [42, 43]. This model assumes that the H_2 molecule is a rigid spherical elastic particle which collides with one cube of U atoms. These U atoms are also assumed to be elastic particles and their cube moves like an oscillator only in one direction normal to the assumed perfectly smooth surface [46]. This model suggests an initial sticking of ~ 0.25 at 3 meV as seen in **figure VII.11**, assuming that all physisorbed molecules go on to dissociate.

Between 65 and 160 meV, the initial sticking was found to be quite constant (within the experimental errors) around 0.05±0.02, which suggests that there are at least two processes occurring at the surface. In fact the dissociative adsorption of H_2 might occur through an indirect channel associated with the presence of defects on the surface as well as through a weak direct channel at high energies.

Results obtained from a slightly contaminated surface (see **figure VII.11**) suggest that impurities cause a blocking of hydrogen adsorption in the whole energy range. Hence it was decided to dose oxygen prior to hydrogen in order to study the effects of surface contamination on H_2 adsorption (by TPD measurements).

VII.3.4 Consequences of Pre-adsorbed Oxygen on Hydrogen TPD

The U sample initially obtained was largely oxidised on the surface and carbon free. Thus the stages of cleaning observed in **figures VII.3** to **VII.5**, showed that the presence of oxygen atoms on the U surface strongly influences the hydrogen adsorption. However, the precise effects of the oxygen contamination were difficult to interpret. Therefore, the following experiments allowed a direct observation of the influence of adsorbed oxygen on

the hydrogen adsorption and a confirmation of the attributions of the TPD peaks in **figures VII.3** to **VII.5**.

After numerous phases of sputtering, the U surface appeared free of contaminants, thus it was exposed to specific amounts of O_2 gas varying between 0.1 and 0.8 L, each of them followed by a constant H_2 coverage of 0.3 ML. **Figure VII.12** was obtained by dosing O_2 and H_2 at $T_s = 310$ K, while **figure VII.13** was acquired at $T_s = 180$ K. Note that the anneal performed after each experiment was found to be insufficient to completely remove the adsorbed oxygen which adsorbs irreversibly on the U surface (only removed by sputtering). Thus the oxygen exposures specified in **figures VII.12** and **VII.13** do not correspond to the doses performed by the experimentalist but to the sum of all the previous exposures (e. g. 1.6 L = 0+0.1+0.1+0.2+0.4+0.8).

The insert in **figure VII.12** shows that an oxygen exposure of 0.1 L gives rise to an increase of the hydrogen TPD area, while the following exposures show it to decrease. In most cases the presence of a pre-adsorbed substance on the surface will reduce the sticking coefficient for hydrogen by blocking the most active sites, especially for polycrystalline and stepped surfaces. But in certain cases, like here and for the densely packed Ni(111) surface [47], we observed that hydrogen has a very small sticking, however in the presence of a small amount of pre-adsorbed oxygen $S(H_2)$ increases. Hence Winkler and Rendulic [47] conclude in the existence of a precursor state and two different types of adsorption sites on the surface. Note that their results were also obtained by thermal desorption of hydrogen. In the same way in the present study, a very small amount of chemisorbed O atoms seems to increase the H_2 adsorption while a higher O coverage blocks the adsorption.
The same remark can be made from the insert in **figure VII.13**.

Figure VII.12 represents the adsorption of 0.3 ML of hydrogen on a O_2 pre-covered U surface at 310 K and shows 3 main peaks. While in **figure VII.13** there is one more feature around 250 K.
The peak located around 410 – 450 K decreases in intensity when the oxygen coverage increases. This is in agreement with Balooch *et al.* data [10] who associated it with recombinative desorption of H atoms adsorbed on U metal. Thus, more O atoms are present on the surface more uranium oxide is formed and less U metal sites are free for this specific hydrogen adsorption.

The peak situated around 500 – 600 K increases with the oxygen coverage, which is consistant with our previous deductions that H_2 desorbing from the oxide layer. The peak around 300-350 K was previously associated with OH species formed on the metal, which is confirmed by the fact that the intensity of this peak is higher for a 0.1 L oxygen pre-covered U surface than for a clean U surface. As the oxygen atoms concentration increases, the small islands originally deposited link together to start the formation of an oxide layer, thus there are less sites for the previous hydrogen to form isolated OH groups which leads to the decrease of this hydrogen TPD feature.

Figure VII.3 shows a peak around 240 K on a completely oxidised surface which was thought to be related to OH species adsorbed on the U surface. Note that **figures VII.3** to **VII.5** did correspond to the cleaning of an U surface highly oxidised in air, meaning that it has been sputtered and annealed regularly before dosing any hydrogen gas. While the present experiments correspond to a clean U sample oxidised with pure O_2 gas, followed directly by H_2 exposure hence the oxide layer does not undergo any prior reconstruction, hence these results are quite difficult to compare. In fact the 220-270 K in **figures VII.3** to **VII.5** did not show any obvious decrease as the cleaning procedure progressed while in **figure VII.13** this peak seems to disappear slowly with increasing O coverage. At this early stage it is too difficult to rich any conclusion on these observations especially because of the polycrystalline nature of the sample, hence it would be interesting to study some single crystal of uranium to simplify the experiments.

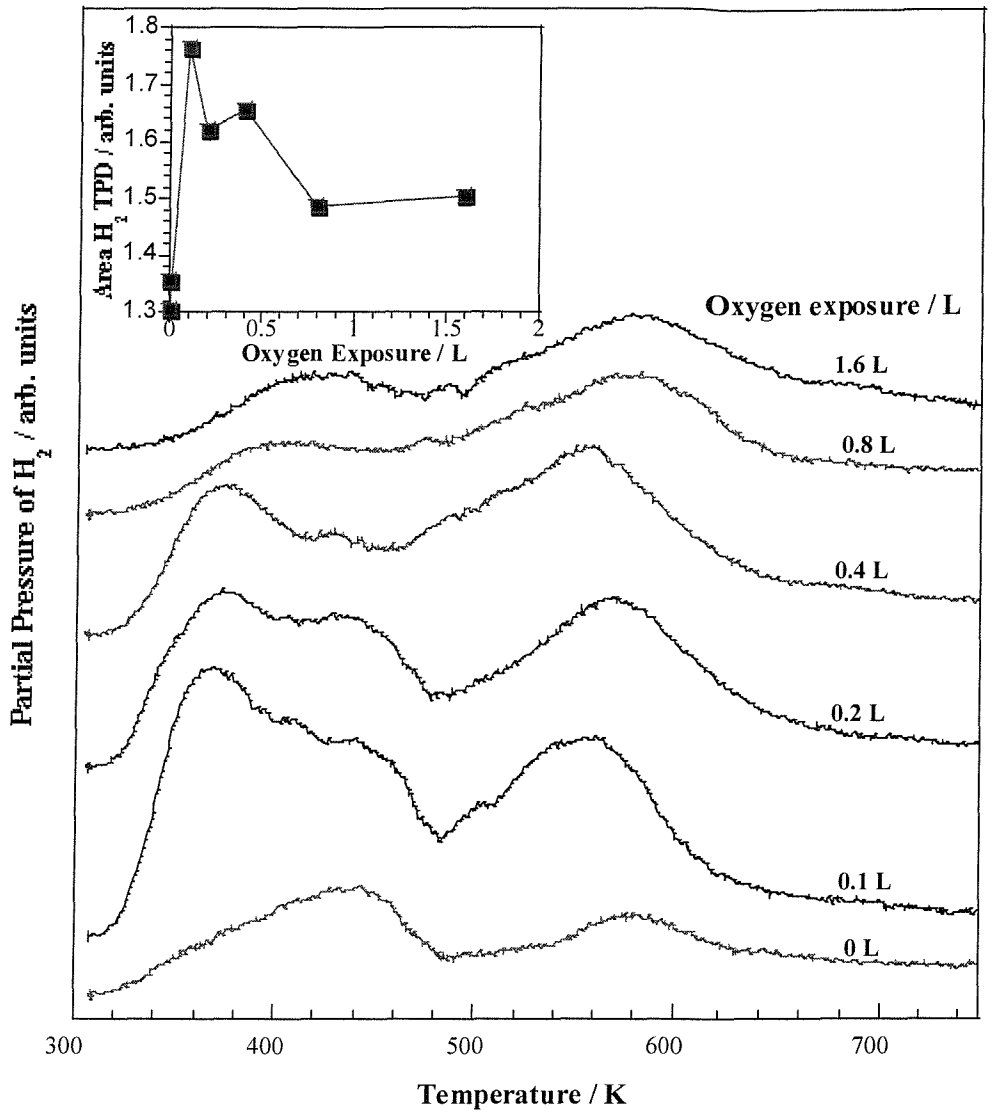

Figure VII.12: Hydrogen TPD spectra from the U surface pre-covered with an oxygen exposure varying from 0 to 1.6 L at $T_s = 310$ K, followed by a constant 0.3 ML coverage of H_2 at $T_s = 310$ K. The oxygen exposures are marked for each spectrum. An insert corresponding to the areas of these spectra versus the oxygen exposure is also available.

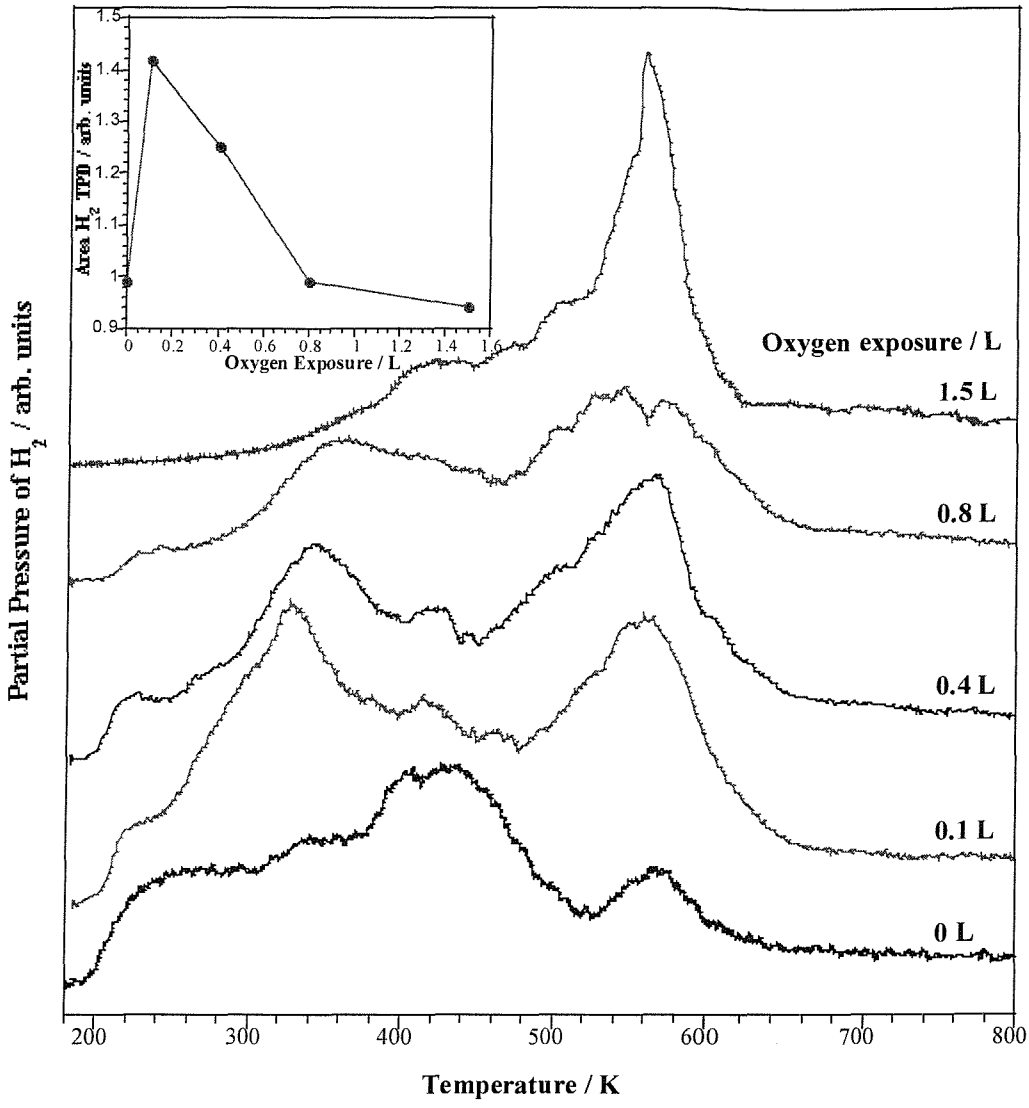

Figure VII.13: Hydrogen TPD spectra from the U surface pre-covered with an oxygen exposure varying from 0 to 1.5 L at T_s = 180 K, followed by a constant 0.3 ML coverage of H_2 at T_s = 180 K. The oxygen exposures are marked for each spectrum. An insert corresponding to the areas of these spectra versus the oxygen exposure is also available.

VII.3.5 Dependence of S_0 of Oxygen on Incident Energy

Initial sticking probability measurements of oxygen on clean uranium as a function of incident beam energy have been performed in the energy range 50 to 150 meV. The results are shown in **figure VII.14**. Beam energies were controlled by a combination of nozzle temperature and seeding. From these data it should become apparent as to the dissociation channels available at the surface for oxygen and why the uranium oxidises readily.

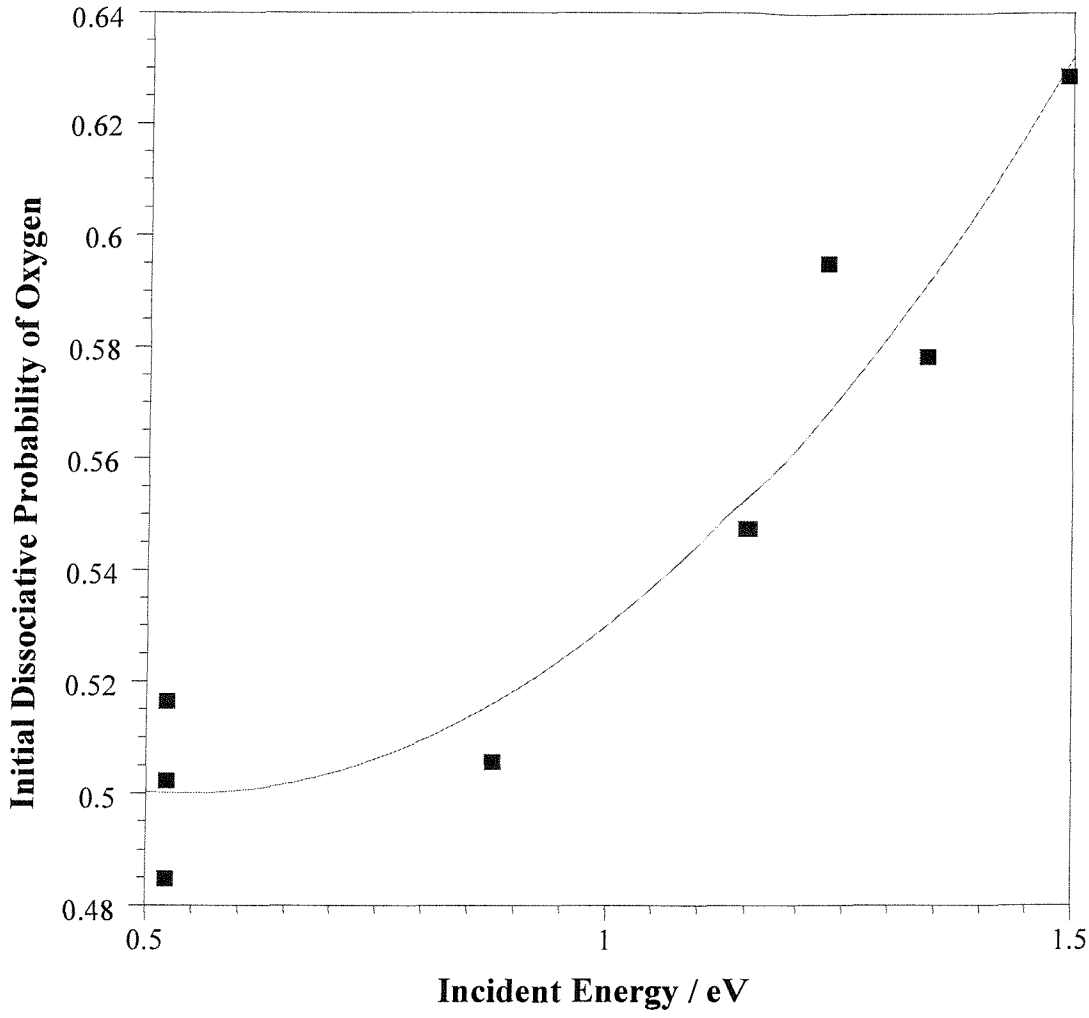

Figure VII.14: Initial sticking probability of O_2 on clean polycrystalline U as a function of nozzle temperature, $T_s = 300$ K, $\Theta_i = 0°$.

The initial sticking probability of O_2 on U, measured at $\Theta_i = 0°$ and at $E_i = 0.5$ eV, is relatively high (0.5 in average) and increases with incident energy. Thus the dissociation of O_2 molecules happens via a non-activated direct dissociation channel. The increase in the sticking with translational energy is due to the effective opening of a dynamical window giving access to barriers along non-optimal reactive trajectories. Further measurements need to be performed in order to know the $S_0(O_2)$ behaviour at low energies.

It is not possible at this early stage to relate the oxygen sticking to any specific sites on the surface, as the U sample is of polycrystalline nature. Thus it would be of great interest to study O_2 sticking on different U single crystal planes.

VII.4 CONCLUSION

Temperature programmed desorption measurements of hydrogen over clean and oxygen-precovered polycrystalline uranium indicate that recombinative desorption of hydrogen from the clean U metal is observed around 410-440 K. The peak around 500-600 K corresponds to hydrogen desorbing from an oxide layer. The 300-350 K feature is associated with recombinative hydrogen desorption from hydroxyl species formed on the metal. When the oxygen atoms concentration increases, the small islands originally deposited link together to start the formation of an oxide layer, thus there are less sites available for this last H adsorption which explains the increase of the 500-600 K feature and the decrease of the 350 K one. The origin of the 240 K peak, present on clean and partly oxidised U, is believed to be related to recombinative desorption of H atoms adsorbed in the crystal bulk, but more experiments would need to be performed in order to confirm it.

The initial dissociative sticking probability of hydrogen on polycrystalline U seems rather constant over the range $60 < Ei\ (meV) < 160$ with an average value of 0.05 ± 0.02, while at low energy (3 meV) it is much higher at 0.185. Previous results on H_2/U obtained a sticking coefficient of 0.04 by TPD spectroscopy dosing hydrogen with an effusive source [10] that are in good agreement with the present results.

The initial dissociative sticking probability of oxygen on clean U is relatively high 0.5 at an incident energy of 0.52 eV and increases with incident energy. Thus the dissociation of O_2 molecules happens via a non-activated direct dissociation channel.

VII.5 REFERENCES

[1] website: www.world-nuclear.org.

[2] website: www.treasure-troves.com/bios/Becquerel

[3] website : ccnr.org/fission_ana-f.html

[4] website: www.uic.com.au

[5] website: www.gse.ic.uk/phd/phd_materials_high_spot_res.html

[6] Mintz M. H. and Bloch J., *Prog. Solid State Chem.*, 16: 163, **1985**.

[7] Bloch J., Brami D. and Kremner A., *J. Less. Comm. Met.*, 139: 371, **1988**.

[8] Owen L. W. and Scudamore R. A., *Corr. Sci.*, 6: 461, **1966**.

[9] website : www.isis-online.org

[10] Balooch M. and Hamza A. V., *J. of Nucl. Mat*, 230: 259, **1996**.

[11] Balooch M. and Siekhaus W. .J., *J. of Nucl. Mat*, 255: 263, **1998**.

[12] Cohen D., Zeiri Y. and Mintz M. H., *J. of Alloys Compd.*, 184: 11, **1992**.

[13] Arkush R., Venkert A., Aizenshtein M., Zalkind S., Moreno D., Brill M., Mintz M. H. and Shamir N., *J. of Alloys Compd.*, 244: 197, **1996**.

[14] Danon A., Koresh J. E. and Mintz M. H., *Langmuir*, 15: 5913, **1999**.

[15] Moreno D., Arkush R., Zalkind S. and Shamir N., *J. Nucl. Mater.*, 230: 181, **1996**.

[16] Swissa E., Jacob I., Atzmony U., Shamir N. and Mintz M. H., *Surf. Sci.*, 223: 607, **1989**.

[17] Muggelberg C., Castell M. R., Briggs G. A. D. and Goddard D. T., *Surf. Sci.*, 404: 673, **1998.**

[18] Allen G. C., Trickle I. R. and Tucker P. M., *Philosophical Magazine B*, 43: 689, **1981**.

[19] Lander G. H. and Fisher E. S. and Bader S. D., *Advan. Phys.*, 43: 1, **1994**.

[20] Nornes S. B. and Meisenheimer R. G., *Surf. Sci.*, 88: 191, **1979**.

[21] Winer K., Colmenares C. A., Smith R. L. and Wooten F., *Surf. Sci.*, 183: 67, **1987**.

[22] Allen G. C., Tucker P. M. and Lewis R. A., *J. Chem. Soc., Faraday Trans.* II, 80: 991, **1984**.

[23] Colmenares C. A., *Prog. Solid State Chem.*, 15: 257, **1984**.

[24] Manner W. L., Lloyd J. A., Hanrahan R. J. and Paffett M. T., *Appl. Surf. Sci.*, 150: 73, **1999**.

[25] Eberhardt W., Greuter F. and Plummer E. W., *Phys. Rev. Lett.*, 46: 1085, **1981**.

[26] Greuter F. and Plummer E. W., *Solid State Commun.*, 48: 37, **1983**.

[27] Hofmann P. and Menzel D., *Surf. Sci.*, 152/153: 382, **1985**.

[28] Yates J. T., Peden C. H. F., Houston J. E. and Goodman D. W., *Surf. Sci.*, 160: 37, **1985**.

[29] Comsa G. and David R., *Surf. Sci.*, 117: 77, **1982**.

[30] Rieder K. H., Baumberger M. and Stocker W., *Phys. Rev. Lett.*, 51: 1799, **1983**.

[31] Hayden B. E., Lackey D. and Schott J., *Surf. Sci.*, 239: 119, **1990**.

[32] Behm R. J., Penka V., Cattania M. G., Christmann K. and Ertl G., *J. Chem. Phys.*, 78: 7486, **1981**.

[33] Briggs D. and Seah M. P., "*Practical Surface Analysis, by Auger and X-ray Photoelectron Spectroscopy*", Ed. John Wiley & Sons, Chichester, chap.5, **1983**.

[34] Briggs D. and Seah M. P., "*Practical Surface Analysis, by Auger and X-ray Photoelectron Spectroscopy*", Ed. John Wiley & Sons, Chichester, chap.3, **1983**.

[35] Wagner C. D., Riggs W. M., Davis L. E., Moulder J. F. and (ed.) Muilenberg G. E., "*Handbook of X-ray*", Perkin-Elmer Corp., Eden Praire, **1979**.

[36] Manner W. L., Lloyd J. A. and Paffett M. T., *J. of Nucl. Mat.*, 275: 37, **1999**.

[37] Swissa E., Bloch J., Atzmony U. and Mintz M. H., *Surf. Sci.*, 214: 323, **1989**.

[38] Fuggle J. C., Burr A. F., Watson L. M., Fabian D. J. and Lang W., *J. Phys. F*, 4: 335, **1974**.

[39] Allen G. C. and Tucker P. M., *J. Chem. Soc. Dalton Trans.*, p. 470, **1973**.

[40] King D. A. and Wells M. G., *Surf. Sci.*, 29: 454, **1972**.

[41] Butler D.A., Hayden B. E. and Jones J. D., *Chem. Phys. Lett.*, 217: 423, **1994**.

[42] Butler D.A. and Hayden B. E., *Chem. Phys. Lett.*, 232: 542, **1995**.

[43] Gee A. E., Hayden B. E., Mormiche C. and Nunney T. S., *J. Chem. Phys.*, 112: 7660, **2000**.

[44] Hayden B. E. and Lamont C. L. A., *Chem. Phys. Lett.*, 160: 331, **1989**.

[45] Gee A.T., Hayden B. E., Mormiche C., Nunney T.S., *Surf. Sci.*, 512: 165, **2002**.

[46] Jones J. D., Ph. D. thesis, University of Southampton, p.10, **1994**.

[47] Winkler A. and Rendulic K. D., *Surf. Sci.*, 118: 19, **1982**.

CONCLUSION

Supersonic molecular beam techniques and temperature programmed desorption spectroscopy have been used to study the adsorption and desorption of CH_4, H_2 and NH_3 on a stepped platinum (533) surface and H_2 on a polycrystalline uranium surface.

The strong dependency of the initial sticking probability, S_0, of CH_4 with the surface temperature for $120 < T_s(K) < 800$ (at $E_i = 700$ meV) and the incident energy for $26 < E_i(meV) < 1455$ (at $T_s = 600$ K) are compatible with the existence of a thermally assisted tunneling channel caused by a coupling of the tunnel barrier (direct channel component) to the lattice (indirect channel component) which dominates over most of the accessible temperature and energy range. This phenomena dominates the dissociation of a CH_4 molecule into a CH_3 radical and an H atom on stepped surfaces as on flat surfaces.

S_0 has also been measured as a function of angle of incidence, Θ, for $E_i = 1450$ meV and $T_s = 600$ K and it is found that the maximum sticking occurs at -5° to the surface normal which indicates that dissociation is most efficient for molecules which impinge nearly perpendicularly to the (533) surface normal. This behaviour suggests that dissociation at the step proceeds via a concerted interaction with two surface planes.

The steps have been shown to offer a low energetic bypass to dissociative chemisorption with a reduction of the barrier height of roughly 300 meV compared to Pt(111). This channel most likely saturates and at incident energies above 700 meV the observed increase in activity can be attributed to dissociation on the (111) terraces.

TPD of H_2 from a Pt(533) surface indicates recombinative H_2 desorption from the (100) step sites at $E_{des} = 94$kJ mol^{-1} and from the (111) terrace sites at $E_{des} = 70$kJ mol^{-1}. Saturation of the steps and of the whole surface takes place at 0.18 ± 0.02 and 0.84 ± 0.05 ML respectively.

$S_0(H_2)$ has been measured for $3 < E_i(meV) < 180$ at $T_s = 300$ K on oxygen and CO decorated Pt(533) surfaces. At oxygen coverage $\theta_O = 0.12$ ML, corresponding to saturation of the step sites, $S_0(H_2)$ exhibits a rapid decrease from 3 to 30 meV associated with an accommodated indirect channel component, and a linear increase above 30 meV

corresponding to a direct channel. Removing the contribution of the step sites responsible for the low energy component of $S_0(H_2)$ through decoration of step sites (*i.e.* an unaccommodated indirect channel component) creates a "virtual" Pt(111) surface. Decorating the step sites with 0.12 ML of CO instead of O has a stronger influence on $S_0(H_2)$ due to a strongly repulsive CO-H interaction, therefore $S_0(H_2)$ is lower across the whole energy range studied.

At high energy $S_0(H_2)$ is found to exhibit a negligible T_s dependence on O/Pt(533) and CO/Pt(533). At $E_i = 6.6$ meV a more significant T_s dependence is associated with the accommodated indirect channel component. At intermediate energy $E_i = 18$ meV both channels are available hence a very weak T_s dependence is observed.

On O/Pt(533) and CO/Pt(533) the trend of $S(H_2)$ with hydrogen coverage is near to second order Langmurian at high energy while at low energy it is characteristic of the accommodated indirect channel.

The dominance of the indirect channels to dissociation in the overall dissociation process in the presence of step sites on Pt(533) is highlighted by demonstrating that, for a simulated isotropic thermal source, 76 % of the sticking is blocked by oxygen adsorbed at the (100) step sites (a similar result is expected for CO).

At 6.6 meV, the production of water from hydrogen adsorption on the step sites of the O/Pt(533) surface is observed above 244 K, and reaches a maximum at $T_s \sim 340$ K, while on CO/Pt(533) there is no water formation due to the lack of free oxygen adsorbates.

TPD of NH_3 from a Pt(533) surface indicate molecular adsorption at $T_s < 400$ K which does not seem to depend strongly on the platinum surface plane. The first layer corresponds to α-molecules bound to the metal through the lone pair on the nitrogen and to β-molecules at $E_{des} = 39$ kJ mol^{-1} held with a hydrogen bond to the α ones. Desorption from the steps is evidenced by the α' shoulder and the β' one at 46 kJ mol^{-1}. The poor resolution of the TPD spectra did not allow any measurements of the α and α' phases desorption energies.

Decomposition of NH_3 on Pt(533) is observed at $T_s > 360$ K evidenced by H_2 and N_2 productions on the (100) steps. $NH_3 \rightarrow NH_2 + H$ giving rise to the first maximum of H_2 production at 400 K and $NH_2 \rightarrow N + 2H$ producing N_2 and H_2 at 530 K. The coverages of atomic H and atomic N coming from NH_3 decomposition have been estimated to saturate around 0.03 and 0.01 ML, hence the coverage of NH_3 undergoing decomposition represents

only ~ 4 % of the total amount of NH_3 adsorbed on the Pt(533) surface (estimated at 0.25 ML).

The initial dissociative sticking probability of NH_3, $S_0(NH_3)$, has been measured in the energy range $27 < E_i(meV) < 825$, at $T_s = 400$ K where the initial NH_3 decomposition has already taken place. The decrease of $S_0(NH_3)$ observed with increasing E_i is indicative of precursor mediated dissociation of NH_3. The decrease in $S(NH_3)$ as a function of coverage and the T_s dependence indicate that the blocking of the dissociation sites quickly enhances desorption of the precursor rather than dissociation.

$S_0(NH_3)$ and TPD measurements have also been performed on O_2 and CO decorated Pt(533) surfaces. $\theta_{CO} \sim 0.19$ ML or $\theta_{O2} \sim 0.12$ ML were found to correspond to the saturation of the (100) step sites. The NH_3, N_2 and H_2 TPD measurements on both precovered surfaces reveal that dissociation of ammonia is not entirely blocked by the preadsorbed species. On O_2/Pt(533) surface the oxidation of NH_3 molecules on both (100) steps and (111) terraces is established by the production of H_2, H_2O, N_2 and NO. On CO/Pt(533) the steric effect of CO slowly blocks the adsorption and decomposition of NH_3.

At 400 K, the $S_0(NH_3)$ measurements on the CO/Pt(533) surface show a similar trend with E_i as on the clean surface. However the values are slightly smaller for corresponding values of E_i showing that some of the ammonia adsorption step sites have been blocked by CO.

At 400 K, the oxygen is adsorbed dissociatively and the $S_0(NH_3)$ measurements on the O/Pt(533) surface show a similar trend with E_i as on the clean surface. However the values are slightly higher than on the clean surface for corresponding values of E_i illustrating the enhancement of NH_3 decomposition by oxygen.

The coverage dependencies of $S(NH_3)$ on both precovered surfaces are similar to that found on the clean surface.

Temperature programmed desorption measurements of hydrogen over clean and oxygen-precovered polycrystalline uranium indicate that recombinative desorption of hydrogen from the clean U metal is observed around 410-440 K. The peak around 500-600 K corresponds to hydrogen desorbing from an oxide layer. The 300-350 K feature is associated with recombinative hydrogen desorption from OH species formed on the metal. The origin of the 240 K peak, present on clean and partly oxidised U, is believed to be

related to recombinative desorption of H atoms adsorbed in the crystal bulk, but more experiments would need to be performed in order to confirm it.

$S(H_2)$ on U seems rather constant over the range $60 < E_i\,(meV) < 160$ with an average value of 0.05±0.02, while at low energy (3 meV) it is much higher at 0.185.

$S(O_2)$ on U is relatively high at 0.5 at $E_i = 0.52$ eV and increases with incident energy. Thus the dissociation of O_2 molecules happens via a non-activated direct dissociation channel.

FUTURE WORK

There are still many experiments to be performed in order to complete the study of the four present systems. For example:

In the case of H_2 on platinum, the first experiment to perform concerns the dissociative adsorption of H_2 on Pt(111). There is no data for the initial dissociative sticking probability below 40 meV, which would be essential to confirm if the indirect accommodated channel observed below 30 meV on the Pt(533) surface is due to adsorption on the whole surface or only on the (100) steps. Moreover it would be useful to obtain some XPS data of the interaction of hydrogen on the atomic O-precovered Pt(533) surface, so as to confirm the presence or absence of OH species. An angular dependency of $S_0(H_2)$ on both O and CO precovered stepped surfaces might differ from $S_0(H_2)$ on the clean Pt(533) surface due to the influence of these pre-adsorbates, hence possibly showing a different favoured orientation of the incident hydrogen molecules.

In the case of ammonia adsorption on a stepped Pt(533) surface, it would be useful to perform some XPS measurements at various surface temperatures after deposition. This would allow the verification of our conclusions concerning the mechanism of NH_3 decomposition on the (100) steps. The initial dissociative sticking probability of NH_3 needs to be measured over a wider range of energies to check the possibility of a direct channel to dissociation above 800 meV. TPD of NH_3, N_2 and H_2 on an O_2-precovered surface have been obtained but it would be useful to complete similar measurements on an atomic O-precovered Pt(533) surface. Performing identical experiments on slightly different surfaces (i.e. increasing the width of the terraces or of the steps, changing the nature of these planes (111), (110), (100)), might simplify the identification of the processes involved in NH_3 adsorption and decomposition.

In the case of H_2 on U, much still needs to be done. The main problem arose from the polycrystalline nature of the sample studied, which strongly complicated the present results notably the TPD data. Hence a single crystal would be essential in order to simplify the processes taking place during H_2 adsorption. $S_0(H_2)$ at low energies was impossible to

obtain by the King and Wells method due to the rapid contamination of the surface, making it crucial to improve the experimental conditions.

APPENDIX A: DERIVATION OF THE HARD-CUBE TRAPPING PROBABILITY

The hard-cube model described here was originally developed by Goodman [1], Trilling [2] and Oman [3]. Due to the lack of computational power at the time, the thermal motion of the surface in any collision was neglected. Logan and Stickney [4] then proposed a simple classical model for the scattering of gas atoms from a solid surface. This model includes the thermal motion of the surface and is based on the following assumptions:

(a) The interaction of a gas atom with a surface atom is represented by an impulsive force of repulsion, meaning that both the incident gas particle and the surface atom may be considered as rigid elastic particles.

(b) The gas-surface intermolecular potential is uniform in the plane of the surface (i.e. the surface is perfectly smooth), hence the interaction does not change the tangential velocity of the gas particle, thus there are no forces acting parallel to the surface.

In order to combine the two previous assumptions, it is convenient to think of the surface atoms as cubes oriented with one face parallel to the surface plane and with motion only in the direction normal to the surface plane. Each gas particle (spherical, rigid and elastic) interact with just one of these cubes. The tangential velocity component is unchanged but the normal component changes according to Newton's laws.

(c) The surface atoms are represented by independent particles (cubes) confined by square-well potentials (i.e. rigid boxes). A gas particle interacts with a single surface atom by entering the "box", colliding with the surface particle, and then departing. Although it would be more realistic to consider the surface atoms as harmonic oscillators.

(d) A temperature-dependent velocity distribution is assigned to the surface atoms. A one-dimensional Maxwellian distribution is chosen for the component of velocity of the cubes in the direction normal to the surface. This may not be an appropriate distribution for surface atoms but it does satisfy certain equilibrium conditions.

A consequence of this approach is the restriction that, for only single collision to occur, the mass ratio of the gas to surface particles, μ, must be less than 1/3. This is not too great a restriction as, practically, it is often the case.

Molecular velocity in the potential well: V_{well}

The velocity, V_{vac}, of the molecule before entering the potential well is:

$$V_{vac} = -\sqrt{\frac{2E_i}{M}}$$

The depth of the potential well U is:

$$U = \frac{MV_{add}^2}{2}$$

Hence the additional velocity to the incident molecule as a result of the well is:

$$V_{add} = -\sqrt{\frac{2U}{M}}$$

with M the mass of the incident molecule.

Note that the velocities are taken to be positive when moving away from the surface and negative when impinging.

$$V_{well} = -\sqrt{\left(V_{vac}^2 + \frac{2U}{M}\right)} \qquad (1)$$

Molecular velocity after impact: V'_{well}

The conservation of the momentum leads to:

$$MV_{well} + mV_{cube} = MV'_{well} + mV'_{cube} \qquad (2)$$

Where V_{cube} is the velocity of the surface cube before impact, V'_{cube} is the velocity after impact, and m is the mass of the surface site.

From Newton's Experimental Law for an elastic collision:

$$V'_{well} - V'_{cube} = V_{cube} - V_{well}$$

$$V'_{cube} = V'_{well} - V_{cube} + V_{well} \qquad (3)$$

Combining equation (2) and (3) gives:

$$MV_{well} + mV_{cube} = MV_{well}^{'} + m\left(V_{well}^{'} - V_{cube} + V_{well}\right)$$

$$MV_{well} + mV_{cube} = MV_{well}^{'} + m\left(V_{well}^{'} - V_{cube} + V_{well}\right)$$

Hence:

$$V_{well}^{'} = \frac{V_{well}(\mu - 1) + 2V_{cube}}{(\mu + 1)}$$

With μ the reduced mass (M/m).

Velocity of the cube below which the incident molecule will trap

The energy required to escape the potential well after impact is U.

Hence the minimum velocity required to escape the well is:

$$V_{escape} = +\sqrt{\frac{2U}{M}}$$

To remain trapped:

$$V_{well}^{'} < \sqrt{\frac{2U}{M}}$$

$$\frac{V_{well}(\mu - 1) + V_{cube}}{(\mu + 1)} < \sqrt{\frac{2U}{M}}$$

$$V_{cube} < \frac{(\mu + 1)}{2}\sqrt{\frac{2U}{M}} - \frac{V_{well}(\mu - 1)}{2}$$

With V_{well} from equation (1):

$$V_{cube} < \frac{(\mu + 1)}{2}\sqrt{\frac{2U}{M}} + \frac{(\mu - 1)}{2}\sqrt{\left(V_{vac}^2 + \frac{2U}{M}\right)}$$

By stating:

$$V_{\lim it} = \frac{(\mu + 1)}{2}\sqrt{\frac{2U}{M}} + \frac{(\mu - 1)}{2}\sqrt{\left(V_{vac}^2 + \frac{2U}{M}\right)}$$

Hence to be trapped a molecule has to verify:

$$V_{cube} < V_{limit} \qquad (4)$$

Fraction of surface cubes capable of collision and verifying equation (4): $P_c(v)$

The probability of a surface cube having a velocity v, P(v), is dependent on the energy of the 'state', E, and the surface temperature, T_s. The probability of occupying a particular state is depicted by the Boltzmann distribution.

With:

$$E = \frac{1}{2} m v^2$$

Pc(v) being the probability of colliding with a surface site of velocity v, hence:

$$P_c(v) = \int_{-\infty}^{V_{limit}} Pc(v).P(v)\, dv$$

a) With the probability of a surface site having the velocity v: P(v)

$$P(v) = \frac{\exp\left(-\frac{mv^2}{2kT}\right)}{Q}$$

Where Q is the partition function:

$$Q = \int_{-\infty}^{+\infty} \exp\left(-\frac{mv^2}{2kT}\right) dv \qquad (5)$$

Using the standard integral:

$$\int_0^{+\infty} \exp\left(-bv^2\right) dv = \frac{1}{2}\sqrt{\frac{\pi}{b}}$$

And substituing in equation (5):

$$a^2 = \frac{m}{2kT}$$

Hence:

$$\int_0^{+\infty} \exp\left(-a^2 v^2\right) dv = \frac{1}{2}\sqrt{\frac{\pi}{a^2}}$$

Therefore:

$$Q = 2 \times \int_{-\infty}^{+\infty} \exp\left(-\frac{m v^2}{2kT}\right) dv = \frac{\sqrt{\pi}}{a}$$

Concluding:

$$P(v) = \frac{a}{\sqrt{\pi}} \exp\left(-a^2 v^2\right)$$

b) With the probability of colliding with a surface site of velocity v: Pc(v)

If the surface is receding from the incoming molecule this probability will be small, falling to zero when the surface is receding with the same velocity as the incident molecule V_{well}. The maximum probability will be when the surface and molecule are moving in opposite directions.

Hence:

$$Pc(v) = \frac{V_{well} - v}{V_{well}} = 1 - \frac{v}{V_{well}}$$

c) $P_c(v)$

$$P_c(v) = \int_{-\infty}^{V_{limit}} \left(1 - \frac{v}{V_{well}}\right)\left(\frac{a}{\sqrt{\pi}} \exp\left(-a^2 v^2\right)\right) dv$$

d) to evaluate $P_c(v)$

$$P_c(v) = \int_{-\infty}^{V_{limit}} \left(\frac{a}{\sqrt{\pi}} \exp\left(-a^2 v^2\right)\right) dv - \int_{-\infty}^{V_{limit}} \frac{v}{V_{well}} \left(\frac{a}{\sqrt{\pi}} \exp\left(-a^2 v^2\right)\right) dv$$

$$P_c(v) = A - B \qquad (6)$$

Evaluation of A:

$$A = \int_{-\infty}^{0} \left(\frac{a}{\sqrt{\pi}} \exp\left(-a^2 v^2\right)\right) dv + \int_{0}^{V_{limit}} \left(\frac{a}{\sqrt{\pi}} \exp\left(-a^2 v^2\right)\right) dv$$

With:

$$\int_{-\infty}^{0} \exp\left(-a^2 v^2\right) dv = \int_{0}^{+\infty} \exp\left(-a^2 v^2\right) dv = \frac{1}{2}\sqrt{\frac{\pi}{a^2}}$$

Hence:

$$\int_{-\infty}^{0}\left(\frac{a}{\sqrt{\pi}}\exp\left(-a^2v^2\right)\right)dv=\frac{1}{2}$$

And by substituting:

$$u=av$$

$$du=a\,dv$$

$$\int_{0}^{V_{limit}}\left(\frac{a}{\sqrt{\pi}}\exp\left(-a^2v^2\right)\right)dv=\int_{0}^{aV_{limit}}\left(\frac{a}{\sqrt{\pi}}\exp\left(-u^2\right)\right)\frac{du}{a}$$

$$\int_{0}^{V_{limit}}\left(\frac{a}{\sqrt{\pi}}\exp\left(-a^2v^2\right)\right)dv=\frac{1}{\sqrt{\pi}}\int_{0}^{aV_{limit}}\exp\left(-u^2\right)du$$

As:

$$erf(z)=\frac{2}{\sqrt{\pi}}\int_{0}^{z}\left(-x^2\right)dx \qquad (7)$$

Hence:

$$\int_{0}^{V_{limit}}\left(\frac{a}{\sqrt{\pi}}\exp\left(-a^2v^2\right)\right)dv=\frac{erf(aV_{limit})}{2}$$

Therefore A is: $$A=\frac{1}{2}+\frac{erf(aV_{limit})}{2}$$

Evaluation of B:

$$\int_{-\infty}^{V_{limit}}\frac{v}{V_{well}}\left(\frac{a}{\sqrt{\pi}}\exp\left(-a^2v^2\right)\right)dv=\frac{a}{\sqrt{\pi}V_{well}}\int_{-\infty}^{V_{limit}}v\exp(-a^2v^2)\;dv$$

By substituting: $u=-a^2v^2$

$$du=-2a^2v\,dv$$

So:

$$B=\frac{a}{\sqrt{\pi}V_{well}}\int_{-\infty}^{-a^2V_{limit}^2}\frac{v}{-2a^2v}\exp(u)du$$

$$B = -\frac{1}{2a\sqrt{\pi}V_{well}} \int_{-\infty}^{-a^2V_{lim\,it}^2} \exp(u)du$$

With equation (7):

$$B = -\frac{1}{2a\sqrt{\pi}V_{well}} \exp(-a^2V_{lim\,it}^2)$$

From equation (6) $P_c(\nu)$:

$$P_c(\nu) = \frac{1}{2} + \frac{erf(aV_{lim\,it})}{2} + \frac{1}{2a\sqrt{\pi}V_{well}} \exp(-a^2V_{lim\,it}^2)$$

REFERENCES

[1] Goodman F. O., *in Proc. Intern. Symp. Rarified Gas Dyn. 4th Toronto 1964*, 2: 366, **1965**.

[2] Trilling L., *de Mecanique*, 3: 215, **1964**.

[3] Oman R. A., Bogan A. and Li C. H., *in Proc. Intern. Symp. Rarified Gas Dyn. 4th Toronto 1964*, 2: 396, **1965**.

[4] Logan R. M., Stickney R. E., *J. Chem. Phys.*, 44: 195, **1966**.

APPENDIX B: THE MAXWELL-BOLTZMANN DISTRIBUTION

When a chemical system achieves equilibrium, it is through a process of energy transfer between the components, with energetic parts constantly giving energy away. This means that the probability distribution should tend towards situations where the energy is spread throughout the system in favor of situations where any system component has a great deal of energy. The exact form of the probability distribution is an exponential function:

$$P(i) = C\exp\left(-\frac{E_i}{k_B T}\right)$$

With ***P(i)*** the probability of finding a particle in state ***i***, E_i the energy of the state i, k_B the Boltzmann's constant and ***T*** the temperature of the particles.

For an atom in an ideal gas, each state has particular values of the three velocity components u_x, u_y, and u_z. States of a molecule can be indexed by the same three velocity components, plus vibrational and rotational energy levels. Since we know that any probability distribution must be normalized, we can determine the constant ***C*** explicitly:

$$P(i) = \frac{\exp\left(-\frac{E_i}{k_B T}\right)}{\sum_{j=1}^{N}\exp\left(-\frac{E_j}{k_B T}\right)}$$

With $\sum_{j=1}^{N}\exp\left(-\frac{E_j}{k_B T}\right)$ the partition function. This probability distribution, ***P(i)***, describes how energy is distributed at equilibrium for an amazingly wide variety of chemical and physical systems. This probability distribution is the Maxwell-Boltzmann distribution.

For many systems, including the ideal gas, the Maxwell-Boltzmann distribution provides the probability of finding a component in a particular state with a particular amount of energy. In the case of the gas, many different states have the same speed; a particle could be going left, right, up, down, back, front, or at any angle, and still be traveling at the same speed. To find the probability of a particle having a particular speed,

we must compute how many states have the same speed, and add up the probabilities of being in any of these states. The kinetic energy of a particle with mass m and speed u is:

$$E = \frac{1}{2}mu^2 \qquad (1)$$

So the probability of finding the particle in any one state is:

$$P(\vec{u} = (u_x, u_y, u_z)) = C\exp\left(-\frac{E}{k_B T}\right) = C\exp\left(-\frac{mu^2}{2k_B T}\right)$$

The number of states with the same speed is given by the surface area of a spherical shell:

$$4\pi u^2$$

Every state has a different velocity vector. All the states with the same speed have velocity vectors with the same length u, pointing in different directions. All these velocity vectors sweep out a spherical shell with radius ***u***. Therefore, the probability of finding an atom with a particular speed is:

$$P(u) = 4\pi u^2 C\exp\left(-\frac{mu^2}{2k_B T}\right)$$

Evaluation of C

The next step is to evaluate the normalization constant ***C***. Since ***P(u)*** is a continuous distribution, we must integrate over all values of ***u*** (from 0 to infinity). Moreover, the probability distribution must be normalised, hence:

$$\int_{u\,\min}^{u\,\max} P(u)du = \int_{x\,\min}^{x\,\max} Bu^2\exp\left(-Au^2\right)du = 1 \qquad (2)$$

With $B=4\pi C$ and $A=m/2k_BT$.

By defining the following equations:

$$I_n(A) = \int_0^{\infty} u^n\exp\left(-Au^2\right)du \qquad (3)$$

With:

$$I_0(A) = \int_0^\infty \exp\left(-Au^2\right)\, du = \frac{\sqrt{\pi}}{2} A^{-\frac{1}{2}}$$

And using the differentiation method, $I_2(c)$ can be obtained by:

$$\frac{d}{dA}\left(I_0(A)\right) = \int_0^\infty \frac{d}{dA}\left(\exp\left(-Au^2\right)\right)\, du = \frac{d}{dA}\left(\frac{\sqrt{\pi}}{2} A^{-\frac{1}{2}}\right)$$

$$\frac{d}{dA}\left(I_0(A)\right) = \int_0^\infty -u^2 \exp\left(-Au^2\right)\, du = -\frac{\sqrt{\pi}}{4} A^{-\frac{3}{2}}$$

Which gives:

$$I_2(A) = \int_0^\infty u^2 \exp(-Au^2)\, du = \frac{\sqrt{\pi}}{4} A^{-\frac{3}{2}}$$

By substitution in equation (2):

$$\int_{u\,\min}^{u\,\max} P(u)du = \frac{4\pi C\sqrt{\pi}}{4}\left(\frac{m}{2k_B T}\right)^{-\frac{3}{2}} = 1$$

Hence:

$$C = \left(\frac{m}{2k_B \pi T}\right)^{\frac{3}{2}}$$

Therefore:

$$P(u) = 4\pi\left(\frac{m}{2\pi k_B T}\right)^{\frac{3}{2}} u^2 \exp\left(-\frac{mu^2}{2k_B T}\right)$$

Overall properties of the gas as a whole

The average speed

The average value of the speed is just the speed value in each state, weighted by the probability of finding the system in this state. For each speed u, the probability of finding a molecule with this speed is simply $P(u)$. So the average speed, $\bar{u}$, is:

$$\bar{u} = \int_0^{\infty} uP(u)du = \int_{x\,\min}^{x\,\max} Bu^3 \exp\left(-Au^2\right)\, du = BI_3(A)$$

Equation (3) gives:

$$I_1(A) = \int_0^{\infty} u^1 \exp\left(-Au^2\right)\, du$$

By posing $x=u^2$, hence:

$$du = \frac{1}{2}x^{-\frac{1}{2}}$$

$$I_1(A) = \int_0^{\infty} \sqrt{x}\exp(-Ax)\frac{1}{2\sqrt{x}}dx = \frac{1}{2}\int_0^{\infty}\exp(-Ax)\, dx = \frac{1}{2}A^{-1}$$

Using the differentiation method:

$$\frac{d}{dA}\left(I_1(A)\right) = \frac{1}{2}\int_0^{\infty}\frac{d}{dA}\left(\exp(-Ax)\right)\, dx = \frac{d}{dA}\left(\frac{1}{2}A^{-1}\right)$$

$$\frac{d}{dA}(I_1(A)) = \frac{1}{2}\int_0^{\infty} -x\exp(-Ax)dx = -\frac{1}{2}A^{-2}$$

$$\int_0^{\infty} x\exp(-Ax)dx = \int_0^{\infty} u^2\exp(-Au^2)2udu = \int_0^{\infty} 2u^3\exp(-Au^2)du = I_3(A)$$

$$I_3(A) = \frac{1}{2}A^{-2} = 2\left(\frac{k_BT}{m}\right)^2$$

Therefore by replacing A, B and C by their values:

$$\bar{u} = \left(\frac{8k_BT}{m}\right)^{\frac{1}{2}}$$

The average kinetic energy

The kinetic energy for one molecule has been defined in equation (1), hence the average is:

$$\bar{E} = \frac{1}{2}m\overline{u^2}$$

because the mass m is the same for all the gas particles, the only speed changes.

$$\overline{u^2} = \int_0^{\infty} u^2 P(u)du = \int_{x\,\min}^{x\,\max} Bu^4 \exp\left(-Au^2\right)\, du = BI_4(A)$$

$I_4(A)$ is found by differentiation of $I_2(A)$, hence we find:

$$\overline{u^2} = \frac{3k_BT}{m} \text{ and } \overline{E}(u) = \frac{3k_BT}{2}$$

The most probable speed

The most probable speed is the speed u_p for which $P(u_p)$ has a maximum. For a function to have a maximum or minimum, its first derivative must equal 0, hence:

$$\frac{d}{du}P(u_p) = 4\pi\left(\frac{m}{2\pi k_BT}\right)^{\frac{3}{2}} \times \frac{d}{du}\left(u_p^2 \exp\left(-\frac{mu_p^2}{2k_BT}\right)\right) = 0$$

$$\frac{d}{du}P(u_p) = 4\pi\left(\frac{m}{2\pi k_BT}\right)^{\frac{3}{2}} \times \left[2u_p \exp\left(-\frac{mu_p^2}{2k_BT}\right) - \frac{m}{k_BT}u_p^3 \exp\left(-\frac{mu_p^2}{2k_BT}\right)\right] \quad (4)$$

$$u_p = \left(\frac{2k_BT}{m}\right)^{\frac{1}{2}}$$

Note that from equation (4) the solution $u_p=0$ is also possible, however we are looking for a speed $u>0$, hence this latter solution is not valid here.

Energy distribution

It is customary in gas-surface dynamics to discuss angular dependence in terms of "energies" and energy scaling. So instead of normal momentum, we would say normal energy. In fact the normal energy is just the energy associated with the normal component of momentum. Hence to convert the Maxwell-Boltzmann distribution of speeds into energy, equation (1) leads to:

$$P(u) = 4\pi u^2 \left(\frac{m}{2k_B \pi T} \right)^{\frac{3}{2}} \exp\left(-\frac{mu^2}{2k_B T} \right)$$

$$P(E) = 8\pi \frac{E}{m} \left(\frac{m}{2k_B \pi T} \right)^{\frac{3}{2}} \exp\left(-\frac{E}{k_B T} \right)$$

Calculation of E

The incident particle is characterised by a speed vector $\vec{u}$ and an energy $E(\vec{u})$ (incident beam energy) with an angle θ to the normal to the surface.

When θ and $\vec{u}$ vary, the particle is in fact defined on a cone of area A:

$$A = \pi Rh + \pi R^2$$

Only the outside of the cone is of interest not the base, hence A':

$$A' = \pi Rh$$

With $R = E(\vec{u}) \sin\theta$ and $h = E(\vec{u}) \cos\theta$

Hence:

$$A' = \pi \sin\theta \times \cos\theta \times E(\vec{u})^2$$

Then to perform the energy scaling, we have to chose the value of n such that:

$$S(E^{(n)}, \theta_i) \approx S(E^{(n)}, 0)$$

Where:

$$E^{(n)} = E \cos^n \theta_i$$

What these equations mean is that if you take the dissociation probability at off-normal incidence and plot it not as a function of E, but as a function of $E^{(n)}$ instead, then it will lie exactly on top of the normal incidence data, for which $E^{(n)} = E$ anyway since the angle of incidence is zero.

The most common example of normal energy scaling is when ***n=2***.

In the present case, only the normal component of the energy $E_{\perp}(\vec{u})$ is of interest, and:

$$E_{\perp}^{(2)}(\vec{u}) = E(\vec{u})\cos^2\theta_i$$

Hence: to scale the energy we have:

$$E = \frac{A'}{E_{\perp}^{(2)}(\vec{u})} = \frac{\pi \sin\theta \times \cos\theta \times E(\vec{u})^2}{E\cos^2\theta_i}$$

$$E = \frac{\pi \sin\theta \times E(\vec{u})}{\cos\theta_i}$$

Hence:

$$P(E) = 8\pi^2 \frac{\sin\theta \times E(\vec{u})}{m\cos\theta_i}\left(\frac{m}{2k_B\pi T}\right)^{\frac{3}{2}} \exp\left(-\frac{\pi \sin\theta \times E(\vec{u})}{k_B T\cos\theta_i}\right)$$

The Maxwell-Boltzmann distribution of energies for hydrogen at 300 K is shown in **figure 1**, with θ varying between 0 and 80°.

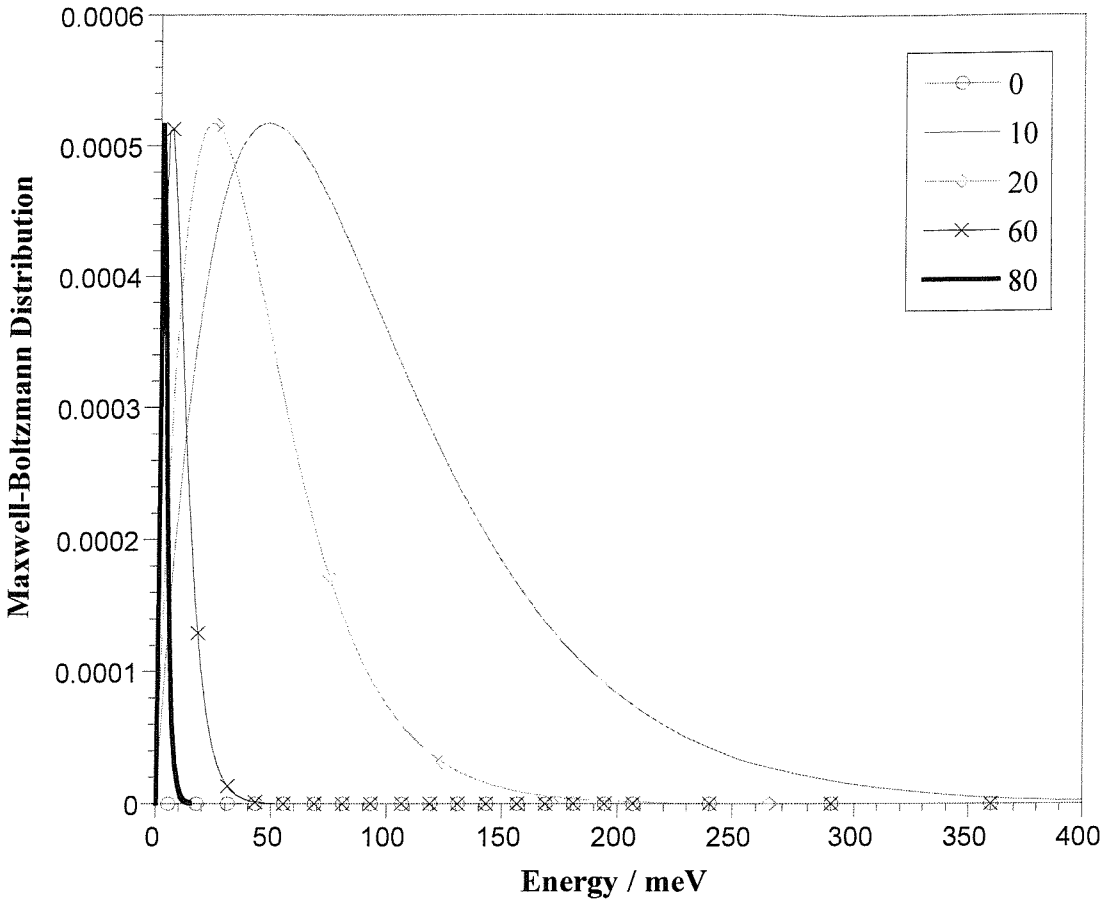

Figure 1: Maxwell-Boltzmann distribution of energies for a gas at T = 300 K, $0 < \theta < 80$, and for a beam energy $0 < E(meV) < 400$.